TESIS DE LA UNIVERSIDAD DE ZARAGOZA
2021
109

Francisco Manuel Navarro Serrano

Análisis del comportamiento altitudinal de la temperatura del aire superficial en áreas de montaña

Director/es
López Moreno, Juan Ignacio
Azorín Molina, César

ISSN 2254-7606

Prensas de la Universidad
Universidad Zaragoza

ISSN 2254-7606

Universidad Zaragoza
1542

Tesis Doctoral

ANÁLISIS DEL COMPORTAMIENTO ALTITUDINAL DE LA TEMPERATURA DEL AIRE SUPERFICIAL EN ÁREAS DE MONTAÑA

Autor

Francisco Manuel Navarro Serrano

Director/es

López Moreno, Juan Ignacio
Azorín Molina, César

UNIVERSIDAD DE ZARAGOZA
Escuela de Doctorado

Programa de Doctorado en Ordenación del Territorio y Medio Ambiente

2020

Universidad Zaragoza
1542

Tesis Doctoral

ANÁLISIS DEL COMPORTAMIENTO ALTITUDINAL DE LA TEMPERATURA DEL AIRE SUPERFICIAL EN ÁREAS DE MONTAÑA

Autor

Francisco Manuel Navarro Serrano

Directores

Juan Ignacio López Moreno
Cesar Azorín Molina

UNIVERSIDAD DE ZARAGOZA
Ordenación del Territorio y Medio Ambiente

2020

Universidad de Zaragoza

TESIS DOCTORAL

ANÁLISIS DEL COMPORTAMIENTO ALTITUDINAL DE LA TEMPERATURA DEL AIRE SUPERFICIAL EN ÁREAS DE MONTAÑA

Francisco Manuel Navarro Serrano

Directores: Juan Ignacio López Moreno y César Azorín Molina

Doctorado en Ordenación del Territorio y Medio Ambiente
Zaragoza, 2020

La presente Tesis Doctoral ha sido financiada por el Ministerio de Educación, Cultura y Deporte a través de un contrato del Programa de Formación de Profesorado Universitario, convocatoria 2015 (FPU15/00742, Resolución de 5 de agosto de 2016 por la que se conceden ayudas FPU), disfrutado en el Instituto Pirenaico de Ecología (Consejo Superior de Investigaciones Científicas, IPE-CSIC).

Los trabajos llevados a cabo han sido financiados por el Ministerio de Economía y Competitividad (Programa I+D: excelencia. CGL2014-52599 [2015-2017] y CGL2014-52135-C3-1-R [2015-2018]), por el Ministerio de Economía, Industria y Competitividad (Programa I+D orientada a los retos de la sociedad [2018-2021]. CGL2017-82216-R), y por el Fondo Europeo de Desarrollo Regional (FEDER, Programa Interreg-POCTEFA [2016-2019]. CLIMPY).

Imagen de Portada: Pico Balaitús (en aragonés, *Pico Os Moros*), 3.145 m s.n.m. Fotografía original tomada desde Formigal por Francisco M. Navarro Serrano, en 2014. Procesada posteriormente.

De acuerdo a la posibilidad ofrecida por el Programa de Doctorado de la Universidad de Zaragoza, se presenta esta Tesis Doctoral como un compendio de artículos de investigación, siendo el estudiante de doctorado autor de todos ellos:

1. **Navarro-Serrano, F.**, López-Moreno, J.I., Azorin-Molina, C., Alonso-González, E., Tomás-Burguera, M., Sanmiguel-Vallelado, A., Revuelto, J., Vicente-Serrano, S.M. 2018. Estimation of near-surface air temperature lapse rates over continental Spain and its mountain areas. *International Journal of Climatology* 38: 3233-3249. DOI: https://doi.org/10.1002/joc.5497.

2. **Navarro-Serrano, F.**, López-Moreno, J.I., Domínguez-Castro, F., Alonso-González, E., Azorin-Molina, C., El-Kenawy, A., Vicente-Serrano, S.M. 2020. Maximum and Minimum air temperature lapse rates in the Andean region of Ecuador and Peru. *International Journal of Climatology*. En Prensa. DOI: https://doi.org/10.1002/joc.6574.

3. **Navarro-Serrano, F.**, López-Moreno, J.I., Azorin-Molina, C., Buisán, S., Domínguez-Castro, F., Sanmiguel-Vallelado, A., Alonso-González, E., Khorchani, M. 2019. Air temperature measurements using autonomous self-recording dataloggers in mountainous and snow covered areas. *Atmospheric Research* 224: 168-179. DOI: https://doi.org/10.1016/j.atmosres.2019.03.034.

4. **Navarro-Serrano, F.**, López-Moreno, J.I., Azorin-Molina, C., Alonso-González, E., Aznárez-Balta, M., Buisán, S., Revuelto, J. 2020. Elevation effects on air temperature in a topographically complex mountain valley in the Spanish Pyrenees. *Atmosphere* 11(6): 656. DOI: https://doi.org/10.3390/atmos11060656.

5. López-Moreno, J.I., **Navarro-Serrano, F.**, Azorin-Molina, C., Sánchez-Navarrete, P., González-Alonso, E., Rico, I., Morán-Tejeda, E., Buisán, S., Revuelto, J., Pons, M., Vicente-Serrano, S.M. 2019. Air and wet bulb temperature lapse rates and their impact on snowmaking in a Pyrenean ski area. *Theoretical and Applied Climatology* 135(3-4): 1361-1373. DOI: https://doi.org/10.1007/s00704-018-2448-y.

Francisco Manuel Navarro Serrano, con DNI 29495369-P expone:

Siendo el autor principal del artículo titulado: "Estimation of near-surface air temperature lapse rates over continental Spain and its mountain areas", afirmo haber contribuido en todo el proceso de elaboración de este trabajo de investigación, incluyendo los análisis estadísticos, la interpretación de los datos así como la redacción y corrección del manuscrito. El resto de co-autores no doctores ha renunciado a presentar este trabajo como parte de una tesis doctoral en la modalidad de compendio de publicaciones.

En Zaragoza, a 23 de junio de 2020

Fdo. Francisco Manuel Navarro Serrano

Francisco Manuel Navarro Serrano, con DNI 29495369-P expone:

Siendo el autor principal del artículo titulado: "Maximum and Minimum air temperature lapse rates in the Andean region of Ecuador and Peru", afirmo haber contribuido en todo el proceso de elaboración de este trabajo de investigación, incluyendo los análisis estadísticos, la interpretación de los datos así como la redacción y corrección del manuscrito. El resto de co-autores no doctores ha renunciado a presentar este trabajo como parte de una tesis doctoral en la modalidad de compendio de publicaciones.

En Zaragoza, a 23 de junio de 2020

Fdo. Francisco Manuel Navarro Serrano

Francisco Manuel Navarro Serrano, con DNI 29495369-P expone:

Siendo el autor principal del artículo titulado: "Air temperature measurements using autonomous self-recording dataloggers in mountainous and snow covered areas", afirmo haber contribuido en todo el proceso de elaboración de este trabajo de investigación, incluyendo los análisis estadísticos, la interpretación de los datos así como la redacción y corrección del manuscrito. El resto de co-autores no doctores ha renunciado a presentar este trabajo como parte de una tesis doctoral en la modalidad de compendio de publicaciones.

En Zaragoza, a 23 de junio de 2020

Fdo. Francisco Manuel Navarro Serrano

Francisco Manuel Navarro Serrano, con DNI 29495369-P expone:

Siendo el segundo autor del artículo titulado: "Elevation effects on air temperature in a topographically complex mountain valley in the Spanish Pyrenees", afirmo haber contribuido en todo el proceso de elaboración de este trabajo de investigación, incluyendo los análisis estadísticos, la interpretación de los datos así como la redacción y corrección del manuscrito. El resto de co-autores no doctores ha renunciado a presentar este trabajo como parte de una tesis doctoral en la modalidad de compendio de publicaciones.

En Zaragoza, a 23 de junio de 2020

Fdo. Francisco Manuel Navarro Serrano

Francisco Manuel Navarro Serrano, con DNI 29495369-P expone:

Siendo el segundo autor del artículo titulado: "Air and wet bulb temperature lapse rates and their impact on snowmaking in a Pyrenean ski area", afirmo haber contribuido activamente en el diseño experimental, así como en la contextualización de la investigación y discusión de los resultados, trabajando activamente en la redacción del manuscrito y en las distintas fases metodológicas. El resto de co-autores no doctores ha renunciado a presentar este trabajo como parte de una tesis doctoral en la modalidad de compendio de publicaciones.

En Zaragoza, a 23 de junio de 2020

Fdo. Francisco Manuel Navarro Serrano

Dr. D. Juan Ignacio López Moreno, Investigador Científico en el Instituto Pirenaico de Ecología del Consejo Superior de Investigaciones Científicas (IPE – CSIC), AUTORIZA:

La presentación de la Tesis Doctoral en la modalidad de compendio de publicaciones y titulada "Análisis del comportamiento altitudinal de la temperatura del aire superficial en áreas de montaña", realizada por Francisco Manuel Navarro Serrano, bajo mi inmediata supervisión y dirección, en el Departamento de Geografía y Ordenación del Territorio.

En Zaragoza, junio de 2020

Fdo. Juan Ignacio López Moreno

Dr. D. Cesar Azorín Molina, contratado Ramón y Cajal en el Centro de Investigaciones sobre Desertificación (Consejo Superior de Investigaciones Científicas y Universidad de Valencia, CIDE – CSIC – UV), AUTORIZA:

La presentación de la Tesis Doctoral en la modalidad de compendio de publicaciones y titulada "Análisis del comportamiento altitudinal de la temperatura del aire superficial en áreas de montaña", realizada por Francisco Manuel Navarro Serrano, bajo mi inmediata supervisión y dirección, en el Departamento de Geografía y Ordenación del Territorio.

En Zaragoza, junio de 2020

Fdo. Cesar Azorín Molina

Dr. D. José María Cuadrat Prats, Catedrático de Geografía Física en el Departamento de Geografía y Ordenación del Territorio de la Universidad de Zaragoza, AUTORIZA:

La presentación de la Tesis Doctoral en la modalidad de compendio de publicaciones y titulada "Análisis del comportamiento altitudinal de la temperatura del aire superficial en áreas de montaña", realizada por Francisco Manuel Navarro Serrano, bajo mi inmediata supervisión y tutorización, en el Departamento de Geografía y Ordenación del Territorio.

En Zaragoza, junio de 2020

Fdo. José María Cuadrat Prats

El progreso no sirve…si éste ha de traducirse inexorablemente en un aumento de la incomunicación y la violencia, de la autocracia y la desconfianza, de la injusticia y la prostitución del medio natural, de la explotación del hombre por el hombre, y de la exaltación del dinero como único valor

Miguel Delibes

Agradecimientos

Son muchas las personas que han contribuido de alguna u otra forma a que esta Tesis Doctoral cogiera forma y se desarrollara hasta esta fase final.

En primer lugar, me gustaría agradecer a mi director, Nacho López Moreno, quien ha confiado en mí desde ya hace tantos años y el cual me ha dedicado muchas, muchas horas de paciente enseñanza, acompañada siempre de una empatía y comprensión desbordante en todos los sentidos. La realización de esta Tesis Doctoral hubiera sido imposible sin su trabajo como guía y su conocimiento del entorno, tanto ambiental como del puramente académico. Gracias por confiar en mí más que yo mismo, y por enseñarme a hacer ciencia a partir de la curiosidad.

En segundo lugar, quiero agradecer a mi codirector César Azorín Molina, por su disposición y dedicación constante por ayudar, por mejorar los textos, los análisis, y por hacer que tuviera otro *meteo friki* en el ámbito laboral. Me alegro muchísimo de que ya estés por casa y puedas desarrollar todo tu potencial con los tuyos, pero ten cuidado con esas maratones. En tercer lugar, a mi tutor en la Universidad de Zaragoza José Mª Cuadrat por sus ánimos y optimismo pleno durante todas las fases del trabajo y, por supuesto, por su total disposición a ayudar en todas las cuestiones docentes y administrativas.

Asimismo, en este punto es obligado mencionar a otros investigadores y compañeros que han estado día a día y codo con codo haciendo que cada trabajo mejorara en cuanto pasaba por sus manos, como es el caso de Fernando Domínguez (qué sería de las tesis del Despacho 3 sin tu ayuda incansable), Sergio M. Vicente Serrano, Jesús Revuelto, Miquel Tomás, Ahmed…

Quisiera extender mis agradecimientos a otras personas que han colaborado, tanto desde el ámbito científico como del logístico, para que esta tesis marchara para adelante. Gracias Samuel Buisán por tus ganas de colaborar en todos los trabajos, y a Pedro Sánchez (Navarrete) por hacer que las salidas de campo fueran mucho más llevaderas, especialmente a la altura de Lanave, y por tus dosis de cariño siempre. Eres como un hermano mayor para muchos, por si no lo sabes.

Agradezco también a mis compañeros del Grupo de Investigación de Hidrología Ambiental y del Despacho 3 (Makki, Fergus, Javi, Iván, Alba, Esteban, Natalia y Marina Aznárez) por haber hecho piña durante estos años, permitiendo que el trabajo se haya hecho mucho más llevadero, y aprendiendo muchísimo sobre las cosas más variopintas ("*Makki, ¿en tu país...?*"). Os llevo conmigo para Sevilla, espero veros por allí.

Del mismo modo, doy gracias a todas aquellas personas que, gracias a su labor administrativa y técnica, han hecho posible cumplir con todos los plazos, requisitos, papeles y burocracia exigida. Especial mención al personal del Instituto Pirenaico de Ecología, Cecilia y Trini, pero también a José Manuel y Antonio. En la Universidad de Zaragoza, gracias principalmente a Juan de la Riva, creo que no ha habido mejor representante de los doctorandos "externos" que él, muchísimas gracias por tu labor incansable y por tus enseñanzas durante el Máster de SIG y Teledetección.

Quisiera tener un especial recuerdo de gratitud hacia mis profesores de Geografía de Sevilla, que hicieron crecer en mí aún más el amor por esta disciplina, como Fernando Díaz del Olmo y Leandro del Moral, guías y referentes en mi visión geográfica del territorio. Pero, especialmente, gracias a Rafael Cámara, con el que compartí jornadas maratonianas de campo en las arenas de Doñana, estando además presente desde el inicio de mi vocación como geógrafo a mediados y finales de los años noventa por tierras del Aljarafe. Espero y deseo que este trabajo lo consideréis también vuestro.

Me gustaría dar las gracias a mis amigos de siempre, especialmente a Luís, por estar ahí aunque pasen los años y nos hayamos tenido que reencontrar en la otra punta, siendo siempre buen momento para hablar de fútbol, política, Semana Santa, itinerarios y hasta de regatas si se tercia. No sabes lo que se agradece poder desconectar a veces; a mis trece primos y cinco tíos que tan poco he podido ver estos años, a mi familia "araeña" que con tanta intensidad y cariño me han acogido desde el principio, sobre todo el Rubete y la Gordis, me llenáis de alegría siempre.

Finalmente, gracias a mi abuela Catalina, que cree que soy una especie de agricultor de termómetros; a mi abuelo Paco y a mi tito Manolo, que se perdieron todo este camino, pero que seguro que lo están viendo desde algún sitio; a mi hermano, perdóname la falta de paciencia, sabes que en realidad estaremos ahí para lo que haga falta, más aún después de los sustos que nos estamos llevando desde el pasado año, a ver si todo encaja para poder volver; y a mis padres, que habéis hecho, cada uno a vuestra manera, que todo esto fuera posible desde el principio de los principios, haciendo que nunca nos faltara de nada. Siempre era buen momento para regalarme un libro de geografía, tuviera seis, dieciséis o veintiséis años. Siempre era buen momento para prepararme una merienda a pesar de mi cabezonería por no parar de estudiar ni diez minutos durante las largas tardes del Instituto y la Facultad. Siempre era buen momento para escuchar mis dudas y preguntas, o para darme un achuchón, aunque fuera el más 'despegao' de la casa. Por ello, y por veintiocho años más de razones, siempre será buen momento para deciros que esto es vuestro y que os quiero, papá y mamá.

…y a ti, Clara, sólo tú sabes lo que ha costado llevar esto para adelante,
los grises andenes de estación y los nudos en la garganta.

Hemos subido este escalón, y ahora vamos a por el siguiente

Sin embargo, esta vez será oliendo a azahar,
y a incienso, por supuesto.

Resumen

Las sociedades se encuentran en un estado de continua interrelación con el medio ambiente que las rodea y del que forman parte. En esa relación multidireccional, el sistema climático y, más concretamente, la temperatura del aire, juega un papel imprescindible a la hora de entender multitud de procesos que nos afectan directa o indirectamente, tales como la disponibilidad de recursos hídricos, los movimientos de población, o la viabilidad de determinadas actividades económicas. En este sentido, las áreas montañosas son especialmente sensibles a los cambios bruscos y rápidos que están produciéndose en el medio ambiente, con el agravante de que, debido a la mayor complejidad topográfica y de procesos, la difícil accesibilidad y el menor poblamiento de estas áreas, son territorios en los que el conocimiento de la temperatura del aire es mucho más reducido que en otros entornos a más baja altitud y de topografía más sencilla. Sin embargo, a pesar de ser áreas menos pobladas y menos estudiadas, en las zonas montañosas se generan multitud de recursos, así como riesgos naturales que nos afectan como sociedad. Por ello, creemos que el estudio de una de las variables más importantes del sistema climático, como es la temperatura del aire superficial, justifica la realización de este trabajo, que permitirá conocer mejor las condiciones ambientales que se observan en las zonas de montaña, así como su efecto consecuente en la totalidad del territorio.

En esta Tesis Doctoral se ha analizado la medición y la dinámica espacio-temporal de la temperatura del aire superficial (habitualmente medida a 1.25 - 2 metros sobre el nivel de suelo) en las áreas de montaña, con especial énfasis en su relación con la altitud. Para ello se ha procedido a realizar estudios a escalas de trabajo diferenciadas (regional y local) con el objetivo de analizar las diferentes influencias de los factores explicativos de su variabilidad. El análisis ha sido realizado combinando redes oficiales de observación meteorológica con las mediciones tomadas por el propio Grupo de Investigación de Hidrología Ambiental (IPE – CSIC) mediante temporadas de trabajo de campo, lo cual otorga un interés añadido a los resultados obtenidos. Además, se añade una propuesta metodológica para el diseño de redes de observación a escalas de trabajo local sobre áreas de montaña, lo cual podrá ayudar a la comparabilidad de nuestros resultados con otras investigaciones.

La Tesis Doctoral es presentada como un compendio de artículos de investigación publicados en los que se da respuesta a una serie de objetivos específicos planteados. El primer manuscrito consistió en analizar el comportamiento espacio-temporal de la temperatura del aire a escala

regional sobre la España continental y sus áreas montañosas. El segundo estudio consistió en un análisis regional sobre la región andina tropical de Ecuador y Perú. El tercer trabajo trató de establecer una serie de criterios metodológicos que permitieran el diseño de redes de observación a escalas de trabajo local con unas condiciones de calidad y homogeneidad. La cuarta publicación analizó el comportamiento espacio-temporal de la temperatura del aire a escala local sobre un área montañosa del Pirineo Aragonés, focalizándose en el análisis de la topografía y el efecto que produce sobre la insolación. La quinta y última publicación aplicó los conocimientos y análisis anteriores en el estudio de la producción de nieve artificial en una estación de esquí del Pirineo Aragonés.

Los resultados han demostrado la existencia de una variabilidad espacio-temporal muy reseñable en los ámbitos de montaña, siendo una variable extremadamente compleja de modelizar. Además, los factores explicativos de su comportamiento son múltiples y variados en función de la escala de análisis. La gran variabilidad espacio-temporal de la temperatura del aire a escala local obliga a una mayor monitorización de estos territorios y al abandono de los enfoques regionales para el análisis de esta variable. Debido al efecto de la topografía, la estacionalidad, las condiciones sinópticas o las coberturas forestales, cada territorio montañoso puede responder de manera diferenciada y ni las escalas regionales ni las relaciones simplistas entre temperatura del aire y altitud pueden detectar esta variabilidad.

Por todo ello, la presente Tesis Doctoral, titulada "Análisis del comportamiento altitudinal de la Temperatura del Aire Superficial en áreas de montaña" supone la puesta en marcha de una línea de trabajo interesante y, sobre todo, útil a la hora de aplicar sus avances en otras disciplinas relacionadas como la Hidrología o los estudios de viabilidad en el sector de los deportes de montaña.

Abstract

Society is in a state of continuous interrelation with its surrounding environment. The climate system, and more specifically, the air temperature, plays a key role in this multidirectional relationship. The availability of water resources, the population movements, or the viability of economic activities, is dependent (directly or indirectly) on air temperature. In this sense, mountain areas are very sensitive to the sudden and rapid changes that are taking place in the environment. Furthermore, due to the complex topography and natural process, in addition to the poor accessibility, mountainous areas are less well-known territories than in more crowded areas, especially in scientific terms. However, despite the lack of knowledge, mountainous areas are essential in generating natural resources and risks that affect society. Therefore, the study of surface air temperature justifies the completion of this Doctoral Thesis, since this knowledge will allow us to better understand the mountain process, the consequences of which are further propagated the whole territory.

This work has analyzed the monitoring and the spatiotemporal variability of surface air temperature (generally measured at 1.25 – 2 meters above ground) in mountainous areas, and its relationship with altitude. For this purpose, different analyzes have been carried out at different spatial scales (regional and local). The analyses have combined official meteorological observation data with measurements taken directly by the Research Group in field campaigns. Besides, a methodological proposal is added for designing own networks for measuring surface air temperature in mountainous and local areas. This will help the comparability of the results.

The Doctoral Thesis has been presented as a compilation of five research publications, in which different specific objectives are answered. The first was to analyze the spatio-temporal behavior of surface air temperature on a regional scale over continental Spain and its mountainous areas. The second tried to analyze the spatiotemporal mechanisms at the regional scale too but in the Andean region of Ecuador and Peru. The third attempted to establish methodological criteria in the design of monitoring networks for surface air temperature in mountain areas. The fourth publication analyzed the spatio-temporal behavior of surface air temperature on a local scale over a mountainous area of the Aragonese Pyrenees, with a special interest in the effects of topography and insolation. The fifth and last publication applied the previous knowledge and analysis in the study of the effect of temperature lapse rates on snowmaking production in a ski resort of the Aragonese Pyrenees.

The results have shown the existence of large spatiotemporal variability in surface air temperature, being extremely complex the modeling of surface air temperature at the local scale. Furthermore, the explanatory factors are multiple and varied depending on the scale of analysis. Results highlight the need of more intense and well-designed monitoring of the mountain areas, discarding direct extrapolation from large scale approaches. The effects of topography, seasonality, synoptic conditions and vegetation cover, among others, can generate different responses in each mountainous territory, making the local approach the most suitable for detecting the variability.

For all these reasons, this Doctoral Thesis entitled "Analysis of the altitudinal behavior of surface air temperature in mountainous areas" means the launch of an interesting and useful work line of interest for other disciplines, such as Hydrology, Ecology or viability studies in the winter tourism industry.

Índice de Contenidos

Índice de Figuras

Índice de Tablas

Capítulo 1

INTRODUCCIÓN

Este capítulo actúa de presentación de la Memoria de Tesis Doctoral. En primer lugar, se indica la función de los estudios realizados en el marco del Programa de Doctorado en Ordenación del Territorio y Medio Ambiente. En segundo lugar, se describen algunos conceptos y contenidos básicos y genéricos de la ciencia climática, la temperatura del aire superficial, así como su relación con la sociedad. En tercer lugar, se muestra la importancia de las áreas montañosas, así como los trabajos previos realizados en el estudio de la temperatura del aire superficial en estos entornos. Por último, se desarrolla la justificación de la presente Tesis Doctoral, indicando sus objetivos generales y específicos, así como la estructura seguida.

1.1. La Geografía: Entre el territorio, el medio ambiente y la sociedad

Las primeras líneas de la presente memoria, para optar al grado de Doctor en el Programa de Doctorado de Ordenación del Territorio y Medio Ambiente, no podrían ser otras que las que definen a las palabras que componen la nomenclatura del Programa de Doctorado.

En primer lugar, ¿qué es el territorio? Según la Real Academia Española (2014), el territorio es, en su primera acepción, "una porción de la superficie terrestre perteneciente a una nación, región o provincia". En segundo lugar, ¿qué es ordenar? De la misma fuente puede obtenerse una definición bastante certera, siendo aquella acción de "encaminar y dirigir algo a un fin de acuerdo a un plan o modo conveniente".

En este punto podríamos afirmar que la Ordenación del Territorio es, en su sentido más literal, la acción de encaminar y dirigir una porción de la superficie terrestre a un fin, de acuerdo a un plan establecido. De manera subyacente, la Ordenación del Territorio ha estado presente en la humanidad, al menos, desde el paso hacia las sociedades sedentarias. Es en ese momento cuando el territorio comienza a ser clasificado en función de sus usos y actividades, tales como los primeros cultivos o explotaciones ganaderas, que debían ocupar espacios reservados y estar adecuadamente gestionados. La Ordenación del Territorio puede realizarse desde multitud de enfoques y criterios, que establecen el plan o modo de actuar. Es en este punto cuando interviene la última de las palabras clave: el medio ambiente.

Por tanto, ¿qué es el medio ambiente? Este interesante término es definido como "el conjunto de componentes físicos, químicos, y biológicos externos con los que interactúan los seres vivos".

Una vez presentadas, al menos de manera literal, las definiciones parciales de la nomenclatura del Programa de Doctorado, es posible leerla de nuevo de manera integral: ordenación del territorio y medio ambiente. Este nombre nos evoca a una ordenación territorial implicada con los agentes ambientales y, más concretamente, implicada con la interacción entre estos elementos y los seres humanos. Este enfoque insta a que el territorio sea estudiado mediante una visión holística, que permita no solo abarcar la continuidad del espacio, sino también la continuidad del tiempo y su afección cambiante sobre el territorio. Sólo mediante el entendimiento de las actividades humanas, el conocimiento del territorio y el estudio de sus interrelaciones podremos llegar a esta concepción integradora entre la ordenación del territorio y el medio ambiente, la cual abre las puertas a una visión poliédrica del planeta en el que vivimos.

Aunque haya hecho falta toda una primera página para describir la interrelación existente entre las palabras "territorio", "ordenar" y "medio ambiente", estas podrían haberse resumido rápidamente con una sola palabra: Geografía. Disciplina que recibió una de las mejores valoraciones posibles, la realizada por El Principito allá en el sexto planeta de su magnífico viaje[1]:

"La sixième planète était une planète dix fois plus vaste. Elle était habitée par un vieux Monsieur qui écrivait d'énormes libres.

- Je suis géographe, dit le vieux Monsieur.

- Ça c'est bien intéressant, ça c'est en fin un véritable métier!
Et le petit prince jeta un coup d'œil autour de lui sur la planète du géographe. Il n'avait jamais vu encore une planète aussi majestueuse"

"El sexto planeta era un planeta diez veces más grande. El planeta estaba habitado por un viejo señor que escribía enormes libros.

- Yo soy geógrafo, dijo el viejo señor.

- ¡Eso es muy interesante! ¡Por fin un verdadero oficio!

Y el Principito miró a su alrededor hacia el planeta del Geógrafo. Nunca había visto un planeta tan majestuoso"

En este punto, y dada la ocasión, me permito el privilegio de interpretar a este respecto el texto original, y añadir que lo que realmente hacía majestuoso al planeta del Geógrafo no era el propio planeta, sino la visión que el Geógrafo tenía de él.

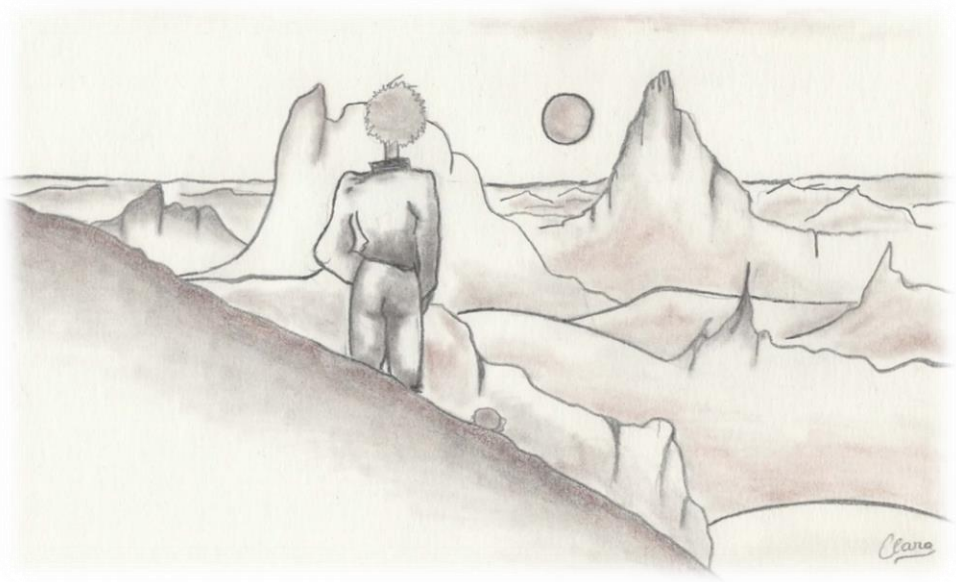

Figura 1. El Principito, basado en las acuarelas originales, por Clara María Martín Brenes (2020).

[1] Este capítulo, perteneciente a la obra El Principito, de Antoine de Saint-Exupéry (1943), fue el primer texto que leímos, hace más de diez años, en septiembre de 2009, en el primer día del Grado de Geografía y Gestión del Territorio (Universidad de Sevilla) a instancias del Catedrático de Geografía Física D. Fernando Díaz del Olmo.

1.2. El Sistema Climático, la temperatura del aire superficial y la sociedad

1.2.1. El Sistema Climático y la atmósfera

Tras la presentación del epígrafe anterior, llega el momento de describir uno de los elementos del medio ambiente que más incide en el territorio y, por ende, en la sociedad: el sistema climático. El sistema climático es un amplio sistema físico, sumamente complejo y rico en conexiones, cuyo funcionamiento está dominado por los intercambios energéticos (Barry y Chorley, 2003), especialmente de energía solar, tanto con el exterior del planeta Tierra, como dentro del mismo. Tradicionalmente, la literatura de referencia (Barry y Chorley, 2003; Cuadrat Prats y Pita López, 2006) ha tratado a este sistema como la integración de cinco heterogéneos y complejos subsistemas (Figura 2): la atmósfera, la hidrosfera, la criosfera, la litosfera y la biosfera, que se relacionan entre sí mediante procesos dinámicos basados en las propiedades físicas de sus elementos y en el intercambio de energía (Figura 3). Como parte de la biosfera, las sociedades humanas estamos interrelacionadas con el resto de subsistemas en el día a día.

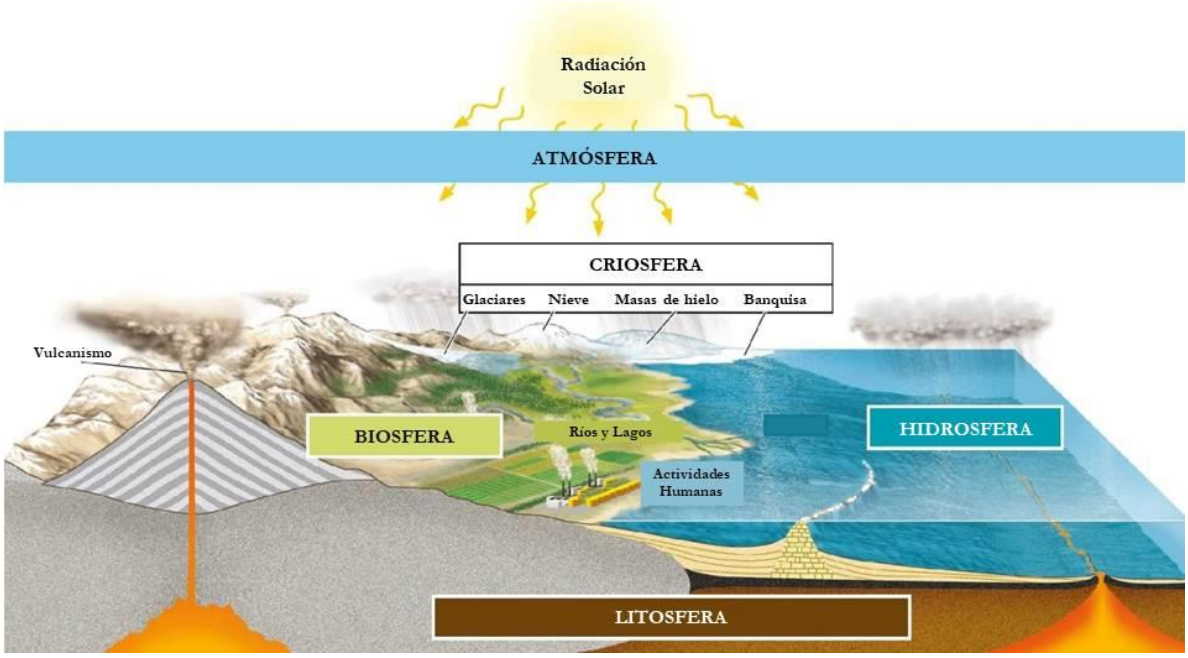

Figura 2. Subsistemas terrestres: atmósfera, hidrosfera, criosfera, litosfera y biosfera. Tomada y traducida de Razik (2014).

En este sentido, la atmósfera es el subsistema principal del sistema climático, ya que controla la cantidad de radiación que llega a la superficie terrestre, y la cantidad de radiación terrestre liberada hacia el exterior, siendo además el principal medio de transferencia de calor entre las regiones del planeta mediante un sistema de balance energético entre áreas con balance positivo y áreas con balance negativo (tropicales y polares, respectivamente).

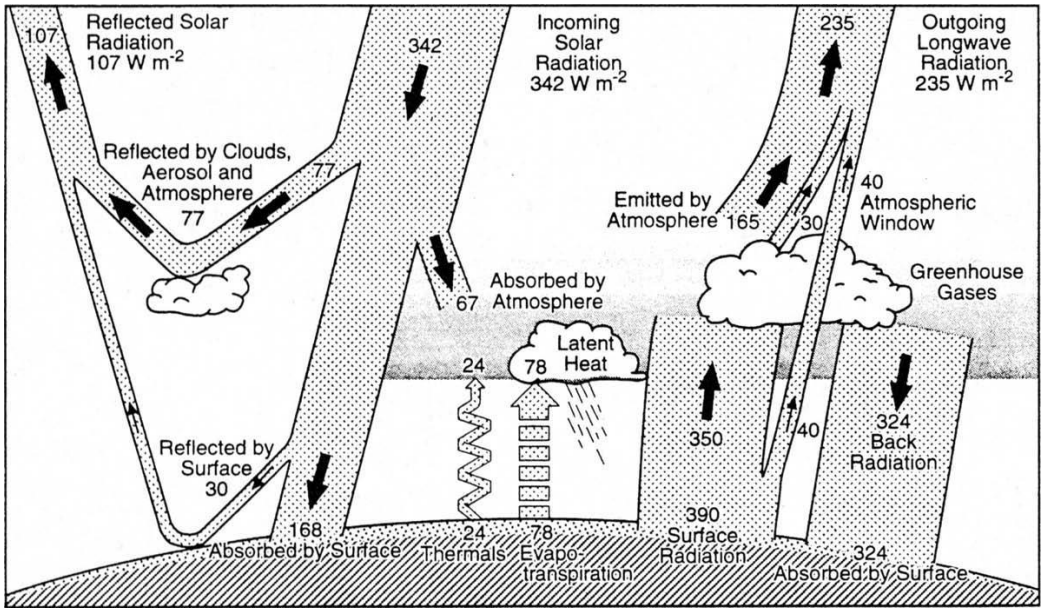

Figura 3. Balance energético anual de la atmósfera, procedente originalmente de la radiación solar que llega a la parte alta de la atmósfera (equivalente a 342 W m^{-2}). Tomada de Kiehl y Trenbreth (1997).

La atmósfera está formada por gases, aerosoles y partículas líquidas en suspensión que cubren la totalidad del planeta gracias al efecto de la gravedad (Strahler y Strahler, 1997). Esta capa, mayormente gaseosa, tiene un límite exterior poco claro, en el que difícilmente se distingue del espacio exterior, estableciendo algunos autores ese límite en la capa magnética de la Tierra, a unos 15,000 km de la superficie terrestre. Sin embargo, la atmósfera no es homogénea en su interior, por lo que ha sido clasificada tradicionalmente mediante diversos criterios (Cuadrat Prats y Pita López, 2006). El más habitual clasifica la estructura de la atmósfera en base al comportamiento de la temperatura del aire con respecto a la altitud (Figura 4), estableciéndose una clasificación que, desde la capa superior a la inferior, está constituida por: la atmósfera superior (magnetosfera-exosfera, termosfera, mesosfera), la estratosfera y, por último, la troposfera.

La troposfera es la capa que se encuentra en contacto con la superficie terrestre, alcanzando un espesor promedio de unos 12 km desde la superficie en las latitudes medias (aunque en las zonas polares tiene 8 – 9 km, y en las ecuatoriales puede alcanzar los 18 km). Esta capa es, por tanto, la de contacto más directo con el territorio. La troposfera es la capa más densa de todas debido al efecto de la gravedad terrestre, que es más intenso conforme nos acercamos a la superficie. Esto provoca que aglutine un 75% de la masa molecular atmosférica y la práctica totalidad del vapor de agua, del dióxido de carbono y de los aerosoles (Barry y Chorley, 2003). Por todo ello, los procesos y características propios de la troposfera son los que afectan más directamente al medio que nos rodea y del que formamos parte en el día a día, tales como la nubosidad, las precipitaciones, el viento o la temperatura del aire, esto es, las condiciones meteorológicas.

Estas condiciones meteorológicas, y su plasmación continua a lo largo del tiempo: el clima, marcan a otros elementos como la vegetación, las masas de agua o el relieve. Es decir, al territorio y, por tanto, a las sociedades humanas.

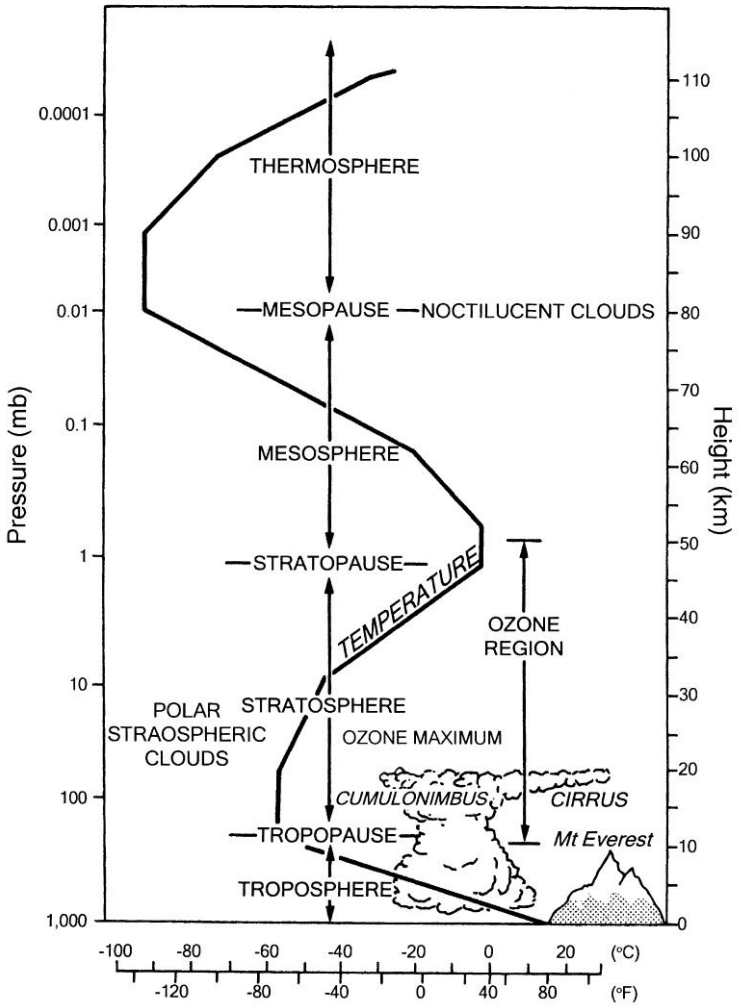

Figura 4. Distribución vertical de la temperatura y presión del aire hasta una altura de 110 km. Se indican algunas altitudes de referencia. Tomada de Barry y Chorley (2003).

1.2.2. La temperatura del aire superficial

La troposfera se ha presentado como una capa atmosférica en la que la temperatura del aire aumenta conforme se desciende en altura. Esto se debe al incremento de la presión atmosférica, que hace aumentar la densidad del aire y, por tanto, los impactos moleculares, liberando calor. Sin embargo, la cercanía y contacto de la troposfera con la superficie terrestre provoca la existencia de continuos intercambios energéticos que pueden matizar y variar esa relación, lo cual obliga a subdividir la troposfera en función del efecto que la superficie terrestre tiene en ella (Figura 5), obteniendo la troposfera libre y la capa límite planetaria que, a su vez, también puede subdividirse:

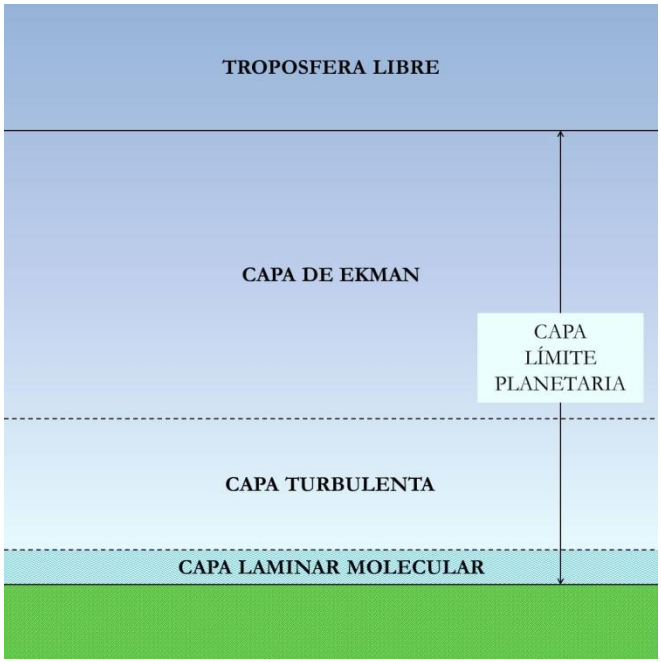

Figura 5. Estructura de la troposfera, prestando especial atención en la Capa Límite Planetaria. Modificada de Cuadrat Prats y Pita López (2006).

- Troposfera libre: A veces también llamada atmósfera libre, tiene un aire más limpio y menos denso. En ella la temperatura del aire desciende con respecto a la altitud a un ritmo promedio de -6.5º C km^{-1} (NOAA y NASA, 1976; Barry, 2008), el cual es un estándar usado ampliamente en meteorología y aviación hasta un límite de 11.000 metros sobre el nivel del mar, y denominado habitualmente como gradiente vertical ambiental.
- Capa Límite Planetaria (*Planetary Boundary-layer*, en inglés): Influenciada por la rugosidad del terreno, predominando la mezcla turbulenta del aire, generada por el roce permanente con la superficie rugosa del suelo y por la elevación convectiva de burbujas de aire al calentarse. La topografía, la rugosidad de la superficie, la cubierta vegetal, la intensidad del viento, el grado de enfriamiento y calentamiento del suelo, la advecciones de calor y humedad, etc. pueden influir activamente en el espesor de esta capa (Barry y Chorley, 2003; Barry, 2008). En algunas ocasiones, y siguiendo la estructura propuesta por Cuadrat Prats y Pita López (2006), puede subdividirse en las siguientes partes:
  - Capa de Ekman: este nivel superior está en transición entre los efectos de la fuerza de Coriolis sobre el viento, y los efectos ya presentes de las turbulencias.
  - Capa turbulenta: caracterizada por la intensa turbulencia del aire, pudiendo alcanzar varias decenas de metros.
  - Capa laminar molecular: en contacto con la superficie, de sólo milímetros de espesor y dominada por los efectos de la viscosidad superficial.

La gran mayoría de actividades humanas y procesos que nos afectan como parte de la biosfera tienen lugar en esta Capa Límite Planetaria y, más concretamente, en la Capa Turbulenta. Por ello, es la temperatura del aire de esta capa la que ha venido interesando a la Climatología y demás ciencias ambientales, así como a los organismos meteorológicos desde hace siglos (Camuffo y Bertolin, 2012) y la que se llamará, en esta memoria de Tesis Doctoral: Temperatura del aire superficial, en contraposición a la temperatura de la troposfera libre.

1.2.3. Factores explicativos y medición de la temperatura del aire superficial

Antes de mencionar los factores que explican la distribución de la temperatura del aire superficial en el territorio, es necesario recordar la importancia de la energía. El almacenamiento de la misma por parte del aire superficial provoca un incremento de su calor y, por tanto, de su temperatura (Strahler y Strahler, 1997). Sin embargo, este proceso es multidireccional, ya que el almacenamiento depende del balance resultante entre las salidas y entradas de calor con respecto a los cuerpos circundantes (Barry y Chorley, 2003), basadas en las diferencias de temperatura. Por todo ello decimos que el principal factor explicativo de la distribución de la temperatura del aire superficial es la propia distribución de la energía. En ese sentido, existen factores que intervienen directamente en la distribución de la energía:

1.2.3.a. Latitud

Debido a la inclinación del eje de rotación terrestre se producen dos efectos que varían latitudinalmente: la duración de los días a lo largo del año y la perpendicularidad con la que los rayos solares atraviesan la atmósfera (Strahler y Strahler, 1997). La conjunción de ambos efectos provoca que la cantidad de radiación solar recibida venga determinada, en una buena medida, de la latitud de dicho territorio (Figura 6).

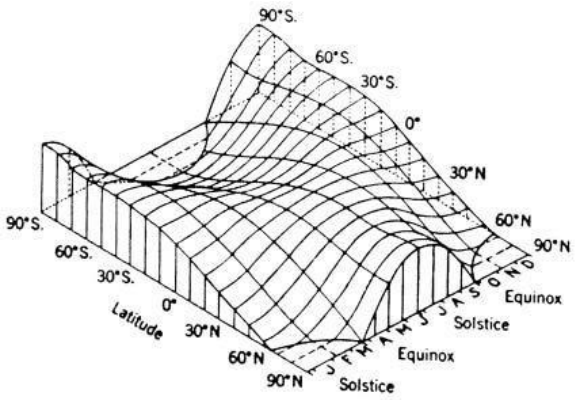

Figura 6. Variación de la radiación solar con respecto a la latitud y la estacionalidad para todo el planeta, asumiendo que no existe atmósfera. Tomada de Barry y Chorley (2003).

1.2.3.b. Transparencia atmosférica y nubosidad

La radiación solar atraviesa las distintas capas de la atmósfera. En este proceso, los componentes y aerosoles atmosféricos interactúan absorbiendo, reflejando o transformando a onda larga la radiación, que llega mermada a la superficie terrestre. El espesor, la composición y cantidad de los componentes atmosféricos (Kaiser, 2002), tales como el vapor de agua o el dióxido de carbono, afectará en el montante de radiación solar que alcanza la superficie terrestre. Del mismo modo, la atmósfera también actúa en la dirección inversa, como invernadero de la radiación de onda larga emitida por los cuerpos terrestres hacia el exterior, proceso en el cual de nuevo la composición y cantidad de los componentes atmosféricos influye directamente.

En cierta manera, la nubosidad forma parte de la transparencia atmosférica, ya que se interpone en el recorrido directo de la radiación solar entre las capas altas de la atmósfera y la superficie terrestre. Según la cobertura y tipología de la nubosidad, las propiedades varían, de tal forma que las nubes con mayor espesor y contenido de agua (por ejemplo, los cumulonimbus) dejan pasar una menor cantidad de radiación solar que las nubes finas y delgadas, debido al albedo de los cristales de hielo, así como a la absorción del vapor de agua. De igual modo, tienen efectos sobre la radiación de onda larga emitida hacia el exterior, dificultando el "escape" de la misma desde la superficie terrestre, debido al elevado contenido de vapor de agua. Además, esta nubosidad sirve de emisora de onda larga, que tiene especial importancia durante la noche.

1.2.3.c. Circulación atmosférica y oceánica

Las circulaciones atmosférica y oceánica funcionan como agentes transmisores de calor mediante advecciones horizontales entre distintos territorios, actuando como transportadoras de las condiciones generadas en unos lugares del planeta hacia otros en los que estas no podrían haberse dado de la misma manera. A nivel global, el fenómeno de El Niño es un certero ejemplo de cómo las diferentes corrientes oceánicas y atmosféricas pueden trasladar las masas de aire originales a miles de kilómetros, transportando de igual forma sus propiedades de temperatura y humedad (Dijkstra, 2006). En este mismo sentido, la corriente del Golfo permite el transporte de aguas cálidas desde latitudes tropicales del Atlántico Norte hacia las latitudes medias y altas de la fachada atlántica europea, atemperando su clima y haciéndolo más benigno que el de la costa oriental americana (Barry y Chorley, 2003). Por ejemplo, una masa de aire fría generada en latitudes altas por la escasa insolación recibida puede ser desplazada por la circulación atmosférica hacia latitudes medias provocando un descenso en la temperatura del aire de estos lugares de destino.

1.2.3.d. Naturaleza de la superficie terrestre

Cada tipo de superficie completa, mediante sus propiedades físicas, el balance energético de la capa de aire superficial. Las superficies, tales como las de suelos desnudos, las marinas, las forestales o las nevadas, imponen su impronta sobre la temperatura del aire superficial por su comportamiento ante la radiación solar (cuánta energía reflejan en onda corta, cuánta absorben y cuánta emiten en onda larga). Por el día, las superficies naturales suelen absorber más energía de la que emiten, por lo que acumulan calor y suben de temperatura, que van transmitiendo a la capa de aire superficial. Por la noche, tras el cese del flujo de energía solar, las superficies por norma general son energéticamente deficitarias, con lo que pierden calor y temperatura. Sin embargo, estas afirmaciones son fluctuantes en función del calor específico[2] de cada superficie, por lo que hay diferencias notables entre las mismas:

- El suelo desnudo tiene un calor específico reducido, por lo que su inercia térmica es pequeña. Además, la mayor parte de la energía queda concentrada en la capa más superficial debido a que conduce mal el calor hacia las capas más bajas, incrementando su temperatura de la superficie de forma significativa. Esto provoca que emita gran cantidad de energía hacia el aire superficial durante el día, calentándolo; habiendo un flujo inverso desde la capa de aire superficial hacia el suelo durante la noche que hace que el aire se enfríe. Será la composición del suelo la que determine los diferentes matices.
- Las superficies marinas tienen un elevado calor específico, lo que las convierte en unos cuerpos con fuerte inercia térmica. El agua absorbe una gran cantidad de energía, que redistribuye por las distintas profundidades sin apenas variar su propia temperatura. Además, parte de esa energía es devuelta a la atmósfera en forma de calor latente mediante la evaporación. Este vapor producido durante el día es el que, debido al descenso de la temperatura del aire superficial durante la noche, llega al punto de condensación. En ese momento, el calor latente atrapado se libera compensando el descenso térmico nocturno e impidiendo que el descenso de la temperatura del aire sea muy acusado.
- Los bosques son superficies terrestres que interrelacionan las propiedades de las dos superficies anteriores debido al gran contenido en humedad. Por otro lado, existen otras particularidades, como que las copas de los árboles pueden actuar como barrera frente a la radiación solar, disminuyendo la energía disponible. Además, el propio funcionamiento de la vegetación (evapotranspiración y fotosíntesis) hace que gran parte de la insolación

[2] El calor específico se define como la cantidad de calor requerido para incrementar la temperatura de esa sustancia en una unidad (Barry y Chorley, 2003).

recibida sea transformada en la propia planta, por lo que la emisión diurna de calor sensible se reduce. Durante la tarde y la noche, el calor emitido por el suelo subyacente queda retenido en la vegetación, que dificulta su escape hacia las capas de aire superiores acaparando esa energía en la capa de aire superficial. A ello hay que añadir la liberación del calor latente derivado de la evapotranspiración.

- Las superficies nevadas están caracterizadas por su elevado albedo ante la radiación de onda corta, que impide su absorción y posterior emisión como calor sensible hacia la capa de aire superficial. Esta situación genera que sean ambientes en los que la superficie terrestre no aporta apenas calor sensible a la capa de aire superficial.

1.2.3.e. Altitud

Tal y como se presentó con anterioridad para el conjunto de la troposfera, a menor altitud sobre el nivel del mar, mayor es la capacidad de aumentar la temperatura del aire superficial. Esto se debe al incremento de la presión atmosférica, que hace más denso al aire. A mayor densidad del aire, también se incrementan los choques entre las moléculas que lo conforman, con lo que la temperatura aumenta. Esta relación marca el teórico Gradiente Adiabático Seco (DALR, por sus siglas en inglés), establecido en -9.8º C km^{-1}. La altitud es, junto al efecto de la latitud, el efecto más estable y cuantificado, lo cual le ha favorecido a la hora de tenerlo en cuenta en las estimaciones de temperatura del aire.

1.2.3.f. Topografía

La topografía condiciona la temperatura del aire superficial desde diferentes frentes y en distintos aspectos (Figura 7). Por un lado, la pendiente del terreno determina el ángulo con el que los rayos solares inciden sobre la superficie terrestre, marcando la cantidad de energía recibida. Por otro, influye directamente en la cantidad de horas de luz debido a las sombras topográficas, originando importantes diferencias espaciales entre posiciones soleadas frente a otras que permanecen en sombra (Daly et al., 2002; Whiteman et al., 2004). Además, la topografía es generadora de movimientos verticales de las masas de aire (por ejemplo, el efecto Foehn basado en la relación entre los gradientes adiabáticos seco y húmedo, o las brisas de valle derivadas de las diferencias de presión atmosférica) y, por tanto, de la temperatura de la capa de aire superficial (Barry, 2008). Del mismo modo, bajo condiciones de estabilidad atmosférica, el aire frío desciende durante la noche hacia el fondo de los valles, acumulándose si la topografía lo permite, y provocando las llamadas inversiones térmicas.

Figura 7. Valle del río Aragón, a la altura del núcleo de población de Canfranc – Estación (Aragón, España). En este valle, la topografía juega un papel crucial por el día, debido a las sombras topográficas que se forman. Asimismo, durante la noche, el fondo del valle sufre procesos de inversión térmica provocados por el descenso del aire frío desde las laderas, que se acumula en el fondo. Fotografía tomada por Juan I. López Moreno en mayo de 2017.

En cualquier caso, al ser un sistema interrelacionado, todos estos factores específicos influyen de manera más o menos directa en la cantidad de energía disponible (Figura 8). Los efectos de los factores van relacionados con la escala espacial del análisis, de tal forma que los efectos de la latitud no serán perceptibles entre ubicaciones separadas por escasos metros, mientras que las diferencias topográficas sí que pueden llegar a percibirse a esa escala. Si imaginamos un caso hipotético de un territorio situado a una latitud 37.05º N, al mediodía del 20 de septiembre, con polvo en suspensión, cielo cubierto 4/8 de cúmulos, intenso flujo del sureste procedente del Sáhara, temperatura de la porción de mar más cercana (35 km) a 28º C, a 3400 metros sobre el nivel del mar, manto de nieve discontinuo en el suelo, en ladera sur con una pendiente de 15%, en el fondo de una dolina; comprobaremos que la temperatura del aire superficial es resultado de la influencia conjunta de todos estos condicionantes, aunque en magnitudes diferentes.

Por último, y aunque diferente a los factores naturales, está el factor de medición. Este factor no influye en la temperatura del aire superficial, que es la que es, pero influye en cómo se traslada esa temperatura a un dato cuantificado. La medición de esa temperatura debe hacerse siempre de una forma comparable para no confundir la variabilidad espacio-temporal de la misma con los efectos de la medición (distancia al suelo, calidad del sensor, protección, etc.). Es esta temperatura

del aire superficial la que la Organización Meteorológica Mundial recomienda medir a una altura aproximada entre los 1.25 y 2 metros sobre el nivel de suelo y en unas condiciones determinadas (WMO, 2014), precisamente con el objetivo de cuantificar de forma homogénea las condiciones térmicas ambientales que afectan al ser humano y a la inmensa mayoría de actividades realizadas por el mismo.

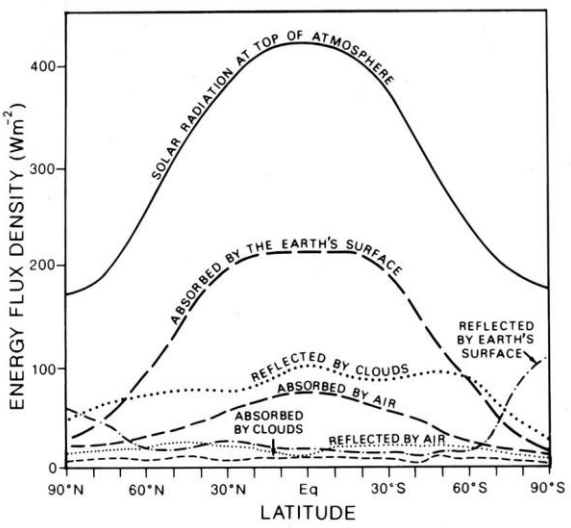

Figura 8. Media anual y distribución latitudinal de la radiación solar, en W m^{-2}. De un 100% de radiación entrante en la parte superior de la atmósfera, sobre un 20% es reflejado de nuevo hacia el espacio por la nubosidad, un 3% por el aire (además de polvo en suspensión y vapor de agua), y un 8% por la superficie terrestre. Alrededor del 3% es absorbido por la nubosidad, el 18% por el aire, y un 48% por la superficie terrestre (donde se incluye también la vegetación y masas de agua). Las diferencias entre latitudes tienen en cuenta diferencias como la mayor extensión del casquete polar del polo sur con respecto del polo norte, que provoca que la reflexión sea mayor en el sur. Tomada de Barry y Chorley (2003).

1.2.4. Relación entre la temperatura del aire superficial y la sociedad

La incidencia y relación de la temperatura del aire superficial en la sociedad es múltiple y heterogénea. En primer lugar, tiene una relación directa con la habitabilidad térmica de los territorios, la cual se puede ver fuertemente limitada por determinados rangos de temperatura del aire, como es el caso de las zonas polares o los desiertos tropicales cálidos. Además, influye directamente sobre el desarrollo de los diferentes sectores económicos, donde los efectos más directos pueden observarse en el sector primario, especialmente en la agricultura y la silvicultura debido a su efecto en la fenología vegetal (Went, 1953; Hatfield y Prueger, 2015); pero también en el sector terciario, donde actividades como el turismo son en gran medida dependientes de las variables meteorológicas (Gómez Martín, 1999; Pons et al., 2012), entre ellas la temperatura del aire superficial.

Aunque de manera indirecta, la temperatura del aire superficial afecta a la gestión de los recursos hídricos, de la cual depende el buen uso y aprovechamiento para poder abastecer a la

población y a sus actividades. Procesos como la evaporación, la fusión de la nieve o del hielo (Figura 9), el tipo de precipitación sobre un territorio (lluvia o nieve) vienen determinados, entre otros factores, por la temperatura del aire (Martinec, 1975; López-Moreno et al., 2009). Además, su influencia en el resto de seres vivos es aún mayor si cabe, puesto que la capacidad de adaptación del resto de seres vivos es limitada. En este sentido, la habitabilidad térmica de los territorios es un factor limitante y excluyente en la flora y fauna salvajes (García et al., 2019), actuando además directamente sobre la fenología vegetal y animal, como es el caso de los movimientos migratorios estacionales de la fauna.

Figura 9. Fase final del deshielo estival (septiembre de 2013) en Bachimaña (Aragón, España). Elaboración propia.

Aunque podrían añadirse infinidad de procesos en los que la temperatura del aire superficial influye en nuestro día a día como sociedad, queremos terminar con el que nos atañe, en cierto modo, como geógrafos y analistas del medio ambiente. Y es que también es necesario analizar la temperatura del aire superficial desde un sentido de ciencia básica, es decir, con el objetivo de conocer los factores que influyen en ella, la distribución espacial de la misma, su evolución a lo largo de tiempos pasados, o la posible evolución futura. El contexto actual en el que se encuentra la humanidad (el llamado cambio global), nos lleva como sociedad a enfrentarnos a cambios rápidos en el medio que nos rodea. Los cambios en los usos del suelo, el posible aumento de las temperaturas, la vulnerabilidad del sector agrícola, el crecimiento demográfico, la gestión de los recursos disponibles (tanto renovables como no renovables) en los escenarios de aumento en la intensidad y frecuencia de las sequías, así como el aumento de consumo energético para refrigeración y calefacción, son todos ellos grandes retos a los que nos enfrentamos como sociedad. Es en ese contexto donde el conocimiento de la temperatura del aire superficial como variable meteorológica que nos rodea, nos cubre y nos influye, es imprescindible.

1.3. Las áreas de montaña y la temperatura del aire superficial

1.3.1. Importancia y problemática

Las áreas de montaña, que definimos como aquellas dominadas por diferencias altimétricas reseñables, fuertes pendientes y topografía abrupta, cubren un significativo porcentaje de la superficie emergida del planeta. En ellas, aunque el poblamiento es disperso y la población escasa, tienen lugar multitud de procesos y actividades imprescindibles para la viabilidad de las sociedades humanas, en los que la temperatura del aire superficial juega un importante papel. Es el caso de los recursos hídricos, en cuya gestión el conocimiento de la temperatura del aire es fundamental para conocer los regímenes y poder gestionar los recursos (Martinec, 1975; García-Ruiz et al., 2011). Estos recursos son esenciales en la producción hidroeléctrica y en el embalsado de agua, lo cual lo convierte en un asunto clave en la gestión del territorio. Usos como el abastecimiento urbano, el regadío agrícola, o los usos para la industria, convierten la gestión de los recursos hídricos en un asunto estratégico. Por otro lado, en ciertas partes del planeta, las áreas de montaña son escenario de un activo aprovechamiento económico en torno al turismo invernal, relacionado habitualmente con el esquí (Pons et al., 2012; Gilaberte-Búrdalo et al., 2014), el cual está basado fundamentalmente en las condiciones meteorológicas del emplazamiento, entre las que la temperatura del aire tiene un papel clave, además evidentemente de las precipitaciones (Alonso-González et al., 2018). En otro orden de ideas, los riesgos naturales desencadenados en áreas montañosas son variados (Bryant, 2005), y se ha comprobado en multitud de ocasiones que sus efectos, en forma de riadas, avalanchas o aludes, entre otros, pueden llegar a áreas alejadas del punto de inicio (Figura 10), como muestran algunos trabajos en nuestro entorno más cercano, como el de García-Ruiz et al. (1996) sobre la riada del camping de Biescas, o el de Ollero Ojeda (2000) sobre las crecidas del río Ebro. Un caso de especial vinculación entre la temperatura del aire superficial en áreas de montaña y los riesgos aguas abajo es el de los episodios de lluvia sobre nieve que ocurren en las cabeceras (Pomeroy et al., 2016). En estos casos, unos pocos grados de diferencia pueden llevar a multiplicar o dividir el pico de avenida de un evento de precipitación, por lo que la predictibilidad es muy complicada. Por todo ello, aunque sean áreas poco pobladas, las condiciones meteorológicas que tienen lugar en estos entornos de montaña influyen en las sociedades humanas más de lo que aparentemente pudiera parecer.

Sin embargo, a pesar de ser un territorio tan importante para la sociedad, y de ocupar una gran extensión de la tierra emergida, la meteorología de las áreas montañosas no se conoce con excesivo detalle. Ello se debe a que, en áreas montañosas, la topografía juega un papel vital a la

hora de comprender la distribución de las temperaturas, generándose grandes diferencias en pequeñas distancias (Barry, 2008). Además, el efecto conjunto de fuertes desniveles, cambios en la cobertura del suelo, una topografía accidentada que genera diferencias en la insolación, en los vientos, o incluso en la nubosidad, grandes contrastes entre laderas por la circulación general, junto a otros procesos como los vientos de valle y las inversiones térmicas, hacen que su estudio sea extremadamente complejo.

Figura 10. Crecida ordinaria del río Ebro en Zaragoza (Aragón, España) en marzo de 2016. El caudal pico medido ese día fue de 1.357 $m^3 s^{-1}$, lejos del caudal de 2.448 $m^3 s^{-1}$ registrado en marzo de 2015, que provocó que buena parte de la ribera del río fuera anegada por las aguas, o los 4.130 $m^3 s^{-1}$ registrados en enero de 1961 (CHE, 2020). Elaboración propia.

Por todo ello, los puntos de observación meteorológica no son lo suficientemente representativos de su entorno, lo que lleva a la necesidad de tener una mayor densidad de observatorios que en otras áreas más homogéneas, algo ya indicado por Brooks (1947). Sin embargo, las áreas de montaña son las que menos estaciones meteorológicas tienen debido a la dificultosa accesibilidad, lo que ha obligado históricamente a medir únicamente en los fondos de valle (donde se ubican tradicionalmente los poblamientos humanos). Estas localizaciones difícilmente representan las condiciones de las laderas y cumbres montañosas. Todo ello obliga a la necesaria instalación de redes de observación más densas, o bien a un cambio metodológico hacia otras técnicas como la teledetección (Vancutsem et al., 2010). En conclusión, las áreas de montaña son, además de muy complejas en el estudio de la distribución espacio-temporal de la temperatura del aire superficial, áreas con un claro déficit de información meteorológica.

1.3.2. Antecedentes bibliográficos

El estudio de la temperatura del aire superficial, los patrones espacio-temporales de su distribución y sus factores explicativos ha sido común desde hace décadas, aunque este formaba parte de trabajos destinados principalmente a las clasificaciones climáticas. Trabajos como los de Ackerman (1941) en América del Norte, Geiger y Pohl (1953) para todo el planeta, Villmow (1962) en Europa y Capel Molina (2000) en la Península Ibérica son algunos ejemplos de esta aproximación. Esta problemática ha hecho que, en la mayoría de clasificaciones climáticas, las áreas montañosas hayan sido infrarrepresentadas, bien clasificándolas como "zonas elevadas" o bien como "clima de montaña", pero sin mayores detalles acerca de la heterogeneidad interna de las mismas. Sin embargo, algunos autores coetáneos a esos trabajos (Greenland et al., 1985) analizaron los climas a una escala local, concluyendo con que las clasificaciones climáticas que se habían venido haciendo habitualmente tenían una aplicabilidad reducida.

El estudio de la distribución de la temperatura del aire implica una aproximación diferente en medios topográficamente complejos y de tamaño reducido como son las áreas de montaña. De este modo, los autores han estado de acuerdo en afirmar que la modelización de la temperatura del aire en estos territorios es un reto y, a pesar de los nuevos avances en la modelización numérica de alta resolución (Karki et al., 2020) y en las técnicas de teledetección (Jiménez-Muñoz y Sobrino, 2003; Khorchani et al., 2018), todavía queda un largo camino a la hora de mejorar la resolución espacial y temporal de estos productos. Por ello, la mayoría de esfuerzos de los últimos lustros se han dirigido a aumentar las redes de monitorización, y poder así mejorar en el conocimiento de estos territorios (Pepin et al., 2005; Buisán et al., 2017). Factores con especial importancia en las áreas montañosas como la altitud o la topografía han sido acompañados además de otros condicionantes, como la circulación atmosférica, el efecto de la continentalidad, o las diferencias entre el día y la noche, en función de la escala espacial analizada.

Trabajos como los de Rolland (2003) en los Alpes; Hubbart et al. (2007), Lundquist & Lott (2008) o Minder et al. (Minder et al., 2010) en los Estados Unidos; Pepin et al. (2016) en África; Kattel et al. (2015) en los Himalayas; Hanna et al. (2017) en los Andes; Braun & Hock (2004) en la Antártida; así como en la Península Ibérica (Benavides et al., 2007; Miró et al., 2017; Pagès et al., 2017), muestran este interés creciente. Los ámbitos y escalas espaciales de estos estudios han sido muy variables, desde trabajos que cubrían todo el planeta (Pepin y Seidel, 2005; Pepin et al., 2015) o grandes regiones como China (Fang y Yoda, 1988; Li et al., 2013), a otros que analizaban escalas regionales más reducidas, como los de Pepin y Losleben (2002), Lunquist y Cayan (Lundquist y

Cayan, 2007), Blandford (2008) y Minder et al. (Minder et al., 2010) en sectores de las Montañas Rocosas, Rolland (2003) en los Alpes, o Bennet et al. (2016) en la región andina.

Además, también se han desarrollado trabajos con un enfoque subregional, que analizan el comportamiento de la temperatura del aire superficial en determinados valles (Duane et al., 2008; Heynen et al., 2016), algunos incluso en los Pirineos (Pagès y Miró, 2010). Por último, otra corriente se ha dirigido hacia el estudio de la temperatura del aire superficial con un enfoque local, sirviendo como estudios experimentales sobre los procesos más locales como las piscinas de aire frío (CAPs[3] en inglés), que se han venido desarrollando a partir principalmente de la tesis doctoral de Whiteman (Whiteman, 1982; Whiteman y McKee, 1982), y que ha continuado con estudios más recientes (Lookingbill y Urban, 2003; Lareau et al., 2013; Lareau y Horel, 2014), con algunas aplicaciones en las montañas españolas (Miró et al., 2017; Pagès et al., 2017; Espín-Sánchez et al., 2018).

El desarrollo tecnológico de dispositivos de medición de la temperatura del aire automáticos y autónomos, así como un progresivo descenso en los costes, ha permitido la monitorización in situ de la temperatura del aire, avanzando en el conocimiento de estos medios tan complejos.

1.4. Justificación, objetivos y estructura

1.4.1. Justificación

La presente Tesis Doctoral se presenta dentro del contexto geográfico y su relación con la ordenación territorial. Partiendo de la necesidad de comprender el medio que nos rodea como sociedad con el objetivo de poder adelantarnos a los diferentes cambios y retos a los que nos enfrentaremos en el futuro. Cambios que influirán en las actividades humanas y, por tanto, en la gestión del territorio tal y como ha sido entendida durante las últimas décadas, poniendo incluso en duda actuaciones hechas en el pasado. Esta posible situación futura exige que la sociedad se adelante a la propia evolución del medio que nos rodea y nos determina, analizando las posibles consecuencias de la inacción y el desconocimiento. El estudio y conocimiento del medio permitirá tener más información a la hora de tomar decisiones en la ordenación territorial y en la gestión de los recursos, dirigiéndonos hacia un nuevo equilibrio adaptativo con el entorno.

[3] Las piscinas de aire frío son acumulaciones, principalmente nocturnas, de aire frío en cubetas topográficas, como por ejemplo las dolinas, valles o poljes. Suelen estar asociadas a condiciones de estabilidad atmosférica, lo cual propicia el descenso del aire frío, más denso, acumulándose en estos recipientes topográficos y provocando intensas inversiones térmicas. Estos fenómenos provocan cambios de temperatura muy intensos en pocos metros de distancia vertical, generando condiciones muy diferenciadas a raíz de las diferencias topográficas, que pueden llegar a influir incluso en la vegetación si se producen con frecuencia.

En este sentido, las áreas de montaña son especialmente sensibles a los cambios que están produciéndose en el medio ambiente, con el agravante de que, debido a su difícil accesibilidad y el reducido poblamiento, son menos conocidas que otros entornos más cotidianos. Sin embargo, y a pesar de ese menor conocimiento, las áreas de montaña son generadoras de multitud de recursos, pero también de riesgos naturales que nos afectan como sociedad. Por ello, el estudio de uno de componentes más importantes como es el sistema climático y, más concretamente, la temperatura del aire superficial, justifica la realización de este trabajo, que permitirá conocer mejor las limitaciones, fortalezas y potencialidades de nuestro modelo como sociedad relacionada con las áreas de montaña.

El comportamiento de la temperatura del aire superficial es resultado de diferentes factores ambientales, tales como la latitud, la circulación atmosférica y marina, o la altitud, entre otros, los cuales se interrelacionan de forma compleja sobre el territorio y, más especialmente, sobre las áreas de montaña. Sin embargo, la magnitud de la influencia de estos factores en la distribución espacio-temporal de la temperatura sobre el territorio es muy dependiente de la escala espacial de los mismos, enfocándose la presente Tesis Doctoral en el estudio multi-escalar. Este es uno de los aspectos que se consideramos de mayor interés, de tal manera que esta aproximación permitirá determinar qué factores están influyendo en la heterogeneidad térmica de los territorios.

Por otro lado, a menudo los trabajos que ahondan en otros aspectos del territorio, tales como los estudios forestales, la distribución y fenología de plantas y animales o la modelización hidrológica, requieren de información sobre la temperatura del aire superficial en áreas de montaña. Sin embargo, la falta de información disponible o la dificultad de tener información precisa, ha llevado al uso de criterios demasiado generales y homogéneos, e incluso erróneos como el uso de gradientes estándares de troposfera libre para estimar la temperatura del aire superficial. En este sentido, también es necesario demostrar los problemas de estas acciones y presentar información veraz que pueda ser utilizada por estas disciplinas.

Las áreas de montaña sufren de una baja densidad de observatorios meteorológicos, por lo que el trabajo de campo es esencial para poder cubrir esas lagunas de información y poder representar mejor estas zonas topográficamente complejas. En este sentido, se ha producido un enorme crecimiento de los trabajos realizados con instrumental de medición propio, lo que ha hecho aumentar la información disponible. Sin embargo, resultado de la falta de trabajos en áreas de montaña, faltan recomendaciones precisas de cómo tomar estas medidas, de forma que sean comparables con las tomadas en otros puntos. Avanzar en la mejora del diseño de redes

experimentales propias de observación es vital para dar una salida adecuada a los próximos trabajos, de tal forma que en esta investigación aportamos algo de luz al respecto en la elección de sensores, protecciones contra la radiación solar, así como elevación de la medición sobre el manto nivoso.

Por estas razones, mejorar en el conocimiento de los patrones que determinan la distribución espacio-temporal de la temperatura del aire superficial en las regiones de montaña es esencial, ya que ello condicionará los resultados de otras disciplinas que requieran de esta información ambiental. En definitiva, la presente Tesis Doctoral trata de aportar en este conocimiento científico, de tal forma que se mejora en la gestión y ordenación territorial mediante el uso de información más precisa.

1.4.2. Objetivos

El objetivo principal de esta Tesis Doctoral es mejorar en el conocimiento de la temperatura del aire superficial en las áreas de montaña desde un enfoque multi-escalar, que permita conocer la influencia de los diferentes factores explicativos de la temperatura del aire en función de la escala de estudio, desde las regionales a las más locales. La cumplimentación de este objetivo principal ha requerido dar respuesta a una serie de objetivos específicos, organizados de la siguiente forma:

- Analizar el comportamiento espacio-temporal de la temperatura del aire superficial a escala regional sobre la España Peninsular, prestando especial atención a las principales regiones montañosas y a factores como la circulación atmosférica y la continentalidad.
- Analizar el comportamiento espacio-temporal de la temperatura del aire superficial a escala regional sobre áreas de montaña de latitudes tropicales y los posibles efectos de factores de teleconexión como el fenómeno de El Niño.

Sin embargo, estas escalas regionales no permiten la identificación de patrones que ocurren a escalas más reducidas, por lo que los siguientes objetivos específicos trataron sobre el estudio de la temperatura del aire superficial en ámbitos locales:

- La falta de información espacial requirió de la instalación de redes de observación propias, con lo que otro objetivo específico fue establecer una serie de criterios metodológicos que permitan el diseño de redes experimentales sobre ámbitos de montaña en cuanto a la elección de los sensores, protecciones contra la radiación solar y elevación sobre el manto de nieve.

- Analizar el comportamiento espacio-temporal de la temperatura del aire superficial a escala local sobre un área montañosa topográficamente compleja del Pirineo Aragonés con especial atención a factores locales como la topografía o el efecto de las condiciones meteorológicas.
- Aplicar estos análisis en el estudio de la variabilidad espacial en la producción potencial de nieve artificial en una estación de esquí del Pirineo Aragonés.

1.4.3. Estructura

La presente memoria de Tesis Doctoral es presentada en el formato de compendio de publicaciones, lo cual modifica la estructura habitual y tradicional siguiendo las indicaciones propias de la Escuela de Doctorado de la Universidad de Zaragoza. La Memoria se estructura de la siguiente forma:

- Introducción (Capítulo 1) que presenta la relación que tiene el presente trabajo con el conjunto de estudios y enseñanzas del Programa de Doctorado en Ordenación del Territorio y Medio Ambiente. Además, se indican los contenidos básicos y esenciales para comprender el funcionamiento de la temperatura del aire, y su especial dificultad de análisis en áreas de montaña, así como la Justificación y Objetivos de la Tesis Doctoral.
- Los diferentes Ámbitos espaciales, Materiales y Métodos (Capítulo 2) se desarrollan en este capítulo, que presenta los diferentes territorios analizados, además de la naturaleza de los datos utilizados y los métodos y análisis con los que se ha llegado a los resultados definitivos.
- Al estructurarse como compendio de publicaciones, los objetivos específicos han sido presentados y desarrollados a lo largo de los capítulos centrales de la Memoria, que reproducen las aportaciones publicadas de las investigaciones realizadas por el doctorando (Capítulos 3, 4, 5, 6 y 7).
- Por último, se desarrollan las Conclusiones Generales y Específicas, así como las próximas líneas de investigación y trabajos futuros (Capítulo 8)

Los contenidos concretos, materiales, técnicas y objetivos específicos de cada capítulo son presentados en la Tabla 1.

Tabla 1. Síntesis de los objetivos específicos, principales técnicas y métodos, así como de las herramientas y publicaciones de la Tesis Doctoral.

Objetivo específico 1	Principales Técnicas y Métodos	Software utilizado
Analizar el comportamiento espacio-temporal de la temperatura a escala regional sobre la España Peninsular	- Control de Calidad de los datos - Adaptación espacio-temporal de los datos - Cálculo de gradientes de temperatura - Clasificación de Tipos de Tiempo - Validación de gradientes - Otros estadísticos - Generación de Cartografía	- Lenguaje y entorno de programación R - ArcGIS 10.4 - Inkscape
Publicación: ***Navarro-Serrano, F.****, López-Moreno, J., Azorin-Molina, C., Alonso-González, E., Tomás-Burguera, M., Sanmiguel-Vallelado, A., Revuelto, J., Vicente-Serrano, S.M. 2018. Estimation of near-surface air temperature lapse rates over continental Spain and its mountain areas. International Journal of Climatology 38: 3233-3249. DOI: 10.1002/joc.5497.*		

Objetivo específico 2	Principales Técnicas y Métodos	Software utilizado
Analizar el comportamiento espacio-temporal de la temperatura a escala regional en áreas de montaña de latitudes tropicales.	- Control de Calidad de los datos - Adaptación espacio-temporal de los datos - Cálculo de gradientes de temperatura - Validación de gradientes - Otros estadísticos - Generación de Cartografía	- Lenguaje y entorno de programación R - ArcGIS 10.4
Publicación: ***Navarro-Serrano, F.****, López-Moreno, J.I., Domínguez-Castro, F., Alonso-González, E., Azorin-Molina, C., El-Kenawy, A., Vicente-Serrano, S.M. 2020. Maximum and minimum air temperature lapse rates in the Andean region of Ecuador and Peru. International Journal of Climatology. En Prensa. DOI: https://doi.org/10.1002/joc.6574.*		

Objetivo específico 3	Principales Técnicas y Métodos	Software utilizado
Establecer una serie de criterios metodológicos que permitan el diseño de redes experimentales sobre ámbitos de montaña.	- Trabajo de Campo - Control de Calidad de los datos - Adaptación espacio-temporal de los datos - Otros estadísticos - Generación de Cartografía	- Lenguaje y entorno de programación R - ArcGIS 10.4 - Tinytag Explorer - 1Wire
Publicación: ***Navarro-Serrano, F.****, López-Moreno, J.I., Azorin-Molina, C., Buisán, S., Domínguez-Castro, F., Sanmiguel-Vallelado, A., Alonso-González, E., Khorchani, M. 2019. Air temperature measurements using autonomous self-recording dataloggers in mountainous and snow covered areas. Atmospheric Research 224: 168-179. DOI: 10.1016/j.atmosres.2019.03.034.*		

Objetivo específico 4	Principales Técnicas y Métodos	Software utilizado
Analizar el comportamiento espacio-temporal de la temperatura a escala local sobre un área topográficamente compleja del Pirineo Aragonés.	- Trabajo de Campo - Control de Calidad de los datos - Adaptación espacio-temporal de los datos - Cálculo de gradientes de temperatura - Clasificación de Tipos de Tiempo - Cálculo de la Insolación estimada - Análisis Clúster - Otros estadísticos - Generación de Cartografía	- Lenguaje y entorno de programación R - ArcGIS 10.4 - Tinytag Explorer
Publicación: ***Navarro-Serrano, F.****, López-Moreno, J.I., Azorin-Molina, C., Alonso-González, E., Aznárez-Balta, M., Buisán, S., Revuelto, J. 2020. Elevation effects on air temperatura in a topographically complex mountain valley in the Spanish Pyrenees. Atmosphere 11(6): 656. DOI: https://doi.org/10.3390/atmos11060656.*		

Objetivo específico 5	Principales Técnicas y Métodos	Software utilizado
Aplicar estos análisis en el estudio de la fragilidad de determinadas actividades económicas de ámbitos de montaña del Pirineo Aragonés.	- Trabajo de Campo - Control de Calidad de los datos - Adaptación espacio-temporal de los datos - Cálculo de temperatura húmeda y de horas de Producción de nieve artificial - Cálculo de gradientes de temperatura seca, de temperatura húmeda y de horas de producción de nieve artificial. - Clasificación de Tipos de Tiempo - Modelos de Árboles de regresión - Otros estadísticos - Generación de Cartografía	- Lenguaje y entorno de programación R - ArcGIS 10.4 - SPSS Windows V.26 - Tinytag Explorer
Publicación: *López-Moreno, J.I., **Navarro-Serrano, F.**, Azorin-Molina, C., Sánchez-Navarrete, P., González-Alonso, E., Rico, I., Morán-Tejeda, E., Buisán, S., Revuelto-Benedí, J., Pons, M., Vicente-Serrano, S.M. 2019. Air and wet bulb temperature lapse rates and their impact on snowmaking in a Pyrenean ski area. Theoretical and Applied Climatology 135(3-4): 1361-1373. DOI: 10.1007/s00704-018-2448-y.*		

Capítulo 2

ÁMBITO ESPACIAL, MATERIALES Y MÉTODOS

Tras situar la presente investigación en el contexto de la Geografía y de los estudios sobre procesos meteorológicos y climáticos en áreas de montaña, este capítulo presenta los diferentes ámbitos espaciales y escalas de trabajo, compuestos por tres escalas bien diferencias (regional, local y experimental), así como los materiales y métodos empleados para la consecución de los diferentes objetivos. La escala regional ha sido representada por: 1) España Peninsular y, 2) Andes de Ecuador y Perú. La escala local por: 1) Valle del río Aragón y, 2) Estación de esquí Aramón – Formigal. Por último, la escala experimental se ha desarrollado en: 1) Daroca, 2) Canfranc, 3) Parcela Formigal – SPICE y, 4) Valle de Panticosa. La sección Materiales muestra los datos utilizados, tomados tanto por organismos oficiales, como por el propio trabajo de campo. Por último, la sección Métodos indica las técnicas empleadas para la consecución de los resultados.

2.1. Ámbito espacial y escalas de trabajo

Todo estudio científico que implique el análisis del territorio debe enfrentarse, en primer lugar, a dos cuestiones imprescindibles como son la elección del ámbito y la escala de trabajo. Esto ocurre en la Geografía, pero también en el resto de disciplinas con implantación territorial.

La elección del ámbito espacial es determinante, y de ella depende gran parte de una investigación. Esta decisión marcará qué factores influyen, y de qué manera, sobre el fenómeno de implantación territorial que se esté analizando, ya sea económico, demográfico, botánico, geomorfológico, turístico o, en este caso, climático. En el estudio de la temperatura del aire superficial, la elección del ámbito espacial es básica y de una importancia capital, ya que todos los factores explicativos (véase Sección 1.2.3 Factores explicativos y medición de la temperatura del aire superficial) son dependientes del área en el que nos situemos. Factores como la latitud, la transparencia atmosférica, la altitud o la exposición a la circulación atmosférica y oceánica basan su influencia en la temperatura del aire en función de la localización de esa área analizada, de tal modo que los factores no influyen de la misma manera si la investigación se realiza en un punto localizado en la selva amazónica que si se realiza en la tundra siberiana, por la conjunción de todos estos factores. Esta es la base del estudio espacial de la temperatura del aire superficial, pero también de cualquier otro fenómeno ambiental. En la presente Tesis Doctoral, las elecciones de los ámbitos de estudio se han realizado en base a un objetivo fundamental, que ha sido la necesidad científica de mejorar el conocimiento de las áreas de montaña, especialmente en espacios para nosotros cercanos y de aplicabilidad directa como son los Pirineos y las montañas españolas. Sin embargo, las áreas con déficit de información, y con aplicabilidad de estos conocimientos, son amplias y numerosas a lo largo del planeta. Es por ello que, al presentarse la oportunidad de realizar un estudio preliminar sobre los Andes, se decidiera acometer su análisis. La elección concreta de cada punto de observación para los diferentes trabajos presentados en el Compendio de publicaciones, se ha detallado en los epígrafes siguientes.

Por otro lado se presenta la escala de trabajo. Este es un concepto también determinante en toda disciplina de implantación territorial, como son los estudios de fenómenos climáticos. Habitualmente, la escala de trabajo se ha referido a la extensión geográfica o espacial de los fenómenos analizados, indicando también en este sentido cuestiones metodológicas de la investigación, especialmente en relación a la toma de datos (Ruiz Rivera y Galicia, 2016). Las propiedades de los fenómenos ambientales se dejan ver de manera más o menos directa en función de la escala desde la que se observa, por lo que habría que hacer un ejercicio de análisis en

determinar cuál es la escala en la que dicho fenómeno ambiental deja ver mejor su propia variabilidad (McMaster y Sheppard, 2004), siendo esa su escala ideal de trabajo. Sin embargo, en trabajos como el que aquí se muestra, la escala de trabajo viene determinada e impuesta por restricciones logísticas (en este caso, la cantidad disponible de observatorios meteorológicos), por lo que la comprensión real de los fenómenos analizados puede resentirse al no analizar el fenómeno a la escala ambientalmente exigida. Esta es la razón del déficit de información y, por tanto, de conocimientos sobre los fenómenos meteorológicos y climáticos en áreas de montaña. Además, en términos jerárquicos, puede darse la situación de que los factores explicativos en unas escalas no sean detectables en otras, y viceversa (Ruiz Rivera y Galicia, 2016), siendo, por tanto, clave entender cómo se dejan ver los factores explicativos en función de la escala de análisis. El conocimiento de esta diferente visibilidad interescalar es parte fundamental de la comprensión final del comportamiento del fenómeno, en este caso la temperatura del aire superficial.

La presente Tesis Doctoral pretende analizar la relación de la temperatura del aire superficial con la altitud bajo diferentes condiciones de ámbitos de estudio y escalas de trabajo (Figura 11), lo cual ha permitido el análisis de este fenómeno con diferentes enfoques: desde el regional realizado sobre la España Peninsular y las regiones andinas de Ecuador y Perú, hasta los trabajos realizados con un enfoque local en el valle del río Aragón y en la estación de esquí de Aramón – Formigal. Asimismo, se ha tratado también el análisis de la temperatura del aire superficial bajo un prisma experimental en los observatorios meteorológicos de Daroca, Canfranc, la parcela experimental del proyecto SPICE en Formigal, y el valle de Panticosa.

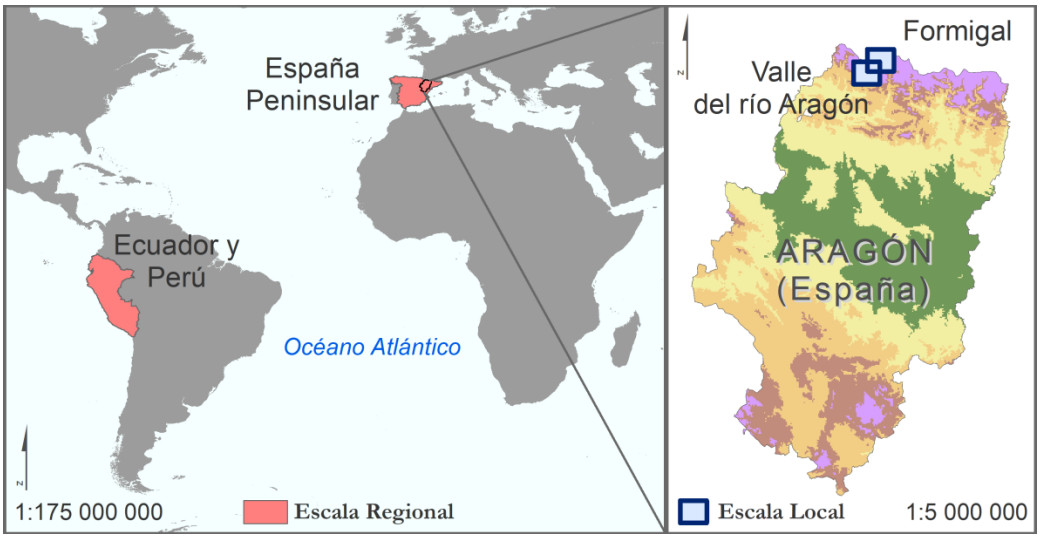

Figura 11. Cartografía de las escalas de trabajo regional y local empleadas en la presente Tesis Doctoral. La escala regional fue representada por la región andina de Ecuador y Perú, así como por la España Peninsular. La escala local se representó mediante el valle del río Aragón (entorno de Canfranc – Estación) y la estación de esquí de Aramón – Formigal. La escala experimental se representa en la Figura 16. Elaboración propia.

2.1.1. Estudios regionales

2.1.1.a. España peninsular y regiones montañosas (aplicación en Capítulo 3)

España forma parte de la Península Ibérica, que se sitúa al suroeste del continente europeo (36º - 43.8º N; 9.3º O – 4.3º E, Figura 12), entre los continentes europeo y africano, así como entre el océano Atlántico y el mar Mediterráneo, lo que la convierte en una región de transición entre diversas realidades, tanto climáticas, como biogeográficas. Las dos principales razones que justifican la elección de este ámbito de trabajo para la escala regional son: 1) la disponibilidad de una red operativa de información meteorológica, procedente de la Agencia Estatal de Meteorología (AEMET) para el conjunto del territorio español y, 2) la necesidad de ampliar y profundizar en el conocimiento de la temperatura del aire superficial en las áreas montañosas españolas que, como veremos, influyen en gran medida en las actividades humanas del resto del territorio del Estado.

El relieve y la orografía peninsular son tremendamente complejos, resultado de una dilatada historia geológica que ha provocado que, hoy en día, la litología superficial tenga muestras de todas las eras geológicas terrestres (IGME, 1994). Los efectos de las diferentes orogenias, la existencia de una gran meseta central y la disposición general oeste – este de los principales sistemas montañosos ha hecho que se genere un espacio de gran heterogeneidad climática (Cuadrat Prats y Pita López, 2006). Aunque el clima general es el propio de latitudes medias y templadas, tanto las precipitaciones como las temperaturas varían intensamente a lo largo del territorio, teniendo por común que el verano corresponde con una estación cálida y eminentemente seca, mientras que el invierno es la estación fría y húmeda, aunque con matices territoriales. Este clima es dependiente de la circulación general atmosférica y de su comportamiento a lo largo del año, que puede verse interrumpido por irrupciones esporádicas procedentes del continente africano (especialmente en verano) y del interior del europeo (principalmente en invierno). A pesar de estar hablando de una región peninsular, la significativa altitud media de algunas cuencas hidrográficas, como las del río Duero, Tajo y Guadiana, marcan un alto grado de continentalidad en estos territorios.

Las regiones montañosas reciben habitualmente precipitaciones en forma de nieve durante el invierno (Alonso-González et al., 2020), y ocasionalmente durante el otoño y la primavera, marcando los regímenes hídricos de los tributarios de los grandes ríos españoles, tales como el Ebro o el Duero (Morán-Tejeda et al., 2014).

La región analizada cuenta con una población total de unos 44 millones de habitantes, en la que un 83.8% es población urbana, concentrada en un 16% del territorio (INE, 2019b; Ministerio de Agricultura Pesca y Alimentación, 2019). Ese territorio densamente poblado es el de las áreas costeras y las circundantes a la Comunidad de Madrid, siendo las áreas montañosas y elevadas un desierto demográfico con densidades inferiores a los 10 hab. por kilómetro cuadrado (Goerlich y Cantarino, 2013). El principal sector por Producto Interior Bruto y por empleabilidad es el de Servicios (66% del PIB y 75% de los empleos), mientras que el sector primario apenas genera un 3% del PIB y un 4% de los empleos (INE, 2019a).

Estos datos podrían llevar a una falsa idea de que, en España, existe una escasa vinculación entre el medio físico, el clima y las actividades humanas. Sin embargo, España es también un país agrícola, principalmente en términos de superficie, con unos 170.000 km^2 de cultivos (~33% de la superficie), aumentando hasta el 88% si incluimos prados y bosques. Buena muestra de ello son las exportaciones de productos agrícolas hacia el resto de la Unión Europea. Sin embargo, el clima peninsular es variable e irregular, por lo que gran parte de esta producción agroalimentaria depende de la disponibilidad de recursos hídricos, que tienen lugar y son recogidos fundamentalmente en las áreas de montaña, donde se concentra un altísimo porcentaje de la capacidad de embalsado del país. Es decir, las despobladas áreas montañosas abastecen de agua a las ciudades litorales y a los grandes valles del interior, además de a las actividades industriales y, en una gran medida, al sector primario. Por todo ello, es una región dependiente de las áreas montañosas, aunque los datos económicos y demográficos muestren una sociedad alejada del mundo rural y de montaña.

Más específicamente, existen algunas zonas en las que se dan precipitaciones muy escasas (inferiores a los 350 mm anuales) pero que, sin embargo, cuentan con potentes industrias agroalimentarias y ganaderas basadas en el uso del agua, como son los regadíos e industrias cárnicas de los valles del Ebro, Cinca y Segre, así como los de las cuencas litorales mediterráneas. Al analizar las áreas con precipitaciones inferiores a 450 mm, estas cuentan con áreas extensas de cultivo de frutales, olivar y vid que, en ocasiones, cuentan con aportaciones puntuales de riego por goteo, lo cual incrementa la dependencia hacia los recursos hídricos en estas regiones sensibles. En este sentido, se ha procedido también a analizar de manera diferenciada cada una de las regiones montañosas de la España Peninsular, debido a sus especiales circunstancias climáticas, diferenciado entre la Cordillera Cantábrica, Pirineos, Sistema Central, Sistemas Béticos y Sistema Ibérico (Figura 12). Puede encontrarse más información en el Capítulo 3.

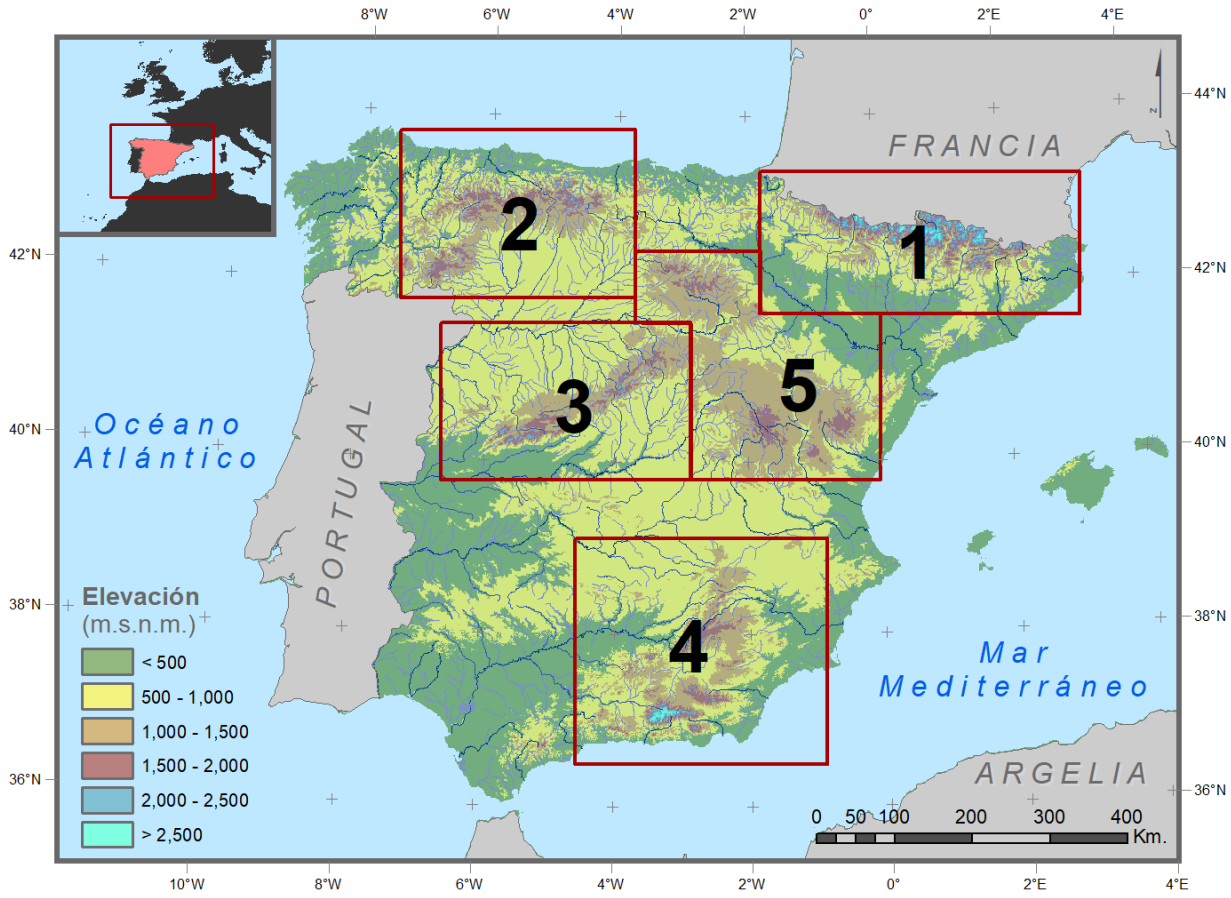

Figura 12. Cartografía de la España Peninsular, prestando atención especial en las 5 subregiones seleccionadas en la publicación del Compendio, esto es: 1) Pirineos, 2) Cordillera Cantábrica, 3) Sistema Central, 4) Sistemas Béticos, y 5) Sistema Ibérico. Elaboración propia.

2.1.1.b. Región andina de Perú y Ecuador (aplicación en Capítulo 4)

Perú y Ecuador están localizados en la costa occidental de América del Sur (1.3º N – 18º S; 81.3º – 68.5º O, Figura 13), bañados por el océano Pacífico y la corriente fría de Humboldt. Estos países son atravesados latitudinalmente por la cordillera de los Andes, que determina grandes diferencias climáticas entre la vertiente pacífica y la amazónica. Las principales razones que hicieron elegir esta región como ámbito de estudio fueron: 1) la posibilidad presentada de poder analizar, de manera similar al caso español, el comportamiento de la temperatura con una red operativa en un ámbito diferente como es el tropical, permitiendo así la comparación entre territorios distantes y con casuísticas diferentes; y 2) cubrir un hueco en el conocimiento de la temperatura del aire en estos territorios, que son de los menos analizados por la literatura científica (Barry, 2008), a pesar de los recientes intentos mencionados en el Capítulo 4. A ello hay que sumar la dependencia de la población local a los extremos climáticos, como las precipitaciones torrenciales (Rollenbeck y Bendix, 2011), que se dejan sentir con su peor cara y demasiada frecuencia en estos puntos del planeta.

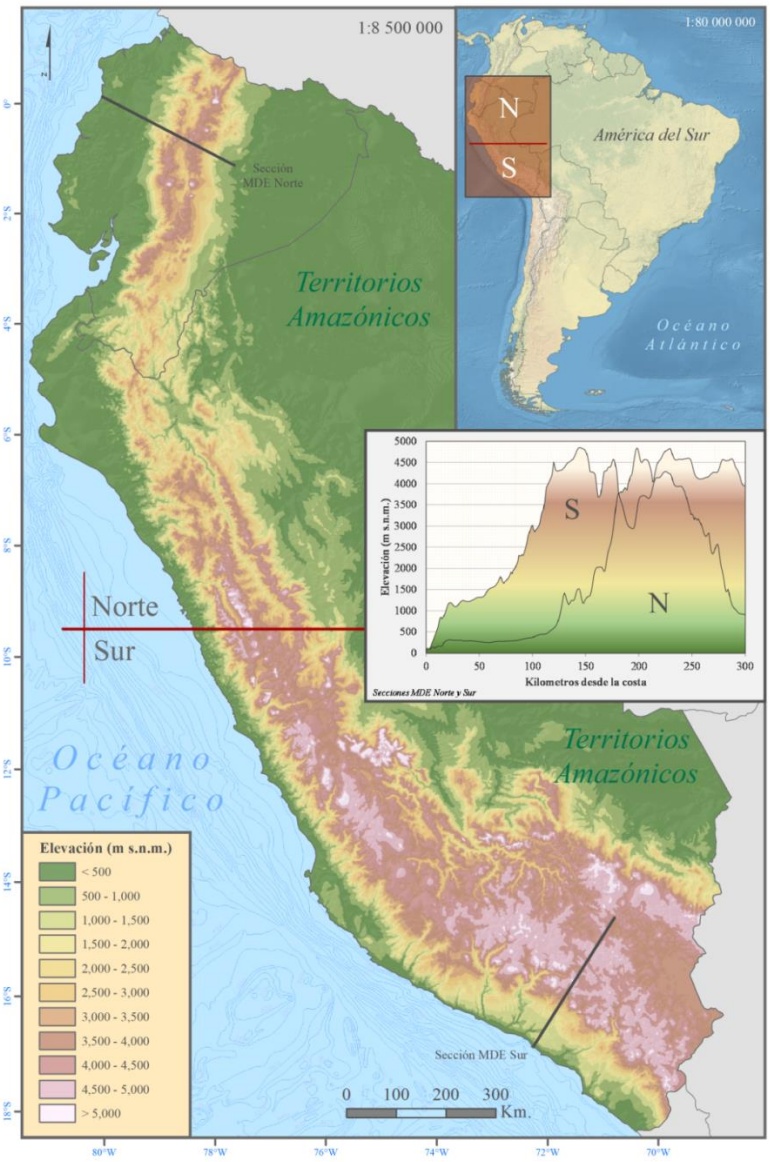

Figura 13. Cartografía de la región andina de Ecuador y Perú. Se han delimitado las subregiones norte y sur por el paralelo latitudinal 9º 30º S. Se ha representado, mediante líneas grises, dos secciones que marcan el perfil topográfico para las dos subregiones. Elaboración propia.

Entender el relieve y la orografía de esta región es relativamente sencillo desde el punto de vista estructural, distinguiéndose tres grandes áreas como son la costera, la amazónica e, intercalada entre ambas, la andina. La región andina es estrecha y larga, y viene delimitada por sus flancos por las estribaciones pacíficas y amazónicas de las montañas. La disposición norte – sur de la región y del área montañosa hace que las condiciones climáticas sean muy diferentes entre las áreas más septentrionales y meridionales de la región andina, además de entre las regiones costera, andina y amazónica, en función del efecto de factores como la latitud y el efecto barrera de la cordillera, respectivamente.

Debido a la posición de la región andina, hay tres elementos clave que afectan al clima de la misma (Barry y Chorley, 2003): 1) la latitud, que oscila entre la línea del Ecuador y el Trópico de Capricornio, con lo que el paso de la Zona de Convergencia Intertropical es determinante; 2) la corriente oceánica fría de Humboldt, que otorga unas características concretas de escasas precipitaciones y persistentes nieblas costeras estacionales en la vertiente del Pacífico; y 3) la disposición latitudinal de la cordillera de los Andes, que marca fuertemente los contrastes entre vertientes. Todo ello hace que exista un gradiente climático norte – sur, además de otro entre costa – interior, que se ha plasmado tradicionalmente en la división de estos dos países entre región costera, andina (o sierra) y amazónica. En este trabajo, debido al especial interés por las áreas de montaña, se ha elegido como ámbito espacial la región andina de ambos países, descartando la región costera y la amazónica por no tener cambios altitudinales de entidad y por no estar referidas a áreas montañosas. La región andina cuenta con una depresión interna localizada a más de 3000 m sobre el nivel del mar, con amplias superficies por encima incluso de este límite, lo que le otorga unas condiciones climáticas muy concretas (SENAMHI, 2020). En el océano Pacífico tiene lugar el fenómeno de El Niño (ENSO, por sus siglas en inglés) que, esporádicamente, puede llegar a afectar intensamente sobre las condiciones meteorológicas de la región. Este fenómeno viene provocado por cambios en la temperatura de la superficie marina, lo cual provoca graves trastornos como sequías, inundaciones o cambios en la temperatura del aire, en función de la fase del fenómeno y su intensidad (Dijkstra, 2006; Grimm et al., 2009; Vicente-Serrano et al., 2017).

Los países de Ecuador y Perú cuentan con una población conjunta de, aproximadamente, 47 millones de habitantes, según la proyecciones y datos oficiales para 2017 (INEC, 2012; INEI, 2017), localizados generalmente en la región costera y en la depresión interna de la región andina (García y Santiago Ochoa, 2012). La economía de estos países está dedicada, fundamentalmente, al sector servicios, pero también tiene una importancia significativa el sector extractivo e industrial, volcado hacia las exportaciones (INEI, 2018; Pino Peralta et al., 2018), que en buena medida son de productos agrícolas, pero también de derivados del petróleo. Por otra parte, la producción hidroeléctrica tiene una importancia capital y un gran potencial de desarrollo futuro (ARCE, 2018; MINEM, 2019), a pesar de disponer de reservas propias de gas y petróleo, especialmente Ecuador. Esta fuente de producción hidroeléctrica copa alrededor del 60% de la producción total, por lo que es capital en el desarrollo económico. El origen de esta producción hidroeléctrica, y de la capacidad de embalsado, está en la región andina, que se presenta como la fuente de recursos hídricos y eléctricos para las regiones costera, andina y amazónica. En áreas con un déficit tan marcado de precipitación, especialmente las áreas meridionales, son los recursos

hídricos de la montaña (esencialmente provenientes del deshielo de la nieve y del hielo), los que permiten la continuidad de las actividades humanas. Estos países, aunque con un rápido desarrollo en las últimas décadas, todavía son vulnerables y están expuestos ante los riesgos naturales (Vicente-Serrano et al., 2017).

Por todo ello, las condiciones ambientales que tienen lugar en la región andina tienen gran impacto en las actividades humanas, ya sea por cuestiones directas (inundaciones o sequías), o indirectas (descenso en la producción hidroeléctrica, aumento del precio de la electricidad, falta de abastecimiento de agua, crisis económicas o desestabilización social), tal y como han indicado algunos autores (Dávila y Olazával, 2006; Paredes y De la Puente, 2014). Por tanto, en esta situación, la temperatura del aire superficial es de nuevo una variable vital en el control y gestión de los recursos hídricos y, de manera indirecta, en la viabilidad de la actividad económica de la región. Por otra parte, con el objetivo de poder observar diferencias latitudinales en la distribución de la temperatura del aire, se ha subdividido la región andina por el paralelo 9.5º S. Puede encontrarse más información en el Capítulo 4.

2.1.2. Estudios locales

2.1.2.a. Valle del río Aragón – Canfranc Estación (aplicación en Capítulo 6)

Con el objetivo específico de analizar el comportamiento espacio-temporal de la temperatura del aire superficial a escala local sobre un área montañosa y topográficamente compleja, se eligió un ámbito espacial cercano, y que cumplió con los requisitos topográficos, altitudinales y de acceso para poder instalar una red de observación propia. Este ámbito fue un sector del tramo alto del valle del río Aragón (42.75º N, 0.52º O, Figura 14), cercano al núcleo poblacional de Canfranc – Estación. El río Aragón es uno de los principales afluentes del río Ebro (se estima que aporta anualmente unos 1000 hm^3), situándose en su margen izquierda y drenando una superficie de 8524 km^2. Debido a su marcado régimen nivo-pluvial, especialmente en su sector de cabecera (García-Ruiz et al., 2001; López-Moreno et al., 2004), sufre avenidas estacionales debido al deshielo (López-Moreno et al., 2002). El sector fue escogido por sus características topográficas y climáticas, ya que cuenta con un rango altimétrico que cubre desde los 1100 m s.n.m. (nivel del río) hasta los 2573 m s.n.m. (Pico de la Moleta). Además, el clima de este sector es frío y húmedo (Canfranc – Estación: 9º C y alrededor de 1400 mm anuales), siendo las nevadas muy comunes durante los meses de invierno (25 días de nevada al año en Canfranc – Estación), lo que genera un manto de nieve continuo a lo largo del invierno en el fondo del valle, y que se alarga hasta bien entrado el verano en las cumbres (López-Moreno, 2006).

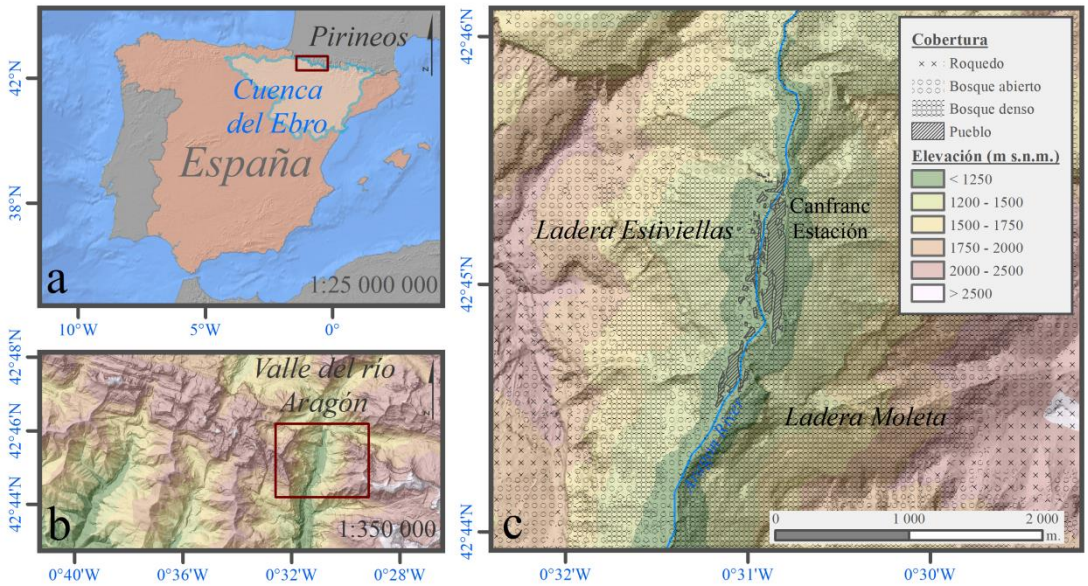

Figura 14. Cartografía que muestra la localización y características principales del valle del río Aragón, en el sector analizado del entorno de Canfranc – Estación. Se indica la situación de las laderas de Estiviellas y Moleta, localizadas a los lados del río Aragón, que discurre por el centro del mapa de norte a sur. Elaboración propia.

El río cruza el ámbito de estudio desde el norte hacia el sur, generando dos laderas enfrentadas a los lados. Es en estas laderas en las que se ha procedido a realizar los diferentes análisis, recibiendo la nomenclatura de ladera de Estiviellas y ladera de la Moleta, orientándose hacia el SSE (solana) y hacia el NNO (umbría), respectivamente. Esto permite un estudio comparativo entre laderas con características opuestas, en las que la radiación solar puede verse fuertemente afectada por las sombras topográficas y sus efectos estacionales. Además, un bosque denso cubre la mayor parte de las laderas hasta los 2000 m s.n.m., con dominancia de *Pinus* spp., así como algunas especies de hoja caduca en las áreas más húmedas (Pueyo y Beguería, 2007; Nadal-Romero et al., 2016). Por encima de 2000 m s.n.m. el bosque va dando paso progresivamente a una vegetación subalpina, e incluso periglacial en las cumbres.

La población es escasa (INE, 2019b), y se encuentra concentrada en pequeños núcleos de población ubicados en el fondo del valle, tales como Canfranc – Estación (463 habs.), Canfranc (77 habs.), Villanúa (398 habs.) o Castiello de Jaca (201 habs.), un poco aguas abajo. La influencia de los condicionantes climáticos en las actividades humanas van más allá del propio tramo alto del río Aragón, aunque a veces los riesgos naturales se han dejado sentir también en las poblaciones anteriormente citadas (López-Moreno et al., 2002), como fue el caso de la crecida de Villanúa en el año 2012 (Bayona, 2012), o de otras crecidas ordinarias (Villanueva, 2018) debidas al deshielo

repentino provocado por una subida brusca de temperaturas y de lluvias intensas, mostrando que los impactos e influencias del medio montañoso en la población nunca deben dejarse de lado. Por otro lado, debido a la importante cuenca hidrográfica del río Aragón, y a su productividad en forma de acumulación de nieve (Alonso-González et al., 2020), es un río estratégico en la gestión de los recursos hídricos de la Confederación Hidrográfica del Ebro, ya que drena una gran superficie, y permite el abastecimiento de más de 50.000 personas y 81.000 has. de regadío gracias al embalse de Yesa y a la creación del canal de Bardenas. Por todo ello, pese a la situación del enclave estudiado, en un lugar remoto de la montaña española, este territorio influye activamente en las actividades económicas y humanas, por lo que un conocimiento preciso y certero de las condiciones climáticas que se dan en él ayudará en la gestión de los recursos y en la adaptación del hombre a los mismos. Puede encontrarse más información en el Capítulo 6.

2.1.2.b. Estación de esquí de Aramón – Formigal (aplicación en Capítulo 7)

Tras plantear el objetivo específico de aplicar los análisis del comportamiento de la temperatura del aire superficial a la fragilidad de determinadas actividades humanas, se decidió que este análisis debía ser a una escala de trabajo local con el objetivo de poder analizar los efectos sobre una actividad en concreto. Es por ello que elegimos una actividad y ámbito de estudio con dependencia directa hacia las condiciones meteorológicas como son las estaciones de esquí del Pirineo aragonés. En esta región, al encontrarnos en un territorio de transición entre los efectos atlánticos y mediterráneos, las precipitaciones, tanto en forma de lluvia como de nieve, son irregulares, y la insolación elevada, por lo que el manto de nieve es irregular. Esto lleva a una situación de vulnerabilidad a las actividades dependientes de la nieve, como son las estaciones de esquí, sobre todo las que se encuentran a menor altitud (López-Moreno et al., 2009; Pons et al., 2015). Esta situación provoca que, ocasionalmente, estos complejos se encuentren al borde del colapso, teniendo que acortar la temporada a unas pocas semanas. Por ello, todas las estaciones de esquí del entorno han ido ampliando la capacidad de producción de nieve artificial, lo cual les permite mantener la actividad durante toda la temporada de esquí (generalmente, desde diciembre hasta abril), salvaguardando los envites más fuertes de la irregularidad meteorológica. Sin embargo, la producción de nieve artificial no es ajena a las condiciones meteorológicas, ya que su viabilidad depende, fundamentalmente, de la temperatura del aire superficial y de la humedad relativa, por lo que el conocimiento espacio-temporal de estas variables es básico para conocer la viabilidad de la actividad. Por estas cuestiones, tras una serie de contactos y colaboraciones previas, se decidió elegir como ámbito de estudio una estación de esquí de amplio impacto sobre toda la región como es la de Aramón – Formigal (en adelante, Formigal).

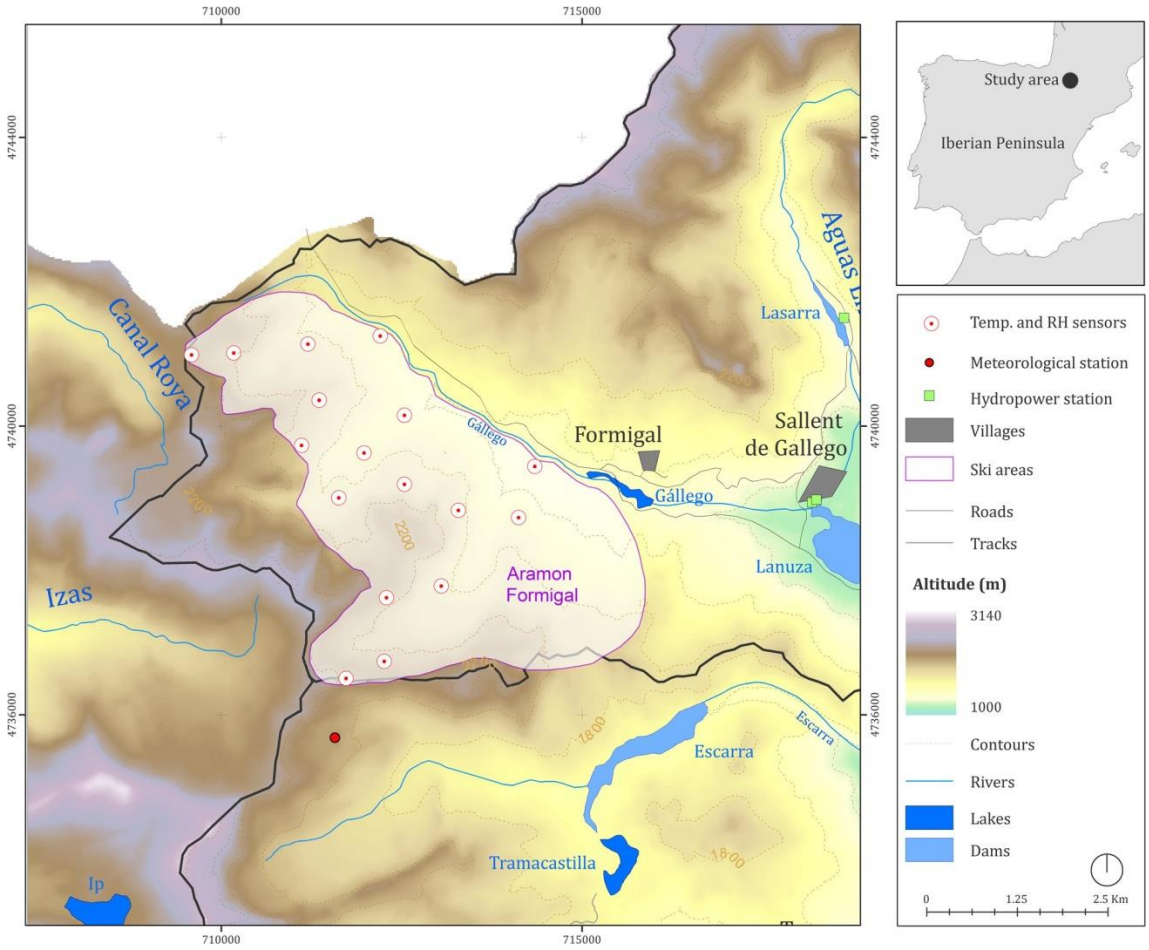

Figura 15. Cartografía y localización de la estación de esquí de Aramón – Formigal. Tomada de López-Moreno et al. (2019).

La estación de esquí de Formigal se encuentra situada en la cabecera del río Gállego (42.5º N, 0.25º O, Figura 15), en los Pirineos centrales y a escasa distancia de la frontera entre España y Francia, y contando con un rango altimétrico desde los 1550 hasta los 2300 m s.n.m., cubriendo una superficie de unas 2500 hectáreas, generalmente en la vertiente norte del macizo montañoso en el que se encuentra. El clima del entorno (medido en una ubicación próxima, a 2056 m s.n.m.) es frío y húmedo, mostrando una temperatura media anual de 3º C y unas precipitaciones de, aproximadamente, 2000 mm anuales, de los cuáles más de un 50% son en forma de nieve (López-Moreno et al., 2013). Además, se dan una media de 130 días anuales en los que no se supera la barrera de los 0º C en ningún momento del día (Revuelto et al., 2017). Aunque la media de temperatura durante el invierno es inferior a 0º C, el ámbito de estudio está sujeto a episodios esporádicos de lluvia durante el invierno, que pueden acelerar la fusión de la nieve y la transformación del manto a lo largo de la temporada de esquí. Estamos por tanto ante un territorio de marcado carácter montañoso, en el que la nieve hace acto de aparición con frecuencia y las temperaturas pasan buena parte del año por debajo del umbral de la helada.

Formigal es una de las estaciones de esquí más importantes del Pirineo y, por tanto, del país. En la actualidad cuenta con 137 km esquiables, distribuidos en más de 115 pistas, teniendo los telesillas una capacidad máxima de 35.920 esquiadores por hora, que se incrementan hasta los 50.000 añadiendo las vecinas instalaciones del valle de Panticosa, conformando el complejo invernal de Aramón Formigal – Panticosa. La importancia económica de Formigal en la comarca es incalculable, tanto desde el punto de vista económico como demográfico, ya que permite la fijación de parte de la población joven del entorno. Sin embargo, a pesar de su importancia y potencial, su situación no escapa a la vulnerabilidad que cubre a la práctica totalidad de estaciones de esquí españolas en relación a las temperaturas y la irregularidad de las precipitaciones en forma de nieve (Gilaberte-Búrdalo et al., 2017). En un contexto de cambio global, en el que parece que las zonas elevadas sufrirán antes los efectos de una subida de la temperatura del aire, estos entornos situados en el límite altimétrico de las precipitaciones en forma de nieve, se encuentran en una posición delicada, especialmente los kilómetros esquiables situados a menor altitud. Es por ello que Formigal, al igual que otras estaciones de esquí, ha desarrollado un amplio dispositivo de cañones de producción de nieve artificial que permite el sostenimiento de la actividad a pesar de las irregulares precipitaciones. Por todo ello, es imprescindible un mayor conocimiento sobre el comportamiento de la temperatura del aire superficial en estos entornos, ya que de ella depende la viabilidad de estas actividades. Puede encontrarse más información en el Capítulo 7.

2.1.3. Estudios experimentales: Daroca, Canfranc, Formigal – SPICE y valle de Panticosa (aplicación en Capítulo 5)

La necesidad de trabajar sobre el objetivo específico de establecer una serie de criterios metodológicos que permitan el diseño de redes experimentales sobre ámbitos de montaña requirió de la disposición de observatorios meteorológicos de referencia, accesibles y controlados, en los que se pudieran llevar a cabo los análisis específicos contando con mediciones de referencia homologadas. Para ello, contamos con la inestimable ayuda y colaboración de la Delegación Territorial en Aragón de la Agencia Estatal de Meteorología (AEMET), que propuso algunos observatorios de referencia en su red que cumplían con los requisitos de nuestra investigación: ambientes fríos, con precipitaciones en forma de nieve y, a poder ser, de ámbitos de alta montaña. Además, se requería que, a ser posible, fueran unos observatorios automáticos, que permitieran almacenar la información a elevada resolución temporal. Se requería también la disponibilidad de información de velocidad de viento y radiación, además de temperatura del aire y precipitación.

La selección final de ámbitos de trabajo a esta escala experimental fueron los observatorios de: Daroca, Canfranc y Formigal – SPICE (Figura 16). Además, otro de los experimentos se desarrolló en parcelas experimentales propias del Grupo de Investigación en el valle de Panticosa.

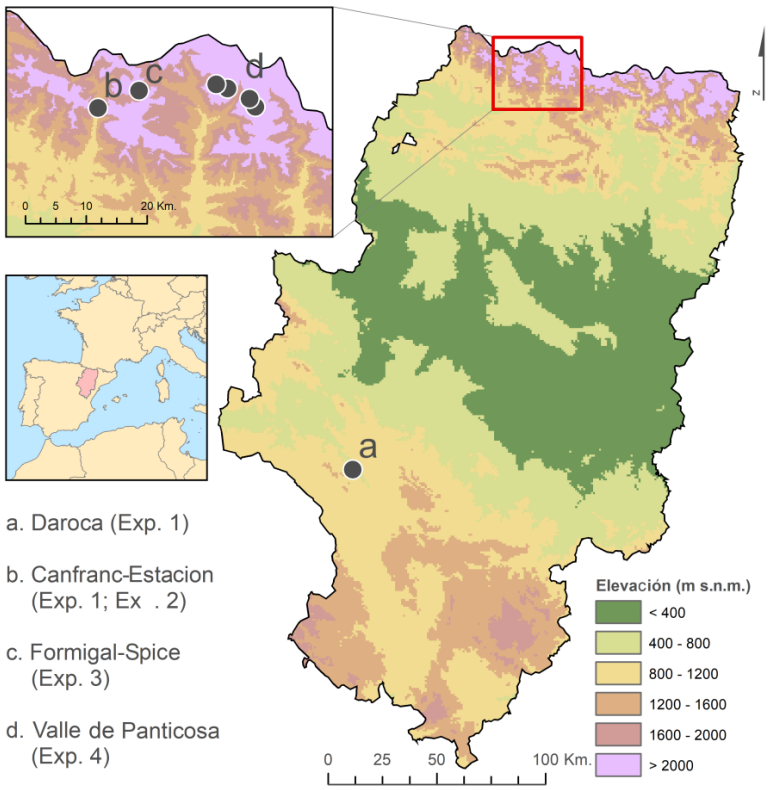

Figura 16. Localizaciones de las parcelas experimentales en el contexto de Aragón (España). Daroca (a), Canfranc (b), Formigal-SPICE (c), y Valle de Panticosa (d). Elaboración propia.

El observatorio de Daroca (identificador '9390') está ubicado en el área montañosa del Sistema Ibérico (779 m s.n.m., 41.11º N, 1.41º O, Figura 16.a). Es un entorno que cuenta con un clima de carácter continental dentro del contexto peninsular, en el que las temperaturas tienen grandes oscilaciones térmicas (media de las máximas de 30.8º C en julio, y media de temperaturas mínimas de -0.6º C en enero). Las precipitaciones son escasas (393 mm anuales), aunque durante el invierno pueden ser, ocasionalmente, en forma de nieve (12 días de nieve al año). La elección de esta localización se debió a la conjunción entre clima muy frío, con nevadas ocasionales, pero en un contexto de sequedad, aridez y fuerte insolación diurna, lo que permitiría contrastar con las condiciones de los observatorios de alta montaña.

El observatorio de Canfranc (identificador '9198X') está ubicado en la población de Canfranc – Estación (1170 m s.n.m., 42.75º N, 0.52º O, Figura 16.b), ya desarrollada en el punto anterior. Su clima es frío y húmedo, siendo las nevadas muy comunes durante el invierno (25 días de nieve

al año), y teniendo una cobertura de nieve generalmente continua a lo largo del invierno. Esta condición permitió analizar diferentes modelos de protección contra la radiación solar sobre suelo nevado, contando con las medidas de referencia del observatorio de AEMET.

El tercer estudio a escala experimental se desarrolló en la parcela (1820 m s.n.m., 42.76º N, 0.39º O, Figura 16.c) que AEMET dispone en la estación de esquí de Aramón – Formigal, en el contexto del Proyecto SPICE (*WMO Solid Precipitation Intercomparison Experiment*). Además del espíritu original del Proyecto SPICE, es deseo de AEMET que esta parcela sea un campo de prueba y de experimentación de diferentes proyectos meteorológicos, por lo que contamos con su plena disposición a colaborar. En esta parcela se toman mediciones de una gran cantidad de variables meteorológicas, entre las que está la toma automática de espesor de nieve. Esta localización está expuesta a los flujos de aire fríos y húmedos del norte, siendo las nevadas muy comunes y regulares, pudiendo alcanzar la nieve espesores de hasta 200 – 300 cm. en años propicios (Buisán et al., 2017). Las condiciones climáticas resultan en una cobertura de nieve continua desde finales de otoño hasta primeros de verano. La parcela de Formigal – SPICE fue elegida como ubicación para este experimento debido a que el principal objetivo fue analizar la distribución vertical de la temperatura del aire sobre áreas cubiertas de nieve. En esta localización la cubierta de nieve es continua, y la disposición de datos automáticos sobre espesor de nieve permitió analizar la temperatura continuamente a varias alturas sobre la superficie nevada.

Por último, el cuarto ámbito de estudio de la escala de trabajo experimental fueron cuatro parcelas experimentales propias en el valle de Panticosa (42.76º N, 0.23º O, Figura 16.d), instalada con motivo de otras investigaciones del Grupo de Investigación de Hidrología Ambiental (IPE – CSIC), que se han plasmado en algunas publicaciones recientes (Sanmiguel-Vallelado et al., 2020). Es un valle elevado del Pirineo, perteneciente a la cuenca del río Gállego. El valle está cubierto por un bosque denso perenne de *Pinus mugo* subsp. *uncinata*. Las cuatro parcelas experimentales se establecieron en varias combinaciones en cara norte y sur a dos bandas altimétricas, conformando: Norte-Arriba (2195 – 2213 m s.n.m.), Norte abajo (1742 – 1757 m s.n.m.), Sur Arriba (2039 – 2053 m s.n.m.) y Sur Abajo (1854 – 1882 m s.n.m.). El valle de Panticosa fue elegido debido a su bosque perenne y la presencia continua de nieve durante varios meses al año, que permitiría encontrar unas condiciones homogéneas dentro de cada parcela. En esta zona se pudo comparar la variabilidad térmica mostrada por grupos de termómetros ubicados a una altura muy similar en cuatro zonas situadas a una orientación y altitud contrastadas. Puede encontrarse más información en el Capítulo 5.

2.2. Materiales

En este punto es necesaria al menos una concisa introducción al método científico. Una vez establecidos los diferentes objetivos específicos de la Tesis Doctoral, así como los ámbitos espaciales y escalas de trabajo, todo trabajo científico debe regirse por este método. El método científico es una forma de trabajar en la que la disciplina, el orden y la sistematización de los procesos garantiza la aceptabilidad de los resultados, así como la reproducibilidad y validez de los mismos, permitiendo así establecer teorías (Jensen, 1992). El método científico tiene una base sólida, que son los datos empíricos, esto es, basados en la observación directa de la realidad, que permiten la cuantificación y documentación de la misma, permitiendo además la comprobación de las diferentes hipótesis. En los siguientes epígrafes describimos brevemente las características principales de los materiales empleados en la consecución de los distintos objetivos específicos de la Tesis Doctoral. Los materiales han sido clasificados en función de su origen (redes oficiales de observación meteorológica, trabajo de campo realizado por el doctorando, y otras fuentes), y resumidos en la Tabla 2:

Tabla 2. Síntesis de los Materiales Empleados, clasificados por los Capítulos y Publicaciones.

Capítulo y Publicación	Materiales Empleados
Capítulo 3 ***Navarro-Serrano, F.**, López-Moreno, J., Azorin-Molina, C., Alonso-González, E., Tomás-Burguera, M., Sanmiguel-Vallelado, A., Revuelto, J., Vicente-Serrano, S.M. 2018. Estimation of near-surface air temperature lapse rates over continental Spain and its mountain areas. International Journal of Climatology 38: 3233-3249.*	▪ Temperaturas máximas y mínimas diarias del aire superficial (Red Aemet) y garitas de tipo Stevenson (Buisán et al., 2015) ▪ Presión atmosférica a nivel del mar procedente de NCEP-NCAR Reanálisis (Basnett y Parker, 1997). ▪ Modelo Digital de Elevaciones (MDT200), de IGN (2020). ▪ Red Hidrográfica derivada del World Map Vector (VMap0), de USDMA (2000).

Capítulo y Publicación	Materiales Empleados
Capítulo 4 ***Navarro-Serrano, F.**, López-Moreno, J.I., Domínguez-Castro, F., Alonso-González, E., Azorin-Molina, C., El-Kenawy, A., Vicente-Serrano, S.M. 2020. Maximum and minimum air temperature lapse rates in the Andean region of Ecuador and Peru. International Journal of Climatology (En Prensa).*	▪ Temperaturas máximas y mínimas diarias del aire superficial (Red INAMHI y SENAMHI). Observaciones manuales y garitas Stevenson. ▪ Humedad específica a la altura geopotencial 500 hPa procedente de ERA-Interim Reanálisis (Berrisford et al., 2011). ▪ Modelo Digital de Elevaciones (GTOPO30), de Gesch et al. (1999). ▪ Índices Fenómeno El Niño: ONI e ICEN (Takahashi et al., 2014; Huang et al., 2017). ▪ Imágenes MODIS (USGS, 2020).

Tabla 2. Síntesis de los Materiales Empleados, clasificados por los Capítulos y Publicaciones (continuación).

Capítulo y Publicación	Materiales Empleados
Capítulo 5 ***Navarro-Serrano, F.**, López-Moreno, J.I., Azorin-Molina, C., Buisán, S., Domínguez-Castro, F., Sanmiguel-Vallelado, A., Alonso-González, E., Khorchani, M. 2019. Air temperature measurements using autonomous self-recording dataloggers in mountainous and snow covered areas. Atmospheric Research 224: 168-179.*	▪ Trabajo de Campo: Temperatura del aire superficial. Sensores Tinytag-Plus-2 (modelo TGP4017) e iButton (modelos DS-1922 y DS-1921G). ▪ Garitas Stevenson (Buisán et al., 2015), Datamate (basada en Gill, 1983), de Tubo (Pepin y Kidd, 2006) y de Embudos (Hubbart, 2011). ▪ Radiación incidente, medida por piranómetro Kipp&Zonen (modelo de piranómetro CM11). ▪ Espesor de nieve, medida por un sensor acústico de espesor Campbell Scientific (modelo SR50A). ▪ Precipitación, medida por pluviómetro totalizados automático OTT (modelo Pluvio2, de 1500 mm de capacidad), e instalado dentro de un DFIR (Buisán et al., 2017). ▪ Intensidad del viento (Red Aemet), medido por anemómetro Thies Clima, a una altura estándar de 10 m. ▪ Existencia y espesor de nieve en suelo (Red Aemet), por pértigas y observación de colaboradores de AEMET en Canfranc y Daroca (Aragón, España).

Capítulo y Publicación	Materiales Empleados
Capítulo 6 ***Navarro-Serrano, F.**, López-Moreno, J.I., Azorin-Molina, C., Alonso-González, E., Aznarez-Balta, M., Buisan, S. Revuelto, J. 2020. Elevation effects on air temperature in a topographically complex mountain valley in the Spanish Pyrenees. Atmosphere 11(6): 656. DOI: https://doi.org/10.3390/atmos11060656.*	▪ Trabajo de Campo: Temperatura del aire superficial. Sensor Tinytag-Plus-2 (TGP4017) ▪ Temperaturas y Humedad Relativa a escala diezminutal del aire superficial (Red Aemet), por termistor Thies Clima (modelo PT100), y garitas de tipo Stevenson (Buisán et al., 2015) ▪ Intensidad del viento (Red Aemet), medido por anemómetro Thies Clima, a una altura estándar de 10 m. ▪ Presión atmosférica (Red Aemet), medida por barómetro Vaisala (modelo PMT) ▪ Presión atmosférica a nivel del mar procedente de NCEP-NCAR Reanálisis (Basnett y Parker, 1997). ▪ Modelo Digital de Elevaciones (MDT05), de IGN (2020) ▪ Imagen Sentinel (Sinergise Ltd, 2020)

Capítulo y Publicación	Materiales Empleados
Capítulo 7 *López-Moreno, J.I.**, Navarro-Serrano, F.**, Azorín-Molina, C., Sánchez-Navarrete, P., Alonso-González, E., Rico, I., Morán-Tejeda, E. et al. 2019. Air and wet bulb temperature lapse rates and their impact on snowmaking in a Pyrenean ski resort. Theoretical and Applied Climatology 135: 1361-1373.*	▪ Trabajo de Campo: Temperatura del aire superficial. Sensor Tinytag-Plus-2 (TGP4500) y garitas Datamate ▪ Trabajo de Campo: Humedad relativa del aire superficial. Sensor Tinytag-Plus-2 (TGP4500) y garitas Datamate ▪ Temperatura del aire, velocidad del viento, humedad relativa y presión atmosférica tomada por estación completa del Grupo de Investigación de Hidrología Ambiental, situada en la Cuenca de Izas. ▪ Presión atmosférica a nivel del mar procedente de NCEP-NCAR Reanálisis (Basnett y Parker, 1997).

2.2.1. Redes oficiales de observación meteorológica

2.2.1.a. Agencia Estatal de Meteorología (AEMET – España)

Gracias a la disposición y colaboración plena de AEMET, el acceso a la información meteorológica ha sido posible siempre que se necesitara, tanto dentro del marco de colaboración del proyecto DESEMON (Ref. CGL2014-52135-C3-1-R, del Ministerio de Economía y Competitividad. Investigador Principal, Dr. S.M. Vicente Serrano), como por las investigaciones conjuntas realizadas con la Delegación Territorial en Aragón en la presente Tesis Doctoral. En este punto, nos referimos fundamentalmente a los datos de temperatura del aire superficial disponibles, tanto de máximas como de mínimas diarias, de los observatorios y estaciones meteorológicas del conjunto de la España Peninsular (un total de 3950 series) desde el año 1951 hasta la actualidad.

Las fechas operativas varían entre observatorios, pero es la década de los años noventa la de mayor cantidad simultánea de observatorios en funcionamiento, período en el cual se empezaron a sustituir parte de los observatorios manuales originales por las estaciones meteorológicas automáticas, lo cual permite la generación de una mayor cantidad de información. Además de las mediciones de temperatura del aire superficial, AEMET también ha facilitado datos de otras variables en los observatorios en los que se han requerido (Canfranc – '9198X', Daroca – '9390' y Aragüés del Puerto – '9208E'), como humedad relativa, presión atmosférica, velocidad y dirección del viento, espesores de nieve, así como precipitaciones.

Todas las mediciones realizadas por el instrumental de AEMET siguen las recomendaciones fijadas por la Organización Meteorológica Mundial (WMO, 2014) en materia de inter-comparabilidad y homogeneidad de los datos. La homologación y calibración de sensores de medición y garitas de protección ante la radiación, además del mantenimiento de los observatorios, son una de las tareas fundamentales del departamento de Servicios Básicos de AEMET. Los distintos modelos de sensores empleados han sido recopilados en la Tabla 2.

La distribución de los observatorios es homogénea a lo largo de la España Peninsular, aunque la mayoría se encuentran localizados en puntos poblados, lo que sesga los puntos de muestreo hacia ubicaciones de escasa altitud y de fácil acceso. Para más información sobre la ubicación, periodicidad de los datos, procesado y aplicabilidad de los mismos, pueden consultarse los capítulos específicos de los artículos de investigación publicados en los que se han empleado (Capítulos 3, 5 y 6).

2.2.1.b. Instituto Nacional de Meteorología e Hidrología (INAMHI – Ecuador) y Servicio Nacional de Meteorología e Hidrología (SENAMHI – Perú)

Gracias a la disposición y colaboración plena de los servicios meteorológicos de INAMHI y SENAMHI, el acceso a la información meteorológica de Ecuador y Perú ha sido posible. Esta colaboración se plasmó en los datos históricos completos de temperaturas máximas y mínimas diarias de 694 observatorios manuales, entre los aportados por los dos servicios meteorológicos para la región andina de ambos países. Los datos fueron tomados en su mayoría de forma manual por observadores especializados y siguiendo las recomendaciones de la WMO (2014). El instrumental específico empleado ha sido recopilado en la Tabla 2.

La distribución de los observatorios es dependiente, al igual que la red de AEMET, de la ubicación de los puntos poblados, lo que ha provocado una mayor densidad de observatorios en las áreas de la depresión intra andina y en las zonas bajas cercanas a la costa. Además, pudo observarse una mayor densidad de observatorios en la red de observación procedente del INAMHI (Ecuador), aunque derivada de un impulso demasiado reciente como para poder ser aprovechada en un estudio de gran amplitud temporal como el realizado. Para más información sobre la ubicación, periodicidad de los datos, procesado y aplicabilidad de los mismos, puede consultarse el capítulo específico de la publicación en la que se han empleado (Capítulo 4).

2.2.1.c. WMO Solid Precipitation Intercomparison Experiment (Proyecto SPICE)

El Proyecto SPICE es un trabajo internacional coordinado por la WMO y por la Comisión de Instrumentación y Métodos de Observación (CIMO), que tiene el objetivo de analizar el rendimiento de los sensores de medición de la precipitación en forma de nieve bajo diferentes condiciones, tanto geográficas como ambientales (Nitu et al., 2018). Un total de veinte parcelas experimentales fueron instaladas en todo el mundo, estando una de ellas localizada en la estación de esquí de Aramón – Formigal (Figura 17), bajo la gestión y supervisión de AEMET (Buisán et al., 2017). Estas parcelas experimentales tienen el objetivo también de servir como punto de referencia en otros trabajos sobre rendimiento y calibración de sensores. Esto provoca que se midan, de forma simultánea, multitud de variables meteorológicas con diferente instrumental. De ellas, se han podido aprovechar en la presente Tesis Doctoral datos sobre precipitación acumulada, espesor del manto de nieve, velocidad del viento y radiación incidente (Tabla 2). Para más información sobre la ubicación, sensores, periodicidad de los datos, procesado y aplicabilidad de los mismos, puede consultarse el capítulo específico de la publicación en la que se han empleado (Capítulo 5).

Figura 17. Parcela experimental de Formigal – SPICE. La fotografía superior izquierda fue tomada por el equipo de monitorización de AEMET (abril de 2018). En la fotografía inferior (elaboración propia) se muestra parte del instrumental anexo.

2.2.2. Trabajo de campo

En aquellos análisis realizados a escala local (Capítulos 6 y 7) y experimental (Capítulo 5) en los que las redes oficiales de observación no permitían tener la suficiente información sobre temperatura del aire superficial, se tomaron datos mediante instrumental propio. Los sensores empleados fueron los Tinytag-Plus-2 (modelos TGP-4017 y TGP-4500, Figura 18.a). El modelo TGP-4500 permite, además, la medición de la humedad relativa. Estos sensores son autónomos, auto-grabables e impermeables, lo que permite su uso y exposición al aire libre. Además, también se emplearon datos tomados por sensores iButton (modelos DS-1922 y DS-1921G). Los dispositivos de medición fueron introducidos dentro de garitas Datamate (modelo ACS-5050, Figura 18.b), basadas en los modelos de platos de Gill (1983) e instalados a diferentes alturas sobre el nivel de suelo, en función de los objetivos de cada uno de los análisis. Este instrumental, además de otras alternativas no comerciales para proteger de la radiación solar, fue validado mediante dos de los experimentos de la publicación que conforma el Capítulo 5.

Además de estos dispositivos, también se han utilizado los datos de temperatura del aire provenientes de la estación meteorológica automática de Izas, instalada por el Grupo de Investigación de Hidrología Ambiental (IPE – CSIC) para la realización de otras investigaciones (Revuelto et al., 2017), pero que permitió disponer de datos para la presente Tesis Doctoral. Estos datos fueron tomados por un sensor Vaisala (modelo HMP155), conectado a un datalogger Campbell Scientific gestionado por el Instituto Pirenaico de Ecología.

Las especificaciones de estos sensores y protectores de radiación pueden encontrarse en la Tabla 2. Para más información sobre la ubicación, periodicidad y procesado de los datos, pueden consultarse los capítulos específicos de las publicaciones en las que se han empleado (Capítulos 5, 6 y 7).

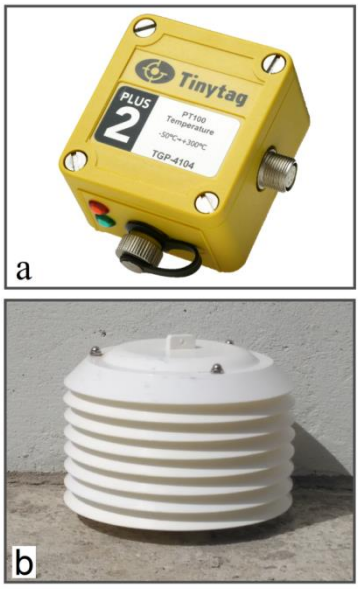

Figura 18. Tinytag-Plus-2 (a), y (b) garita de protección Datamate modelo ACS-5050.

2.2.3. Otras fuentes

2.2.3.a. Modelos Digitales de Elevaciones

Los Modelos Digitales de Elevaciones (MDE) son representaciones visuales del relieve del territorio que muestran la altitud sobre el nivel del mar, permitiendo caracterizar la topografía. La característica más importante de los MDE es la resolución espacial, que marca la capacidad de representar fielmente el territorio. Sin embargo, las limitaciones computacionales son, habitualmente, el mayor impedimento en el uso de MDE de gran detalle. Los MDE tienen diversas aplicaciones en la presente Tesis Doctoral, desde las puramente cartográficas en el diseño de mapas, hasta las más técnicas, como el cálculo de las horas de sol sobre un punto. Se han empleado diferentes MDE en función de los objetivos específicos de cada investigación. En el ámbito español, estos han sido tomados del Instituto Geográfico Nacional (IGN, 2020) bajo diferentes resoluciones espaciales desde los 200 m (MDT200) hasta los 5 m (MDT05/MDT05-LIDAR) de lado de píxel, mientras que en el caso de los Andes peruanos y ecuatorianos, se han utilizado los MDT globales 'GTOPO30' (Gesch et al., 1999) y 'SRTM' (Farr et al., 2007), de 1 km y 30 m de resolución espacial, respectivamente. Ambos son distribuidos por el portal web Earth Explorer (USGS, 2020).

2.2.3.b. Índices para la medición del fenómeno de El Niño

El fenómeno del ENSO es, como hemos indicado anteriormente, un fenómeno natural que se da a causa del calentamiento y enfriamiento de la superficie marina del océano Pacífico. Para su cuantificación se han desarrollado índices que comparan esta temperatura con respecto a los valores normales o habituales. Además, es necesario determinar qué región del océano se escoge para la medición (Figura 19). En este trabajo se han comparado las regiones 3.4 y 1+2 (Rasmusson y Carpenter, 1982) mediante los índices Oceanic Niño Index (ONI) e Índice-Costero-El-Niño (ICEN), respectivamente. Los datos ONI han sido proporcionados por el NOAA – Climate Prediction Center, dependiente del Gobierno de Estados Unidos (https://origin.cpc.ncep.noaa.gov/products/analysis_monitoring/ensostuff/ONI_v5.php, último acceso el 2 de junio de 2020) a una resolución de media móvil de 3 meses, basándose en los datos de Extended Reconstructed Sea Surface Temperature v.5 (Huang et al., 2017).

Los datos ICEN fueron proporcionados a escala mensual por el Gobierno Peruano (http://www.met.igp.gob.pe/variabclim/indices.html, último acceso el 2 de junio de 2020), basándose en ENFEN (2012) y la actualización posterior de Takahashi et al. (2014). Siguiendo el criterio de cada metodología original, las fases positivas de El Niño fueron identificadas tal y como sigue: (ONI): 5 meses (construidos con la media móvil de 3 meses) con valores por encima de +0.5 (por debajo de -0.5 se identifican como fases negativas de La Niña); (ICEN): 3 meses (construidos con la media móvil de 3 meses) con valores por encima de +0.4 (por debajo de -1.0 son identificadas como fases negativas de La Niña).

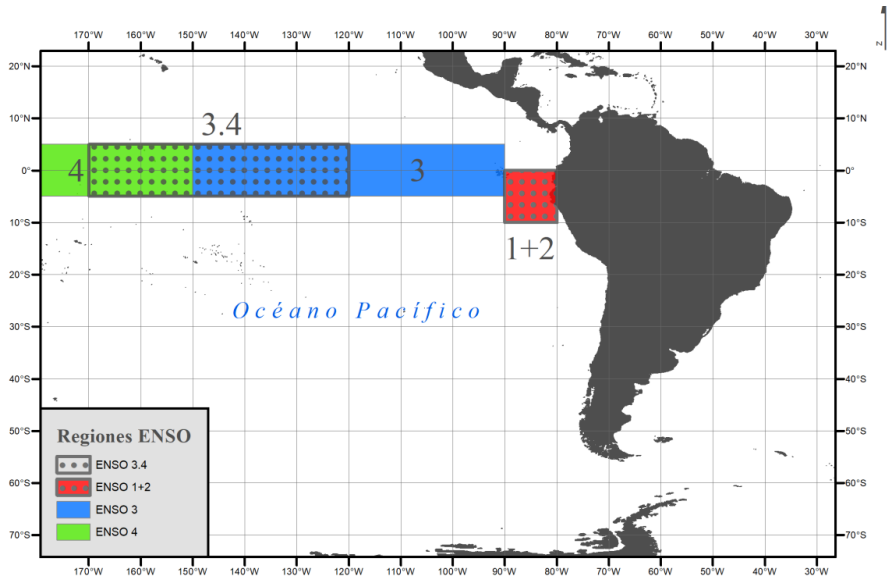

Figura 19. Regiones de referencia para el cálculo de los diferentes índices ENSO. Elaboración propia.

2.2.3.c. Datos procedentes de reanálisis

Los reanálisis son una técnica que permite, tras el procesado de datos observados, la reconstrucción y modelización de las condiciones meteorológicas en un área determinada. Todas las variables meteorológicas pueden ser objeto de un reanálisis, aunque la exactitud y precisión del mismo dependerá de la variable en cuestión y la escala de trabajo. En este sentido, los datos de reanálisis permiten obtener información sobre áreas en las que no existen datos empíricos, aunque siempre con cierta cautela, sobre todo a nivel superficial (Bumke, 2016). Sus limitaciones son evidentes, puesto que son productos modelizados, pero en función del ámbito de estudio, la escala espacial y temporal de trabajo, pueden llegar a ser bastante precisos (Zou et al., 2014; Gao et al., 2017).

En la presente Tesis Doctoral nos servimos de la base de datos del reanálisis del NCEP-NCAR (Basnett y Parker, 1997) para obtener datos de presión atmosférica a nivel del mar sobre la Península Ibérica (https://climatedataguide.ucar.edu/climate-data/ncar-sea-level-pressure, último acceso 2 de junio de 2020). Además, accedimos a la base de datos del reanálisis del ERA-Interim (Berrisford et al., 2011) para obtener datos de humedad específica a la altura geopotencial de 500 hPa sobre la región andina de Ecuador y Perú, con objetivos desarrollados en el Capítulo 4 (https://www.ecmwf.int/en/forecassts/datasets/reanalysis-datasets/era-interim, último acceso 2 de junio de 2020).

2.2.3.d. Otros materiales

Además de los datos anteriormente mencionados, a lo largo de la Tesis Doctoral se han empleado diferentes fuentes para casos y análisis concretos, como capas de información vectorial sobre redes hidrográficas (USDMA, 2000), imágenes del sensor Terra del satélite MODIS para detectar las nieblas de la costa peruana y ecuatoriana (USGS, 2020), así como Sentinel-2B para establecer las coberturas de suelo en la cabecera del valle del río Aragón (Sinergise Ltd, 2020). Estas fuentes son desarrolladas en los capítulos específicos de las publicaciones que componen el Compendio (Capítulos 3, 4, 5, 6 y 7).

2.3. Procedimientos metodológicos

Esta sección de procedimientos metodológicos trata de indicar los principales procesos y técnicas empleados en la Tesis Doctoral, los cuales no tienen por qué haber sido empleados en la totalidad de artículos de investigación que forman el Compendio. Se trata de contextualizar su uso, así como las principales referencias bibliográficas que los soportan. Para más información, pueden consultar los capítulos referidos a las contribuciones del doctorando (Capítulos 3, 4, 5, 6 y 7), así como la bibliografía referenciada.

2.3.1. Pre-procesamiento de los datos

Los materiales adquiridos no empiezan a generar resultados desde el primer momento, sino que son procesados previamente. Esta fase previa trata, en primer lugar, de la comprobación de la fiabilidad y veracidad de los datos y, en segundo lugar, de la adaptación de los mismos a los requerimientos de nuestra investigación, especialmente en materia del ámbito de estudio y de la resolución temporal.

2.3.1.a. Control de calidad

Los datos meteorológicos deben seguir unos criterios técnicos objetivos que permitan la comparabilidad entre ellos en materia de instrumental y forma de medición. Por ello, la Organización Meteorológica Mundial (WMO, 2014) ha desarrollado una guía de recomendaciones fundamentales en este sentido. Entre otros aspectos, se indican los requisitos de precisión y exactitud de las mediciones, así como la altura de las mismas sobre el nivel de suelo. Los organismos oficiales de observación meteorológica, tales como AEMET, INAMHI y SENAMHI, que han colaborado aportando datos a esta presente Tesis Doctoral, son miembros permanentes de la Organización Meteorológica Mundial (WMO, 2020), lo que indica que están sujetos a sus condiciones y requisitos. Es por ello que damos por válida la calidad del instrumental y la homogeneidad en la toma de los datos. Sin embargo, un instrumental homologado no impide la existencia de errores puntuales en las mediciones, provocados por un mantenimiento deficiente o por problemas en la transcripción digital de los datos manuales, entre otras causas (Tomás-Burguera et al., 2016). Por ello, el control de calidad de los datos meteorológicos es imprescindible antes de cualquier análisis. En este punto desarrollaremos los aspectos más importantes de los controles de calidad realizados en las diferentes publicaciones que componen la Tesis Doctoral, que se profundizan convenientemente en los capítulos específicos de las publicaciones en las que se han ejecutado:

Los datos procedentes de los organismos oficiales de observación meteorológica han pasado un control de calidad para asegurar la precisión de los mismos y la eliminación de valores erróneos, como valores fuera de rango, o procedentes de errores de transcripción. Este proceso se realiza siguiendo la metodología propuesta por Tomás-Burgera et al. (2016), basada en el trabajo de Durre et al. (2010). En la misma, se descartan valores tomados en fechas erróneas, valores repetidos, escritura como 0º C en días sin dato, unidades de medición erróneas, temperaturas máximas inferiores a las temperaturas mínimas, oscilaciones térmicas diarias mayores a 35º C, así como valores fuera de rango (-35 a 50º C). Además, en función del tipo de análisis, se han descartado también las estaciones meteorológicas con un porcentaje de dato válido inferior al 20% de días del período de análisis. Si llegada esta fase, los valores presentaran algún tipo de duda, se procedió a su total descarte en pos de la calidad de la base de datos.

Los datos procedentes del trabajo de campo tuvieron un profundo control de calidad y validación con la cumplimentación del objetivo específico nº 3 de la Tesis Doctoral "*establecer una serie de criterios metodológicos que permitan el diseño de redes experimentales sobre ámbitos de montaña"* en cuanto a la elección de los sensores, protecciones contra la radiación y elevación sobre el manto de nieve (desarrollado íntegramente en el Capítulo 5), que trató de analizar el rendimiento y precisión de diferentes sensores y protectores de radiación. Además, se analizó la altura sobre el suelo nevado a la que debían instalarse estos dispositivos con el objetivo de lograr la comparabilidad de las mediciones. Con todo ello, se consiguieron establecer unos criterios que se emplearon en los análisis posteriores (Capítulos 6 y 7). De esta forma lograríamos la comparabilidad de sensores e instalaciones, aunque esto es insuficiente para dar validez a los datos finales. Al tratarse de datos automáticos, pueden aparecer problemas derivados de la falta de mantenimiento, tales como enterramientos bajo la nieve, fallos electrónicos por saturación, o el agotamiento de baterías. Se establecieron criterios objetivos para la detección de estos problemas con el fin de eliminar los registros dudosos y poder mantener una base de datos de calidad.

2.3.1.b. Adaptación a ámbitos de estudio y escalas temporales

El otro paso obligado antes de empezar a analizar aspectos propios de la investigación es la adaptación de las bases de datos al ámbito de estudio y escalas temporales en los que estamos trabajando. La adaptación al ámbito de estudio es una fase que se basa en la selección de los observatorios meteorológicos que nos interesen de las redes oficiales de observación meteorológica, o bien en el diseño de la red experimental de nuestros propios sensores instalados mediante trabajo de campo.

Por otro lado, la adaptación de las escalas temporales es necesaria para poder cruzar e interrelacionar información de distintas variables y adaptarnos a la disponibilidad de los datos originales y al fenómeno observado (Figura 20). Los 'saltos' de escala siempre se realizan hacia arriba (esto es, de datos horarios a diarios, de diarios a mensuales, etc.), generalmente mediante promedios o medianas, aunque depende del objetivo específico de cada análisis pueden interesar otras variables como las máximas o las mínimas de cada escala temporal, por ejemplo. La escala estacional sobre la Península Ibérica se ha realizado mediante la agrupación de meses: invierno (diciembre a febrero), primavera (marzo a mayo), verano (junio a agosto) y otoño (septiembre a noviembre). En el caso de las estaciones sobre la región andina de Perú y Ecuador, esta se ha adaptado a las estaciones seca (junio a septiembre) y húmeda (octubre a mayo).

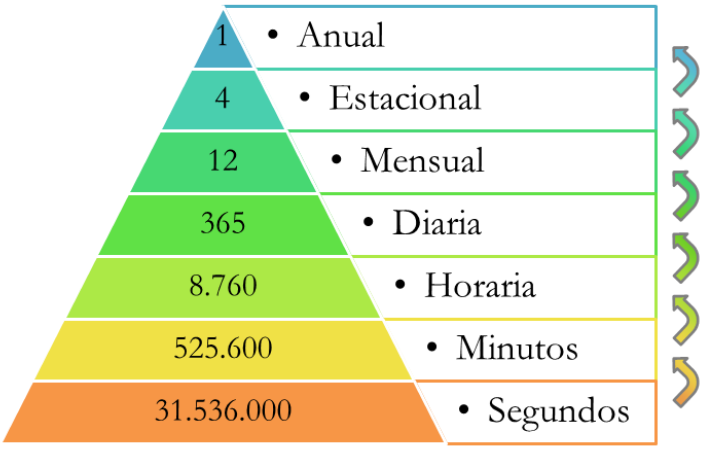

Figura 20. Esquema conceptual del número de muestras posibles bajo diferentes escalas temporales. La aplicación estacional se ha realizado tomando el ejemplo de los trabajos sobre la Península Ibérica, donde generalmente se usan cuatro estaciones de referencia. Elaboración propia.

2.3.2. Gradientes de temperatura del aire

En los ámbitos de montaña, el procedimiento más habitual para estimar y modelizar la temperatura del aire superficial por el territorio es el uso de los gradientes altimétricos, que son definidos como el ratio de cambio en la temperatura del aire por cada unidad de elevación, generalmente medido en grados descendidos por 1000 m ascendidos ($^{o}C\ km^{-1}$) (Fang y Yoda, 1988). Su uso viene derivado del conocido comportamiento de la temperatura del aire en base a la presión atmosférica del mismo, comentado anteriormente (véase Sección 1.2.3 Factores explicativos y medición de la temperatura del aire superficial), y por el cual la temperatura del aire en troposfera libre incrementa con el aumento de presión y, por tanto, con la disminución de altitud sobre el nivel del mar. Estos cambios de temperatura en los que no existen cambios energéticos con otro cuerpo se denominan adiabáticos (Barry y Chorley, 2003).

Cuando el ascenso de aire y el consiguiente enfriamiento del mismo no llega a la temperatura de condensación del vapor de agua contenido, se marca una relación de -9.8º C km^{-1}, denominado gradiente adiabático seco (DALR, por sus siglas en inglés). Sin embargo, si el enfriamiento provoca la condensación del vapor de agua, esta provoca la liberación del calor latente del mismo, compensando en cierta medida el descenso de temperatura, alcanzando el denominado gradiente adiabático húmedo (SALR, por sus siglas en inglés), de unos -6.5º C km^{-1}. Sin embargo, mientras que el DALR es constante, el SALR puede variar con la temperatura, debido que esta influye en la capacidad de almacenar vapor de agua. Por ello, con altas temperaturas el contenido de vapor de agua es mayor, por lo que la liberación de calor latente durante la condensación también lo es, pudiendo debilitar al SALR hasta una relación de -4º C km^{-1} con temperaturas elevadas, e intensificarlo hasta los -9º C km^{-1} con temperaturas extremadamente frías (-40º C) en las que apenas existe capacidad de almacenamiento (Barry y Chorley, 2003).

Sin embargo, estos conceptos teóricos son relativos a la distribución vertical de la temperatura del aire en troposfera libre, fuera de la compleja y multifactorial capa de aire superficial en la que la insolación, la topografía, la orientación o el tipo de superficie afectan de manera crucial. Por ello, en la capa de aire superficial, la mayor parte de los cambios de temperatura no son adiabáticos (consigo mismos), sino diabáticos (procedentes de los intercambios energéticos con los cuerpos circundantes), debido a la constante transferencia energética con la superficie terrestre y a la capacidad del aire para mezclarse y modificar sus características mediante movimientos laterales y turbulentos. La conjunción de todos estos factores genera el llamado gradiente ambiental (ELR, por sus siglas en inglés), que es dinámico espacio-temporalmente, tal y como han mostrado diversos trabajos (Lundquist y Cayan, 2007; Blandford et al., 2008; Pagès et al., 2017), pudiendo ser más intenso que el DALR y más débil que el SALR, ya que no es resultado únicamente de la relación presión atmosférica-altitud, sino de múltiples procesos ambientales.

Debido al enorme dinamismo y complejidad del ELR, habitualmente se ha procedido a estandarizarlo mediante valores de gradientes fijos y constantes que sirvieran de referencia para el comportamiento vertical de la temperatura en la troposfera libre. De esta forma, y con fines relacionados con la aviación, nace el llamado gradiente ambiental medio (MELR, por sus siglas en ingles), al que asignan un valor de -6.5º C km^{-1} (NOAA y NASA, 1976). Sin embargo, y a pesar de que fue diseñado con fines de aplicación en troposfera libre, la falta de información sobre el comportamiento del aire superficial, y su complejidad, hicieron que sirviera muy a menudo como valor de referencia también para aplicaciones superficiales. Esto genera un grave problema espacio-temporal, ya que la relación entre la temperatura del aire superficial y la altitud varía a lo

largo del tiempo y del espacio en función de los factores anteriormente mencionados, por lo que el uso de estos gradientes fijos asume que no existen cambios de ningún tipo y que la relación es constante, pudiendo ser un problema crítico en aplicaciones que requieran gran precisión, como la búsqueda de refugios climáticos o aquellos trabajos que estén basados en reducidas escalas de estudio.

Debido a los problemas generados por el uso de gradientes altitudinales fijos, multitud de trabajos han tratado de encontrar sus propios valores en diversos ámbitos de trabajo como las montañas Rocosas (Hubbart et al., 2007), los Himalayas (Kattel et al., 2015) o los Andes (Hanna et al., 2017), entre otros. Debido a la influencia de múltiples factores, es necesario aislarlos en la medida de lo posible de la variable altitud para conocer su verdadera relación. De esta forma, posteriormente se ha podido analizar esta relación entre altitud y temperatura del aire superficial para intentar detectar qué factores no aislados están provocando que los gradientes oscilen. Es decir, si consiguiéramos aislar completamente la variable altitud, y tuviéramos una masa de aire no saturada, el gradiente debería ser el propio del DALR (-9.8º C km^{-1}), ¿por qué esto no suele suceder? La respuesta está en que en esta relación también interfieren otros factores, como la inestabilidad atmosférica, la diferente insolación de los puntos de muestreo, la topografía, etc. (Lookingbill y Urban, 2003).

En la presente Tesis Doctoral los gradientes altitudinales han sido calculados mediante un método comúnmente aplicado con estos objetivos como es el análisis de regresión (Regniere y Bolstad, 1994; Bolstad et al., 1998; Rolland, 2003; Pepin y Kidd, 2006; Marshall et al., 2007; Blandford et al., 2008; Gardner et al., 2009; Du et al., 2010; Bonnardot et al., 2012; Li et al., 2013; Dumas, 2013; Immerzeel et al., 2014; Kattel et al., 2015, 2018; Joshi y Sambhav, 2018). De este modo se trata de buscar la relación existe entre las variables explicativas y la variable explicada (la temperatura del aire superficial) de una forma rápida y fácilmente aplicable. En la ecuación resultante de los modelos de regresión, cada variable explicativa tendrá un coeficiente que determinará su relación con la variable explicada, por lo que el gradiente altitudinal se corresponde con el coeficiente de la variable altitud (Ecuación 1):

$$(\text{Ec. } 1)\ T' = a_0 + a_1 Alt + a_2 Var_2 + \ldots + a_n Var_n + e$$

La introducción de unas variables explicativas o de otras dependerá, principalmente, de la disponibilidad de datos y de la escala de estudio de cada trabajo, de tal forma que la introducción de variables como la latitud o la distancia al mar tiene sentido en estudios a escala regional, pero no tanto a escala local, donde las distancias entre observatorios son de escasos metros.

Del mismo modo, la introducción de variables micro-topográficas en estudios regionales también podría distorsionar los resultados finales. La variabilidad del gradiente altitudinal resultante implica la existencia de cambios en la relación entre la temperatura del aire superficial y la altitud, que provendrán del efecto distorsionador de otros factores no incorporados en la formulación del modelo. Estos factores distorsionadores son los analizados en esta Tesis Doctoral. El uso de esta metodología es sencillo y fácilmente aplicable, aunque es posible que su linealidad impida en algunos casos representar correctamente la variable (Lundquist et al., 2008). Sin embargo, permite una gran agilidad logística a la hora de calcular los valores, aspecto que hace que sea replicable en cualquier sitio con pocos medios técnicos y avanzar en el conocimiento de una variable muy poco tratada sobre las montañas del planeta. El propio desarrollo y avance en la disciplina tratará de ir complejizando estos métodos en pos de una mejor estimación de la temperatura del aire superficial y un mejor conocimiento de los fenómenos que la determinan.

Durante la Tesis Doctoral, estos cálculos se han realizado con diferentes poblaciones de observatorios meteorológicos, desde las redes operativas de AEMET en España y el INAMHI-SENAMHI en la región andina, hasta los gradientes calculados a partir de nuestros propios registradores en las laderas del valle del río Aragón en Canfranc. En todos los casos, se han introducido la mayor cantidad de observatorios de calidad disponibles tras el control de calidad, puesto que hemos pretendido representar la mayor variabilidad posible. Estos cálculos se realizan a diferentes escalas temporales mediante la aplicación de la misma ecuación, y en función de los diferentes objetivos específicos. Cada escala temporal visibiliza una serie de procesos que son interesantes a la hora de profundizar en el conocimiento de la distribución espacio-temporal de la temperatura del aire superficial, por lo que todas las escalas tienen su interés, desde la horaria para las diferencias noche-día, a las diarias, las mensuales o las estacionales.

2.3.3. Clasificación de tipos de tiempo

Uno de los factores que inciden directamente en la distribución de la temperatura del aire superficial es el movimiento horizontal y vertical de las masas de aire, que viene determinado por la situación atmosférica y las diferentes corrientes (Cuadrat Prats y Pita López, 2006). La circulación general desplaza masas de aire con características propias de los lugares de origen hacia otros territorios (Barry y Chorley, 2003), alterando las condiciones meteorológicas a su paso (temperatura del aire, precipitaciones, contenido de humedad o la presión atmosférica, entre otras). Estos procesos son dinámicos y no responden a un comportamiento fijo y establecido, por lo que existe una variabilidad que se refleja en las condiciones meteorológicas.

Por ello, a menudo se han tratado de clasificar los diferentes estados atmosféricos (o tipos de tiempo) que afectan a un territorio, con el objetivo de describirlos y analizar sus causas y consecuencia. Uno de los primeros intentos de clasificación fue el desarrollado por Lamb (1972) para las Islas Británicas. El método de Lamb está basado en la distribución de la presión atmosférica superficial, la cual marca la dirección e intensidad de los flujos atmosféricos, derivando en una sintética clasificación de siete tipos, adaptados a las Islas Británicas (*ciclónico, anticiclónico, del norte, del noroeste, del oeste, del este y del sur*). Sin embargo, aunque esta metodología estaba basada en la observación diaria de los mapas de presión, era subjetiva y dependía del criterio del experto. Posteriormente, con el objetivo de cuantificar estas direcciones e intensidades de flujo, y respondiendo a la demanda de una clasificación objetiva y replicable en otras áreas, se desarrolla la propuesta de Jenkinson y Collison (1977), finalmente escogida en la presente Tesis Doctoral.

Este método parte de una malla de 16 puntos de presión atmosférica a nivel del mar (Figura 21) sobre la región estudiada para generar una clasificación precisa de 27 tipos de tiempo diferentes, entre los que hay 10 tipos de tiempo básicos (C-ciclónico, A-anticiclónico, N-norte, NE-noreste, E-este, SE-sureste, S-sur, SW-suroeste, W-oeste y NW-noroeste), 16 tipos de tiempo híbridos (CN, CNE, CE, CSE, CS, CSW, CW, CNW, AN, ANE, AE, ASE, AS, ASW, AW y ANW), y 1 para los días que no se ajustan a ninguna categoría (U-inclasificable). El proceso se basa en el cálculo de 4 variables básicas (*W*, *S*, *ZW* y *ZS*, Ecuaciones 2, 3, 4 y 5), relacionadas con la dirección e intensidad de los flujos atmosféricos, y 2 variables derivadas (*F* y *Z*, Ecuaciones 6 y 7), siendo *P* el valor de presión atmosférica a nivel del mar de esa posición dentro de la malla de 16 puntos:

$$\text{(Ec. 2) } W = \big(0.5(P12 + P13)\big) - \big(0.5(P4 + P5)\big)$$

$$\text{(Ec. 3) } S = \left(\frac{1}{\cos(latP8)}\right) \times \Big(\big(0.25(P5 + 2P9 + P13)\big) - \big(0.25(P4 + 2P8 + P12)\big)\Big)$$

$$\text{(Ec. 4) } ZW = \left(\left(\frac{\sin(latP8)}{\sin(latP12)}\right) \times \big(0.5(P15 + P16)\big) - \big(0.5(P8 + P9)\big)\right) - \left(\left(\frac{\sin(latP8)}{\sin(latP4)}\right) \times \Big(\big(0.5(P8 + P9)\big) - \big(0.5(P1 + P2)\big)\Big)\right)$$

$$\text{(Ec. 5) } ZS = \left(\frac{1}{2 \times ((\cos(latP8))^2)}\right) \times$$
$$\Big(\big(0.25(P6 + 2P10 + P14)\big) - \big(0.25(P5 + 2P9 + P13)\big) - \big(0.25(P4 + 2P8 + P12)\big) + \big(0.25(P3 + 2P7 + P11)\big)\Big)$$

$$\text{(Ec. 6) } F = \sqrt{W^2 + S^2}$$

$$\text{(Ec. 7) } Z = ZW + ZS$$

En estas fórmulas, la latitud debe ser incorporada en radianes. Posteriormente, estas variables permiten la obtención de los tipos de tiempo en base a una serie de reglas, que pueden consultarse en los trabajos de Jenkinson y Collison (1977) y de Jones et al. (1993). Aunque este método fue desarrollado originalmente para la región de Gales, pronto fue replicado en diferentes regiones del hemisferio norte (Jones et al., 1993; Buishand y Brandsma, 1997), e incluso fue modificado para poderlo replicar en el hemisferio sur (Sarricolea et al., 2018), debido a su facilidad de cálculo y precisión en los resultados. El método de Jenkinson y Collison también ha sido replicado sobre la Península Ibérica en trabajos previos con el objetivo de caracterizar los diferentes regímenes de precipitación y de temperatura del aire (Spellman, 2000; Trigo y DaCamara, 2000; Cortesi et al., 2014; Peña-Angulo et al., 2016). En algunos casos, y con objetivo de sintetizar los 27 tipos de tiempo originales, se ha procedido a agruparlos en base a diferentes criterios (Jones et al., 1993; Trigo y DaCamara, 2000; Rasilla Álvarez et al., 2002; Sarricolea et al., 2018).

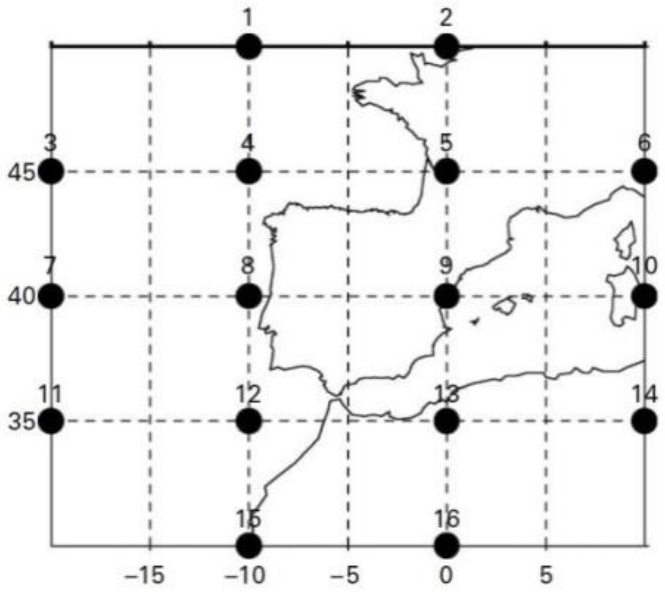

Figura 21. Malla de puntos de presión atmosférica a nivel del mar usada para calcular los tipos de tiempo centrados sobre la España Peninsular. Tomada de López-Moreno y Vicente-Serrano (2007).

La presente Tesis Doctoral ha aplicado esta metodología desarrollada por Jenkinson y Collison para calcular la clasificación original de 27 tipos de tiempo a escala diaria, procediendo posteriormente a realizar algunas agrupaciones y modificaciones puntuales en base a los diferentes objetivos específicos de la investigación. Para ello, se ha desarrollado un código en lenguaje de programación R con el objetivo de automatizar y facilitar el proceso de cálculo para latitudes medias del hemisferio norte (30 – 70º N), tanto para el doctorando como para los diferentes usuarios, disponible en https://github.com/fconavser/TesisCWTs.

2.3.4. Cálculo de la temperatura húmeda y de las horas de producción de nieve

La temperatura húmeda (*TWB*) es la temperatura de un volumen de aire llevado a la saturación y evaporación, siendo por tanto siempre igual o inferior a la temperatura seca (*T*). El cambio de estado a vapor de agua provoca una transformación de la energía como calor latente, causando la pérdida de temperatura en la masa de aire (Cuadrat Prats y Pita López, 2006). Esta variable está interrelacionada directamente con la humedad relativa del aire (*HR*), ya que es esta humedad la que determina el ritmo de evaporación y, por tanto, de enfriado del termómetro húmedo, de tal forma que con una atmósfera saturada, el ritmo de evaporación del termómetro húmedo es muy bajo, con lo que apenas se enfriará con respecto al termómetro seco. La temperatura húmeda fue obtenida para los distintos puntos de muestreo mediante los datos de temperatura del aire y humedad relativa, mediante la relación de la formulación (Ecuación 8) de Stull (2011), que mostró un MAE inferior a 0.3º C:

$$(\text{Ec. } 8)\ TWB = T\ \text{atan}\left[0.151977(HR + 8.313659)^{1/2}\right] + \text{atan}(T + HR) - \text{atan}(HR - 1.676331) + \left(0.00391838(HR)^{3/2}\ \text{atan}\left(0.023101(HR)\right)\right) - 4.686035$$

Para una producción exitosa y eficiente de nieve artificial se necesitan unas condiciones particulares de temperatura del aire y de humedad relativa, generalmente sintetizadas por un umbral de temperatura húmeda. Estas condiciones permiten que, por encima de ese umbral la posibilidad de generar nieve sea descartada, debido a la incapacidad de poder congelar las micro-partículas de agua. Por debajo de ese umbral, al existir menos calor latente en la masa de aire, y estar más cercanos a la temperatura de congelación del agua, la generación de nieve artificial es posible. Este umbral limitante no es fijo, oscilando comúnmente entre una temperatura húmeda de -4 y -1º C, según la tecnología empleada en los cañones de producción. En la presente Tesis Doctoral se ha calculado el número potencial de horas diarias de producción de nieve artificial (*SM*, por sus siglas en inglés) en base a un umbral de temperatura húmeda de -2º C, obtenido a partir de las especificaciones técnicas de los 440 cañones de producción de la estación de esquí de Aramón – Formigal (Technoalpin TL6 y M18).

2.3.5. Cálculo de la insolación estimada

El montante de radiación solar recibida por el terreno (Lookingbill y Urban, 2003; Barry, 2008) en función de las sombras topográficas y la orientación del terreno es crucial para entender mejor la distribución espacio-temporal de la temperatura del aire, especialmente durante las horas diurnas (Florinsky et al., 1994). Debido a la complejidad logística de instalar medidores de

insolación en campo, estimamos esta información a escala horaria mediante modelización. Para ello, usamos un modelo digital de elevaciones de alta resolución espacial (MDT05-LIDAR).

Esta estimación se hizo bajo condiciones de cielo despejado, aplicando la función "*insolation*" del paquete R "insol" (Corripio, 2019), desarrollado en lenguaje R (R-Core-Team, 2013). La función parte de diferentes variables, tanto meteorológicas (temperatura del aire y humedad relativa), como temporales (fecha del año) o geográficas (ubicación, altitud, topografía del entorno y albedo) para hacer un cómputo total de insolación (en W m^{-2} s^{-1}), teniendo en cuenta también la radiación indirecta (Figura 22). De este modo, la insolación fue estimada a escala horaria en cada una de las diez localizaciones del estudio a escala local del río Aragón.

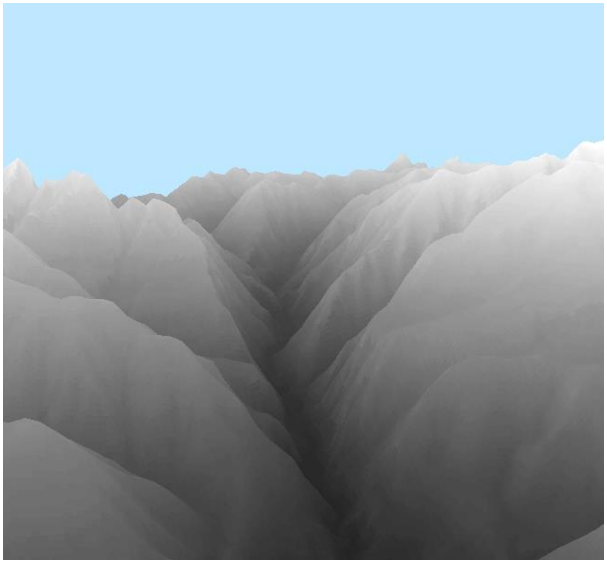

Figura 22. Modelo Digital de Elevaciones del entorno del valle del río Aragón. El MDE es imprescindible en el cálculo de la insolación por parte del paquete "insol", determinando las sombras topográficas y otros condicionantes como la orientación. Elaboración propia.

2.3.6. Análisis clúster

Con el objetivo de clasificar distintos comportamientos de gradientes diarios de temperatura del aire superficial en unos patrones principales, se llevó a cabo un análisis clúster. El análisis clúster es una técnica estadística multivariante, esto es, que analiza el comportamiento de tres o más variables simultáneamente, teniendo como finalidad la creación de clústers o grupos que tengan gran homogeneidad interna y máxima diferencia con respecto al resto de grupos. Este proceso se realiza de forma automática, basándose en el estudio de los casos individuales y en la creación de clústers en base a las distancias existentes entre los individuos. De esta forma, los individuos similares (cercanos) son clasificados en un mismo clúster, mientras que los individuos dispares (distantes) se clasifican en clústers diferentes.

Esta técnica fue aplicada únicamente en el estudio a escala local del valle del río Aragón. De esta forma conseguimos clasificar cada día del período de análisis dentro de un clúster determinado de comportamiento del gradiente. Para ello, y con objeto de estandarizar las unidades, se calcularon las diferencias de temperatura de cada sensor con respecto a un sensor de referencia, en este caso la posición más elevada de cada ladera (Figura 14), convirtiéndose cada una de estas anomalías en una variable, y cada día se convirtió en un caso.

Es necesario indicar que la selección del número de clústers es un motivo de explicación en sí mismo, ya que existen diferentes métodos y aproximaciones. Es por ello que, previamente al desarrollo de esta Tesis Doctoral, fue publicada la función "*NbClust*", dentro del paquete del mismo nombre (Charrad et al., 2014), desarrollada en lenguaje R (R-Core-Team, 2013) y usada en este punto del análisis. Esta función analiza 30 índices diferentes para determinar el número más apropiado de clústers, ofreciendo el de mayor consenso, siendo este el empleado. Para la creación y clasificación de los clústers se empleó la misma función, mediante el método jerárquico Ward.D2 (Murtagh y Legendre, 2014), que minimiza la varianza total dentro del clúster, y usando la distancia euclidiana entre los casos (Figura 23). Este proceso clasificaría, por tanto, cada comportamiento diario de distribución de la temperatura del aire superficial a lo largo de las dos laderas en base al centroide del clúster más próximo. Esto permite la caracterización posterior de esos días mediante el cruce con otras variables de interés, como el viento, la presión atmosférica, o los tipos de tiempo, entre otras.

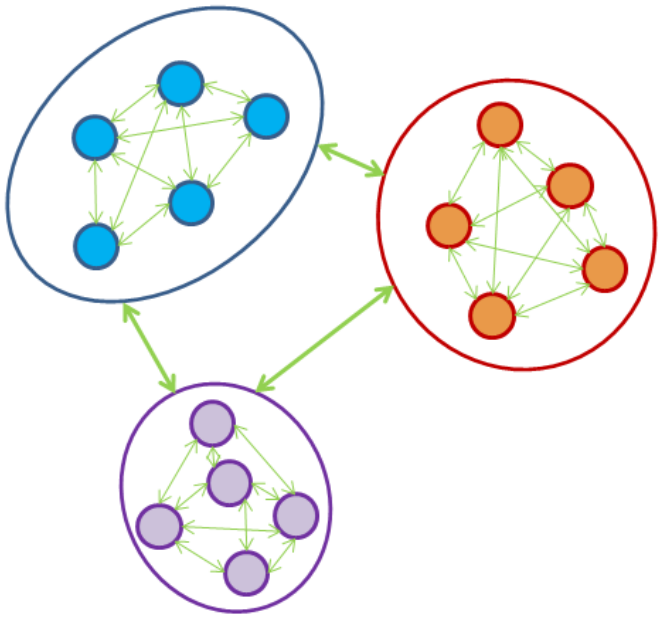

Figura 23. Método de Ward, que minimiza la varianza interna de cada clúster, mientras que maximiza la existente con los otros clústers. Elaboración propia.

2.3.7. Modelos de árboles de regresión

Teniendo el objetivo de establecer una serie de criterios claros de gestión para la estación de esquí de Aramón – Formigal en la producción de nieve artificial, se decidió construir modelos de árboles de regresión, que permiten estimar una variable con pasos poco complejos y fácilmente interpretables. Estos modelos están basados en métodos no paramétricos (Breiman et al., 1984), esto es, que no requieren la distribución normal de sus poblaciones, y tienen el objetivo de crear un modelo predictivo en función de diversas variables explicativas y en función de la suma de los cuadrados de los residuos obtenidos en cada agrupación (o ramificación). Estos árboles de regresión van estableciendo valores predichos mediante ramificaciones jerárquicas de las variables explicativas, siendo así más prácticos a la hora de establecer unos valores predichos concretos. Esta técnica fue aplicada en la estimación de los gradientes altitudinales de horas de temperatura húmeda y de producción de nieve artificial, a partir de las variables explicativas de velocidad de viento, humedad relativa y temperatura del aire.

Para ello, se empleó el método de división CHAID (Kass, 1980), mediante el software IBM-SPSS Statistics (v.26), indicando una máxima profundidad de árbol de 5 niveles, indicando un número mínimo de 20 casos por nodo (20 días). La complejidad del árbol y sus ramificaciones finales están generalmente basadas en el tamaño del árbol, que minimiza la desviación del modelo a partir de un método interno de validación cruzada, maximizando el coeficiente de determinación del modelo (Molotch et al., 2005). Paralelamente, el tamaño del árbol fue ajustado basándonos en un límite de 1% entre las relaciones de varianza. De este modo, la gestión de Aramón – Formigal cuenta con unos criterios concretos y unos umbrales de decisión para conocer los días de mayor o menor productividad de nieve artificial.

2.3.8. Otros estadísticos

2.3.8.a. Error Medio Absoluto

El Error Medio Absoluto (MAE, por sus siglas en inglés) es una medida de la distancia o diferencia entre dos variables, de las cuales una funciona como variable de referencia, frente a otra que está siendo testeada, siempre referidas a un mismo fenómeno. A lo largo de la Tesis Doctoral, los cálculos de MAE han estado referidos a diferentes variables, como la evaluación del rendimiento de diferentes tipos de termómetro o de garitas de protección frente a la radiación, o la comparación entre temperatura del aire observada y estimada mediante la aplicación de un gradiente estimado de temperatura del aire, entre otros.

2.3.8.b. Intervalos de confianza

Con el objetivo de ver la incertidumbre en la estimación de los gradientes de temperatura del aire de la Península Ibérica, se calcularon los intervalos de confianza (a un 95%) para las combinaciones entre tipos de tiempo y mes para cada una de las regiones montañosas. Este intervalo viene determinado a partir de la bondad del ajuste del modelo de regresión y del número de observatorios que formaron parte del cálculo.

2.3.8.c. Validación de gradientes

En el Capítulo 3, referido al estudio a escala regional sobre la España Peninsular, se proponen una serie de valores de referencia para los gradientes de temperatura del aire superficial en base a diferentes criterios (teniendo en cuenta únicamente el mes, mes y tipo de tiempo, sólo el tipo de tiempo, etc.). Estos valores de referencia son testeados para analizar su rendimiento. Para ello, se analizaron las diferencias entre las temperaturas observadas y las estimadas por cada uno de estos valores de referencia. En primer lugar se calculó, para un 20% de observatorios meteorológicos y cada día del período de análisis, la temperatura potencial a nivel del mar, aplicando el modelo de regresión obtenido del 80% restante de ese día. En segundo lugar, se aplicaron a esta temperatura potencial diferentes valores de referencia de gradientes de temperatura del aire para estimar la temperatura a la elevación original del observatorio. Entre ellos, se encontraron el MELR (-6.5º C km^{-1}), pero también valores obtenidos mediante nuestros cálculos, como el valor medio de la zona de estudio, el de ese mes del año, el del tipo de tiempo de ese día, o combinaciones de los mismos. En tercer lugar, se calculó el MAE entre este valor estimado y el valor observado original para determinar cuál de estos gradientes de referencia aplicados tuvo mejor rendimiento.

En el Capítulo 4, referido al estudio a escala regional sobre la región andina de Ecuador y Perú, se llevó a cabo un proceso de validación cruzada sobre un 10% de los observatorios mediante la comparación entre la temperatura del aire observada en ellos y la estimada mediante el modelo calculado con el 90% restante.

2.3.8.d. Comparación de muestras

Con el objetivo de analizar la heterogeneidad entre dos muestras, se llevó a cabo la prueba no paramétrica de Mann-Whitney (Wilcoxon, 1945). De esta forma se identificaron las diferencias estadísticamente significativas existentes entre muestras independientes. El método está basado en la comparación de las muestras, teniendo en cuenta también la población incorporada y la variabilidad de los muestreos. Las diferencias se analizaron con un nivel de significancia de 0.05.

Capítulo 3

GRADIENTES DE TEMPERATURA SOBRE LA ESPAÑA PENINSULAR Y SUS ÁREAS MONTAÑOSAS

Publicado como:

Navarro-Serrano, F., López-Moreno, J., Azorin-Molina, C., Alonso-González, E., Tomás-Burguera, M., Sanmiguel-Vallelado, A., Revuelto, J., Vicente-Serrano, S.M. 2018. Estimation of near-surface air temperature lapse rates over continental Spain and its mountain areas. *International Journal of Climatology* 38: 3233-3249. DOI: https://doi.org/10.1002/joc.5497.

Los autores agradecen a WILEY el permiso para publicar de manera íntegra el contenido de la publicación, que puede encontrarse en https://rmets.onlinelibrary.wiley.com/doi/abs/10.1002/joc.5497.

Received: 6 November 2017 | Revised: 10 February 2018 | Accepted: 14 February 2018 | Published on: 23 March 2018

DOI: 10.1002/joc.5497

International Journal of Climatology RMetS

RESEARCH ARTICLE

Estimation of near-surface air temperature lapse rates over continental Spain and its mountain areas

F. Navarro-Serrano[1] | J. I. López-Moreno[1] | C. Azorin-Molina[2] | E. Alonso-González[1] | M. Tomás-Burguera[3] | A. Sanmiguel-Vallelado[1] | J. Revuelto[4] | S. M. Vicente-Serrano[1]

[1]Department of Geoenvironmental Processes and Global Change, Pyrenean Institute of Ecology, CSIC, Zaragoza, Spain

[2]Regional Climate Group, Department of Earth Sciences, University of Gothenburg, Gothenburg, Sweden

[3]Estación Experimental Aula Dei, CSIC, Zaragoza, Spain

[4]Météo-France, CNRS, CNRM, UMR3589, CEN, Grenoble, France

Correspondence
F. Navarro-Serrano, Department of Geoenvironmental Processes and Global Change, Pyrenean Institute of Ecology, CSIC (Spanish Research Council), Campus de Aula Dei, P.O. Box 202, Zaragoza 50080, Spain.
Email: fnavarro@ipe.csic.es

Funding information
Ministerio de Educación, Cultura y Deporte, Grant/Award Number: FPU Program - FPU13/02976, FPU Program - FPU15/00742; European Union, Grant/Award Number: CLIMPY; Consejo Superior de Investigaciones Científicas, Grant/Award Number: I+D Program - CGL2014-52599-P; Cordis, Grant/Award Number: STILLING project-703733

Although the mean environmental lapse rate (MELR) value (a linear decrease of −6.5 °C/km) is the most widely used, near-surface (i.e., non-free atmosphere) air temperature lapse rates (NSLRs; measured at ~1.5 m height) are variable in space and time because of their dependence on topography and meteorological conditions. In this study we conducted the first analysis of the spatial and temporal variability of NSLRs for continental Spain and their relationship to synoptic atmospheric circulation (circulation weather types [CWTs]), focusing on major mountain areas including the Pyrenees, Cantabrian, Central, Baetic, and Iberian ranges.

The results showed that the NSLR varied markedly at spatial and seasonal scales and depended on the dominant atmospheric conditions. The median NSLR values were weaker (less negative) than the MELR for the mountain areas (Pyrenees −5.17 °C/km; Cantabrian range −5.22 °C/km; Central range −5.78 °C/km; Baetic range −4.83 °C/km; Iberian range −5.79 °C/km) and for the entire continental Spain (−5.28 °C/km). For the entire continental Spain the steepest NSLR values were found in April (−5.80 °C/km), May (−5.58 °C/km), and October (−5.54 °C/km) because of the dominance of northerly and westerly advections of cold air. The weakest NSLR values were found in July (−4.67 °C/km) and August (−4.78 °C/km) because of the inland heating, and in winter because of the occurrence of thermal inversions. As the use of the MELR involves the assumption of large errors, we propose 1 zonal, 12 monthly, 11 CWTs, and 132 hybrid monthly–CWTs NSLRs for each of the mountain ranges and for the entire continental Spain. More regional studies are urgently needed to accurately assess the NSLR as a function of atmospheric circulation conditions.

KEYWORDS
air temperature, complex terrain, lapse rate, mountain climate, weather types

1 | INTRODUCTION

Although near-surface (i.e., ~1.5 m elevation above the ground) air temperature is not a challenging climate variable to extrapolate spatially, modelling in mountain areas can be associated with substantial uncertainties because of the complex topography (Barry, 1992; Whiteman *et al.,* 1999; Minder *et al.,* 2010). In mountain areas the most common procedure for modelling near-surface air temperature involves using air temperature lapse rate, which is defined as the ratio of air temperature change per elevation unit, generally measured in °C/km (Fang and Yoda, 1988). The most widely used spatio-temporal fixed air temperature lapse rate is the mean environmental lapse rate (MELR: −6.5 °C/km); this parameter was presented by Barry and Chorley (1987) as a global lapse rate calculated for the free atmosphere air temperature, and not for near-surface air temperature. However, caution is required in use of the MELR because of the spatio-temporal variability of near-surface air temperature lapse rates (Pepin *et al.,* 1999; 2011;

Rolland, 2003; Lundquist and Cayan, 2007; Blandford *et al.,* 2008; Minder *et al.,* 2010; Dumas, 2013; Kattel *et al.,* 2013; Miró *et al.,* 2018), especially in areas covered by ice or snow (Braun and Hock, 2004). This is because the fixed MELR assumes no changes among seasons, synoptic conditions, or topographic complexity (Barry, 1992).

Near-surface temperature lapse rates (NSLRs) are linear observed ratios between temperature and elevation, and they can be calculated for a specific or aggregated time and space. They are readily calculated, but this requires fine temporal and spatial data resolution to enable most of the variability to be represented. NSLR have been widely used in scientific fields including Glaciology, Hydrology, Forestry, Agricultural Sciences, and Ecology (Martinec *et al.,* 1983; Running *et al.,* 1987; Barringer, 1989; Pepin, 2001; Rolland, 2003; Hanna *et al.,* 2005; Blandford *et al.,* 2008; Minder *et al.,* 2010; Immerzeel *et al.,* 2014). NSLRs can be calculated from maximum ($NSLR_{max}$), minimum ($NSLR_{min}$), or mean ($NSLR_{mean}$) air temperatures, in line with Harlow *et al*. (2004) and Minder *et al*. (2010). Many scientists only used elevation to calculate NSLR (e.g., Immerzeel *et al.,* 2014; Heynen *et al.,* 2016), but air temperature changes are not only due to elevation. Therefore, more complex approaches including regional multiple regression analyses are needed to isolate the effect of elevation on air temperature from other geographical and topographical variables (e.g., latitude, longitude, slope, and continentality), which strongly affect the spatial variability of near-surface air temperatures (Bolstad *et al.,* 1998). In doing so, it may become possible to determine the specific elevation effect on the distribution of temperatures. Observed NSLRs and fixed MELRs can differ because the distribution of air temperatures are strongly dependent on the topography (Barry, 2001; Pepin, 2001; Marshall *et al.,* 2007) and other atmospheric parameters such as air humidity, wind speed and wind direction, cloud cover, and radiative conditions (Kattel *et al*., 2013). Moreover, NSLRs vary between day and night because of the heat flux exchanges between the atmosphere and the ground surface (Gardner *et al*., 2009). In most situations near-surface air temperatures drop with increasing elevation. However, stable atmospheric conditions can reverse this effect forming valley cold pools (i.e., thermal inversions with warm air above, and cold air near the valley floor), especially during the winter months (e.g., Barry, 1992; Whiteman *et al.,* 1999; Pagès and Miró, 2010). Cold-air pools are formed as a result of both cooling of the ground due to long-wave radiation and nocturnal downslope winds, but more complex mechanisms help/avoid in their formation (Whiteman *et al*., 1999).

Several studies have reported significant temporal variability in NSLR at daily and seasonal scales in various mountain regions including the Rocky (Kunkel, 1989; Pepin and Losleben, 2002; Blandford *et al.,* 2008) and Appalachian (Bolstad *et al*., 1998) mountains in the United States, in China (Fang and Yoda, 1988; Tang and Fang, 2006; Du *et al.,* 2010), the Himalayan mountains (Kattel *et al.,* 2013; Immerzeel *et al.,* 2014), the Alps (Rolland, 2003; Dumas, 2013; Kirchner *et al.,* 2013; Nigrelli *et al.,* 2017), and polar areas (Marshall *et al*., 2007). These studies have reported steeper NSLRs under unstable atmospheric conditions, and marked differences in NSLR have been found as a function of synoptic conditions (Pepin *et al.,* 1999; 2011; Pepin, 2001; Blandford *et al.,* 2008; Holden and Rose, 2011; Kirchner *et al.,* 2013; Miró *et al.,* 2018). These findings indicate that these effects need to be taken into account when analysing the temporal and spatial evolution of the NSLR.

Continental Spain (CS) and its mountain areas is a topographically complex region, and several studies have investigated the effect of changes in the frequency of weather types on various climate parameters (Trigo and Dacamara, 2000; Tomás *et al.,* 2004; García-Herrera *et al.,* 2007; López-Moreno and Vicente-Serrano, 2007; Buisan *et al.,* 2015a). However, the spatio-temporal variability of NSLRs in the region has only been investigated in a limited number of local studies in the Pyrenees (Puigdefábregas, 1969; Pepin and Kidd, 2006; Pagès and Miró, 2010). These few previous studies have analysed the effects of regional topography on NSLRs comparing atmospheric model results with observed data, but none of them have investigated how different circulation weather types (CWTs) affect seasonal patterns of NSLR in the main mountain areas of CS. In addition, previous investigations analysed daily maximum temperature lapse rates ($NSLR_{dmax}$), daily minimum temperature lapse rates ($NSLR_{dmin}$), and daily mean temperature lapse rates ($NSLR_{dmean}$) separately, following Harlow *et al.* (2004) and Minder *et al*. (2010). It is important to clarify the sign of lapse rates. A steeper lapse rate indicates a more negative and rapid decrease in air temperature with elevation, while a weaker rate indicates less negative or even positive changes in air temperature with elevation. To assess the similarity of NSLRs among the months, weather types, and regions considered in the present work, Wilcoxon–Mann–Whitney test (Wilcoxon, 1945) was used.

This study is the first attempt to investigate NSLR across CS with focus on assessing the seasonal and synoptic variability of this parameter over the major mountain ranges. The spatio-temporal analysis of NSLRs is strongly needed in Spain because the complex terrain makes air temperature challenging to predict. In addition, this approach helps to improve hydrologic models and snow simulations what is particular useful in areas subject to water scarcity and desertification, as is the case of Spain (Vicente-Serrano, 2007; García-Ruiz *et al.,* 2011). The aims of the study are (a) to define annual and seasonal NSLR reference values; (b) to quantify the effect of seasonality and different weather types on NSLR at a regional scale; and (c) to assess the uncertainty associated with the use of different reference NSLR,

including the MELR (−6.5 °C/km) and other NSLR defined in this study, based on seasonality and weather types.

2 | DATA

2.1 | Study area

CS is characterized by its complex topography, with many mountain ranges located within the area (Figure 1). The average elevation of the entire CS is 688 m above sea level (m a.s.l.; standard deviation = 399 m), and the highest elevation point is the Mulhacén peak (Baetic range) at 3,479 m a.s.l. The climate of CS is mainly influenced by the Atlantic Ocean, the Mediterranean Sea, and its proximity to both subtropical and temperate air mass. The climatic conditions are mainly humid and temperate in the North Atlantic area (defined as Cf in the Köppen classification), and dry and warm in the remainder (Cs in the Köppen classification). Different climates occur depending on exposure to the Atlantic Ocean or the Mediterranean Sea, the continentality, and the complex topography of the region. Based on the variability of annual rainfall, Rodríguez-Puebla *et al*. (1998) identified four main precipitation regions across Spain: northwest, south–southwest, the Mediterranean coast, and the Cantabrian coast. Total annual precipitation ranges from more than 2,000 mm in the northern slopes of the Cantabrian range, the Pyrenees and the Central range to less than 400 mm in the driest areas of the Baetic and the Iberian ranges (Agencia Estatal de Meteorología, 2011). In this study we analysed the NSLR for the entire CS, with focus on its five major mountain ranges (Figure 1): (a) the Pyrenees, in the northeast; (b) the Cantabrian range, in the northwest; (c) the Central range, in the middle west; (d) the Baetic range, in the southeast; and (e) the Iberian range, in the middle east. The elevation ranges and distributions, and the size of the study area for the five mountain ranges are summarized in Table 1.

2.2 | Air temperature data and digital elevation model

Complete records of daily maximum and minimum near-surface (i.e., ∼1.5 m height) air temperature were obtained from the Spanish State Meteorological Agency (AEMET) database. A total of 3,950 air temperature series were

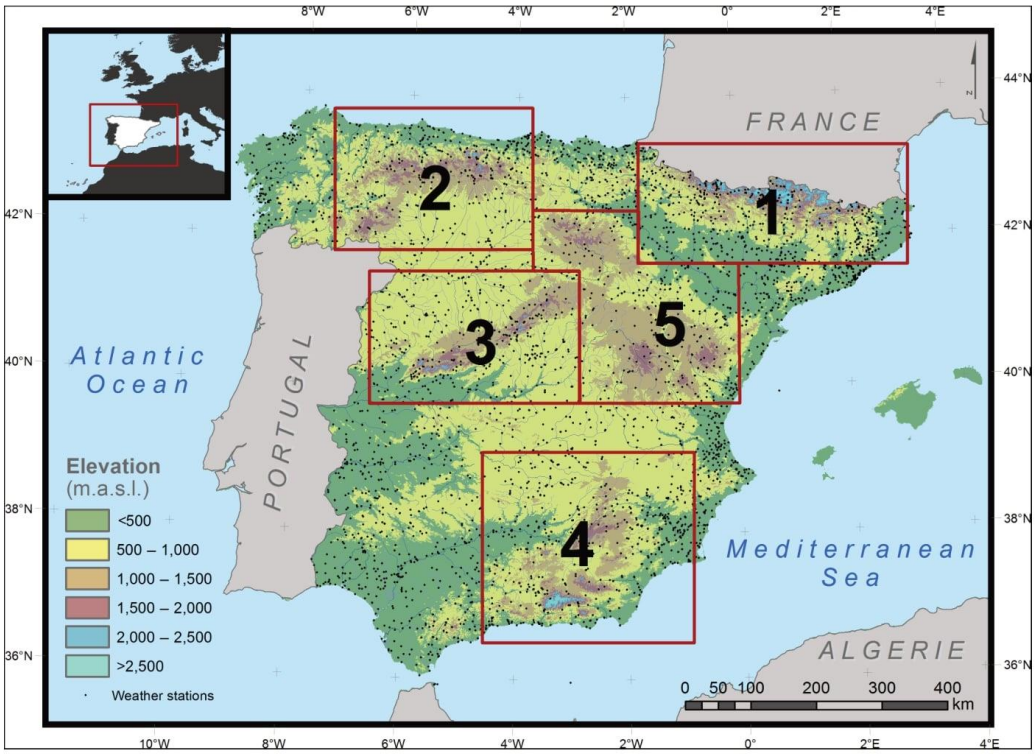

FIGURE 1 Terrain map of CS showing the location of weather stations (black dots) used in this study; red boxes and numbers show to the mountain areas analysed: (1) Pyrenees; (2) Cantabrian range; (3) Central range; (4) Baetic range; and (5) Iberian range [Colour figure can be viewed at wileyonlinelibrary.com]

TABLE 1 Elevations and dimensions of the study areas

Study area	Dimensions	Elevation ranges (m a.s.l.)	Elevation distribution (m a.s.l., in %)					
			<500	500–1,000	1,000–1,500	1,500–2000	2000–2,500	>2,500
Pyrenees	412 × 80 km (≈75,000 km^2)	Coastline (0), Aneto peak (3404)	43.62	29.97	13.02	7.54	4.85	1.00
Cantabrian range	300 × 216 km (≈65,000 km^2)	Coastline (0), Torre Cerredo peak (2648)	13.96	57.75	22.28	5.77	0.24	In.
Central range	320 × 200 km (≈65,000 km^2)	Tagus river (190), Almanzor peak (2592)	14.71	65.55	16.28	3.13	0.33	In.
Baetic range	320 × 290 km (≈93,000 km^2)	Coastline (0), Mulhacén peak (3479)	23.28	56.73	16.00	3.20	0.55	0.24
Iberian range	160 × 90 and 240 × 200 km (≈65,000 km^2)	Coastline (0), Moncayo peak (2314)	14.16	38.73	42.72	4.37	0.02	0

available for the entire CS (the distribution of weather stations is shown in Figure 1). Among them, 664 are located in the Pyrenees, 455 in the Cantabrian range, 376 in the Central range, 650 in the Baetic range, and 390 in the Iberian range. This is the densest network of weather stations available for calculating NSLR across CS. The majority of weather stations are located in the lower parts of valleys (<1,500 m a.s.l.), with <5% being located in high-mountain areas (see the distribution in Figure 1 and elevation ranges in Figure 2).

Near-surface air temperature data were obtained based on recommendations of the World Meteorological Organization (World Meteorological Organization, 2008) in relation to radiation shields and height above the ground. Two types of high-quality thermometer that meet the World Meteorological Organization (WMO) requirements for a measurement range of −30 to 50 °C were used in the station network (Buisan *et al.,* 2015b) and were protected from solar radiation by Stevenson radiation shields. Geographic variables (i.e., latitude, longitude, and elevation) were derived from metadata supplied by the AEMET, and validated using geographical information systems (GISs). With the aim of maximizing long-term analysis and a good station density, we analysed the period from December 1979 to August 2015. The start and end dates for data acquisition from each station, and the number of data gaps varied over time, with the largest number of daily observations available since the 1990s (Figure 2). A digital elevation model (DEM) having a pixel size of 900 m^2, derived from the Shuttle Radar Topography Mission (SRTM) (Farr *et al.*, 2007), was used to calculate the distance of each weather station to the coast. The hydrographic network was obtained from the IECA website (https://www.juntadeandalucia.es/institutodeestadisticaycartografia/DERA/index.htm), which is derived from the World Map Vector (VMap0) developed by United States Defense Mapping Agency (United States Defense Mapping Agency, 2000).

3 | METHODS

3.1 | Quality control and pre-processing

Daily maximum and minimum near-surface air temperature data were subject to quality control to ensure data accuracy. Large weather station networks can contain data outliers introduced by errors during the conversion of manual records. Therefore, we applied the robust quality control procedure described by Tomás-Burguera *et al.* (2016), involving the removal of questionable records according to Durre *et al.* (2010). Following the quality control process a total of 21.21 × 10^6 daily maximum and 21.19 × 10^6 daily minimum records were available covering the entire CS and its mountain areas for the December 1979 to August 2015 period.

3.2 | CWT classification

Daily weather types over CS were determined using the Jenkinson and Collison (1977) classification, which is based on the Lamb's weather type scheme (Lamb, 1972). This method is based on daily sea level pressure (SLP) data from 16 grid points covering the entire Iberian Peninsula (Figure 3). The SLP data were obtained from the NCEP-NCAR reanalysis (5 × 5° longitude–latitude) data set (Basnett and Parker, 1997) (https://climatedataguide.ucar.edu/climate-data/ncar-sea-level-pressure). Equations and rules applied for 40°N are:

$$\mathrm{SF\,(southerly\ flow)} = 1.305[0.25(p5+2\times p9+p13) - 0.25(p4+2\times p8+p12)],$$

$$\mathrm{WF\,(westerly\ flow)} = [0.5(p12+p13) - 0.5(p4+p5)],$$

$$\mathrm{ZS\,(meridional\ vorticity)} = 0.85\times[0.25(p6+2\times p10+p14) - 0.25(p5+2\times p9+p13) - 0.25(p4+2\times p8+p12) + 0.25(p3+2\times p7+p11)],$$

$$\mathrm{ZW\,(zonal\ vorticity)} = 1.12\times[0.5(p15+p16) - 0.5(p8+p9)] - 0.91\times[0.5(p8+p9) - 0.5(p1+p2)],$$

$$F\,(\mathrm{total\ flow}) = 0.5\times\left(\mathrm{SF}^2+\mathrm{WF}^2\right),$$

$$Z\,(\mathrm{total\ vorticity}) = \mathrm{ZS}+\mathrm{ZW},$$

where p is the sea level atmospheric pressure value (in hPa) at grid-point number position.

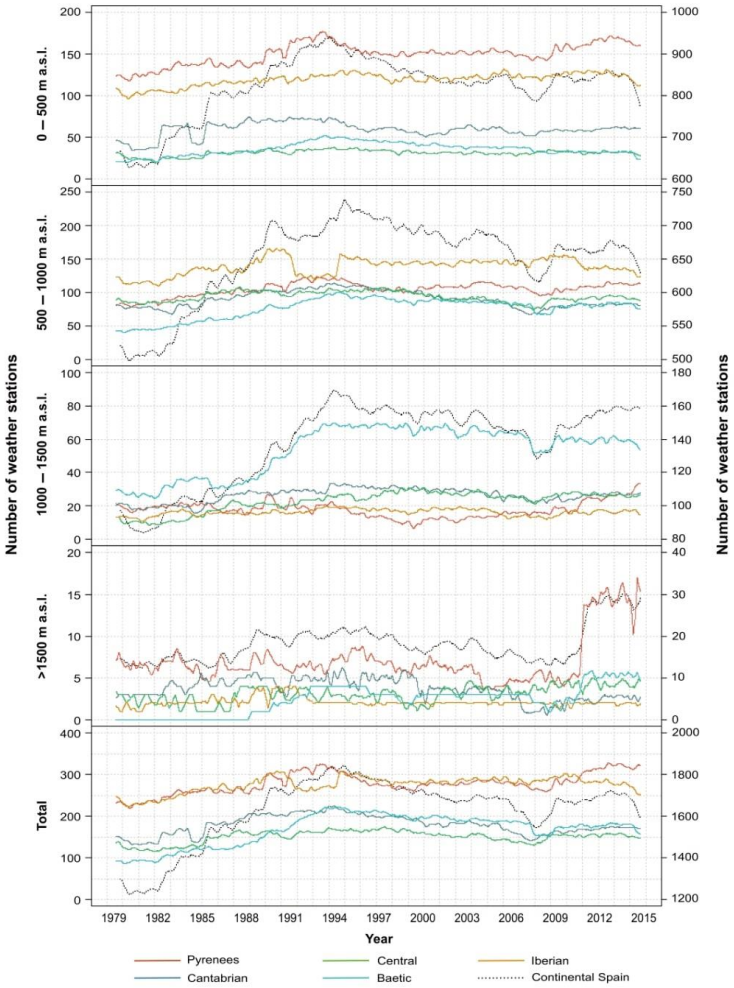

FIGURE 2 Number of weather stations having daily air temperature data as a function of elevation range. Mountain ranges were represented on the left *y* axis. Total amount of CS was represented on the right *y* axis [Colour figure can be viewed at wileyonlinelibrary.com]

Rules:

1. If |Z| is less than *F*, flow is essentially straight, corresponding to a Lamb directional type, for example, *W*.
2. If |Z| is greater than 2*F*, then the pattern is strongly cyclonic or anticyclonic, corresponding to Lamb's C (cyclonic) and A (anticyclonic) types.
3. If |Z| lies between *F* and 2*F*, then the flow in moderately cyclonic or anticyclonic, corresponding to a Lamb hybrid type, with the direction specified, for example, CNW (cyclonic–northwest).
4. If *F* is less than 6, there is light indeterminate flow, corresponding to Lamb's U type (unclassified).

The Jenkinson and Collison's weather type classification has been widely used and successfully applied to the Iberian Peninsula (e.g., Goodess and Palutikof, 1998; Spellman, 2000; Trigo and Dacamara, 2000; López-Moreno and Vicente-Serrano, 2007, to name but a few). The classification includes 27 CWTs including: unclassified (U); anticyclonic (A); cyclonic (C); 8 directional CWTs (N, NE, E, SE, S, SW, W and NW); and 16 hybrid cyclonic or anticyclonic and directional CWTs (CN, CNE, CE, CSE, CS, CSW, CW, CNW, AN, ANE, AE, ASE, AS, ASW, AW, and ANW). To assess the relationships between CWTs and NSLR, the 16 hybrid CWTs were classified according to their directional flow following Trigo and Dacamara (2000), that is, simplifying the interpretation of the results to two pure (A and C) and eight directional (N, NE, E, SE, S, SW, W, and NW) CWTs. We also defined a severe anticyclonic type (A+) as a third pure CWT in order to identify days having strong stability. A day was classified as severe anticyclonic (A+) if: (a) the day was classified as pure anticyclonic (A) and (b) SLP in *p*8 was >1,030 mb.

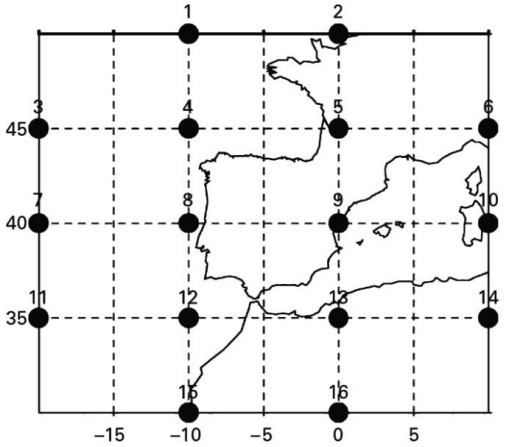

FIGURE 3 Grid of SLP points used to classify the CWTs over the Iberian Peninsula

In addition, unclassified (U) days were reclassified by three rules based on SLP values of $p8$ grid point, following the procedure adopted by Rasilla Álvarez *et al*. (2002): (a) if $p8 < 1{,}020$ mb, the day was reclassified as pure cyclonic (C); (b) if $p8$ is between 1,020 and 1,030 mb, the day was reclassified as pure anticyclonic (A); (c) if $p8 > 1{,}030$ mb, the day was reclassified as severe anticyclonic (A+).

3.3 | Daily NSLR

The daily maximum near-surface air temperature lapse rate ($NSLR_{dmax}$) and the daily minimum near-surface air temperature lapse rate ($NSLR_{dmin}$) were calculated for each mountain range and for the entire CS. $NSLR_{dmax}$ and $NSLR_{dmin}$ were computed using all available simultaneous data (Figure 2). The daily average number of weather stations used in the regression was 279 in the Pyrenees, 179 in the Cantabrian range, 150 in the Central range, 275 in the Baetic range, 167 in the Iberian range, and 1,623 for the entire CS. The daily average equated to one weather station every 266 km^2 in the Pyrenees, 362 km^2 in the Cantabrian range, 426 km^2 in the Central range, 337 km^2 in the Baetic range, 373 km^2 in the Iberian range, and 301 km^2 throughout the entire CS. Figure 2 shows that lower elevation ranges (i.e., 0–500 and 500–1,000 m a.s.l.) were well represented, which contrast with the low density of weather stations at higher elevations for all mountain ranges.

Following the procedure proposed by Rolland (2003), multiple regressions were used to compute daily maximum and minimum NSLRs from maximum and minimum air temperatures (T_{max} and T_{min}, respectively) of stations. Thus, it can be quantified the effect of elevation on air temperature without including other topographic and geographic variables (Bolstad *et al.,* 1998; Blandford *et al.,* 2008; Gardner *et al.,* 2009). For calculating $NSLR_{dmax}$ and $NSLR_{dmin}$, the elevation of each station along with other geographic variables including latitude, longitude, and distance to the sea were taken into account. The distance of each station to the nearest river (until order 4 according to Gravelius classic system, being order 1 the largest stream) was also recorded as a proxy in order to account for the influence of relative micro-topographic features, such as thermal inversions and cold-air pools (Lookingbill and Urban, 2003; Whiteman *et al*., 2004). Equation (1) summarizes this methodology:

$$T'_{max} \text{ and } T'_{min} = a_0 + a_1\text{Elev} + a_2\text{Lat} + a_3\text{Lon} + a_4\text{Sea} + a_5\text{Riv} + e, \quad (1)$$

where T'_{max} and T'_{min} are the maximum and minimum near-surface air temperatures, respectively (in °C); Elev, Lat, Lon, Sea, and Riv are the elevation above sea level (in m a.s.l.), latitude (in UTM), longitude (in UTM), distance to the sea (in km), and distance to the nearest river (in km), respectively; e is a regression error; and a_1, a_2, a_3, a_4, and a_5 are the regression coefficients, with a_1 corresponding to the daily maximum ($NSLR_{dmax}$) or minimum ($NSLR_{dmin}$) lapse rate, following the procedure of Rolland (2003). Confidence intervals (95%) for each $NSLR_{dmax}$ and $NSLR_{dmin}$ were calculated. The mean daily average near-surface air temperature lapse rate ($NSLR_{dmean}$) was obtained by averaging $NSLR_{dmax}$ and $NSLR_{dmin}$. The $NSLR_{dmean}$ was computed on a daily basis and then grouped by months and CWTs, with the aim of developing reference NSLR values (i.e., 1 zonal, 12 monthly, 11 CWTs, and 132 monthly–CWTs) from median values. The Wilcoxon–Mann–Whitney is a nonparametric statistic test that allows the comparison between two independent series to know the similarity between their distributions. In this work, we compare the total amount of daily NSLR, distributed by (a) months in the same study area (396 combinations); (b) study areas in the same month (180 combinations); (c) CWTs in the same study area (396 combinations); and (d) study areas in the same CWTs (180 combinations).

3.4 | Near-surface lapse rate validation

To quantify the accuracy of the proposed NSLR reference values, a validation process was applied. This was based on the use of potential temperature, that is, the air temperature at a common sea level reference applying lapse rates (Marsh, 2009). The following steps were applied: (a) the daily random selection of 20% of weather stations available for a subset of the study period (1981–2010). This subset period was chosen to adapt the analysis to a normalized climate period of 30 years; (b) the sea level potential daily maximum and minimum air temperature was estimated for each of the randomly selected weather stations using a daily multiple regression model (Equation (1)), based on the other 80% of

stations; (c) sea level potential mean air temperature was calculated averaging sea level potential daily maximum and minimum air temperature data calculated (see step b); and (d) real elevation estimated air temperature was calculated to each station from the sea level potential mean air temperature by applying different NSLR proposed reference values (zonal, monthly, CWTs, and hybrid monthly–CWTs NSLRs; explained in section 3.3), and the widely used MELR.

Mean absolute error (MAE) statistics were calculated from the difference between real observed air temperature and estimated (see step d above) and was summarized for winter (December–February: DJF), spring (March–May: MAM), summer (June–August: JJA), and autumn (September–November: SON).

4 | RESULTS

4.1 | Climatology of the $NSLR_{dmean}$

Figure 4 shows the daily mean air temperature lapse rate ($NSLR_{dmean}$) across the CS and its mountain areas for December 1979 to August 2015. We found a marked variability in daily values (measured as the standard deviation), and large differences between each of the five mountain areas and the CS. This variability ranged from 2.06 °C/km for the Central range to 1.40 °C/km for the Pyrenees, being 1.15 °C/km for the entire CS. For the majority of days the daily $NSLR_{dmean}$ was weaker than the MELR, especially in the Pyrenees and the Iberian range. The median daily zonal values (Table 2) were −5.17 °C/km for the Pyrenees, −5.22 °C/km for the Cantabrian range, −5.78 °C/km for the Central range, −4.83 °C/km for the Baetic range, −5.79 °C/km for the Iberian range, and −5.28 °C/km for the CS. The $NSLR_{dmax}$ and $NSLR_{dmin}$ values (see Figures S1 and S2, Supporting information) showed larger daily variability than the $NSLR_{dmean}$, while the median daily zonal values (see Tables S1 and S2) showed steepest lapse rates for the $NSLR_{dmax}$ in the Pyrenees and the Central and the Iberian ranges, and for the $NSLR_{dmin}$ in the Cantabrian and the Baetic ranges.

Figure 5 shows box-and-whisker plots of $NSLR_{dmean}$ for each month and for the various mountain areas, revealing clear differences among them. The Wilcoxon–Mann–Whitney test showed that there were significant differences ($p < .05$) among monthly $NSLR_{dmean}$ values for most of the combinations between months in each mountain area (351 of 396 combinations). Except for the summer months in the Central range, where the $NSLR_{dmean}$ values were very similar to the MELR, the other months showed lapse rates noticeably weaker than −6.5 °C/km. In the Pyrenees and the Central and the Iberian ranges, the steepest monthly $NSLR_{dmean}$ values occurred in summer and spring (May–September), weakening in autumn and winter. In contrast, the steepest monthly $NSLR_{dmean}$ values for the Cantabrian and the Baetic ranges were recorded in the coldest months (i.e., November–February), while decreased in spring and summer. The CS showed the steep NSLR value during each equinoctial seasons (i.e., April–May and October–November), being of lesser magnitude in winter and summer (i.e., December–January and July–August). The Iberian range recorded the least seasonal variability, and the Central range the greatest. The winter months were typically more variable than those in summer. The median monthly NSLR values (Table 2) showed that the two most extreme months for each mountain range were April (−5.71 °C/km) and December (−4.16 °C/km) for the Pyrenees; February (−6.03 °C/km), and July (−4.02 °C/km) for the Cantabrian range; June (−6.71 °C/km) and December (−3.92 °C/km) for the Central range; November (−5.59 °C/km) and July (−3.03 °C/km) for the Baetic range; and April (−6.28 °C/km) and December (−5.28 °C/km) for the Iberian range. CS had the steepest median monthly $NSLR_{dmean}$ in April (−5.80 °C/km) and the weakest in July (−4.67 °C/km). A separate analysis of $NSLR_{dmax}$ and $NSLR_{dmin}$ revealed that the seasonality was less marked for $NSLR_{dmin}$, especially for the Cantabrian range and the CS (see Figures S3 and S4). Median monthly values of $NSLR_{dmax}$ and $NSLR_{dmin}$ were also calculated and can be found in Tables S1 and S2.

4.2 | Synoptic $NSLR_{dmean}$ analysis

The weather type classification revealed that the most frequent CWTs (Figure 6) were the A (23.4%, 85.8 day/year) and C (17.4%, 63.8 day/year) aggregated types, followed by the N type (11.1%, 40.6 day/year). The less frequent CWTs were the S (3.3%, 12 day/year) and the A+ (3.8%, 13.8 day/year) types. Summer months were influenced by the N, NE, A, and C types, whereas in winter the occurrence of CWTs varied, with the A+ and the W advections being the most frequent ones.

The Wilcoxon–Mann–Whitney test identified significant differences ($p < .05$) in $NSLR_{dmean}$ among the CWTs for the majority of combinations between CWTs in each mountain area (347 of 396 combinations). Figure 7 shows that the steepest $NSLR_{dmean}$ occurred with the N, NE, and NW weather types for the majority of mountain ranges and the CS. In contrast, the weakest $NSLR_{dmean}$ took place under the A+ and A types, and southerly advections (S and SE). An exception to this pattern occurred in the Cantabrian range, where the steepest $NSLR_{dmean}$ corresponded to the SW and W advections. In the case of the Baetic range the A and A+ types did not reduce the $NSLR_{dmean}$, as occurred for the rest of mountain areas.

The $NSLR_{dmean}$ for each CWTs and regions are shown in Table 2, being the extreme values as follows: the Pyrenees (N –5.75 °C/km, A+ −3.55 °C/km); the Cantabrian range (SW –7.07 °C/km, SE −3.65 °C/km); the Central range (N –6.70 °C/km, A+ −2.29 °C/km); the Baetic range (NW –5.69 °C/km, A −4.32 °C/km); and the Iberian range (NE −6.83 °C/km, S –4.57 °C/km). CS had the steepest $NSLR_{dmean}$ with the NW type (−6.10 °C/km) and the weakest with the A+ type (−4.30 °C/km). The variability of

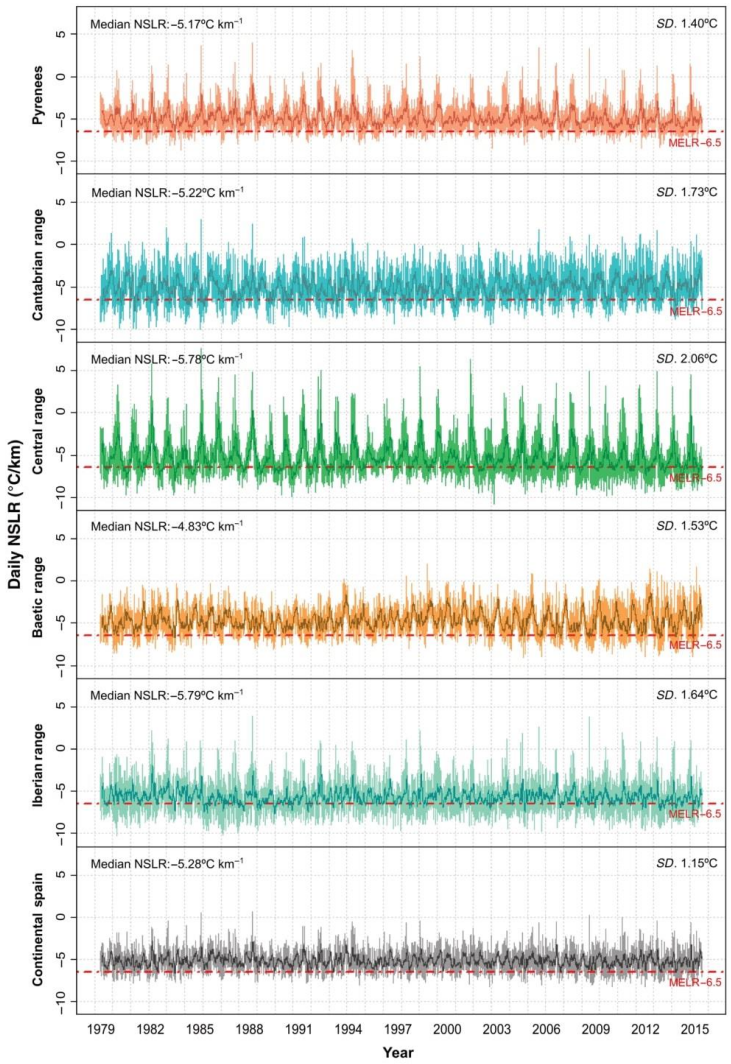

FIGURE 4 $NSLR_{dmean}$ (°C/km). Dark coloured lines show the 30-day running average. Dashed red lines show the standard and fixed MELR of −6.5 °C/km. *SD*: standard deviation [Colour figure can be viewed at wileyonlinelibrary.com]

$NSLR_{dmean}$ was similar for all CWTs, except for A and A+ situations showing large standard deviations values. The behaviour of the $NSLR_{dmax}$ and $NSLR_{dmin}$ (see Figures S5 and S6) was similar, with less variability for the $NSLR_{dmin}$ values. Median values for $NSLR_{dmax}$ and $NSLR_{dmin}$ under the different CWTs were also calculated (see Tables S1 and S2).

4.3 | Combined monthly synoptic analysis

Figure 8 shows the differences in $NSLR_{dmean}$ values for all possible combinations of CWTs and months. These values can be considered to be reference values for NSLR, and 132 monthly–CWTs combinations are being proposed here as reference values for each study area. In the vast majority of cases $NSLR_{dmean}$ values were weaker than the MELR value (−6.5 °C/km). In addition, it was observed that steepest $NSLR_{dmean}$ values tended to occur in spring and early summer months (i.e., April–June), and in autumn (i.e., September–November), associated with northerly CWTs (principally N and NW) and atmospheric instability across CS. On the contrary, the weakest $NSLR_{dmean}$ values occurred in summer (i.e., June–August) and winter (i.e., December–January), associated with southerly (S) and anticyclonic (A and A+) CWTs, respectively, with stable atmospheric conditions dominating across the CS. In particular, the Cantabrian and the Baetic ranges also exhibited very weak $NSLR_{dmean}$ values under all possible CWTs in summer months. Figure 8 shows the accuracy of the proposed values (at the 95% confidence interval), which was

TABLE 2 Proposed monthly and CWTs NSLR (°C/km) reference values

Zonal reference near-surface air temperature lapse rate ($NSLR_{dmean}$)						
	Pyrenees	Cantabrian range	Central range	Baetic range	Iberian range	CS
Zonal	−5.17	−5.22	−5.78	−4.83	−5.79	−5.28
Monthly reference near-surface air temperature lapse rate ($NSLR_{dmean}$)						
Month	**Pyrenees**	**Cantabrian range**	**Central range**	**Baetic range**	**Iberian range**	**CS**
Jan	−4.33	−6.02	−4.10	−5.28	−5.49	−5.16
Feb	−4.97	−6.03	−4.98	−5.58	−5.88	−5.50
Mar	−5.22	−5.80	−5.48	−5.17	−6.00	−5.47
Apr	−5.71	−5.60	−6.28	−5.36	−6.28	−5.80
May	−5.66	−5.12	−6.51	−4.83	−6.19	−5.58
Jun	−5.45	−4.25	−6.71	−3.94	−5.99	−5.09
Jul	−5.21	−4.02	−6.36	−3.03	−5.44	−4.67
Aug	−5.19	−4.28	−6.01	−3.58	−5.45	−4.78
Sep	−5.34	−4.74	−5.82	−4.79	−5.80	−5.39
Oct	−5.21	−5.57	−5.29	−5.31	−5.79	−5.54
Nov	−4.72	−5.82	−4.78	−5.59	−5.78	−5.47
Dec	−4.16	−5.93	−3.92	−5.42	−5.28	−5.15
Synoptical reference (by CWT) near-surface air temperature lapse rate ($NSLR_{dmean}$)						
CWT	**Pyrenees**	**Cantabrian range**	**Central range**	**Baetic range**	**Iberian range**	**CS**
N	−5.75	−5.82	−6.70	−5.29	−6.81	−5.91
NE	−5.52	−5.04	−6.43	−4.62	−6.83	−5.63
E	−5.16	−4.20	−5.85	−4.86	−6.25	−5.49
SE	−4.55	−3.65	−4.85	−5.31	−5.34	−5.02
S	−4.63	−5.58	−4.98	−5.08	−4.57	−4.98
SW	−5.00	−7.07	−5.39	−4.65	−5.09	−5.37
W	−5.58	−6.92	−5.97	−5.23	−6.06	−5.88
NW	−5.71	−6.45	−6.52	−5.69	−6.63	−6.10
C	−5.20	−4.81	−6.13	−4.84	−5.63	−5.15
A	−4.79	−4.62	−4.92	−4.32	−5.25	−4.79
A+	−3.55	−4.87	−2.29	−4.58	−4.97	−4.30

determined from goodness of fit to the model regression and the number of stations involved in the calculation (bolded values in Figure 8 imply <±1.0 °C/km). The Central range was the most difficult region for defining a $NSLR_{dmean}$ value (~±1.6 °C/km), with the Baetic range being the easiest one (~±0.9 °C/km). The CS showed a low absolute error (~±0.4 °C/km) as a result of the large number of stations and the robustness of the regression models. In terms of uncertainty, the southerly (S, SE) and anticyclones (A, A+) CWTs displayed the largest values while the northerly (N, NW) CWTs showed the lowest ones. Finally, the median $NSLR_{dmax}$ and $NSLR_{dmin}$ values for all possible combinations of CWTs and months were calculated and are provided in Figures S7 and S8.

4.4 | Proposed reference $NSLR_{dmean}$ values and validation

Table 2 shows our proposal of zonal, monthly, and CWTs reference $NSLR_{dmean}$ values (Table 2) for CS and the major mountain ranges.

The accuracy of the proposed $NSLR_{dmean}$ values is shown in Table 3 for each study area and season. The fixed MELR and zonal NSLR displayed the largest errors in all study areas, while the hybrid monthly–CWTs showed the smallest errors. For the Cantabrian and the Iberian ranges the proposed monthly values were associated with larger errors than the proposed CWTs values, which contrasts to the findings for the Central and the Baetic ranges. Both monthly and CWTs values were similar for the Pyrenees, which showed the smallest errors, whereas the largest errors were found for the Central and the Iberian ranges. Seasonally, the MAE values revealed marked differences, which were largest for the fixed lapse rates (MELR and zonal).

5 | DISCUSSION

Near-surface air temperature lapse rates based on records of daily averages ($NSLR_{dmean}$) were analysed for the major mountain ranges in CS. Our results found spatial changes in $NSLR_{dmean}$ as a function of the month of the year and synoptic conditions (i.e., CWTs). The weather station network used in this study included a large number of weather stations at elevation ranges from 0 to 1,500 m a.s.l, but with

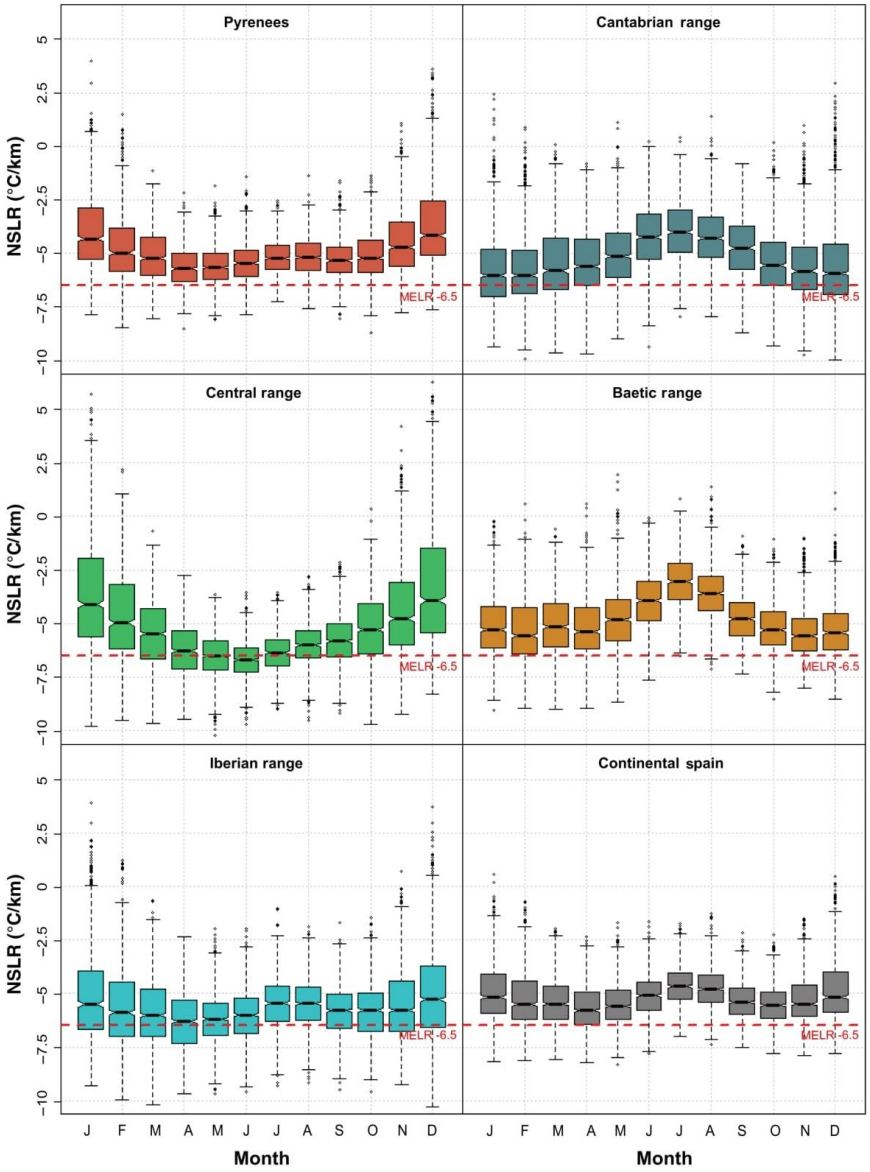

FIGURE 5 Monthly box-and-whisker plots of $NSLR_{dmean}$ (°C/km) for the five mountain ranges and the entire CS. Dashed red lines show the standard and fixed MELR of −6.5 °C/km. The median (black line), 25th and 75th percentile ranges (boxes), 75th + 1.5IQR (upper whisker), 25th − 1.5IQR (bottom whisker), and the extreme values (>75th + 1.5IQR and <25th − 1.5IQR) are represented [Colour figure can be viewed at wileyonlinelibrary.com]

few number of stations above 1,500 m a.s.l. The lack of high-elevation stations is a common problem in many previous studies (e.g., Blöschl, 1991; Rolland, 2003; Benavides *et al.,* 2007; Du *et al.,* 2017). Thus, our results are robust for interpolating air temperatures at low and medium elevations, whereas lapse rate values for high-elevation mountain areas have to be interpreted with caution. For instance, low humidity and katabatic winds could markedly affect the slope of NSLRs (Heynen *et al.*, 2016) in areas of complex topography at high elevations. Therefore, the increase in the density of high-elevation stations would help to overcome this limitation over mountainous areas.

FIGURE 6 Frequency (in number of days per year; day/year) of synthetized CWTs, based on Jenkinson and Collison (1977) classification for December 1979 to August 2015 [Colour figure can be viewed at wileyonlinelibrary.com]

Previous studies have reported a strong inverse relationship between elevation and mean annual air temperature (Barry and Chorley, 1987), highlighting the strength of our methodological approach to calculate NSLR based on changes in elevation. Overall, we found that the $NSLR_{dmean}$ (−5.28 °C/km) was weaker than the standard MELR value (−6.5 °C/km), which is widely used in the scientific literature; this suggests that the use of the MELR to interpolate near-surface air temperatures may lead to large inaccuracies, particularly over high-elevation mountain ranges. Additionally, we found large differences in $NSLR_{dmean}$ values among the studied mountain ranges (the Pyrenees: −5.17 °C/km; the Cantabrian range: −5.22 °C/km; the Central range: −5.78 °C/km; the Baetic range: −4.83 °C/km; and the Iberian range: −5.79 °C/km), and also in the accuracy (standard deviation) of the estimated averages (the Pyrenees: 1.40 °C/km; the Cantabrian range: 1.73 °C/km; the Central range: 2.06 °C/km; the Baetic range: 1.53 °C/km; the Iberian range: 1.64 °C/km; and CS: 1.15 °C/km). Differences in the slope of $NSLR_{dmean}$ and its variability might be due to the degree of continentality and its effect on prevailing atmospheric conditions for each mountain region. This phenomenon has been previously reported for polar (Marshall *et al*., 2007) and Chinese (Fang and Yoda, 1988; Li *et al*., 2013) areas; in the latter case especially for mountain ranges receiving less radiation in the northern slopes (Lookingbill and Urban, 2003), as quantified by McCutchan and Fox (1986). Thus, dry continental conditions (e.g., in the Central and the Iberian ranges) resulted in the highest zonal $NSLR_{dmean}$ values, whereas the increased moisture and exposure to oceanic winds and cloudiness in lowland areas might lead to a reduced zonal $NSLR_{dmean}$, as occurred for the Baetic and the Cantabrian ranges (Capel Molina, 2000). The Pyrenees may present an intermediate pattern, with oceanic/sea influences in the westernmost and easternmost areas, and continental influences (albeit prone to severe winter thermal inversions) in the central area. Regional topography is a key element in understanding the behaviour of near-surface air temperature lapse rates. Beyond the mean annual $NSLR_{dmean}$ values, it is imperative to consider their temporal variability (Bolstad *et al*., 1998; Minder *et al*., 2010). Our results showed a marked seasonality for the entire CS, and also for each of the five mountain areas analysed. The results for CS showed that the steepest $NSLR_{dmean}$ occurred in the equinoctial seasons (autumn and spring), and decreased in winter and summer. The cold season is typically found to be associated with weak $NSLR_{dmean}$ values, because of the prevalence of stable atmospheric conditions and the development of thermal inversions (Blöschl, 1991; Bolstad *et al.,* 1998; Tang and Fang, 2006; Marshall *et al.,* 2007; Blandford *et al.,* 2008; Gardner *et al.,* 2009; Kattel *et al.,* 2013). Our results for thermal inversions are consistent with the findings at local scales reported for the Pyrenees by Pagès and Miró (2010) and Puigdefábregas (1969), who identified a marked weakening of NSLRs under anticyclonic conditions. In the majority of the analysed mountain areas the steepest $NSLR_{dmean}$ values were found in spring, which is consistent with previous studies in the Alps (Dumas, 2013; Kirchner *et al.,* 2013), the Pennines (Pepin, 2001), and the Rocky mountains (Blandford *et al.,* 2008; Pepin and Seidel, 2011). This behaviour might be due to the persistence of snow cover at highest stations in winter and, occasionally, in spring due to heat exchange and albedo as previously proposed by Rolland (2003), Pepin and Kidd (2006), or Pagès *et al*. (2017). In the mountain area nearest to the ocean (the Cantabrian range), the weakest $NSLR_{dmean}$ occurred in summer. This might be associated with the local synoptic effects

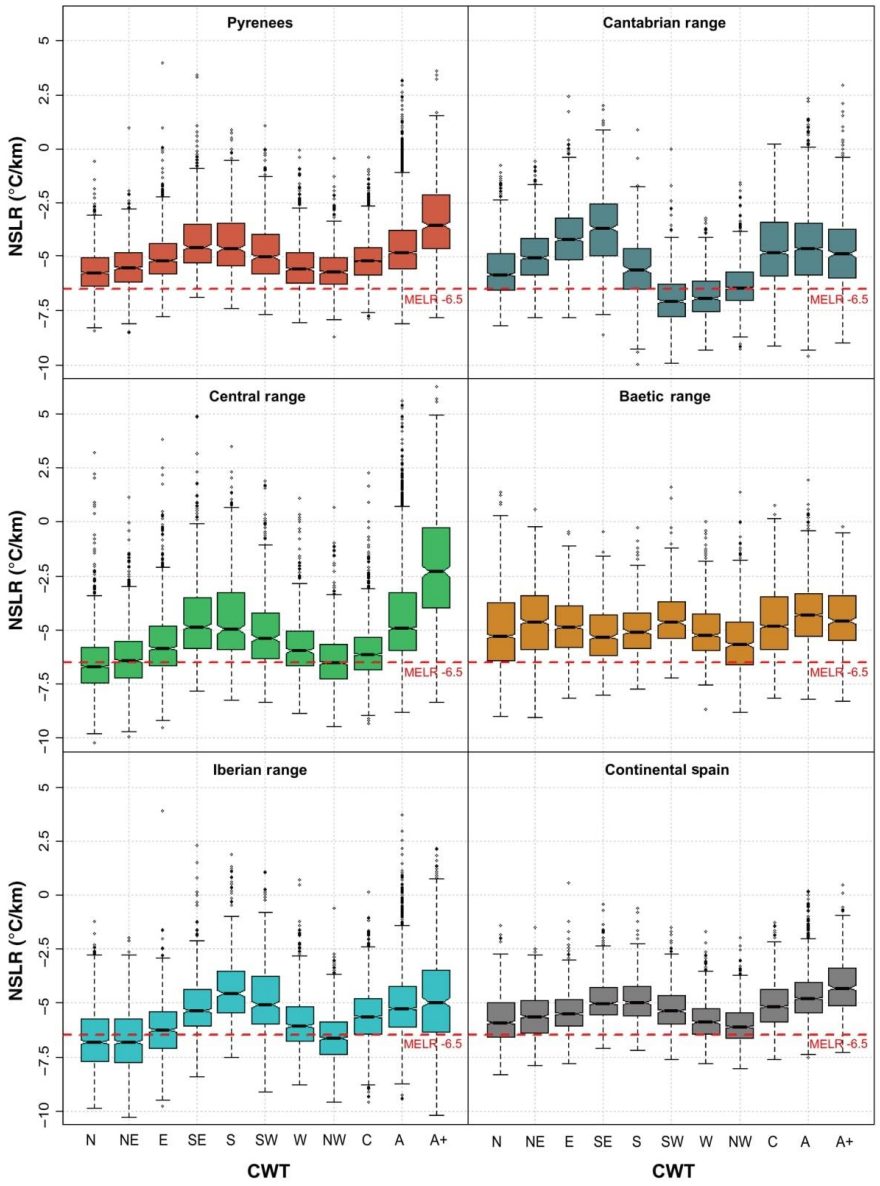

FIGURE 7 Variability in the $NSLR_{dmean}$ (°C/km) for various synthetized CWTs. Dashed red lines show the standard and fixed MELR of −6.5 °C/km. The median (black line), the 25th and 75th percentile range (boxes), 75th + 1.5IQR (upper whisker), 25th − 1.5IQR (bottom whisker), and the extreme values (>75th + 1.5IQR and <25th − 1.5IQR) are represented [Colour figure can be viewed at wileyonlinelibrary.com]

in summer months, in which northerly flows result in low stratiform clouds along the coastal fringe. This also occurred for the Baetic range, but over this mountain are this could be related to the heat in the warm inland valleys, beyond the coastal and temperate locations. Generally, the variability of $NSLR_{dmean}$ values was great in winter for all mountain ranges because the occurrence of both stable and unstable atmospheric circulations.

We also found that weather types have a significant impact on the $NSLR_{dmean}$. This finding, particularly for the Pyrenees and the Central range, is consistent with previous studies showing that the most stable weather types

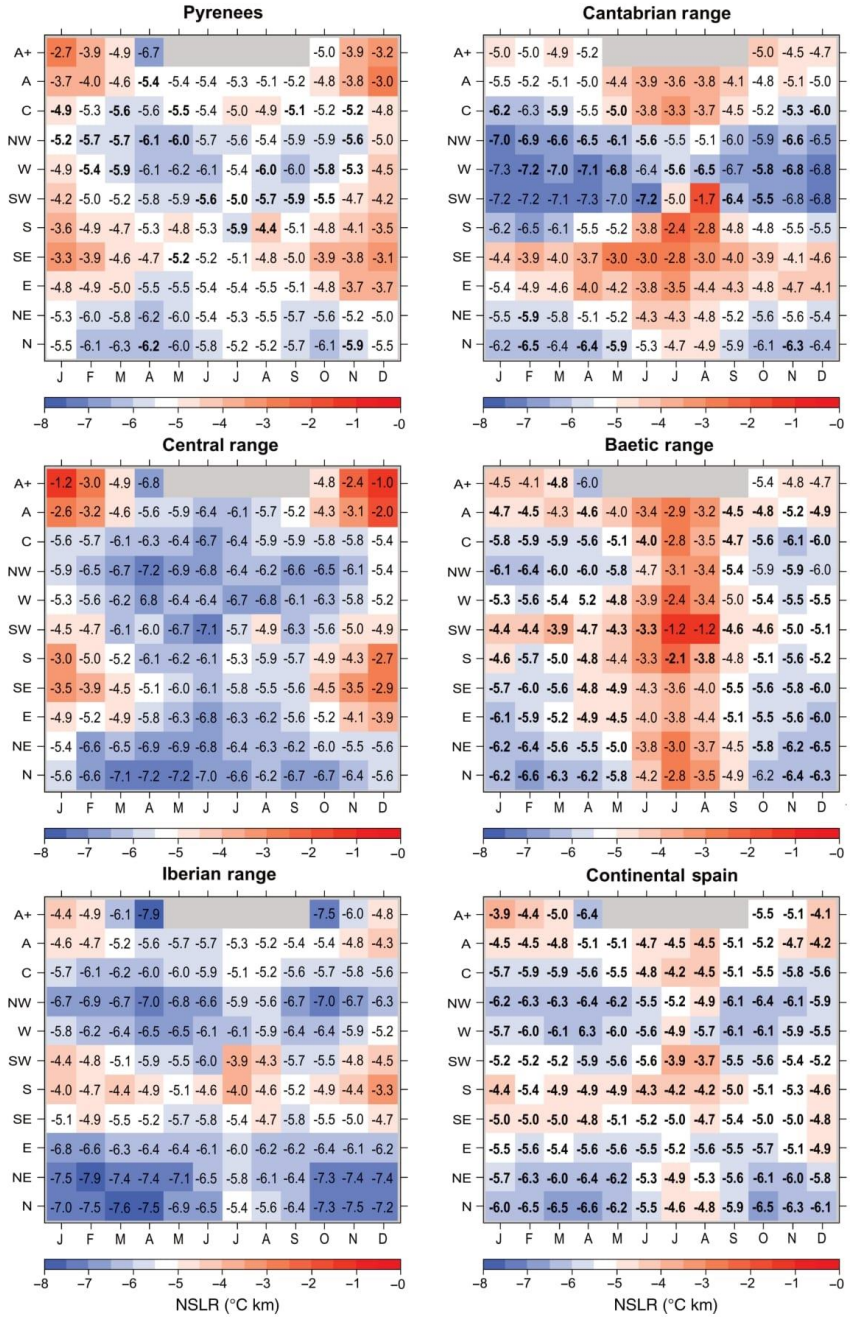

FIGURE 8 Monthly median $NSLR_{dmean}$ (°C/km) for different months and synthetized CWTs. Accuracy ±1 °C (95% confidence interval) is represented by bold values [Colour figure can be viewed at wileyonlinelibrary.com]

TABLE 3 MAEs (°C) derived for the proposed NSLRs by season, based on 20% of the stations

MAE (in °C) derived of proposed NSLR application by seasons (test: 20% of stations)										
	Pyrenees					**Cantabrian range**				
NSLR	**D–J–F**	**M–A–M**	**J–J–A**	**S–O–N**	**Mean**	**D–J–F**	**M–A–M**	**J–J–A**	**S–O–N**	**Mean**
MELR	1.90	1.33	1.42	1.49	1.54	1.68	1.62	2.06	1.64	1.75
Zonal	1.62	1.25	1.27	1.30	1.36	1.68	1.49	1.64	1.51	1.58
Monthly	1.58	1.23	1.26	1.29	1.34	1.64	1.49	1.52	1.49	1.54
CWT	1.57	1.23	1.27	1.28	1.34	1.60	1.41	1.55	1.42	1.50
Monthly–CWT	1.53	1.21	1.26	1.26	1.32	1.55	1.39	1.46	1.40	1.45
	Central range					**Baetic range**				
NSLR	**D–J–F**	**M–A–M**	**J–J–A**	**S–O–N**	**Mean**	**D–J–F**	**M–A–M**	**J–J–A**	**S–O–N**	**Mean**
MELR	2.55	1.56	1.50	1.87	1.87	1.61	1.66	2.18	1.54	1.75
Zonal	2.21	1.58	1.59	1.69	1.77	1.52	1.51	1.70	1.42	1.54
Monthly	2.02	1.51	1.49	1.65	1.67	1.50	1.51	1.58	1.40	1.50
CWT	2.02	1.51	1.54	1.63	1.68	1.50	1.49	1.71	1.42	1.53
Monthly–CWT	1.82	1.45	1.48	1.56	1.58	1.47	1.48	1.56	1.39	1.48
	Iberian range					**CS**				
NSLR	**D–J–F**	**M–A–M**	**J–J–A**	**S–O–N**	**Mean**	**D–J–F**	**M–A–M**	**J–J–A**	**S–O–N**	**Mean**
MELR	2.08	1.59	1.67	1.66	1.75	1.72	1.53	1.81	1.52	1.65
Zonal	1.95	1.59	1.58	1.59	1.68	1.60	1.47	1.63	1.43	1.53
Monthly	1.92	1.57	1.57	1.59	1.66	1.60	1.46	1.61	1.43	1.53
CWT	1.82	1.51	1.59	1.52	1.61	1.57	1.44	1.63	1.42	1.52
Monthly–CWT	1.78	1.48	1.54	1.50	1.58	1.56	1.43	1.60	1.41	1.50

(i.e., anticyclonic situations) are associated with the lowest $NSLR_{dmean}$ values, mainly because of the high occurrence of thermal inversions (Pepin and Kidd, 2006; Marshall *et al.,* 2007), whereas the highest $NSLR_{dmean}$ values occur under unstable synoptic conditions (Kirchner *et al.*, 2013) with cold air in the mid- to high layers of the troposphere. We also found extreme high pressures (A+) were associated with very weak $NSLR_{dmean}$ values. In contrast, northerly weather types showed the steepest $NSLR_{dmean}$ values, consistent with previous studies in Europe (Pepin, 2001; Holden and Rose, 2011), and Antarctica (Southern Hemisphere) (Braun and Hock, 2004). Northerly situations bring cold-air masses over the CS, in particular at high mountain elevations, resulting in increased $NSLR_{dmean}$ values. As an exception, the steepest $NSLR_{dmean}$ values occur under SW flows in the Cantabrian range, where the Foehn effect causes an overheating along the coast. Other atmospheric parameters such as wind, humidity, and atmospheric pressure can also affect the $NSLR_{dmean}$ (Blandford *et al.*, 2008; Dumas, 2013; Li *et al.*, 2013; Immerzeel *et al.*, 2014) and are directly related to the prevailing synoptic conditions. Future studies will be directed towards improving our understanding of the effect of these atmospheric parameters on the $NSLR_{dmean}$. However, the complexity of CS suggests that the relative impact of each atmospheric parameter may vary spatially.

Here we also proposed reference $NSLR_{dmean}$ values as a function of the time of the year, CWTs, and study area. For instance, the combinations of months and CWTs revealed that the effects of the northwest CWT are not the same in January and August. In addition, the analysis of confidence intervals enabled the estimation of uncertainty. In some study areas the seasonality tended to have a large effect (e.g., the Baetic range), while in others the $NSLR_{dmean}$ values were more influenced by synoptic conditions (e.g., the Cantabrian range). The results and reference values obtained in this study are not necessarily representative for other regions, as there was large spatial, seasonal, and synoptic variability, and local factors can play a key role (Nunez and Calhoun, 1986; Pepin and Seidel, 2005; Marshall *et al.,* 2007). However, the approach presented can serve as guide to improving estimates of $NSLR_{dmean}$ in other regions.

Validation of the reference NSLR results showed that the MAE decreased for monthly, CWTs, and hybrid monthly–CWTs. In this context, Marshall *et al.* (2007) and Minder *et al.* (2010) not recommended the use of fixed lapse rates. The study areas showing large variability in $NSLR_{dmean}$, corresponded to regions with high MAE. In this regard seasonal differences were marked, especially between winter (i.e., December–February) and equinoctial seasons (i.e., March–June; September–November). This is because synoptic conditions can usually change from 1 day to the other in winter, while atmospheric instability tends to dominate in spring and autumn. There were no large differences between the proposed monthly and CWTs NSLRs in the validation process. The best approach was the proposed hybrid monthly–CWTs NSLRs. In cases where the proposed reference CWTs values had lower MAEs than monthly values, synoptic conditions better explained the

near-surface air temperature lapse rates than seasonal ones, and vice versa.

In any case, MAE values were large (until ~1.8 °C), which indicates that although the estimates of air temperature took account of latitude, longitude, distance to the sea, and topographic position, others factors could also influence the spatial distribution of near-surface air temperatures (Lookingbill and Urban, 2003). Mountainous areas represent unique environments for detecting climate change and its impacts. Modelling plays a key role in the prediction and amelioration of future climate scenarios, facilitating response actions and preparing the society for change. Improvements in determining NSLRs will help reduce uncertainties in any modelling involving the use of climatic variables, such as hydrological models and mass balance snow and glacier simulations.

6 | CONCLUSION

The major findings of the spatio-temporal analysis of near-surface air temperature lapse rates for CS and its five most important mountain regions for December 1979 to August 2015 are:

- Near-surface air temperature lapse rates based on daily mean air temperatures ($NSLR_{dmean}$) were weaker than the standard MELR value of −6.5 °C/km, which is commonly used for interpolating and extrapolating air temperatures. Moreover, the $NSLR_{dmean}$ varied spatially and seasonally, and depended on the prevailing synoptic conditions. All median $NSLR_{dmean}$ were weaker than −6.5 °C/km, and ranged from −4.83 °C/km for the Baetic range to −5.79 °C/km for the Iberian range. The median $NSLR_{dmean}$ was −5.28 °C/km for CS. The steepest $NSLR_{dmean}$ values occurred in spring and autumn for CS, in spring and early summer for the Pyrenees and the Central and Iberian ranges, and in autumn and early winter for the Cantabrian and the Baetic ranges.
- Anticyclonic and southerly CWTs favoured thermal inversions and the weakening of the $NSLR_{dmean}$. Northerly weather types enhanced steep NSLRs. The same response of $NSLR_{dmean}$ values to CWTs was found for all study areas, except for the weakening effect of high-pressure circulations on $NSLR_{dmean}$ values which was less pronounced in the mountain areas close to oceanic air masses (e.g., the Baetic and the Cantabrian ranges).
- Fixed lapse rates such as the MELR and zonal lapse rates are not recommended because of the large residuals found. Therefore, we strongly encourage the use of well-defined monthly–CWTs lapse rates for future applications.

ACKNOWLEDGEMENTS

This study was funded by the research projects CGL2014-52599-P "Estudio del manto de nieve en la montaña española y su respuesta a la variabilidad y cambio climatico" and CLIMPY "Characterization of the evolution of climate and provision of information for adaptation in the Pyrenees" (FEDER-POCTEFA). We thank the Spanish Meteorological Agency (AEMET) for the air temperature data used in this study. F.N.-S. and M.T.-B. are granted with a pre-doctoral FPU grant (Spanish Ministry of Education, Culture and Sports) and C.A.-M. has received funding from the European Union's Horizon 2020 research and innovation programme under the Marie Skłodowska-Curie grant agreement no. STILLING project-703733. The authors thank all colleagues who helped in the development of the experiments, and wish to acknowledge the three anonymous reviewers for their detailed and helpful comments on the original manuscript.

ORCID

F. Navarro-Serrano http://orcid.org/0000-0002-2975-6472

REFERENCES

Agencia Estatal de Meteorología. (2011) In: Closas-Orcoyen, S.L. (Ed.) *Atlas climático Ibérico*, 1st edition. Madrid: Agencia Estatal de Meteorología–Ministerio de Medio Ambiente y Medio Rural y Marino and Instituto de Meteorología de Portugal.

Barringer, J.R.F. (1989) A variable lapse rate snowline model for the remarkables, Central Otago, New Zealand. *Journal of Hydrology*, 28(1), 32–46.

Barry, R.G. (1992) *Mountain Weather and Climate*, 2nd edition. Cambridge: Cambridge University Psychology Press.

Barry, R.G. (2001) Mountain climate change and cryospheric responses: a review. In: Berger, T. (Ed.) *Mountain of the World. Proceedings of the World Mountain Symposium*. Bern: International Mountain Society.

Barry, R.G. and Chorley, R.J. (1987) *Atmosphere, Weather and Climate*, 1st edition. London: Associated Book Publishers.

Basnett, T.A. and Parker, D.E. (1997) Development of the global mean sea level pressure data set GMSLP2. In: Office, H.C.-M. (Eds.), *Climatic research technical note* (Project Report). Bracknell: CEDA.

Benavides, R., Montes, F., Rubio, A. and Osoro, K. (2007) Geostatistical modelling of air temperature in a mountainous region of northern Spain. *Agricultural and Forest Meteorology*, 146(3), 173–188.

Blandford, T.R., Humes, K.S., Harshburger, B.J., Moore, B.C., Walden, V.P., Ye, H., Blandford, T.R., Humes, K.S., Harshburger, B.J., Moore, B.C., Walden, V.P. and Ye, H. (2008) Seasonal and synoptic variations in near-surface air temperature lapse rates in a mountainous basin. *Journal of Applied Meteorology and Climatology*, 47(1), 249–261.

Blöschl, G. (1991) The influence of uncertainty in air temperature and albedo on snowmelt. *Hydrology Research*, 22(2), 95–108.

Bolstad, P.V., Swift, L., Collins, F. and Régnière, J. (1998) Measured and predicted air temperatures at basin to regional scales in the southern Appalachian mountains. *Agricultural and Forest Meteorology*, 91(3–4), 161–176.

Braun, M. and Hock, R. (2004) Spatially distributed surface energy balance and ablation modelling on the ice cap of King George Island (Antarctica). *Global and Planetary Change*, 42(1), 45–58.

Buisan, S.T., Azorin-Molina, C. and Jimenez, Y. (2015a) Impact of two different sized Stevenson screens on air temperature measurements. *International Journal of Climatology*, 35(14), 4408–4416.

Buisan, S.T., Saz, M.A. and López-Moreno, J.I. (2015b) Spatial and temporal variability of winter snow and precipitation days in the western and central Spanish Pyrenees. *International Journal of Climatology*, 35(2), 259–274.

Capel Molina, J.J. (2000) *El clima de la Península Ibérica* (84-344-3466-0). Barcelona: Editorial Ariel.

Du, M., Liu, J., Zhang, X., Li, Y. and Tang, Y. (2010) Changes of spatial patterns of surface-air-temperature on the Tibetan Plateau. In: *Latest Trends on Theoretical and Applied Mechanics, Fluid Mechanics and Heat & Mass*

Transfer. Greece: World Scientific and Engineering Academy and Society Press (WSEAS), pp. 42–47.

Du, M., Zhang, M., Wang, S., Zhu, X. and Che, Y. (2017) Near-surface air temperature lapse rates in Xinjiang, northwestern China. *Theoretical and Applied Climatology*, 131, 1221–1234.

Dumas, M.D. (2013) Changes in temperature and temperature gradients in the French Northern Alps during the last century. *Theoretical and Applied Climatology*, 111(1–2), 223–233.

Durre, I., Menne, M.J., Gleason, B.E., Houston, T.G., Vose, R.S., Durre, I., Menne, M.J., Gleason, B.E., Houston, T.G. and Vose, R.S. (2010) Comprehensive automated quality assurance of daily surface observations. *Journal of Applied Meteorology and Climatology*, 49(8), 1615–1633.

Fang, J.-Y. and Yoda, K. (1988) Climate and vegetation in China (I). Changes in the altitudinal lapse rate of temperature and distribution of sea level temperature. *Ecological Research*, 3(1), 37–51.

Farr, T.G., Rosen, P.A., Caro, E., Crippen, R., Duren, R., Hensley, S., Kobrick, M., Paller, M., Rodríguez, E., Roth, L., Seal, D., Shaffer, S., Shimada, J., Umland, J., Werner, M., Oskin, M., Burbank, D. and Alsdorf, D. (2007) The Shuttle Radar Topography Mission. *Reviews of Geophysics*, 45(2), RG2004.

García-Herrera, R., Hernández, E., Barriopedro, D., Paredes, D., Trigo, R.M., Trigo, I.F. and Mendes, M.A. (2007) The outstanding 2004/05 drought in the Iberian peninsula: associated atmospheric circulation. *Journal of Hydrometeorology*, 8(3), 483–498.

García-Ruiz, J.M., López-Moreno, J.I., Vicente-Serrano, S.M., Lasanta-Martínez, T. and Beguería, S. (2011) Mediterranean water resources in a global change scenario. *Earth-Science Reviews*, 105(3–4), 121–139.

Gardner, A.S., Sharp, M.J., Koerner, R.M., Labine, C., Boon, S., Marshall, S.J., Burgess, D.O. and Lewis, D. (2009) Near-surface temperature lapse rates over Arctic Glaciers and their implications for temperature downscaling. *Journal of Climate*, 22(16), 4281–4298.

Goodess, C.M. and Palutikof, J.P. (1998) Development of daily rainfall scenarios for southeast Spain using a circulation-type approach to downscaling. *International Journal of Climatology*, 18(10), 1051–1083.

Hanna, E., Huybrechts, P., Janssens, I., Cappelen, J., Steffen, K. and Stephens, A. (2005) Runoff and mass balance of the Greenland ice sheet: 1958–2003. *Journal of Geophysical Research*, 110(D13), D13108.

Harlow, R.C., Burke, E.J., Scott, R.L., Shuttleworth, W.J., Brown, C.M. and Petti, J.R. (2004) Research note: derivation of temperature lapse rates in semi-arid south-eastern Arizona. *Hydrology and Earth System Sciences*, 8(6), 1179–1185.

Heynen, M., Miles, E., Ragettli, S., Buri, P., Immerzeel, W.W. and Pellicciotti, F. (2016) Air temperature variability in a high-elevation Himalayan catchment. *Annals of Glaciology*, 57(71), 212–222.

Holden, J. and Rose, R. (2011) Temperature and surface lapse rate change: a study of the UK's longest upland instrumental record. *International Journal of Climatology*, 31(6), 907–919.

Immerzeel, W.W., Petersen, L., Ragettli, S. and Pellicciotti, F. (2014) The importance of observed gradients of air temperature and precipitation for modeling runoff from a glacierized watershed in the Nepalese Himalayas. *Water Resources Research*, 50(3), 2212–2226.

Jenkinson, A.F. and Collison, P. (1977) *An initial climatology of Wales over the North Sea* (Synoptic Climatology Branch Memorandum 62). State College: Pennsylvania State University.

Kattel, D.B., Yao, T., Yang, K., Tian, L., Yang, G. and Joswiak, D. (2013) Temperature lapse rate in complex mountain terrain on the southern slope of the central Himalayas. *Theoretical and Applied Climatology*, 113(3–4), 671–682.

Kirchner, M., Faus-Kessler, T., Jakobi, G., Leuchner, M., Ries, L., Scheel, H.-E. and Suppan, P. (2013) Altitudinal temperature lapse rates in an Alpine valley: trends and the influence of season and weather patterns. *International Journal of Climatology*, 33(3), 539–555.

Kunkel, K.E. (1989) Simple procedures for extrapolation of humidity variables in the mountainous western United States. *Journal of Climate*, 2(7), 656–670.

Lamb, H.H. (1972) British Isles weather types and a register of daily sequence of circulation patterns, 1861–1971. *Geophysical Memoires*, 116, 1–85.

Li, X., Wang, L., Chen, D., Yang, K., Xue, B. and Sun, L. (2013) Near-surface air temperature lapse rates in the mainland China during 1962–2011. *Journal of Geophysical Research: Atmospheres*, 118(14), 7505–7515.

Lookingbill, T.R. and Urban, D.L. (2003) Spatial estimation of air temperature differences for landscape-scale studies in montane environments. *Agricultural and Forest Meteorology*, 114(3), 141–151.

López-Moreno, J.I. and Vicente-Serrano, S.M. (2007) Atmospheric circulation influence on the interannual variability of snow pack in the Spanish Pyrenees during the second half of the 20th century. *Hydrology Research*, 38(1), 33–44.

Lundquist, J.D. and Cayan, D.R. (2007) Surface temperature patterns in complex terrain: daily variations and long-term change in the central Sierra Nevada, California. *Journal of Geophysical Research*, 112(D11), D11124.

Marsh, C. (2009) Application and comparison of high resolution radiation models in complex terrain. *Geography*, 490(2), 1–47.

Marshall, S.J., Sharp, M.J., Burgess, D.O. and Anslow, F.S. (2007) Near-surface-temperature lapse rates on the Prince of Wales Icefield, Ellesmere Island, Canada: implications for regional downscaling of temperature. *International Journal of Climatology*, 27(3), 385–398.

Martinec, J., Rango, A. and Major, E. (1983) *The Snowmelt-runoff Model (SRM) User's Manual. NASA Reference Publication*, Vol. 1100. Washington, D.C.: National Aeronautics and Space Administration, Scientific and Technical Information Branch.

McCutchan, M.H. and Fox, D.G. (1986) Effect of elevation and aspect on wind, temperature and humidity. *Journal of Climate and Applied Meteorology*, 25(12), 1996–2013.

Minder, J.R., Mote, P.W. and Lundquist, J.D. (2010) Surface temperature lapse rates over complex terrain: lessons from the Cascade Mountains. *Journal of Geophysical Research*, 115(D14), D14122.

Miró, J.R., Peña, J.C., Pepin, N., Sairouni, A. and Aran, M. (2018) Key features of cold-air pool episodes in the northeast of the Iberian Peninsula (Cerdanya, eastern Pyrenees). *International Journal of Climatology*, 38(3), 1105–1115.

Nigrelli, G., Fratianni, S., Zampollo, A., Turconi, L. and Chiarle, M. (2017) The altitudinal temperature lapse rates applied to high elevation rockfalls studies in the Western European Alps. *Theoretical and Applied Climatology*, 131, 1479–1491.

Nunez, M. and Calhoun, E.A. (1986) A note on air temperature lapse rates on Mount Wellington, Tasmania. *Papers and Proceedings of the Royal Society of Tasmania*, 12012(120), 11–15.

Pagès, M. and Miró, J.R. (2010) Determining temperature lapse rates over mountain slopes using vertically weighted regression: a case study from the Pyrenees. *Meteorological Applications*, 17(1), 53–63.

Pagès, M., Pepin, N. and Miró, J.R. (2017) Measurement and modelling of temperature cold pools in the Cerdanya valley (Pyrenees), Spain. *Meteorological Applications*, 24(2), 290–302.

Pepin, N. (2001) Lapse rate changes in northern England. *Theoretical and Applied Climatology*, 68(1–2), 1–16.

Pepin, N. and Kidd, D. (2006) Spatial temperature variation in the eastern Pyrenees. *Weather*, 61(11), 300–310.

Pepin, N. and Losleben, M. (2002) Climate change in the Colorado Rocky Mountains: free air versus surface temperature trends. *International Journal of Climatology*, 22(3), 311–329.

Pepin, N.C. and Seidel, D.J. (2005) A global comparison of surface and free-air temperatures at high elevations. *Journal of Geophysical Research*, 110(D3), D03104.

Pepin, N., Benham, D. and Taylor, K. (1999) Modeling lapse rates in the maritime uplands of northern England: implications for climate change. *Arctic, Antarctic, and Alpine Research*, 31(2), 151–164.

Pepin, N.C., Daly, C. and Lundquist, J. (2011) The influence of surface versus free-air decoupling on temperature trend patterns in the western United States. *Journal of Geophysical Research*, 116(D10), D10109.

Puigdefábregas, J. (1969) Avance para un estudio climatologico del alto aragon. *Pirineos*, 76–80.

Rasilla Álvarez, D.F., García-Codrón, J.C. and Garmendia Pedraja, C. (2002) Los temporales de viento: propuesta metodológica para el análisis de un fenómeno infravalorado. In: *Reunión Nacional de Climatología*. Madrid: Grupo de Clima de la Asociación de Geógrafos Españoles, pp. 129–136.

Rodríguez-Puebla, C., Encinas, A.H., Nieto, S. and Garmendia, J. (1998) Spatial and temporal patterns of annual precipitation variability over the Iberian Peninsula. *International Journal of Climatology*, 18(3), 299–316.

Rolland, C. (2003) Spatial and seasonal variations of air temperature lapse rates in alpine regions. *Journal of Climate*, 16(7), 1032–1046.

Running, S.W., Nemani, R.R. and Hungerford, R.D. (1987) Extrapolation of synoptic meteorological data in mountainous terrain and its use for simulating forest evapotranspiration and photosynthesis. *Canadian Journal of Forest Research*, 17(6), 472–483.

Spellman, G. (2000) The application of an objective weather-typing system to the Iberian Peninsula. *Weather*, 55(10), 375–385.

Tang, Z. and Fang, J. (2006) Temperature variation along the northern and southern slopes of Mt. Taibai, China. *Agricultural and Forest Meteorology*, 139(3), 200–207.

Tomás, C., de Pablo, F. and Rivas Soriano, L. (2004) Circulation weather types and cloud-to-ground flash density over the Iberian Peninsula. *International Journal of Climatology*, 24(1), 109–123.

Tomás-Burguera, M., Jiménez Castañeda, A., Luna Rico, M.Y., Morata, A., Vicente Serrano, S., González-Hidalgo, J.C. and Beguería, S. (2016) Control de calidad de siete variables del banco nacional de datos de AEMET. Asociación Española de Climatología Congreso (10. 2016. Alicante) (Ed.). In: *X Congreso Internacional AEC: Clima, sociedad, riesgos y ordenación del territorio*. Alicante: AEC, pp. 407–415.

Trigo, R.M. and Dacamara, C.C. (2000) Circulation weather types and their influence on the precipitation regime in Portugal. *International Journal of Climatology*, 20(13), 1559–1581.

United States Defense Mapping Agency. (2000) *Vector map level 0 (VMAP0).* Avaialble at: https://www.lib.msu.edu/branches/map/findingaids/VMAP0/.

Vicente-Serrano, S.M. (2007) Evaluating the impact of drought using remote sensing in a Mediterranean, semi-arid region. *Natural Hazards*, 40(1), 173–208.

Whiteman, C.D., Bian, X., Zhong, S., Whiteman, C.D., Bian, X. and Zhong, S. (1999) Wintertime evolution of the temperature inversion in the Colorado Plateau Basin. *Journal of Applied Meteorology*, 38(8), 1103–1117.

Whiteman, C.D., Pospichal, B., Eisenbach, S., Weihs, P., Clements, C.B., Steinacker, R., Mursch-Radlgruber, E. and Dorninger, M. (2004) Inversion breakup in small Rocky Mountain and alpine basins. *Journal of Applied Meteorology*, 43(8), 1069–1082.

Wilcoxon, F. (1945) Individual comparisons by ranking methods. *Biometrics*, 1(6), 80.

World Meteorological Organization. (2008) *Guide to Meteorological Instruments and Methods of Observation*, 1st edition. Geneva: World Meteorological Organization.

SUPPORTING INFORMATION

Additional Supporting Information may be found online in the supporting information tab for this article.

How to cite this article: Navarro-Serrano F, López-Moreno JI, Azorin-Molina C, *et al.* Estimation of near-surface air temperature lapse rates over continental Spain and its mountain areas. *Int J Climatol*. 2018;38:3233–3249. https://doi.org/10.1002/joc.5497

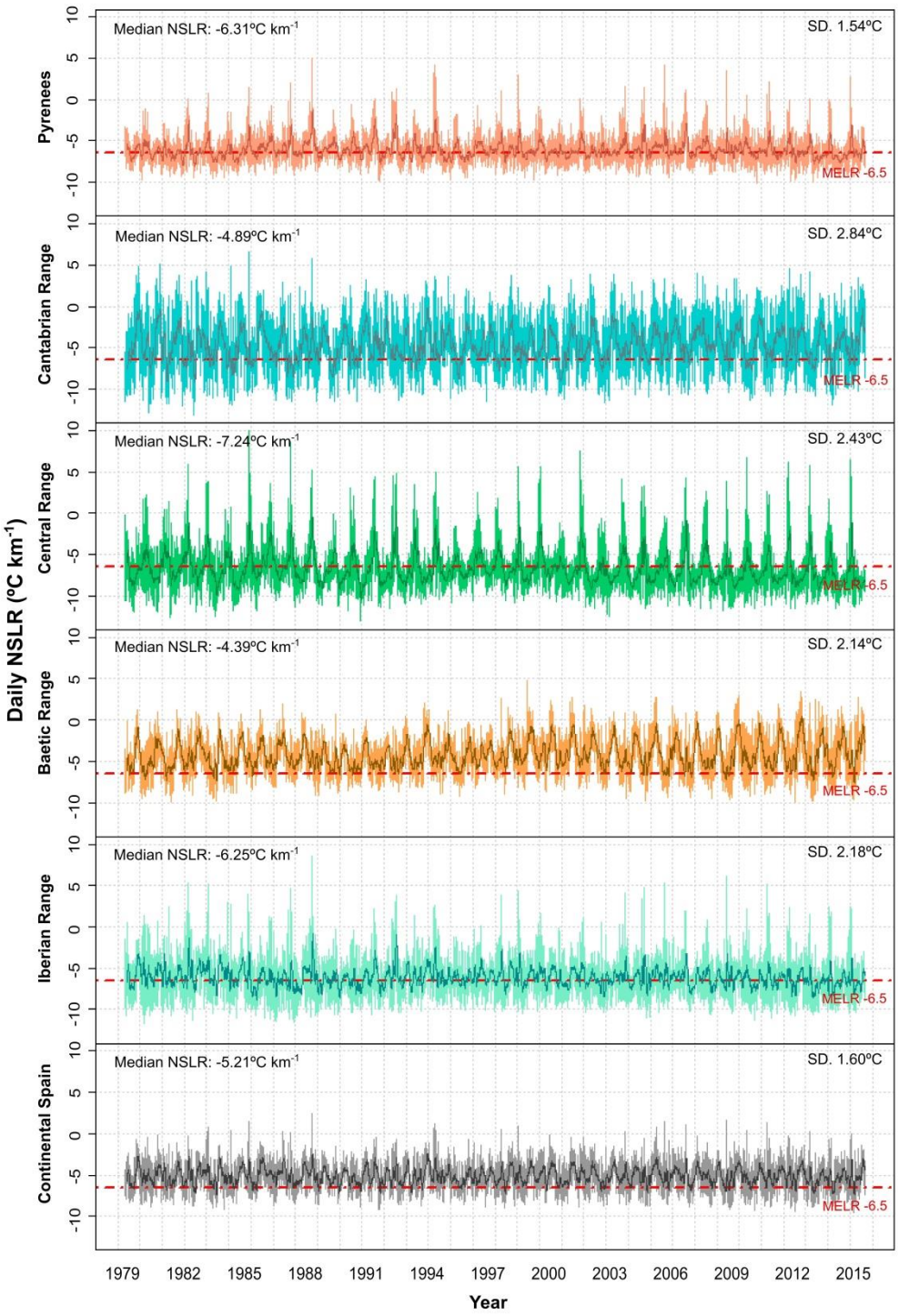

Figure S1. Daily maximum near-surface air temperature lapse rate (NSLRdmax °C/km). Dark colored lines show the 30-day running average. Dashed red lines show the standard and fixed moist adiabatic lapse rate (MALR) of −6.5 °C/km. SD: standard deviation.

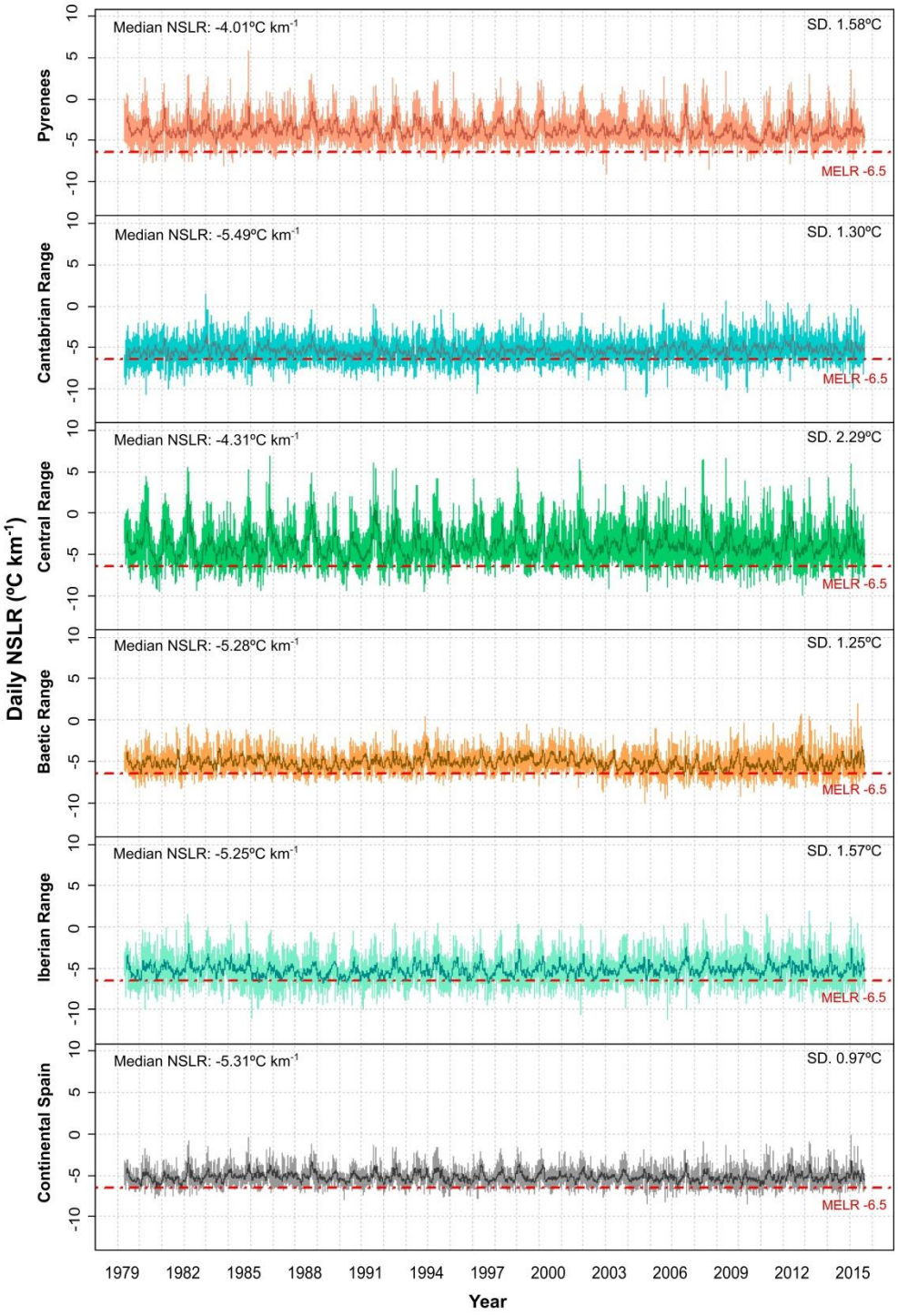

Figure S2. Daily minimum near-surface air temperature lapse rate (NSLRdmin °C/km). Dark colored lines show the 30-day running average. Dashed red lines show the standard and fixed moist adiabatic lapse rate (MALR) of −6.5 °C/km. SD: standard deviation.

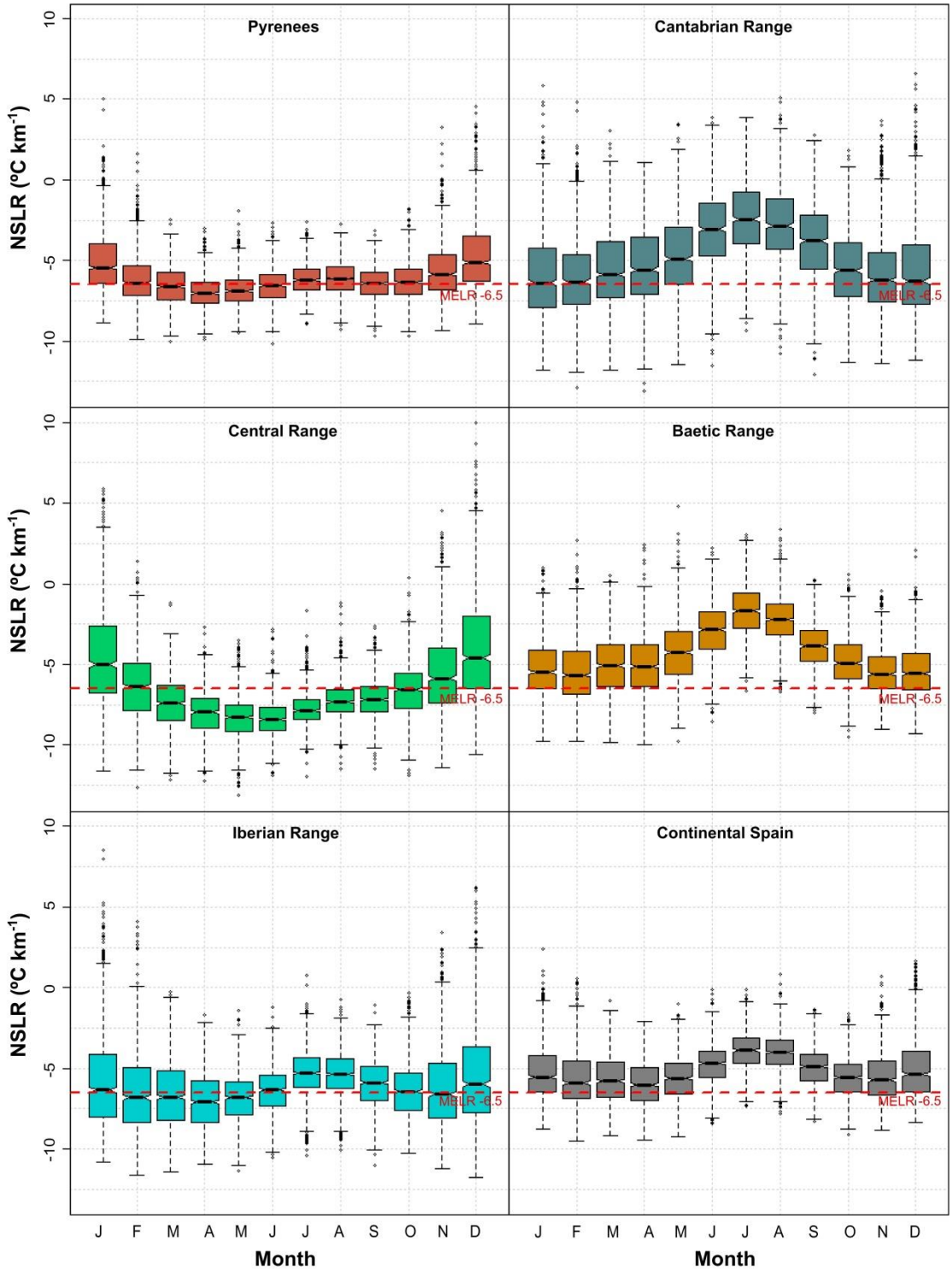

Figure S3. Monthly box-and-whisker plots of near-surface maximum air temperature lapse rate (NSLRdmax: °C/km) for the five mountain ranges and the entire CS. Dashed red lines show the standard and fixed moist adiabatic lapse rate (MALR) of −6.5 °C/km. The median (black line), 25th and 75th percentile ranges (boxes), 75th + 1.5IQR (upper whisker), 25th − 1.5IQR (bottom whisker), and the extreme values (>75th + 1.5IQR and <25th – 1.5IQR) are represented.

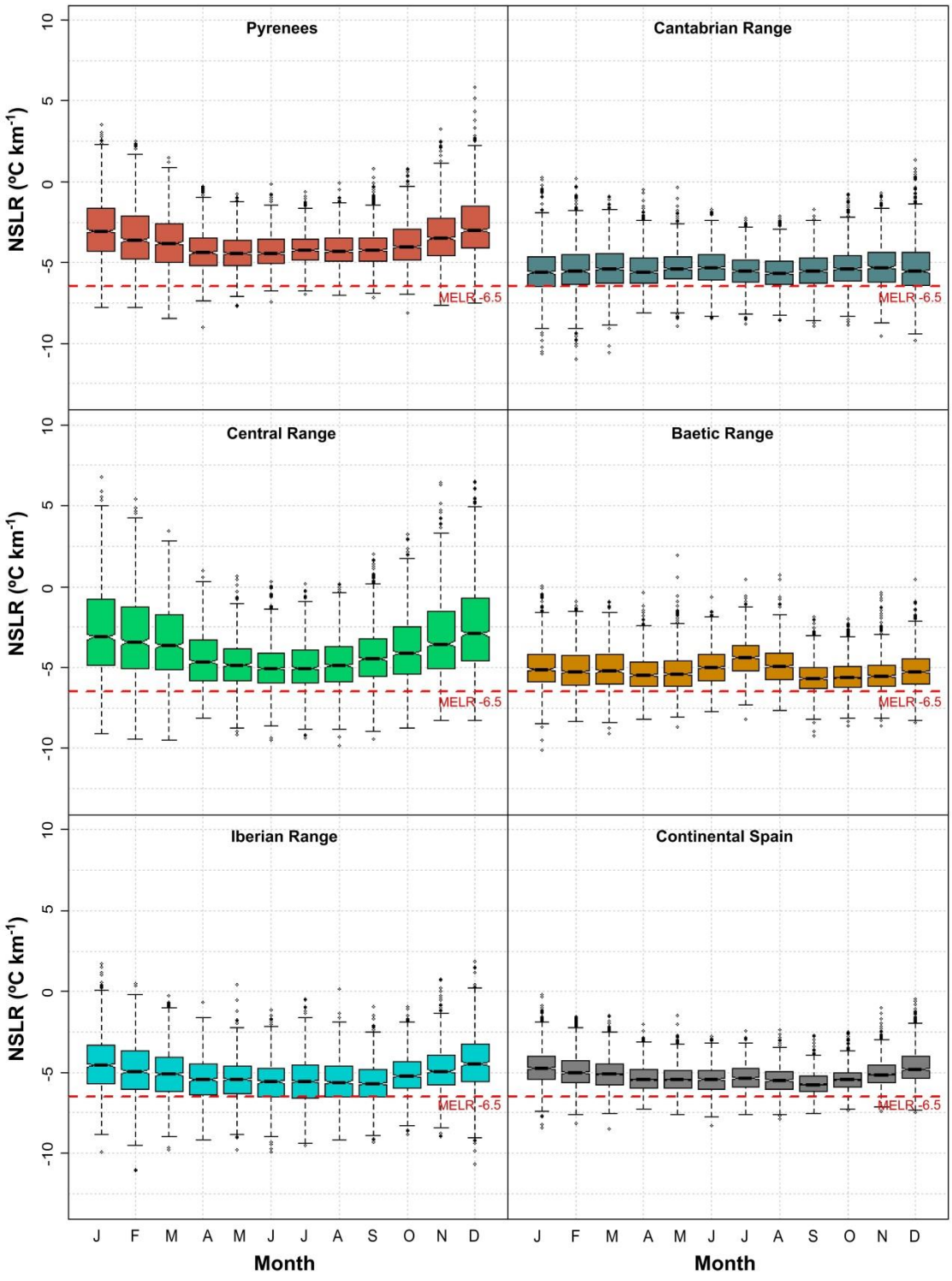

Figure S4. Monthly box-and-whisker plots of near-surface minimum air temperature lapse rate (NSLRdmin: °C/km) for the five mountain ranges and the entire CS. Dashed red lines show the standard and fixed moist adiabatic lapse rate (MALR) of −6.5 °C/km. The median (black line), 25th and 75th percentile ranges (boxes), 75th + 1.5IQR (upper whisker), 25th − 1.5IQR (bottom whisker), and the extreme values (>75th + 1.5IQR and <25th − 1.5IQR) are represented.

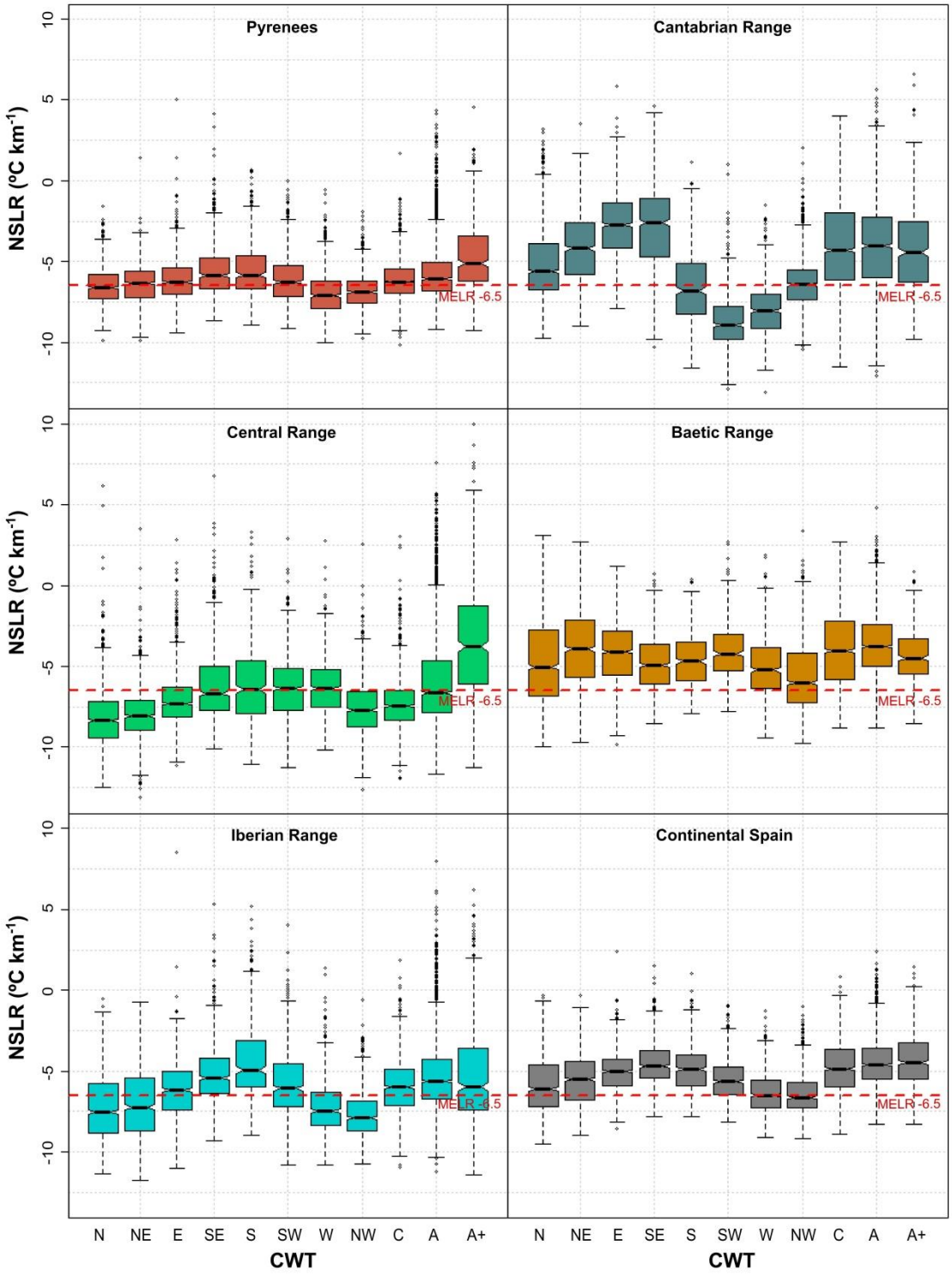

Figure S5. Variability in the near-surface maximum air temperature lapse rate (NSLRdmax: °C/km) for various synthetized circulation weather types (CWTs). Dashed red lines show the standard and fixed moist adiabatic lapse rate (MALR) of −6.5 °C/km. The median (black line), the 25th and 75th percentile range (boxes), the minimum value between daily NSLR and 75th + 1.5IQR (upper whisker), the maximum value between daily NSLR and 25th – 1.5IQR (bottom whisker), and the extreme values (>75th + 1.5IQR and <25th – 1.5IQR) are represented.

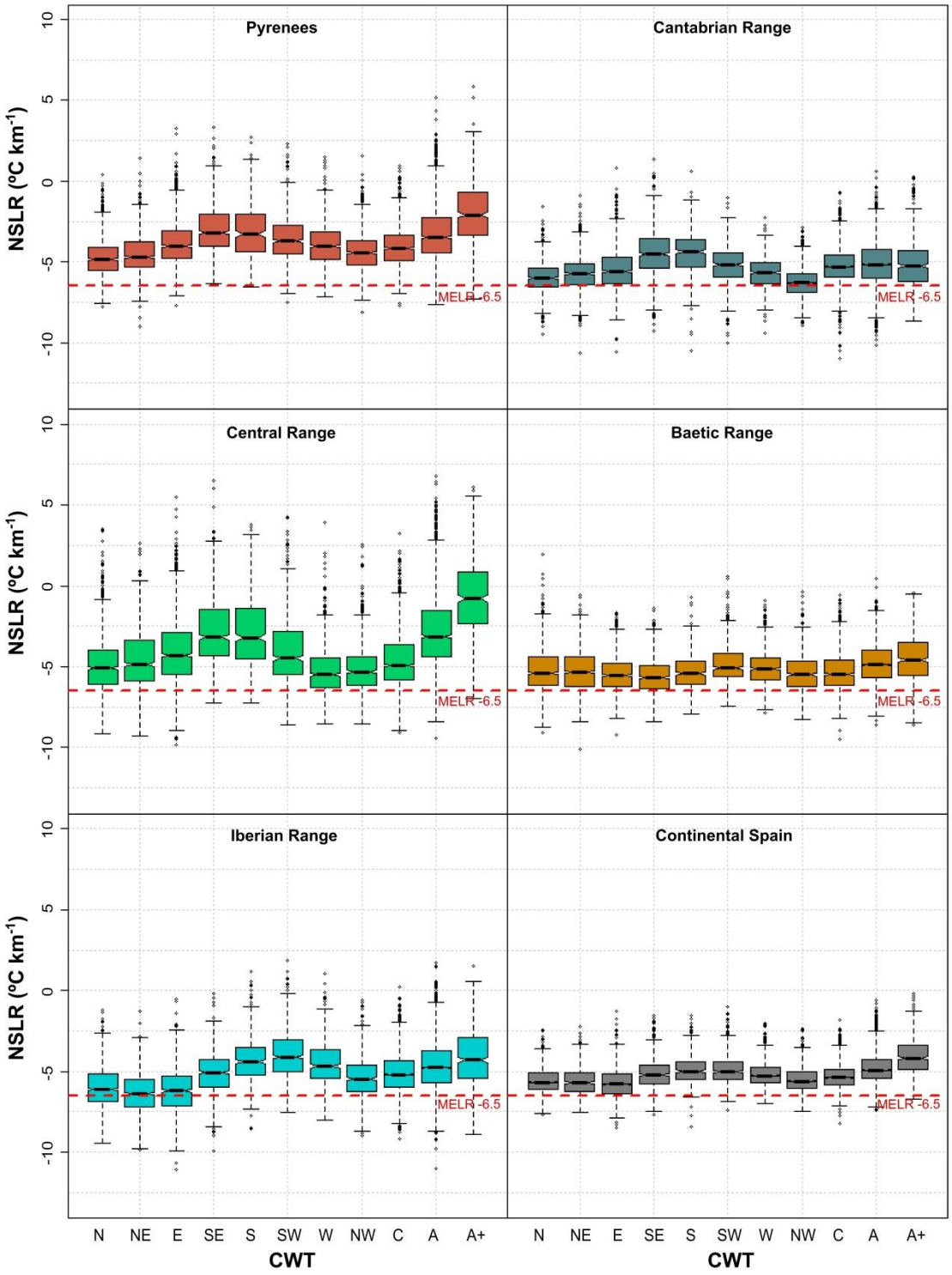

Figure S6. Variability in the near-surface minimum air temperature lapse rate (NSLR dmin: °C/km) for various synthetized circulation weather types (CWTs). Dashed red lines show the standard and fixed moist adiabatic lapse rate (MALR) of −6.5 °C/km. The median (black line), the 25th and 75th percentile range (boxes), the minimum value between daily NSLR and 75th + 1.5IQR (upper whisker), the maximum value between daily NSLR and 25th – 1.5IQR (bottom whisker), and the extreme values (>75th + 1.5IQR and <25th – 1.5IQR) are represented.

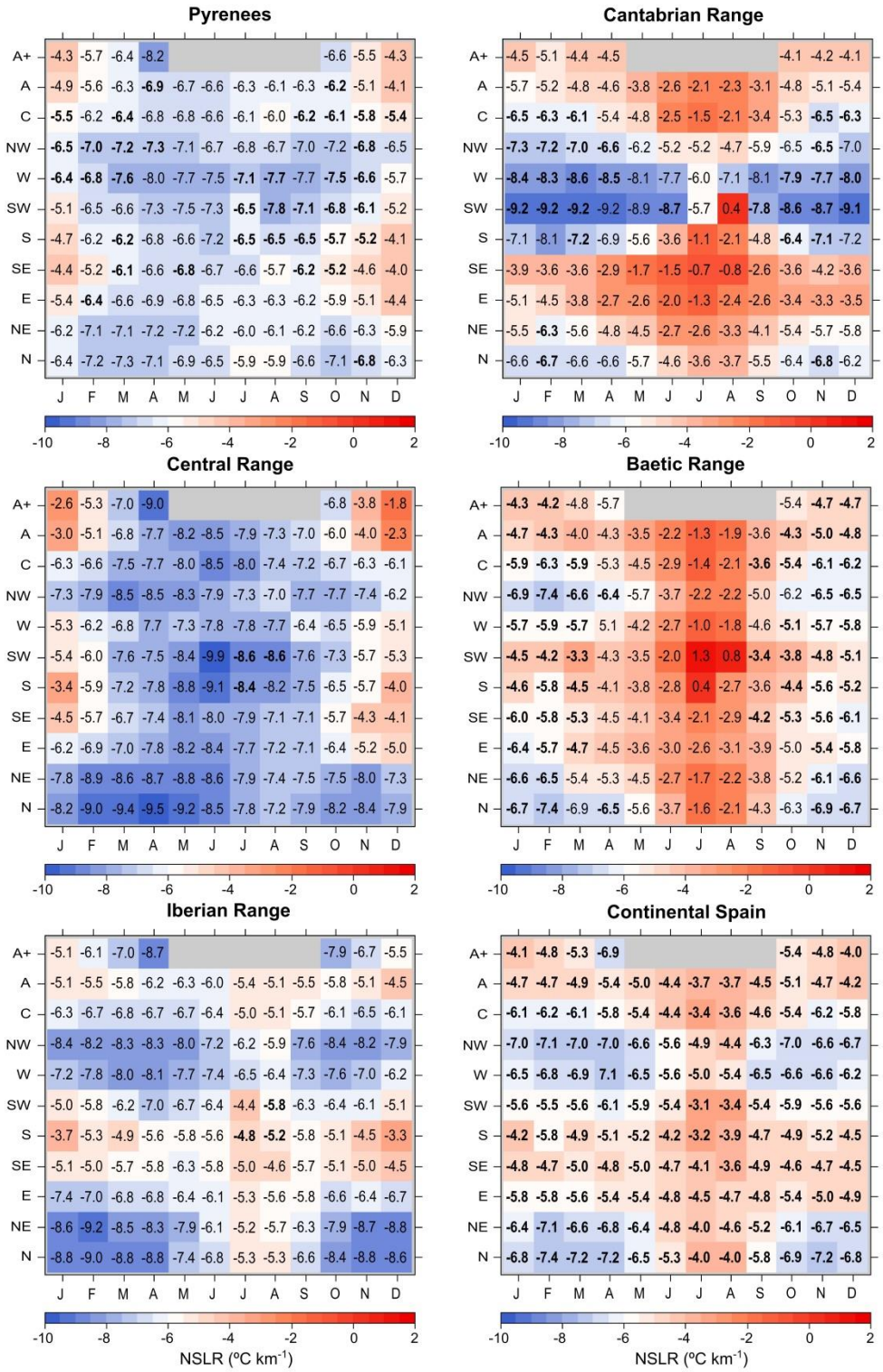

Figure S7. Monthly median near-surface maximum air temperature lapse rate (NSLRdmax: °C/km) for different months and synthetized circulation weather types (CWTs). Accuracy ±1 °C (95% confidence interval) is represented by bold values.

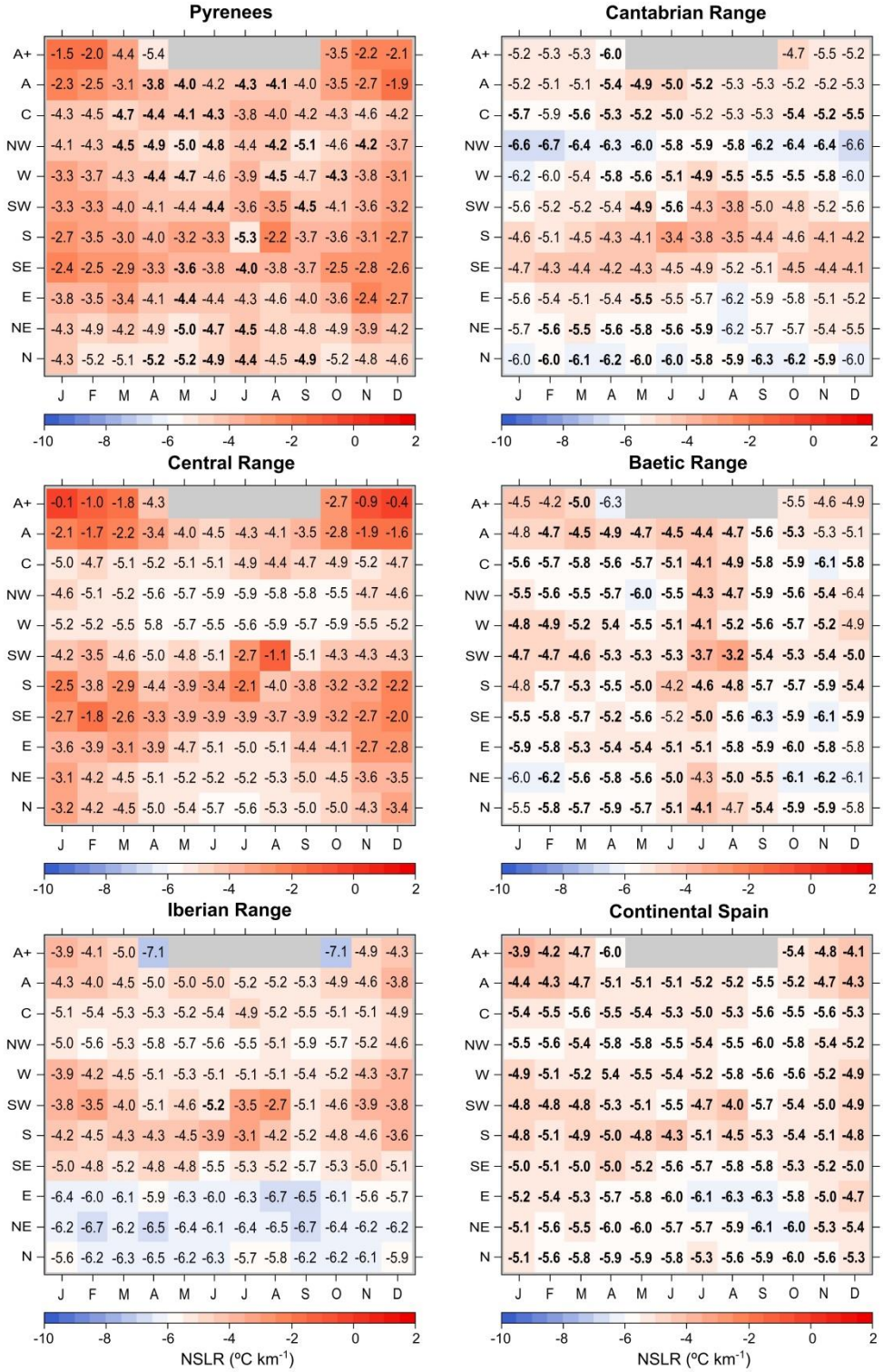

Figure S8. Monthly median near-surface minimum air temperature lapse rate (NSLRdmin: °C/km) for different months and synthetized circulation weather types (CWTs). Accuracy ±1 °C (95% confidence interval) is represented by bold values.

Table S1. Proposed monthly and synoptic near-surface maximum air temperature lapse rate (NSLR: °C/km) reference values.

ZONAL REFERENCE Near-surface air temperature lapse rate ($NSLR_{dmax}$)						
	Pyrenees	Cantabrian Range	Central Range	Baetic Range	Iberian Range	Continental Spain
Zonal	–6.31	–4.89	–7.24	–4.39	–6.25	–5.21
MONTHLY REFERENCE Near–surface air temperature lapse rate ($NSLR_{dmax}$)						
Month	Pyrenees	Cantabrian Range	Central Range	Baetic Range	Iberian Range	Continental Spain
Jan	–5.44	–6.39	–5.02	–5.48	–6.34	–5.57
Feb	–6.39	–6.32	–6.38	–5.66	–6.81	–5.91
Mar	–6.62	–5.87	–7.41	–5.08	–6.81	–5.79
Apr	–7.01	–5.59	–7.95	–5.11	–7.10	–6.03
May	–6.88	–4.89	–8.28	–4.24	–6.82	–5.62
Jun	–6.57	–3.05	–8.45	–2.85	–6.35	–4.69
Jul	–6.19	–2.43	–7.86	–1.69	–5.29	–3.91
Aug	–6.11	–2.85	–7.32	–2.20	–5.36	–4.02
Sep	–6.38	–3.78	–7.20	–3.87	–5.91	–4.90
Oct	–6.34	–5.63	–6.56	–4.93	–6.45	–5.57
Nov	–5.85	–6.22	–5.86	–5.59	–6.61	–5.72
Dec	–5.15	–6.28	–4.61	–5.57	–6.00	–5.39
SYNOPTICAL REFERENCE (by Circulation Weather Types CWT) Near–surface air temperature lapse rate ($NSLR_{dmax}$)						
CWT	Pyrenees	Cantabrian Range	Central Range	Baetic Range	Iberian Range	Continental Spain
N	–6.63	–5.63	–8.37	–5.07	–7.58	–6.12
NE	–6.37	–4.19	–8.09	–3.93	–7.25	–5.53
E	–6.29	–2.72	–7.31	–4.09	–6.20	–5.04
SE	–5.86	–2.59	–6.69	–4.92	–5.42	–4.70
S	–5.85	–6.79	–6.43	–4.69	–4.93	–4.90
SW	–6.30	–8.92	–6.37	–4.23	–6.08	–5.67
W	–7.12	–8.05	–6.40	–5.24	–7.48	–6.52
NW	–6.90	–6.45	–7.72	–6.04	–7.93	–6.63
C	–6.26	–4.28	–7.48	–4.06	–6.01	–4.87
A	–6.09	–4.03	–6.66	–3.79	–5.62	–4.61
A+	–5.14	–4.45	–3.75	–4.50	–6.00	–4.48

Table S2. Proposed monthly and synoptic near-surface minimum air temperature lapse rate (NSLR: °C/km) reference values.

ZONAL REFERENCE Near–surface air temperature lapse rate ($NSLR_{dmin}$)						
	Pyrenees	Cantabrian Range	Central Range	Baetic Range	Iberian Range	Continental Spain
Zonal	–4.01	–5.49	–4.31	–5.28	–5.25	–5.31
MONTHLY REFERENCE Near–surface air temperature lapse rate ($NSLR_{dmin}$)						
Month	Pyrenees	Cantabrian Range	Central Range	Baetic Range	Iberian Range	Continental Spain
Jan	–3.05	–5.63	–3.12	–5.12	–4.58	–4.78
Feb	–3.64	–5.55	–3.45	–5.27	–4.95	–5.05
Mar	–3.81	–5.40	–3.66	–5.24	–5.11	–5.13
Apr	–4.40	–5.60	–4.66	–5.51	–5.46	–5.47
May	–4.42	–5.38	–4.85	–5.43	–5.46	–5.46
Jun	–4.45	–5.34	–5.08	–5.02	–5.6	–5.45
Jul	–4.22	–5.53	–5.06	–4.39	–5.57	–5.37
Aug	–4.32	–5.66	–4.88	–4.96	–5.63	–5.51
Sep	–4.26	–5.53	–4.49	–5.70	–5.69	–5.76
Oct	–4.02	–5.38	–4.11	–5.65	–5.24	–5.47
Nov	–3.50	–5.31	–3.54	–5.57	–4.94	–5.15
Dec	–3.03	–5.54	–2.91	–5.27	–4.49	–4.82
SYNOPTICAL REFERENCE (by Circulation Weather Types CWT) Near–surface air temperature lapse rate ($NSLR_{dmin}$)						
CWT	Pyrenees	Cantabrian Range	Central Range	Baetic Range	Iberian Range	Continental Spain
N	–4.85	–6.01	–5.09	–5.39	–6.11	–5.68
NE	–4.69	–5.73	–4.87	–5.36	–6.39	–5.72
E	–4.04	–5.61	–4.30	–5.57	–6.21	–5.81
SE	–3.19	–4.51	–3.18	–5.69	–5.09	–5.22
S	–3.27	–4.38	–3.20	–5.43	–4.4	–5.01
SW	–3.72	–5.16	–4.48	–5.09	–4.11	–5.05
W	–4.03	–5.67	–5.49	–5.13	–4.69	–5.27
NW	–4.47	–6.30	–5.32	–5.51	–5.48	–5.61
C	–4.18	–5.31	–4.91	–5.50	–5.2	–5.39
A	–3.50	–5.17	–3.15	–4.89	–4.78	–4.94
A+	–2.09	–5.26	–0.81	–4.58	–4.29	–4.19

Capítulo 4

GRADIENTES DE TEMPERATURA EN LA REGIÓN ANDINA DE ECUADOR Y PERÚ

Publicado como:

Navarro-Serrano, F., López-Moreno, J.I., Domínguez-Castro, F., Alonso-González, E., Azorin-Molina, C., El-Kenawy, A., Vicente-Serrano, S.M. Maximum and Minimum air temperature lapse-rates in the Andean region of Ecuador and Peru. *International Journal of Climatology* (En Prensa). DOI: https://doi.org/10.1002/joc.6574.

Los autores agradecen a WILEY el permiso para publicar de manera íntegra el contenido de la publicación, que puede encontrarse en https://rmets.onlinelibrary.wiley.com/doi/abs/10.1002/joc.6574.

Received: 6 July 2019 | Revised: 21 January 2020 | Accepted: 26 March 2020
DOI: 10.1002/joc.6574

RESEARCH ARTICLE

International Journal of Climatology RMetS

Maximum and minimum air temperature lapse rates in the Andean region of Ecuador and Peru

Francisco Navarro-Serrano[1,2] | **Juan I. López-Moreno**[1] | **Fernando Domínguez-Castro**[1,2,3] | **Esteban Alonso-González**[1] | **Cesar Azorin-Molina**[4,5] | **Ahmed El-Kenawy**[6,7] | **Sergio M. Vicente-Serrano**[1]

[1]Department of Geoenvironmental Process and Global Change, Pyrenean Institute of Ecology, CSIC, Zaragoza, Spain

[2]Department of Geography, University of Zaragoza, Zaragoza, Spain

[3]ARAID Foundation, University of Zaragoza, Zaragoza, Spain

[4]Regional Climate Group, Department of Earth Sciences, University of Gothenburg, Gothenburg, Sweden

[5]Centro de Investigaciones sobre Desertificación, Consejo Superior de Investigaciones Científicas (CIDE-CSIC), Montcada, Valencia, Spain

[6]Department of Geography, Sultan Qaboos University, Muscat, Oman

[7]Department of Geography, Mansoura University, Mansoura, Egypt

Correspondence
Francisco Navarro-Serrano, Pyrenean Institute of Ecology, CSIC, Campus de Aula Dei, Avenida de Montañana, P.O. Box 202, Zaragoza 50059, Spain.
Email: fnavarro@ipe.csic.es

Funding information
Ministerio de Ciencia e Innovación, Grant/Award Number: CGL2017-82216-R; Ministerio de Educación, Cultura y Deporte, Grant/Award Number: FPU15/00742; Secretaría de Estado de Investigación, Desarrollo e Innovación, Grant/Award Number: FPI

Abstract

To know the vertical distribution of air temperature is complex, and this is necessary for different applications. The main explanatory variable of air temperature is elevation above sea level, whose relationship with air temperature is measured by air temperature lapse rates (LRs). LRs can vary considerably spatiotemporally due to a wide spectrum of geographical, environmental, and other atmospheric factors. Our study presents the first comprehensive assessment of spatiotemporal changes of LRs over the Tropical Andes. Our study is focused on the Peruvian and Ecuadorian Andes, divided in two subregions by the parallel 9.5° (i.e., north and south). Maximum and minimum air temperatures were employed from 115 quality checked weather stations, for the period 1994–2011. Maximum (LR_{max}) and minimum (LR_{min}) air temperature lapse rates have been calculated for the whole study period. The effects of seasonality, humidity content and ENSO on the variability of LRs have been analysed. Results show that LRs have large spatiotemporal variability, since references values of LR_{max} range from −3.57 (South, dry season) to −4.77 (North, wet season), and LR_{min} range from −3.78 (North, dry season) to −4.93°C·km^{-1} (South, dry season), in function of season and subregion. Results indicate that the ENSO phases contribute significantly to the variability of southern subregion LRs. This study also presents that minimum air temperatures were more unpredictable than maximum air temperatures in terms of error and uncertainty, as a consequence of the larger spatial variability of nocturnal air temperatures, mainly influenced by local topography. In conclusion, this work goes deeper into the need to obtain precise LRs adapted to the study region, and shows that the use of standard LR values can cause significant failures in modelling air temperature in regions of complex terrain, such as the Andes.

KEYWORDS
air temperature, Ecuador, ENSO, lapse rates, Peru, Tropical Andes

1 | INTRODUCTION

Surface air temperature (measured at ~1.5–2.0 m height above ground) is a key climatic variable for a wide range of ecological (Hatfield and Prueger, 2015), environmental and economic applications (Moore and Diaz, 2015), among others. In regions of complex topography, air temperature varies considerably over space and time, even for short distances, which makes it necessary to use a dense network of meteorological information. Unfortunately, meteorological networks in mountainous regions are mostly characterized by uneven distribution of weather stations, especially in remote, elevated and less-populated sites (Barry, 2008). This is typical in the Andean region in Ecuador and Peru. To address this lack of information, some authors have installed their own weather station networks on the territory, mainly in reduced study areas (Lewkowicz and Bonnaventure, 2011; Bonnardot *et al*., 2012; Appelhans *et al*., 2016; Wang *et al*., 2017). Alternatively, many investigations of air temperature in complex terrain regions deployed either reanalysis datasets (Alonso-González *et al*., 2018) or interpolation techniques (Lussana *et al*., 2018; Sadoti *et al*., 2018). This has been evident for the Rocky Mountains (Whiteman *et al*., 1999; Minder *et al*., 2010), the Alps (Rolland, 2003), the Subarctic Scandinavia (Pike *et al*., 2013) and the Ecuadorian Andes (Morán-Tejeda *et al*., 2016), among others.

The elevational lapse rate (LR forward) is simply defined as the change in air temperature per elevation unit, measured in $°C \cdot km^{-1}$ (Fang and Yoda, 1988). In hydroclimatic research, it is common to apply elevation-dependent LRs to interpolate air temperature. As such, they have been widely applied in various disciplines, such as glaciology, hydrology and ecology (Immerzeel *et al*., 2014; Hanna *et al*., 2017; Kulshrestha and Ramsankaran, 2018). Among them, the most used LR is the fixed Mean Environmental Lapse Rate (hereafter MELR: $-6.5°C \cdot km^{-1}$), which assumes free atmospheric conditions (Barry and Chorley, 2003). Nonetheless, the application of the fixed MELR has a degree of uncertainty, as it fails to adequately reveal the high variability of air temperature both vertically or horizontally (Kattel *et al*., 2013; Miró *et al*., 2017) and, accordingly, it does not represent the synoptic behaviours of temperature profiles (Pepin and Losleben, 2002; Du *et al*., 2010). While the calculation of LRs can easily be accomplished, it requires high-resolution air temperature data over space and time, which allows for a more reliable diagnosis of air temperature variability at different scales.

Even under stable atmospheric conditions, LRs can vary considerably from one season to another for maximum and minimum air temperature (Pepin, 2001; Marshall *et al*., 2007; Kattel *et al*., 2013). This notion has been confirmed across the global mountain systems, including the Rocky Mountains (Kunkel, 1989; Pepin and Losleben, 2002), the Himalayas (Immerzeel *et al*., 2014; Romshoo *et al*., 2018; Ojha, 2019) and the Alps (Dumas, 2013; Nigrelli *et al*., 2017), along with other regions (e.g., the Iberian Peninsula; (Navarro-Serrano *et al*., 2018), as well as in the Antarctic Peninsula (Ambrozova *et al*., 2019). In each region, the vertical distribution of air temperature varies between nighttime and daytime due to variations in heat fluxes between the atmosphere and the surface (Duane *et al*., 2008; Gardner *et al*., 2009). These diurnal variations demonstrated that MELR does not represent the regional annual average of LRs. Large errors may be introduced applying MELR on modelling temperature with diverse aims. Unfortunately, except for work at the local scale of Córdova *et al*. (2016) in a specific Ecuadorian valley over 12 months, the dependency between elevation and air temperature is still unexplored in this Andean region, which could have different implications in the countries of this region.

In Ecuador and Peru, the hydrological resources are needed for more than 40 million people, being originate mainly from the Andean mountains due to the strong lack of precipitation in the coastal regions (Mortensen *et al*., 2018). Water-dependent economic sectors in these countries (e.g., agriculture, energy production) are mainly based on the seasonal melting of glaciers (Bradley *et al*., 2006; Mark *et al*., 2017) which have undergone a marked retreat (Kaser, 1999; López-Moreno *et al*., 2014). This makes the mountainous areas of the tropics among the regions most vulnerable to global warming (Vuille *et al*., 2008; Bradley *et al*., 2009). In the Tropical Andes, warming signals are stronger in the most elevated sites compared to low-elevationed locations (Morán-Tejeda *et al*., 2016; Vicente-Serrano *et al*., 2018), although there are also some world regions where this elevation-dependent warming has not been detected, due to diverse factors (Rangwala and Miller, 2012; Pepin *et al*., 2015) in their global studies. Thus, a proper understanding of the spatial and temporal variability of air temperature LRs is needed to improve the understanding of air temperature distribution over complex terrain in the Tropical Andes.

The Ecuadorian and Peruvian climate is influenced by the complex phenomenon of El-Niño-Southern-Oscillation (ENSO). In particular, changes in sea-surface temperatures (SSTs) of the Pacific Ocean can alter meteorological patterns of the South American coast. This phenomenon implies that, during the positive phase, the habitual and dominant trade winds from the east are weakened, allowing overheating of the sea surface and its larger influence on the continental zones from the west (inverse pattern in the negative phase), as Dijkstra (2006) explains. The impacts of the ENSO on the Andean region

are assessed, including precipitation (Barros *et al.*, 2008; Grimm *et al.*, 2009), air temperature (Vuille and Bradley, 2000; Francou *et al.*, 2004; Vuille *et al.*, 2015), drought severity (Vicente-Serrano *et al.*, 2017), but with no investigation of their links to LRs. This investigation is highly desired in the tropical Ecuadorian and Peruvian Andean regions, given the strong seasonality of their climate due to the shift of the Inter Tropical Convergence Zone (ITCZ) during the year.

Within this background, this study endeavoured to assess the spatiotemporal characteristics of air temperature elevation LR in the Ecuadorian and Peruvian Andes, and their links to specific humidity and the ENSO during the period 1994–2011. The overriding objectives of this work are to (a) define annual, seasonal and monthly air temperature LR reference values; (b) analyse the effects of seasonality, specific humidity, ENSO and topography on LRs; and (c) identify subregional representative pair-stations, which allows for estimating air temperature LR in data-scarce areas.

2 | STUDY AREA

The Andean Mountains are located parallel to the Pacific coast of South America, extending for more than 7,000 km to the southern foothills of Cape Horn (Figure 1). The study area includes the Andean areas of Ecuador and Peru, disregarding Amazonian and coastal territories due to our special interest in mountainous regions, the uneven distribution of their weather stations, and their relatively low altitudes (Marengo *et al.*, 2016), affected by the usual coastal fogs. The study domain has a total area of almost 400,000 km^2, mostly above 3,000 m a.s.l., with its highest peaks in Huascarán Peak (Peru) at 6,768 m a.s.l. and Chimborazo volcano (Ecuador) at 6,267 m a.s.l. This steep slope represents almost a barrier for the Pacific and the Amazonian air masses. Here, the study area was divided into two subregions, separated by the latitude 9°30′S: namely the north and south domains. The northern territory (1°N-9°30′S) has a coastal plain that extends inland to the foothills, with widths varying from 10 to 150 km. Next, the land rises to the highlands (∼3,000 m a.s.l.), where a large part of the population is located (García and Santiago Ochoa, 2012). The southern territory (9°30′-18°S) has a narrow coastal plain, which runs 15 km inland at most, generating a sudden rise in elevation from the sea to the highlands. The topographical gradient is very strong, particularly in the Peruvian Altiplano (∼4,000 m a.s.l.), where elevation exceeds 5,500 m within only 85 km from the coast. While the climate of the northern and southern subregions of the study domain is generally tropical, some considerable differences exist due to the impact of latitude. Specifically, the northern subregion is typically equatorial (i.e., warm and rainy climate most of the year, especially on the coastal plain). Once the effect of elevation is removed, annual precipitation clearly decreases from North to South in the whole Tropical Andes, mainly driven by the ITCZ passage, shorter as it approaches the Tropic of Capricorn (Gruber, 1972). In the northern subregion, rainfall mainly occurs during March–April and October–November. The southern subregion is dryer, especially when approaching the Atacama desert in the extreme south (Cárdenas Gaudry *et al.*, 2017). The southern highlands show larger daily thermal amplitude due to a combined impact of aerial extension and elevation, which enhance continental conditions (Vicente-Serrano *et al.*, 2018).

Coastal fogs occur in both the northern and southern subregions. This phenomenon has been studied in depth (Pinche Laurre, 1986; Schemenauer and Cereceda, 1993) and is persistent from June to September, occasionally from April to November and, exceptionally, it can appear in the rest of the year. Fogs are important due to their impact modulating coastal air temperature. This phenomenon is generally affected by the existence of the cold Humboldt Current which laps the coasts, especially the Peruvian coasts, but also those of Ecuador, although it can be generated by other diverse factors. The frequency of coastal fogs increases gradually to the south, causing a marked diurnal cooling in the affected areas.

3 | RAW DATASET DESCRIPTION

3.1 | Observed air temperature data

A daily raw maximum and minimum air temperature database of 694 manually observed weather stations across Ecuador and Peru was provided by the governmental meteorological services of Ecuador (INAMHI) and Peru (SENAMHI). Analysis was restricted to stations located along the highlands, western slopes and those situated along the continental coastlines. First, our analysis selected 363 stations in the northern subregion and 164 stations in the southern subregion. Air temperature data have been measured following World Meteorological Organization guidelines (WMO, 2014), that is, at ∼1.5–2.0 m height above the ground and protected with naturally-ventilated Stevenson screens against solar radiation and weather (van der Meulen and Brandsma, 2008). Air temperature data were subjected to a robust quality-control and homogenization protocol detailed in Section 4. Analysis was restricted to the period October 1994–September 2011, given that this study

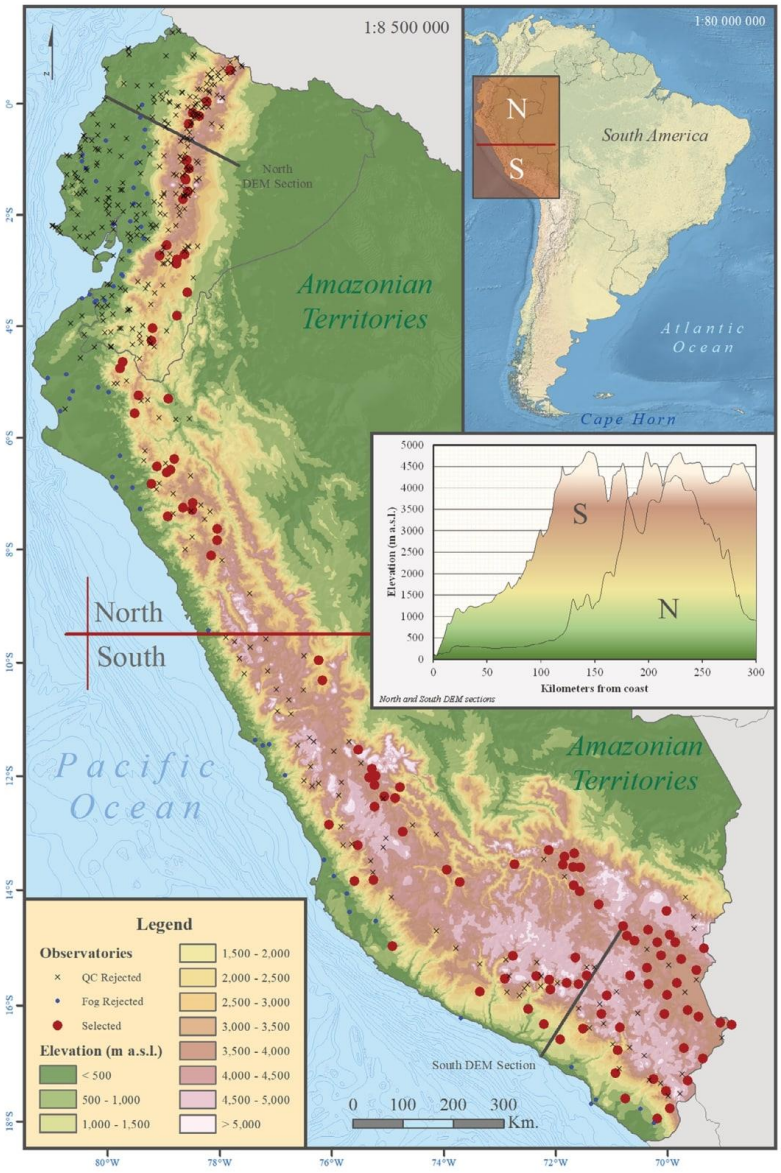

FIGURE 1 Topography of the study domain. The northern and southern subregions are delimited by the 9°30′S parallel. The available, selected, fog rejected, and rejected (denoted with x symbol) weather stations are shown. Two cross-sectional elevation profiles for the northern and southern subregion are also included (solid grey lines)

period guarantees the highest density of climate records. In contrast, the 1970s and 1980s show a relatively lower data density, especially in the northern subregion. Finally, following the quality control and homogeneity testing, data from 76 and 93 weather stations in the northern and southern subregion, respectively (see Table S1 and Figure S1) were retained. The final dataset includes high quality, quasi-complete, and homogenous

time series, which were used for the subsequent analysis. Weather stations have been classified depending on their relative position in relation to elevation within 25 km in the surroundings: Bottom (0–33.3%), Slope (33.3–66.6%) and Summit (66.6–100%).

3.2 | El Niño southern oscillation (ENSO)

In order to analyse the influence of the ENSO phenomenon from different locations, it has been analysed by two different indexes: El Niño 3.4 and El Niño 1 + 2 (i.e., ONI and ICEN, respectively). The widely known Oceanic Niño Index (ONI) has been used to synthesize the behavior of sea surface temperature in the 3.4 Pacific region, defined by Rasmusson and Carpenter (1982) and showed in Figure S2. Data has been provided by the NOAA - Climate Prediction Center (https://origin.cpc.ncep.noaa.gov/products/analysis_monitoring/ensostuff/ONI_v5.php, last accessed on 19th January 2020) at 3 months moving average resolution (Huang *et al*., 2017), based on ERSSTv5 data. To synthesize the behavior of sea surface temperature in the 1 + 2 coastal Pacific region the Índice-Costero-El-Niño (ICEN) was chosen on a monthly basis, used previously in the Ecuadorian territory (Morán-Tejeda *et al*., 2016). ICEN has been provided by the Peruvian Government (http://www.met.igp.gob.pe/variabclim/indices.html, last accessed on 19th January 2020), based on ENFEN (2012) and updated by Takahashi *et al*. (2014). Following the different criteria of the original authors, the El Niño positive phases are identified as follows: (ONI): five consecutive 3 months moving average above +0.5 (below −0.5 are identified as La Niña negative phases); (ICEN): three consecutive 3 months moving average above +0.4 (below −1.0 are identified as La Niña negative phases).

Following the methodology outlined in ENFEN (2012) and Huang *et al*. (2017), the monthly ONI and ICEN values were computed to determine the positive (El Niño), neutral (Neutral) and negative (La Niña) phases of the ENSO phenomenon, as well as intensity. The ICEN and ONI phases showed some common features. However, some differences due to the use of two different thermal anomalies in the Pacific sector were found. This refers to weak differences in the transition from the neutral phases to the positive and negative phases, as well as delays in the start of significant anomalies, which could slightly alter the results. In any case, the two indices identified similar strong and very strong El Niño events (>1.5 ONI; >1.7 ICEN), such as 1972, 1982–1983, 1987, 1992 and 1997–1998). Likewise, strong La Niña events (< −1.5 ONI; < −1.4 ICEN) were also identified by the ICEN and ONI indices, but with weak differences, in which La Niña events were less frequent using the ICEN index. Nonetheless, strong and very strong La Niña events were detected by both indices (e.g., 1973–1976, 1988–1989, 1998–2001, 2007 and 2010).

3.3 | Specific atmospheric humidity

Specific atmospheric humidity ($g \cdot kg^{-1}$) was analysed to delimitate wet and dry seasons. It has been extracted from the ERA-Interim reanalysis (Berrisford *et al*., 2011) at 500 hPa geopotential height at 6-hourly intervals (https://www.ecmwf.int/en/forecasts/datasets/reanalysis-datasets/era-interim, last accessed on 19th January 2020) from the start of available data (January 1979). The spatial horizontal resolution is about 0.7°. The 500 hPa geopotential height (i.e., ∼5,500 m a.s.l.) is above the average elevation of the region but affects surface conditions, while at higher geopotential heights (e.g., 100–300 hPa), the effects of specific humidity on surface air temperature would not be so obvious and direct due to its approximate correspondence with >9,000 m a.s.l.

Raw 6-hourly (UTC + 0) 500 hPa specific humidity data were aggregated to daily scale. Later, two subregional series were created for the northern and southern subregions using an arithmetic average of daily specific humidity for all pixels belonging to each subregion. In this process, raw 6-hourly (UTC + 0) specific humidity data were adapted to local time zone (UTC-5), at the same time as air maximum and minimum daily temperature measurements.

4 | METHODS

4.1 | Quality control and homogenization protocol

The raw dataset (694 weather stations) was subjected to a robust quality control (QC) and homogenization (Hom.) process, which consisted of six defined steps (Figure 2):

- Step 1: (QC) consisted of discarding weather stations without metadata (i.e., latitude, longitude, elevation and recognized identifier), in addition to those located in the Amazon and insular territories, out of the analysed study areas.
- Step 2: (QC) consisted of data screening using the protocol proposed by Tomás-Burguera *et al*. (2016), which removes questionable samples according to Durre *et al*. (2010). This step aims to detect codification errors

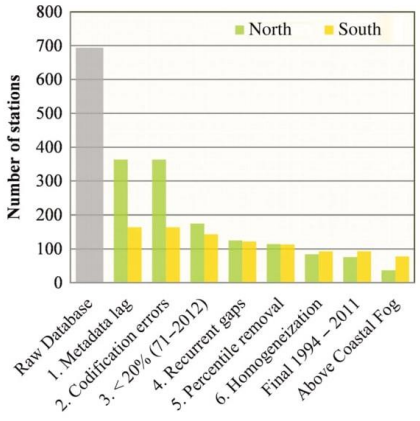

FIGURE 2 The total number of the selected meteorological observatories following the different steps of quality control and homogenization testing for both northern (left bar) and southern (right bar) subregion. Raw database has not subregion distinction due to the location lags

and extreme outliers to ensure data accuracy. The codification errors were: samples recorded on erroneous dates; seven or more consecutive days with identical value; write '0°C' when NA corresponds; invalid data units; $T_{min} \geq T_{max}$; and diurnal variation larger than 35°C. The outliers were identified by comparing with the extremes of the study area to maintain reliable values (i.e., between −35 and 50°C). Step 2 does not imply a reduction in the number of weather stations but a reduction in the amount of daily records.

- Step 3: (QC) consisted of discarding stations with less than 20% daily samples, referred to original temperature raw database period (January 1, 1971–December 31, 2012), which means 3,068 days (> 8 complete years).
- Step 4: (QC) consisted of discarding weather stations affected by continuous and recurrent gaps, despite achieving Step 3, due to doubts about the quality of the data.
- Step 5: (QC) consisted of removing daily records above percentile 99 (P_{99}, extreme warming) and below percentile 1 (P_{01}, extreme cooling) of change in relation to the previous day, along complete weather stations that experienced these repeated problems. During the QC process, it was preferred to remove weather stations of uncertain quality and keep only the truly reliable ones.
- Step 6: (Hom.) consisted of homogenizing air temperature by applying relative homogeneity statistics, following the procedure described by Domínguez-Castro *et al.* (2018) at a daily scale. Daily missing data were not filled using available data from neighbouring stations, due to large variability of temperature even over short distances. Also, this reconstruction process may introduce new inhomogeneities into the series from the candidate closing series, which can add further challenges to LR calculation.

Finally, weather stations without any data in the definitive study period, October 1, 1994–September 30, 2011, and those weather stations located in the coastal areas, where coastal fog exists were discarded. Low-stratiform clouds and coastal fogs have large influences on near-surface air temperatures, leading to noticeable thermal inversion at coastal areas. The inclusion of these coastal areas generates serious noise problems in LR calculations outside the fog layer. Therefore, aiming to know the air temperature distribution in the mountainous area (where air temperature modelling is mainly needed), makes its elimination appropriate. As such, to determine the definition of coastal areas, the elevation threshold based on Pulgar-Vidal (1987) (i.e., 500–600 m a.s.l). and the height of the thermal inversion layer based on cloudiness were analysed. Therefore, August MODIS-Terra satellite daily imagery from 2000 to 2012 was analysed to detect coastal foggy days for the northern and southern subregions (e.g., in the Figure 3). August was chosen due to its central position in the dry and coastal foggy season. The corrected reflectance (True Colour) product was analysed (https://earthdata.nasa.gov/faq#ed-CRvsSR, last accessed on 19th January 2020) in addition to air temperature values of the weather station network to determinate the thermal inversion thresholds. Although there is certain variability in the daily thermal inversion high, 400 m (northern subregion) and 600 m (southern subregion) were defined as the best and conservative thresholds to determine the height of the thermal inversion layer. After applying the coastal fog-elevation threshold filter, a total of 115 stations were used in this study (37 in the northern subregion and 78 in the southern subregion). The vertical distribution of the final dataset is shown in Figure 4. A quick inspection of Figures 1 and 4 reveals that the elevation range between 1,000 and 2,000 m a.s.l is poorly represented in the final dataset. This lack of observations is due to the location of the main cities either below (coastal plain) or above (highlands) these elevation bands.

4.2 | Daily air temperature LR

Maximum (LR_{max}) and minimum (LR_{min}) daily air temperature LR were calculated separately for the northern

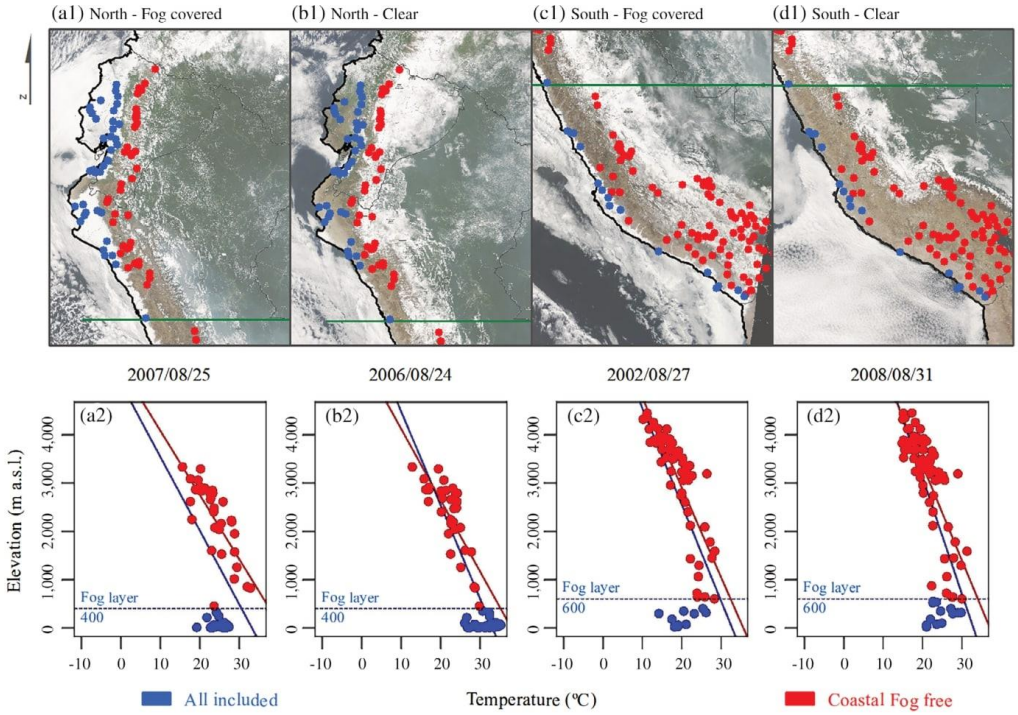

FIGURE 3 Example of MODIS-Terra satellite images in two situations of (i) coastal fog-covered, and (ii) cloud-free days for both (a, b) northerh, and (d, e) southern subregions. The vertical distribution of air temperature is represented in lower panels. Coastal fog-free stations of the northern (> 400 m a.s.l.) and southern subregion (>600 m a.s.l.) are represented in red, while weather stations located below the coastal fog elevation threshold were represented in blue. Lines represent the best linear fitted model between elevation and air temperature using all available weather stations (blue lines) and using only fog-free weather stations (red lines)

and southern subregions for the period October 1994–September 2011 with all selected series. Since the number of available series varies daily, the mean number of weather stations used in the regressions was 31 for the northern subregion and 65 for the southern subregion. Following Rolland (2003) and Navarro-Serrano *et al*. (2018) procedures, multiple daily regressions were used to compute daily air temperature LR. This was conducted by removing the effect of other topographic and geographic variables (i.e., latitude and sea distance), formulated as:

$$T'_{max} \text{ or } T'_{min} = a_0 + a_1 \text{Elev} + a_2 \text{Lat} + a_3 \text{Sea} + e.$$

where T'_{max} and T'_{min} are the daily maximum and minimum air temperatures (in °C), respectively; Elev, Lat and Sea are elevation above sea level (in m a.s.l.), latitude (in decimal degrees), and distance to the sea (in km), respectively; e is the regression error; and a_1, a_2 and a_3 are the regression coefficients, a_1 corresponding to the daily maximum (LR_{max}) or minimum (LR_{min}) lapse rate. These daily LRs were aggregated to months and seasons, and by ENSO phases, in order to develop reference LRs for the northern and southern subregions. LRs at daily, monthly and seasonal scales have been compared by the Wilcox–Mann–Whitney test to identify statistically significant differences among groups (i.e., ENSO phases, seasons, subregions and maximum–minimum). The Wilcoxon–Mann–Whitney (Wilcoxon, 1945) is a nonparametric statistical test that allows for testing the similarity/differences between two independent samples. Differences were tested at 0.05 level of significance.

A validation process was implemented to assess the accuracy of the computed monthly LRs. Herein, 90% of weather stations was randomly selected and the remaining 10% was used for validation purposes. Daily and monthly MAE statistics were computed from the residuals between maximum and minimum air

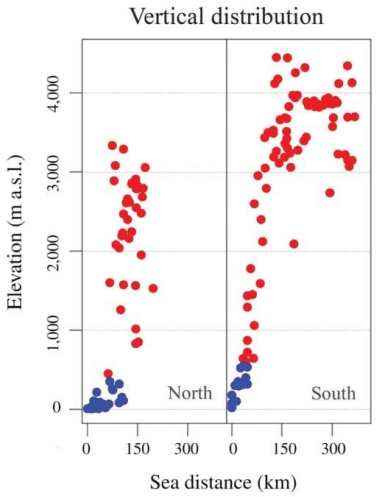

FIGURE 4 Vertical distribution of the selected station network. Coastal and fog-free stations of the northern (threshold 400 m a.s.l.) and southern subregion (threshold 600 m a.s.l.) are represented

temperature observed and the estimated by the regression model derived from 90% of weather stations, and were summarized at monthly basis (in absolute °C).

4.3 | Local versus subregional LRs

The possibility of estimating subregional air temperature LR using data from only two representative weather stations at large elevational ranges (difference, in meters, between the elevation above sea level of the two weather stations) was also tested. Then, the LR obtained from those pairs was compared with the LR obtained from all stations. For this purpose, the same equation (Section 4.2) was used to calculate daily air temperature LR for all combinations between pairs of weather stations, regardless of elevation range. Next, these daily "pair lapse rates" were aggregated at a seasonal scale, compared with those calculated from all stations. A similar procedure for LR calculation from two weather stations was adopted by Holden and Rose (2011) in England and Nigrelli *et al*. (2017) in the Alps, in addition to other old works, due to the absence of a wide observational network or long-term air temperature series. The absolute residuals were summarized by seasons. The Mean Absolute Error (MAE) statistics were computed and correlations between the two LRs were analysed. MAE was tabulated in relation to the elevation range between each pair using different categories of this range, that is, less than 500 m, 500–999 m, 1,000–1,499 m, 1,500–1,999 m, and higher than 2,000 m. In addition, the effect of horizontal distance between pairs was analysed.

4.4 | Wet/dry season definition

Two seasons were identified as a function of the 500 hPa specific atmospheric humidity and frequency of coastal fogs as a sign of seasonal change (Figure S3): (a) Dry Season (June–September) and (b) Wet Season (October–May). Dry season corresponds to the 4 months with smaller atmospheric humidity content. In addition, the dry season corresponds to a more frequent coastal foggy period as shown by MODIS-Terra satellite imagery (Paniagua-Guzmán, 2017), being a clear seasonal signal. The wet and dry seasonal specific atmospheric humidity content was statistically different ($p < .05$), for both the northern and southern subregions.

5 | RESULTS AND DISCUSSION

5.1 | Air temperature LR validation

Figure 5 summarizes two basic patterns: (1) MAE was larger ($p < .05$) for minimum than maximum air temperature in the two subregions, and (2) MAE was larger ($p < .05$) in the northern subregion for both maximum and minimum air temperatures. These results agree with earlier works that suggest more uncertainty modelling minimum/nocturnal air temperatures, especially in mountainous regions. Dodson and Marks (1997) indicate that interpolation methods based on statistical approaches (e.g., IDW, or kriging) have worse yields at nocturnal air temperatures due to specific local topography and aspect.

We also noted that the impact of seasonality is more pronounced in the southern subregion, as MAE increases mainly during the dry season (May–November is ∼2°C in maximum and ∼3°C in minimum air temperatures). In the northern subregion, seasonality is much less pronounced than in the southern region. Larger differences between the northern and southern subregions were identified during the wet season (October–May), while the dry season (June–September) balances both study areas (although the whiskers are larger in the northern subregion). The differences between MAEs of maximum and minimum air temperatures were larger in the north (∼2°C difference), while in the southern subregion they were similar during some wet season months (December–March); these differences increase (∼1.5°C) in the dry season. Non-absolute residuals were compiled in Table S2,

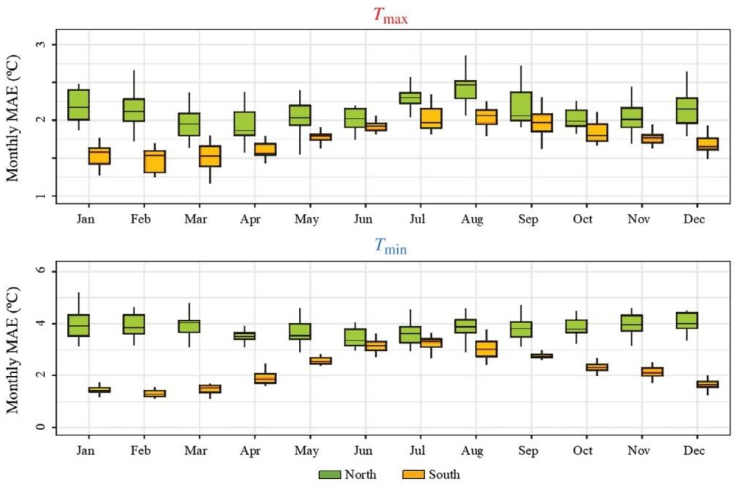

FIGURE 5 Monthly MAE (October 1994–September 2011) between the observed and estimated maximum and minimum air temperatures for the northern (left box) and southern (right box) subregions. The median (black line) and the interquartile range (boxes; *Y*-axis) are shown

and they were around 0°C. The significant differences in LRs as a function of the subregion and season are relevant. The spatial uncertainty and spatial distribution of LRs have already been evident in several studies, coming mainly from environmental factors such as specific humidity (Bolstad *et al.*, 1998; Du *et al.*, 2017), topography, continentality (Lewkowicz and Bonnaventure, 2011), distribution and representativeness of weather stations (Navarro-Serrano *et al.*, 2018).

5.2 | Air temperature LR, specific humidity and ENSO phases

Figure 6 illustrates the data period October 1994–September 2011 (all available data from 1971 are shown in Figure S4). Monthly LR peaks varied from −5.1 and −2.8°C·km^{-1} for the southern LR_{max}; −6.2 and −3.9°C·km^{-1} for the southern LR_{min}; −5.7 and −3.8°C·km^{-1} for the northern LR_{max}; and −5.2 and −2.7°C·km^{-1} for the northern LR_{min}. This supposes a small and reduced range between the steepest and weakest values in comparison with previous works, such as Blandford *et al.* (2008) in the Rocky Mountains, or Li *et al.* (2013). A fact that could be due to reduced thermal range and a climate less variable than the present on mid-latitude territories. This stresses that the use of a fixed MELR (i.e., −6.5°C·km^{-1}) might lead to gross errors (i.e., slightly during the wet season and strongly in the dry season). A similar finding in relation to MELR has been confirmed in previous studies (e.g., Hubbart *et al.*, 2007; Blandford *et al.*, 2008; Gardner *et al.*, 2009; Minder *et al.*, 2010; Kulshrestha and Ramsankaran, 2018). All these studies (located in Rocky Mountains, Arctic or Western Himalayas) showed different values (generally weaker) than −6.5°C·km^{-1}. Indeed, the marked seasonal variability in the calculated LR reference values would be missed when applying a fixed MELR. This was also confirmed by Dumas (2013) for the Alps and Heynen *et al.* (2016) for the Himalayas. The northern LR_{max} showed the smallest difference between maximum and minimum values. LR_{max} was affected largely by seasonality, as LRs exhibited steeper values during the wet season, compared to the dry season. These seasonal patterns were less evident for LR_{min}. The error of regression over the period has been constant (not shown in the figure), responding to the seasonal variability shown in the validation experiment (Figure 5).

Specific atmospheric humidity showed a marked seasonal pattern, with its highest values during the wet season (almost 3 g·kg^{-1} in the northern and southern subregions), while its lowest values were recorded during the dry season (∼1 g·kg^{-1} in both subregions). Nonetheless, the two subregions show statistically significant differences in their specific atmospheric humidity ($p < .05$), particularly in terms of seasonality. Seasonality is more marked in southern subregion. The interannual variability is relatively small in the two subregions during the wet and dry seasons, being remarkable only during some very wet periods (i.e., 1997–1998).

A quick inspection of Figure 6 (and Figure S4) reveals that the strong El Niño events (i.e., positive phases) were often followed by an increase of specific atmospheric humidity and an enhanced increase of LR_{max} and LR_{min} at a monthly scale. A representative example is the El Niño event in 1997–1998, especially in the southern subregion. Contrarily, the strong La Niña events (e.g., 1973–1976 or 2007) did not show significant impact

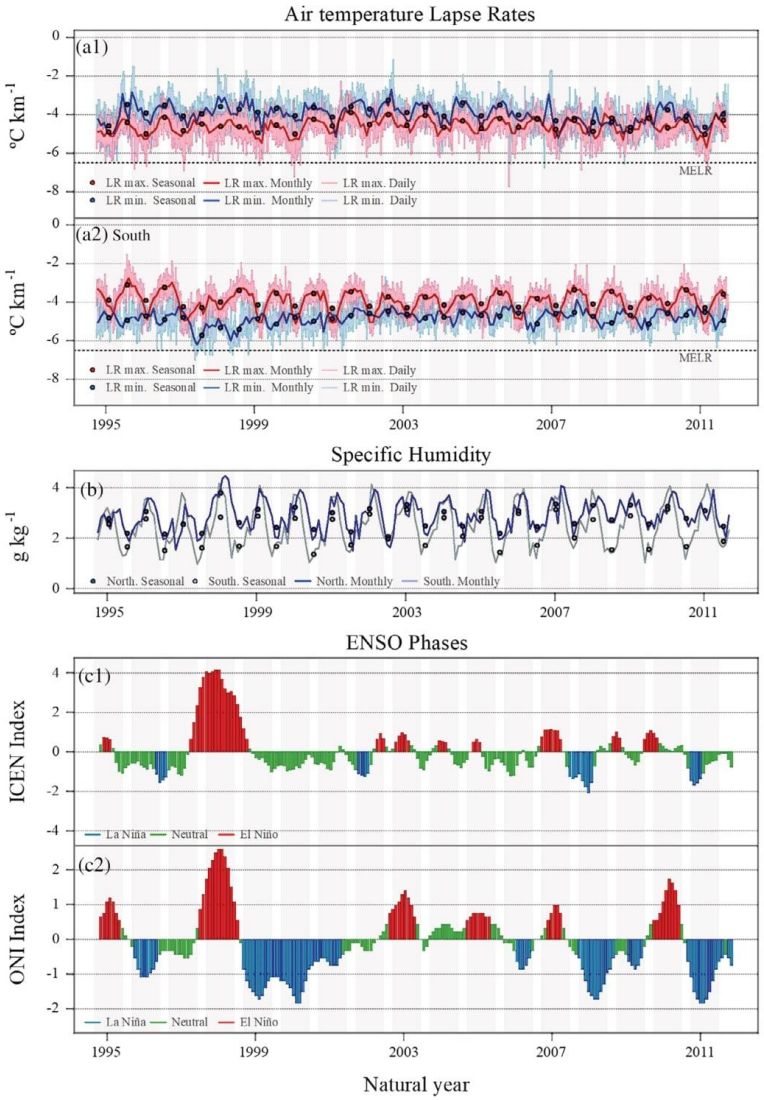

FIGURE 6 (a) Daily, monthly and seasonal north (a.1) and south (a.2) series of LR_{max} and LR_{min}. Mean environmental lapse-rate (MELR $-6.5°C \cdot km^{-1}$) was represented by dashed grey line; (b) monthly and seasonal 500 hPa specific atmospheric humidity (in $g \cdot kg^{-1}$); (c) ENSO El Niño (positive), neutral and La Niña (negative) phases based on the ICEN index (c.1) and the ONI index (c.2)

on LR variability. Overall, this behavior may be expected, given the low interannual variability of specific humidity. As such, specific humidity is more likely to increase during an El Niño positive phase.

5.3 | Reference air temperature LR

Table 1 shows the monthly and seasonal LR_{max} and LR_{min} values for each subregion. In the northern subregion, the steepest LR_{max} (LR_{min}) are during December (March), while the weakest LR_{max} (LR_{min}) are during June (September). In the southern subregion, the steepest LR_{max} (LR_{min}) are during February (May), while the weakest LR_{max} (LR_{min}) are during July (December). The main seasonal reference values for LR_{max} (LR_{min}), in $°C \cdot km^{-1}$, were: −4.77 (−4.10) for North-Wet; −4.26 (−3.78) for North-Dry; −4.16 (−4.74) for South-Wet; and − 3.57 (−4.93) for South-Dry. This implies that LR_{max} was steeper in the northern subregion than in the southern subregion

TABLE 1 Reference monthly and seasonal mean (and 25th/75th percentile information) LR_{max} and LR_{min} (in °C·km^{-1}) to northern and southern subregions

Month	North LR_{max}		North LR_{min}		South LR_{max}		South LR_{min}	
Wet season								
Oct	−4.6 (−4.8/−4.5)	−4.77	−3.8 (−4.2/−3.5)	−4.10	−3.6 (−3.7/−3.4)	−4.16	−4.6 (−4.7/−4.4)	−4.74
Nov	−4.8 (−4.9/−4.7)	(−4.97 /−4.54)	−4.0 (−4.1/−3.8)	(−4.41/−3.78)	−3.6 (−3.6/−3.5)	(−4.56/−3.75)	−4.8 (−5.1/−4.6)	(−4.84/−4.54)
Dec	−5.0 (−5.1/−4.8)		−3.9 (−4.1/−3.7)		−3.9 (−4.0/−3.8)		−4.5 (−4.6/−4.3)	
Jan	−4.9 (−5.1/−4.6)		−4.3 (−4.6/−4.0)		−4.5 (−4.6/−4.3)		−4.6 (−4.7/−4.5)	
Feb	−4.8 (−5.2/−4.5)		−4.3 (−4.7/−4.1)		−4.8 (−5.0/−4.6)		−4.7 (−4.8/−4.6)	
Mar	−4.9 (−5.1/−4.7)		−4.4 (−4.9/−4.3)		−4.7 (−5.0/−4.5)		−4.7 (−4.8/−4.5)	
Apr	−4.7 (−4.8/−4.7)		−4.2 (−4.3/−3.9)		−4.3 (−4.4/−4.2)		−4.8 (−5.0/−4.6)	
May	−4.5 (−4.6/−4.3)		−4.0 (−4.3/−3.7)		−4.0 (−4.1/−3.7)		−5.2 (−5.3/−5.0)	
Dry season								
Jun	−4.2 (−4.3/−4.2)	−4.26	−3.8 (−4.1/−3.5)	−3.78	−3.6 (−3.7/−3.5)	−3.57	−5.2 (−5.4/−5.0)	−4.93
Jul	−4.2 (−4.3/−4.1)	(−4.37/−4.12)	−3.9 (−4.2/−3.7)	(−4.13/−3.49)	−3.5 (−3.7/−3.3)	(−3.72/−3.37)	−5.0 (−5.1/−4.7)	(−5.12/−4.70)
Aug	−4.3 (−4.4/−4.2)		−3.8 (−4.1/−3.5)		−3.6 (−3.8/−3.4)		−4.9 (−5.1/−4.7)	
Sep	−4.3 (−4.6/−4.2)		−3.6 (−3.9/−3.3)		−3.6 (−3.8/−3.4)		−4.6 (−4.9/−4.4)	

($p < .05$), shared by a larger atmospheric instability and lower air pressure, which prevents air subsidence in the northern subregion. The effect of atmospheric instability and synoptic conditions on LRs has been previously indicated by Blandford *et al.* (2008), Gardner *et al.* (2009), Bonnardot *et al.* (2012) and Hanna *et al.* (2017) in different mountain areas of the globe. Thus, the larger instability throughout the year due to the proximity of the ITCZ has been proved analysing atmospheric pressure values, and the more progressive relief towards the highlands might cause steeper values of LR_{max}.

In contrast, LR_{min} was steeper in the southern subregion ($p < .05$), but with slight seasonal variations. LR_{min} was also affected by these north–south differences by the same phenomenon during the unstable and low-pressure characterized wet season. In contrast, during the stable dry season, unexpectedly LR_{min} is steeper than LR_{max} in the southern subregion. It is widely accepted that LR_{min} are weaker than LR_{max}, since they are generally impacted by several processes (e.g., cold air pool formations, thermal inversions in lowlands [Kattel and Yao, 2018]), which can weaken LR, as pointed out by many authors (Bonnardot *et al.*, 2012; Hanna *et al.*, 2017). However, the specific pattern found in the southern subregion could be attributed to some local factors of the database. The topographical position of the weather stations, which can induce the formation of nocturnal cold air pools at the position of the highest weather stations of the network (above 3,000 m a.s.l.), steepening the calculated LR (Duane *et al.*, 2008). This hypothesis has been analysed through the topographical position (bottom–slope–summit) of weather stations as a function of their elevation in relation to the surrounding areas. It has been observed (not shown in the results) that there are few weather stations located at summit topographical positions, being mainly located at the bottom of high valleys, or on sloped areas. In addition, the lower atmospheric humidity content at high elevation leads to steeper values of LR in response to night overcooling in these higher locations. Moreover, the enhanced continentality condition in the southern subregion increases the daily thermal amplitude, and favours a steeper LR_{min} compared to LR_{max}. Continentality, low specific humidity, and location of weather stations could favour the diurnal heating at higher weather stations, usually located at the bottom of high valleys, thus weakening the whole subregional LR_{max}. This feature was less evident in the northern subregion, where there is lower air pressure, more atmospheric instability and higher specific humidity due to the proximity to the ITCZ (Takahashi *et al.*, 2007), in addition to the lower continentality of northern weather stations, causing that LR_{max} and LR_{min} were more balanced to the habitual pattern.

The weakening of LRs during the dry season when the atmosphere is rather stable has been reported in previous works (Richardson *et al.*, 1999; Pepin and Losleben, 2002; Harlow *et al.*, 2004; Marshall *et al.*, 2007), although this is not always valid, as Kattel *et al.* (2015) and Kattel and Yao (2018) show in their Himalayan works; and Córdova *et al.* (2016) in a specific Ecuadorian valley for a 12-month period. Moreover, LR_{max} was more intensified during the wet season. The dispersion of LR values is synthetized by showing values corresponding to the 25 and 75 quantiles. The percentiles are close to the mean values, suggesting low interannual LR variability. LR_{max} and LR_{min} were significant different in the south and in the north ($p < .05$), and northern and southern LRs were significantly different analysing LR_{max} ($p < .05$) and LR_{min} ($p < .05$) data.

5.4 | Links between ENSO and LRs

Table 2 shows the LR_{max} and LR_{min} as a function of the subregion, seasons and ENSO phases. For the ENSO phases, more complex patterns were found:

- LR–ONI: In the northern and southern subregions, the steepest LR_{max} during the wet season occur during La Niña phases, although they were only statistically significant ($p < .05$) in the northern subregion; during the dry season in the south, the steepest LR_{max} occured during El Niño phases ($p < .05$) and in the northern subregion no statistical significant ($p > .05$) ENSO phase differences were found. In terms of LR_{min}, the only statistically significant differences ($p < .05$) were found analysing the northern

TABLE 2 Reference seasonal mean (and 25th/75th percentile information) LR_{max} and LR_{min} (in °C·km^{-1}), as a function of the subregion and ENSO phases

Season	North	South	ENSO index phase	
LR_{max} (in °C·km^{-1})				
Wet season (October–May)	−4.73 (−4.89/−4.55)*	−4.07 (−4.38/−3.79)	El Niño (+)	ONI
	−4.63 (−4.85/−4.43)*	−4.12 (−4.49/−3.71)	Neutral	
	−4.91 (−5.16/−4.67)*	−4.26 (−4.76/−3.73)	La Niña (−)	
	−4.68 (−4.85/−4.51)	−4.09 (−4.37/−3.78)*	El Niño (+)	ICEN
	−4.82 (−5.01/−4.62)	−4.25 (−4.69/−3.85)*	Neutral	
	−4.67 (−4.90/−4.52)	−3.63 (−3.74/−3.52)*	La Niña (−)	
Dry season (June–September)	−4.26 (−4.46/−3.99)	−3.95 (−4.07/−3.76)*	El Niño (+)	ONI
	−4.19 (−4.28/−4.08)	−3.51 (−3.68/−3.35)*	Neutral	
	−4.37 (−4.54/−4.25)	−3.44 (−3.56/−3.36)*	La Niña (−)	
	−4.35 (−4.53/−4.19)	−3.76 (−3.98/−3.43)*	El Niño (+)	ICEN
	−4.22 (−4.34/−4.07)	−3.53 (−3.68/−3.46)*	Neutral	
	−4.23 (−4.33/−4.19)	−3.34 (−3.38/−3.31)*	La Niña (−)	
LR_{min} (in °C·km^{-1})				
Wet season (October–May)	−3.99 (−4.36/−3.62)*	−4.76 (−4.86/−4.53)	El Niño (+)	ONI
	−4.04 (−4.31/−3.73)*	−4.76 (−5.03/−4.52)	Neutral	
	−4.23 (−4.61/−3.90)*	−4.70 (−4.82/−4.56)	La Niña (−)	
	−3.96 (−4.27/−3.70)	−4.87 (−5.16/−4.59)*	El Niño (+)	ICEN
	−4.17 (−4.50/−3.82)	−4.72 (−4.83/−4.55)*	Neutral	
	−3.99 (−4.38/−3.50)	−4.51 (−4.70/−4.33)*	La Niña (−)	
Dry season (June–September)	−3.67 (−3.94/−3.41)	−5.06 (−5.51/−4.42)	El Niño (+)	ONI
	−3.80 (−4.15/−3.45)	−4.90 (−5.08/−4.70)	Neutral	
	−3.81 (−4.08/−3.60)	−4.91 (−5.12/−4.79)	La Niña (−)	
	−3.98 (−4.37/−3.69)	−5.24 (−5.48/−5.05)*	El Niño (+)	ICEN
	−3.66 (−3.90/−3.44)	−4.86 (−5.06/−4.68)*	Neutral	
	−3.92 (−4.14/−3.67)	−4.65 (−4.83/−4.42)*	La Niña (−)	

Note: Asterisk (*) represents significant (<0.05) LRs differences between positive (El Niño) and negative (La Niña) episodes.

subregion during the wet season, with steepest values during La Niña phases.

- LR–ICEN: In the northern subregion, no statistically significant ($p > .05$) differences between ENSO phases and LR_{max} and LR_{min} were found. In the southern subregion, the steepest LR_{max} ($p < .05$) occurred during El Niño phases in the wet and dry seasons.

Figure 7 illustrates the seasonal differences found in all combinations between ENSO indices, seasons and subregions. The differences between ONI and ICEN (comparing the lapse rates during the same ENSO phase calculated from both indices) were weak and statistically non-significant for El Niño ($p > .05$, with the exception of south LR_{min}), while being weak and statistically significant for La Niña ($p < .05$, with the exception of north LR_{min}) phases. However, the differences among the ENSO phases were statistically significant ($p < .05$), with the exception of ICEN phases in the northern subregion ($p > .05$), and ONI phases ($p > .05$) for the southern LR_{min}, in addition to ONI phases during the dry season. The differences between ENSO phases were smaller than the seasonal variability. In the southern subregion, it was possible to detect a weak and statistically significant steepness of LRs when the El Niño phase occurs, especially following ICEN phases. In the northern subregion, only ONI phases and during the wet season was statistically significant, showing a steepness during La Niña phases. In summary, it seems that ENSO effects were more detectable in the southern subregion, compared to the northern subregion, showing better response of the southern subregion to ICEN phases, and northern subregion to ONI phases, although with nuances in relation to El Niño and La Niña effects.

Therefore, similar to other studies (Bennett *et al.*, 2016; Morán-Tejeda *et al.*, 2016) in Puna (Bolivia and Chile) and Ecuador, respectively, the dependency between air temperature and the ENSO was not statistically significant in all cases. Moreover, ENSO effects are spatially variable and not equal over the whole south American coast (Morán-Tejeda *et al.*, 2016). The ENSO effects were stronger in the southern subregion, since its low variability and high temporal stability facilitate strong air mass irruptions from the west (i.e., strong positive ENSO episodes). This relationship only during extreme episodes implies that the neutral and weak positive ENSO episodes fail to penetrate inland sufficiently (Dijkstra, 2006) to affect the weather station network and change the subregional LRs. Contrarily, during strong and very strong El Niño episodes, the west-to-east associated pattern could reach the mainland and the Andean lands in Ecuador and Peru, largely covering the weather station network and, thus, could alter air temperature conditions over the whole study area. Comparative analysis between ENSO indices has shown that the ICEN index is more appropriate for the southern subregion, as ENFEN (2012) and Takahashi *et al.* (2014) actively seek with the development of this index for the Peruvian territory, while ONI has higher influence in the northern subregion.

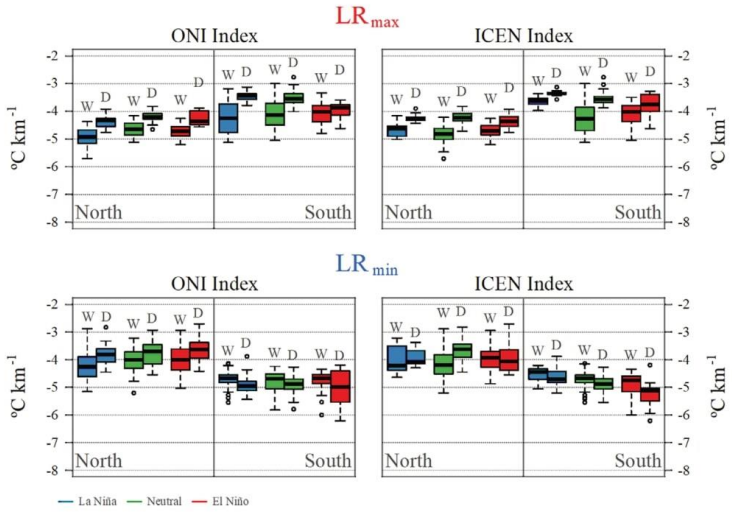

FIGURE 7 LR_{max} and LR_{min} by means of the ENSO phases and indices distribution for both the wet (W) and dry (D) seasons during the common period October 1994–September 2011. La Niña (left pair boxes), neutral (central pair boxes) and El Niño (right pair boxes) are represented

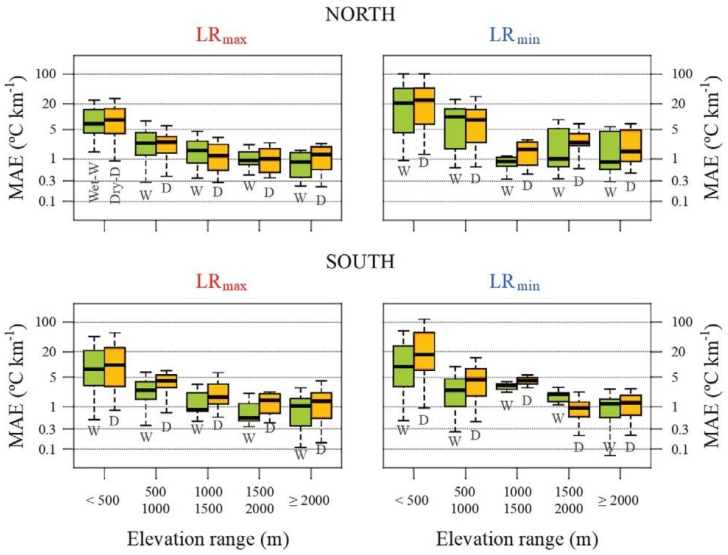

FIGURE 8 Seasonal LR_{max} and LR_{min} MAE distribution by season (i.e., wet and dry) and elevation range between pairs (in meters) for both the northern and southern subregions. MAE is represented by a logarithmic *y*-axis from 0.1 to 100ºC·km^{-1} due to aberrant values found. The median (black line), the interquartile range (boxes), and whiskers are shown

5.5 | Comparison of local and regional lapse rates

Figure 8 depicts the MAE between seasonal LRs calculated from the pairs of weather stations and those calculated using the whole network. Box-plots illustrate that MAE is less when elevation range between pairs is larger than 1,500 m, as their vertical range allows for properly detecting the vertical air temperature profile. On the other hand, box-plots showing extremely higher values (>20°C·km^{-1}) when elevation range is <500 m. For all situations, the differences between the wet and dry seasons were detected, but with no clear pattern. MAE for LR_{max} was lower than LR_{min} for the northern and southern subregions. It can be observed that the median MAE tended to stabilize around 1°C·km^{-1} for elevation ranges larger than 1,500 m. Euclidean distance between the most representative pairs (Figure S5) have been analysed, but no significant patterns were found. The topographic position of pairs in relation to MAE have been analysed (Figure S6b), showing that it is not appropriate to choose only bottom located weather stations, since these pairs are not usually representative of the general behaviour. The most representative pairs (shown in Figures S7b) in almost all combinations had MAE values <0.3°C·km^{-1}. Seasonally, the wet season had better scores, in terms of MAE.

The findings suggest that there is a possibility to properly estimate the subregional seasonal LR using only a pair of stations. These findings imply that previous works carried out with few data can incur errors of low representativeness of the regional LRs. In the southern subregion, the most representative territory was the southeast, which has a large number of the most representative pairs. This allows for obtaining the subregional seasonal LR behavior for both the coastal and highlands territories. However, in all cases, the errors obtained using these representative stations were lower than those derived from the use of a fixed LR (e.g., the MELR). The low correlations in the majority of the selected pairs occurred due to the compensation between weak underestimations and overestimations of LRs along the study period. The remarkable low MAE values inform the reliability of the paired LRs. According to our findings in both northern and southern subregion, the calculation of LR from only two stations is possible, although it is necessary to choose weather stations representative of regional behavior, in addition to choosing weather stations with a minimum elevation range of at least 1,500 m; and studying the minimum number of weather stations needed to better represent lapse-rates.

To conclude, our findings indicate that due to various geographic, climatic, and topographic variables, LR is highly variable over space and time in the Andean region in Ecuador and Peru. This stresses the need to consider specific LRs rather than universal and fixed LRs (e.g., the MELR). However, it is noteworthy that the reference LR values are regionally specific and cannot be extrapolated to other regions, considering the large spatial and seasonal variability of air temperature on one hand and the possible impacts of local environmental factors on the other hand (Marshall *et al*., 2007). It is not recommended

to use the MELR, as it introduces large biases to air temperature estimations. Increasing the number of weather stations in mountain areas can improve estimation of air temperature LRs. This study contributes to better understanding of the factors controlling snow hydrology and water resources availability in dry areas. In this way, it has been possible to advance knowledge of the explanatory factors for its variability.

6 | CONCLUSIONS

This study assessed, for the first time, changes in air temperature LRs over the Andean region in Ecuador and Peru using in situ temperature data from 1994 to 2011. The major findings of this study can be summarized as follows:

1 It is more complex to estimate LR_{min} than LR_{max}, given that Tmin has more spatial heterogeneity and is more influenced by local meteorological processes.
2 The calculated LR_{max} and LR_{min} are weaker than the fixed Mean Environmental Lapse Rate (MELR $-6.5°C \cdot km^{-1}$), which has been widely used to interpolate and extrapolate air temperatures with multiple aims. Importantly, the calculated LRs are spatiotemporally more variable. This study stresses the need to calculate specific LR for each study area and season, as the fixed and standard MELR cannot adequately reveal the large spatial and temporal variability of air temperature in regions of complex topography.
3 LR_{max} and LR_{min} show steeper values during the wet season (October–May), with the exception of LR_{min} in the southern subregion, where continentality, topography, and specific humidity content could influence air temperature conditions.
4 The ENSO phenomenon significantly influences LR variability in the southern subregion, while its impact is more variable in the north. In some exceptional events corresponding mainly to the strong and very strong positive ENSO (El Niño) events (e.g., 1997–1998), LRs can support an intense steepness.
5 LRs can be calculated using limited data (i.e., pair of weather stations); however, this was mainly restricted to weather stations with an elevation range over 1,500 m, where MAE is generally around $1°C \cdot km^{-1}$.

These findings show the need to continue researching this issue for other spatial scales and geographical areas, so observed variability and patterns might be larger than commonly assumed by lapse rate users. In the future, it is necessary to advance in the assessment of the spatiotemporal variability and causes of LRs for other regions. Thus, based on our findings, the extrapolation of air temperature from lowlands to summits would be not recommended. In addition, an increase in the number of weather stations located in the summits is crucial to retrieve air temperature data over miles of km^2 in which they are generally extrapolated without using empirical data. Thus, a comprehensive monitoring of highest elevation areas and summits are needed to better obtain LRs for the whole study region, which may indirectly influence common human activities (e.g., water resources) or climate products as air temperature grid datasets.

ACKNOWLEDGEMENTS

This study was funded by the research project CGL2017-82216-R (HIDROIBERNIEVE) funded by the Spanish Ministry of Science, Innovation and Universities. We thank the Instituto Nacional de Meteorología e Hidrología de Ecuador (INAMHI) and the Servicio Nacional de Meteorología e Hidrología del Perú (SENAMHI) for providing the meteorological data used in this study. Navarro-Serrano, F. (FPU15/00742) is granted with a pre-doctoral FPU grant (Spanish Ministry of Education, Culture and Sports). Alonso-González, E. is granted with a pre-doctoral FPI grant (Spanish Ministry of Economy and Competitiveness). The authors thank all colleagues who helped in the development of the study. The authors wish to acknowledge anonymous reviewers for their detailed and helpful comments to the original manuscript.

ORCID

Francisco Navarro-Serrano https://orcid.org/0000-0002-2975-6472
Juan I. López-Moreno https://orcid.org/0000-0002-7270-9313
Fernando Domínguez-Castro https://orcid.org/0000-0003-3085-7040
Esteban Alonso-González https://orcid.org/0000-0002-1883-3823
Cesar Azorin-Molina https://orcid.org/0000-0001-5913-7026
Ahmed El-Kenawy https://orcid.org/0000-0001-6639-6253
Sergio M. Vicente-Serrano https://orcid.org/0000-0003-2892-518X

REFERENCES

Alonso-González, E., Ignacio López-Moreno, J., Gascoin, S., García-Valdecasas Ojeda, M., Sanmiguel-Vallelado, A., Navarro-Serrano, F., Revuelto, J., Ceballos, A., Esteban-Parra, M.J. and Essery, R. (2018) Daily gridded datasets of snow depth and snow water equivalent for the Iberian Peninsula from 1980 to 2014. *Earth System Science Data*, 10(1), 303–315. https://doi.org/10.5194/essd-10-303-2018.

Ambrozova, K., Laska, K., Hrbacek, F., Kavan, J. and Ondruch, J. (2019) Air temperature and lapse rate variation in the ice-free and glaciated areas of northern James Ross Island, Antarctic peninsula, during 2013-2016. *International Journal of Climatology*, 39(2), 643–657. https://doi.org/10.1002/joc.5832.

Appelhans, T., Mwangomo, E., Otte, I., Detsch, F., Nauss, T. and Hemp, A. (2016) Eco-meteorological characteristics of the southern slopes of Kilimanjaro, Tanzania. *International Journal of Climatology*, 36(9), 3245–3258. https://doi.org/10.1002/joc.4552.

Barros, V.R., Doyle, M.E. and Camilloni, I.A. (2008) Precipitation trends in southeastern South America: relationship with ENSO phases and with low-level circulation. *Theoretical and Applied Climatology*, 93(1–2), 19–33. https://doi.org/10.1007/s00704-007-0329-x.

Barry, R. (2008) *Mountain Weather and Climate*. Cambridge, UK: Cambridge University Press.

Barry, R. and Chorley, R. (2003) *Atmosphere, Weather and Climate* (8th edition). London: Routledge.

Bennett, M., New, M., Marino, J. and Sillero-Zubiri, C. (2016) Climate complexity in the Central Andes: a study case on empirically-based local variations in the dry Puna. *Journal of Arid Environments*, 128, 40–49. https://doi.org/10.1016/J.JARIDENV.2016.01.004.

Berrisford, P., Dee, D., Poli, P., Brugge, R., Fielding, K., Fuentes, M., Kallberg, P., Kobayashi, S., Uppala, S. and Simmons, A. (2011) The ERA-interim archive, version 2.0. *ERA Report Series*, 1, 1–23.

Blandford, T.R., Humes, K.S., Harshburger, B.J., Moore, B.C., Walden, V.P., Ye, H., Blandford, T.R., Humes, K.S., Harshburger, B.J., Moore, B.C., Walden, V.P. and Ye, H. (2008) Seasonal and synoptic variations in near-surface air temperature lapse rates in a Mountainous Basin. *Journal of Applied Meteorology and Climatology*, 47(1), 249–261. https://doi.org/10.1175/2007JAMC1565.1.

Bolstad, P.V., Swift, L., Collins, F. and Régnière, J. (1998) Measured and predicted air temperatures at basin to regional scales in the southern Appalachian mountains. *Agricultural and Forest Meteorology*, 91(3–4), 161–176. https://doi.org/10.1016/S0168-1923(98)00076-8.

Bonnardot, V., Carey, V., Madelin, M., Cautenet, S., Coetzee, Z. and Quénol, H. (2012) Spatial variability of night temperatures at a fine scale over the Stellenbosch Wine District, South Africa. *Journal International des Sciences de la Vigne et du Vin*, 46(1), 1–13.

Bradley, R.S., Vuille, M., Diaz, H.F. and Vergara, W. (2006) Climate change. Threats to water supplies in the tropical Andes. *Science (New York, N.Y.)*, 312(5781), 1755–1756. https://doi.org/10.1126/science.1128087.

Bradley, R.S., Keimig, F.T., Diaz, H.F. and Hardy, D.R. (2009) Recent changes in freezing level heights in the tropics with implications for the deglacierization of high mountain regions. *Geophysical Research Letters*, 36(17), L17701. https://doi.org/10.1029/2009GL037712.

Cárdenas Gaudry, M.M., Gutknecht, D., Parajka, J., Perdigão, R.A.P. and Blöschl, G. (2017) Seasonality of runoff and precipitation regimes along transects in Peru and Austria. *Journal of Hydrology and Hydromechanics*, 65, 347–358. https://doi.org/10.1515/johh-2017-0018.

Córdova, M., Célleri, R., Shellito, C.J., Orellana-Alvear, J., Abril, A. and Carrillo-Rojas, G. (2016) Near-surface air temperature lapse rate over complex terrain in the southern Ecuadorian Andes: implications for temperature mapping. *Arctic, Antarctic, and Alpine Research*, 48(4), 673–684. https://doi.org/10.1657/AAAR0015-077.

Dijkstra, H.A. (2006) The ENSO phenomenon: theory and mechanisms. *Advances in Geosciences*, 6, 3–15. https://doi.org/10.5194/adgeo-6-3-2006.

Dodson, R. and Marks, D. (1997) Daily air temperature interpolated at high spatial resolution over a large mountainous region. *Climate Research*, 8(1), 1–20. https://doi.org/10.3354/cr008001.

Domínguez-Castro, F., Vicente-Serrano, S.M., López-Moreno, J.I., Correa, K., Ávalos, G., Azorin-Molina, C., El-Kenawy, A., Tomas-Burguera, M., Navarro-Serrano, F., Peña-Gallardo, M., Gimeno, L. and Nieto, R. (2018) Mapping seasonal and annual extreme precipitation over the Peruvian Andes. *International Journal of Climatology*, 38(15), 5459–5475. https://doi.org/10.1002/joc.5739.

Du, M., Liu, J., Zhang, X., Li, Y., and Tang, Y. (2010). Changes of spatial patterns of surface-air-temperature on the Tibetan Plateau. Latest Trends on Theoretical and Applied Mechanics, Fluid Mechanics and Heat & Mass Transfer.

Du, M., Zhang, M., Wang, S., Zhu, X. and Che, Y. (2017) Near-surface air temperature lapse rates in Xinjiang, northwestern China. *Theoretical and Applied Climatology*, 131, 1–14. https://doi.org/10.1007/s00704-017-2040-x.

Duane, W.J., Pepin, N.C., Losleben, M.L. and Hardy, D.R. (2008) General characteristics of temperature and humidity variability on Kilimanjaro, Tanzania. *Arctic, Antarctic, and Alpine Research*, 40(2), 323–334. https://doi.org/10.1657/1523-0430(06-127).

Dumas, M.D. (2013) Changes in temperature and temperature gradients in the French northern Alps during the last century. *Theoretical and Applied Climatology*, 111(1–2), 223–233. https://doi.org/10.1007/s00704-012-0659-1.

Durre, I., Menne, M.J., Gleason, B.E., Houston, T.G., Vose, R.S., Durre, I., Menne, M.J., Gleason, B.E., Houston, T.G. and Vose, R.S. (2010) Comprehensive automated quality assurance of daily surface observations. *Journal of Applied Meteorology and Climatology*, 49(8), 1615–1633. https://doi.org/10.1175/2010JAMC2375.1.

ENFEN. (2012) *Definición operacional de los eventos El Niño y La Niña y sus magnitudes en la costa del Perú*. Lima: ENFEN.

Fang, J.-Y. and Yoda, K. (1988) Climate and vegetation in China (I). Changes in the altitudinal lapse rate of temperature and distribution of sea level temperature. *Ecological Research*, 3(1), 37–51. https://doi.org/10.1007/BF02348693.

Francou, B., Vuille, M., Favier, V. and Cáceres, B. (2004) New evidence for an ENSO impact on low-latitude glaciers: Antizana 15, Andes of Ecuador, 0°28′S. *Journal of Geophysical Research*, 109(D18), D18106. https://doi.org/10.1029/2003JD004484.

García, D. and Santiago Ochoa, W. (2012) Relación entre crecimiento económico y medio ambiente en Ecuador a nivel provincial (Promedio 2010-2015). *Revista Amazónica Ciencia y Tecnología*, 6(2), 99–112.

Gardner, A.S., Sharp, M.J., Koerner, R.M., Labine, C., Boon, S., Marshall, S.J., Burgess, D.O. and Lewis, D. (2009) Near-surface temperature lapse rates over Arctic glaciers and their implications for temperature downscaling. *Journal of Climate*, 22(16), 4281–4298. https://doi.org/10.1175/2009JCLI2845.1.

Grimm, A.M., Tedeschi, R.G., Grimm, A.M. and Tedeschi, R.G. (2009) ENSO and extreme rainfall events in South America. *Journal of Climate*, 22(7), 1589–1609. https://doi.org/10.1175/2008JCLI2429.1.

Gruber, A. (1972) Fluctuations in the position of the ITCZ in the Atlantic and Pacific oceans. *Journal of the Atmospheric Sciences*, 29(1), 193–197. https://doi.org/10.1175/1520-0469(1972)029<0193:fitpot>2.0.co;2.

Hanna, E., Mernild, S., Yde, J. and Villiers, S. (2017) Surface air temperature fluctuations and lapse rates on Olivares gamma glacier, Rio Olivares basin, Central Chile, from a novel meteorological sensor network. *Advances in Meteorology*, 2017, 1–15. https://doi.org/10.1155/2017/6581537.

Harlow, R.C., Burke, E.J., Scott, R.L., Shuttleworth, W.J., Brown, C. M. and Petti, J.R. (2004) Research note: derivation of temperature lapse rates in semi-arid South-Eastern Arizona. *Hydrology and Earth System Sciences*, 8(6), 1179–1185.

Hatfield, J.L. and Prueger, J.H. (2015) Temperature extremes: effect on plant growth and development. *Weather and Climate Extremes*, 10, 4–10. https://doi.org/10.1016/J.WACE.2015.08.001.

Heynen, M., Miles, E., Ragettli, S., Buri, P., Immerzeel, W.W. and Pellicciotti, F. (2016) Air temperature variability in a high-elevation Himalayan catchment. *Annals of Glaciology*, 57(71), 212–222. https://doi.org/10.3189/2016AoG71A076.

Holden, J. and Rose, R. (2011) Temperature and surface lapse rate change: a study of the UK's longest upland instrumental record. *International Journal of Climatology*, 31(6), 907–919. https://doi.org/10.1002/joc.2136.

Huang, B., Thorne, P.W., Banzon, V.F., Boyer, T., Chepurin, G., Lawrimore, J.H., Menne, M.J., Smith, T.M., Vose, R.S., Zhang, H.-M., Huang, B., Thorne, P.W., Banzon, V.F., Boyer, T., Chepurin, G., Lawrimore, J.H., Menne, M.J., Smith, T.M., Vose, R.S. and Zhang, H.-M. (2017) Extended Reconstructed Sea surface temperature, version 5 (ERSSTv5): upgrades, validations, and Intercomparisons. *Journal of Climate*, 30(20), 8179–8205. https://doi.org/10.1175/JCLI-D-16-0836.1.

Hubbart, J., Kavanagh, K., Pangle, R., Link, T. and Schotzko, A. (2007) Cold air drainage and modeled nocturnal leaf water potential in complex forested terrain. *Tree Physiology*, 27(4), 631–639. https://doi.org/10.1093/treephys/27.4.631.

Immerzeel, W.W., Petersen, L., Ragettli, S. and Pellicciotti, F. (2014) The importance of observed gradients of air temperature and precipitation for modeling runoff from a glacierized watershed in the Nepalese Himalayas. *Water Resources Research*, 50 (3), 2212–2226. https://doi.org/10.1002/2013WR014506.

Kaser, G. (1999) A review of the modern fluctuations of tropical glaciers. *Global and Planetary Change*, 22(1–4), 93–103. https://doi.org/10.1016/S0921-8181(99)00028-4.

Kattel, D.B. and Yao, T. (2018) Temperature-topographic elevation relationship for high mountain terrain: an example from the southeastern Tibetan plateau. *International Journal of Climatology*, 38, e901–e920. https://doi.org/10.1002/joc.5418.

Kattel, D.B., Yao, T., Yang, K., Tian, L., Yang, G. and Joswiak, D. (2013) Temperature lapse rate in complex mountain terrain on the southern slope of the Central Himalayas. *Theoretical and Applied Climatology*, 113(3–4), 671–682. https://doi.org/10.1007/s00704-012-0816-6.

Kattel, D.B., Yao, T., Yang, W., Gao, Y. and Tian, L. (2015) Comparison of temperature lapse rates from the northern to the southern slopes of the Himalayas. *International Journal of Climatology*, 35 (15), 4431–4443. https://doi.org/10.1002/joc.4297.

Kulshrestha, S. and Ramsankaran, R. (2018) Investigating the performance of snowmelt runoff model using temporally varying near-surface lapse rate in Western Himalayas. *Current Science*, 114, 808–813. https://doi.org/10.18520/cs/v114/i04/808-813.

Kunkel, K.E. (1989) Simple procedures for extrapolation of humidity variables in the mountainous Western United States. *Journal of Climate*, 2(7), 656–670. https://doi.org/10.1175/1520-0442(1989)002<0656:SPFEOH>2.0.CO;2.

Lewkowicz, A.G. and Bonnaventure, P.P. (2011) Equivalent elevation: a New method to incorporate variable surface lapse rates into mountain permafrost modelling. *Permafrost and Periglacial Processes*, 22(2), 153–162. https://doi.org/10.1002/ppp.720.

Li, X., Wang, L., Chen, D., Yang, K., Xue, B. and Sun, L. (2013) Near-surface air temperature lapse rates in the mainland China during 1962-2011. *Journal of Geophysical Research-Atmospheres*, 118(14), 7505–7515. https://doi.org/10.1002/jgrd.50553.

López-Moreno, J.I., Fontaneda, S., Bazo, J., Revuelto, J., Azorin-Molina, C., Valero-Garcés, B., Morán-Tejeda, E., Vicente-Serrano, S.M., Zubieta, R. and Alejo-Cochachín, J. (2014) Recent glacier retreat and climate trends in cordillera Huaytapallana, Peru. *Global and Planetary Change*, 112, 1–11. https://doi.org/10.1016/J.GLOPLACHA.2013.10.010.

Lussana, C., Tveito, O.E. and Uboldi, F. (2018) Three-dimensional spatial interpolation of 2 m temperature over Norway. *Quarterly Journal of the Royal Meteorological Society*, 144(711), 344–364. https://doi.org/10.1002/qj.3208.

Marengo, J.A., Williams, E.R., Alves, L.M., Soares, W.R. and Rodriguez, D.A. (2016) *Extreme Seasonal Climate Variations in the Amazon Basin: Droughts and Floods*. Berlin, Heidelberg: Springer, pp. 55–76.

Mark, B.G., French, A., Baraer, M., Carey, M., Bury, J., Young, K.R., Polk, M.H., Wigmore, O., Lagos, P., Crumley, R., McKenzie, J.M. and Lautz, L. (2017) Glacier loss and hydro-social risks in the Peruvian Andes. *Global and Planetary Change*, 159, 61–76. https://doi.org/10.1016/J.GLOPLACHA.2017.10.003.

Marshall, S.J., Sharp, M.J., Burgess, D.O. and Anslow, F.S. (2007) Near-surface-temperature lapse rates on the prince of Wales icefield, Ellesmere Island, Canada: implications for regional downscaling of temperature. *International Journal of Climatology*, 27(3), 385–398. https://doi.org/10.1002/joc.1396.

van der Meulen, J.P. and Brandsma, T. (2008) Thermometer screen intercomparison in De Bilt (The Netherlands), part I: understanding the weather-dependent temperature differences. *International Journal of Climatology*, 28(3), 371–387. https://doi.org/10.1002/joc.1531.

Minder, J.R., Mote, P.W. and Lundquist, J.D. (2010) Surface temperature lapse rates over complex terrain: lessons from the Cascade Mountains. *Journal of Geophysical Research*, 115(D14), D14122. https://doi.org/10.1029/2009JD013493.

Miró, J.R., Peña, J.C., Pepin, N., Sairouni, A. and Aran, M. (2017) Key Features of Cold-Air Pool Episodes in the Northeast of the Iberian Peninsula (Cerdanya, Eastern Pyrenees). *International Journal of Climatology*, 38(3), 1105–1115. https://doi.org/10.1002/joc.5236.

Moore, F.C. and Diaz, D.B. (2015) Temperature impacts on economic growth warrant stringent mitigation policy. *Nature Climate Change*, 5(2), 127–131. https://doi.org/10.1038/nclimate2481.

Morán-Tejeda, E., Bazo, J., López-Moreno, J.I., Aguilar, E., Azorín-Molina, C., Sanchez-Lorenzo, A., Martínez, R., Nieto, J.J., Mejía, R., Martín-Hernández, N. and Vicente-Serrano, S.M. (2016) Climate trends and variability in Ecuador (1966-2011). *International Journal of Climatology*, 36(11), 3839–3855. https://doi.org/10.1002/joc.4597.

Mortensen, E., Wu, S., Notaro, M., Vavrus, S., Montgomery, R., De Piérola, J., Sánchez, C. and Block, P. (2018) Regression-based season-ahead drought prediction for southern Peru conditioned on large-scale climate variables. *Hydrology and Earth System Sciences*, 22, 287–303. https://doi.org/10.5194/hess-22-287-2018.

Navarro-Serrano, F., López-Moreno, J., Azorin-Molina, C., Alonso-González, E., Tomás-Burguera, M., Sanmiguel-Vallelado, A., Revuelto, J. and Vicente-Serrano, S.M. (2018) Estimation of near-surface air temperature lapse rates over continental Spain and its mountain areas. *International Journal of Climatology*, 38, 3233–3249. https://doi.org/10.1002/joc.5497.

Nigrelli, G., Fratianni, S., Zampollo, A., Turconi, L. and Chiarle, M. (2017) The altitudinal temperature lapse rates applied to high elevation rockfalls studies in the Western European Alps. *Theoretical and Applied Climatology*, 131, 1479–1491. https://doi.org/10.1007/s00704-017-2066-0.

Ojha, R. (2019) Identification of Homogeneous Regions of near Surface Air Temperature Lapse Rates across India. *International Journal of Climatology*, 39(11), 4288–4304. https://doi.org/10.1002/joc.6073.

Paniagua-Guzmán, L.J. (2017) Condiciones microclimáticas en las lomas costeras y riesgos a la salud de los pobladores en Lima Metropolitana. In: del EGAL, A. (Ed.) *Observatorio Geográfico de América Latina*, Vol. XVI. La Paz, Bolivia: Observatorio Geográfico de América Latina, p. 15.

Pepin, N. (2001) Lapse rate changes in northern England. *Theoretical and Applied Climatology*, 68(1–2), 1–16. https://doi.org/10.1007/s007040170049.

Pepin, N.C. and Losleben, M. (2002) Climate change in the Colorado Rocky Mountains: free air versus surface temperature trends. *International Journal of Climatology*, 22(3), 311–329. https://doi.org/10.1002/joc.740.

Pepin, N., Bradley, R.S., Diaz, H.F., Baraer, M., Caceres, E.B., Forsythe, N., Fowler, H., Greenwood, G., Hashmi, M.Z., Liu, X. D., Miller, J.R., Ning, L., Ohmura, A., Palazzi, E., Rangwala, I., Schöner, W., Severskiy, I., Shahgedanova, M., Wang, M.B., Williamson, S.N. and Yang, D.Q. (2015) Elevation-dependent warming in mountain regions of the world. *Nature Climate Change*, 5, 424–430.

Pike, G., Pepin, N.C. and Schaefer, M. (2013) High latitude local scale temperature complexity: the example of Kevo Valley, Finnish Lapland. *International Journal of Climatology*, 33(8), 2050–2067. https://doi.org/10.1002/joc.3573.

Pinche Laurre, C. (1986) *Estudio de las condiciones climáticas y de la niebla en la costa norte de Lima*. Lima (Perú): Universidad Nacional Agraria La Molina.

Pulgar-Vidal, J. (1987). Geografía del Perú: las ocho regiones naturales, la regionalización transversal, la microregionalización.

Rangwala, I. and Miller, J.R. (2012) Climate change in mountains: a review of elevation-dependent warming and its possible causes. *Climatic Change*, 114(3–4), 527–547. https://doi.org/10.1007/s10584-012-0419-3.

Rasmusson, E.M. and Carpenter, T.H. (1982) Variations in Tropical Sea surface temperature and surface wind fields associated with the southern oscillation/El Niño. *Monthly Weather Review*, 110 (5), 354–384. https://doi.org/10.1175/1520-0493(1982)110<0354:VITSST>2.0.CO;2.

Richardson, S., Brock, F., Semmer, S. and Jirak, C. (1999) Minimizing errors associated with multiplate radiation shields. *Journal of Atmospheric and Oceanic Technology*, 16(11), 1862–1872. https://doi.org/10.1175/1520-0426(1999)016<1862:MEAWMR>2.0.CO;2.

Rolland, C. (2003) Spatial and seasonal variations of air temperature lapse rates in alpine regions. *Journal of Climate*, 16(7), 1032–1046. https://doi.org/10.1175/1520-0442(2003)016<1032:SASVOA>2.0.CO;2.

Romshoo, S.A., Rafiq, M. and Rashid, I. (2018) Spatio-temporal variation of land surface temperature and temperature lapse rate over mountainous Kashmir Himalaya. *Journal of Mountain Science*, 15(3), 563–576. https://doi.org/10.1007/s11629-017-4566-x.

Sadoti, G., McAfee, S.A., Roland, C.A., Fleur Nicklen, E. and Sousanes, P.J. (2018) Modelling high-latitude summer temperature patterns using physiographic variables. *International Journal of Climatology*, 38(10), 4033–4042. https://doi.org/10.1002/joc.5538.

Schemenauer, R.S. and Cereceda, P. (1993) Meteorological conditions at a coastal fog collection site in Peru. *Atmosfera*, 6(3), 175–188.

Takahashi, K., Battisti, D.S., Takahashi, K. and Battisti, D.S. (2007) Processes controlling the mean tropical Pacific precipitation pattern. Part I: the Andes and the eastern Pacific ITCZ. *Journal of Climate*, 20(14), 3434–3451. https://doi.org/10.1175/JCLI4198.1.

Takahashi, K., Mosquera, K. and Reupo, J. (2014) El Índice Costero El Niño (ICEN): Historia y actualización. *Boletín Técnico del Instituto Geofísico del Perú*, 1(2), 8–9.

Tomás-Burguera, M., Jiménez Castañeda, A., Luna Rico, M.Y., Morata, A., Vicente Serrano, S., González-Hidalgo, J.C. and Beguería, S. (2016) Control de calidad de siete variables del banco nacional de datos de AEMET. In: *Asociación Española de Climatología Congreso (10. 2016. Alicante)*. Alicante, Spain: *X Congreso Internacional AEC: Clima, sociedad, riesgos y ordenación del territorio*, pp. 407–415.

Vicente-Serrano, S.M., Aguilar, E., Martínez, R., Martín-Hernández, N., Azorin-Molina, C., Sanchez-Lorenzo, A., El-Kenawy, A., Tomás-Burguera, M., Moran-Tejeda, E., López-Moreno, J.I., Revuelto, J., Beguería, S., Nieto, J.J., Drumond, A., Gimeno, L. and Nieto, R. (2017) The complex influence of ENSO on droughts in Ecuador. *Climate Dynamics*, 48(1–2), 405–427. https://doi.org/10.1007/s00382-016-3082-y.

Vicente-Serrano, S.M., López-Moreno, J.I., Correa, K., Avalos, G., Bazo, J., Azorin-Molina, C., Domínguez-Castro, F., El-Kenawy, A., Gimeno, L. and Nieto, R. (2018) Recent changes in monthly surface air temperature over Peru, 1964-2014. *International Journal of Climatology*, 38, 283–306. https://doi.org/10.1002/joc.5176.

Vuille, M. and Bradley, R.S. (2000) Mean annual temperature trends and their vertical structure in the tropical Andes. *Geophysical Research Letters*, 27(23), 3885–3888. https://doi.org/10.1029/2000GL011871.

Vuille, M., Francou, B., Wagnon, P., Juen, I., Kaser, G., Mark, B.G. and Bradley, R.S. (2008) Climate change and tropical Andean

glaciers: past, present and future. *Earth-Science Reviews*, 89(3–4), 79–96. https://doi.org/10.1016/J.EARSCIREV.2008.04.002.

Vuille, M., Franquist, E., Garreaud, R., Lavado Casimiro, W.S. and Cáceres, B. (2015) Impact of the global warming hiatus on Andean temperature. *Journal of Geophysical Research-Atmospheres*, 120(9), 3745–3757. https://doi.org/10.1002/2015JD023126.

Whiteman, C.D., Bian, X., Zhong, S., Whiteman, C.D., Bian, X. and Zhong, S. (1999) Wintertime evolution of the temperature inversion in the Colorado Plateau Basin. *Journal of Applied Meteorology*, 38(8), 1103–1117. https://doi.org/10.1175/1520-0450(1999)038<1103:WEOTTI>2.0.CO;2.

Wilcoxon, F. (1945) Individual comparisons by ranking methods. *Biometrics Bulletin*, 1(6), 80. https://doi.org/10.2307/3001968.

WMO. (2014) *Guide to Meteorological Instruments and Methods of Observation*. Geneva: Switzerland.

Wang, G.Y., Zhao, M.F., Kang, M.Y., Xing, K.X., Wang, Y.H., Xue, F. and Chen, C. (2017) Diurnal and seasonal variation of the elevation gradient of air temperature in the northern flank of the western Qinling Mountain range, China. *Journal of Mountain Science*, 14(1), 94–105. https://doi.org/10.1007/s11629-016-4107-z.

SUPPORTING INFORMATION

Additional supporting information may be found online in the Supporting Information section at the end of this article.

How to cite this article: Navarro-Serrano F, López-Moreno JI, Domínguez-Castro F, *et al.* Maximum and minimum air temperature lapse rates in the Andean region of Ecuador and Peru. *Int J Climatol*. 2020;1–19. https://doi.org/10.1002/joc.6574

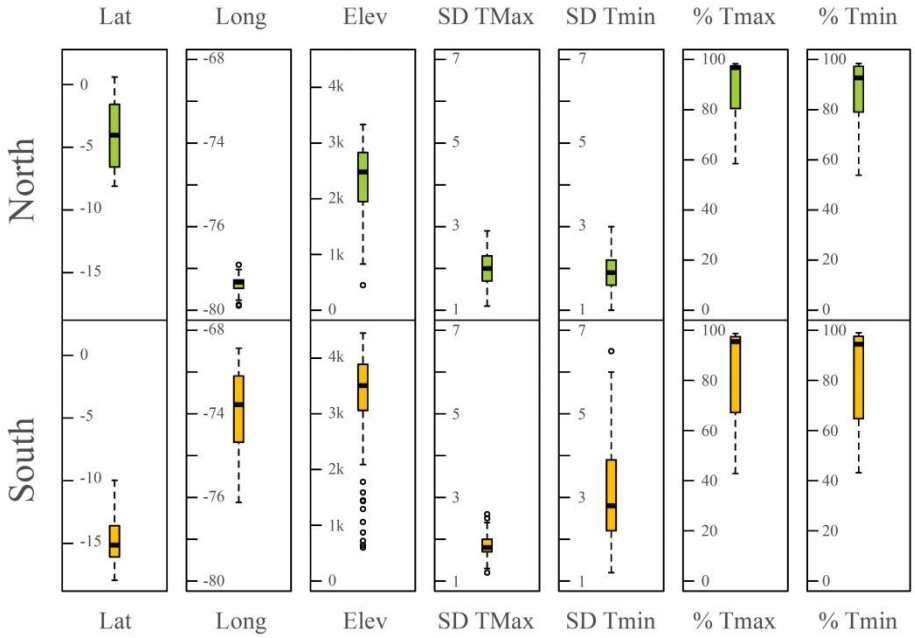

Supplementary Material – Figure 1. The main characteristics of the meteorological observatories dataset used in this study.

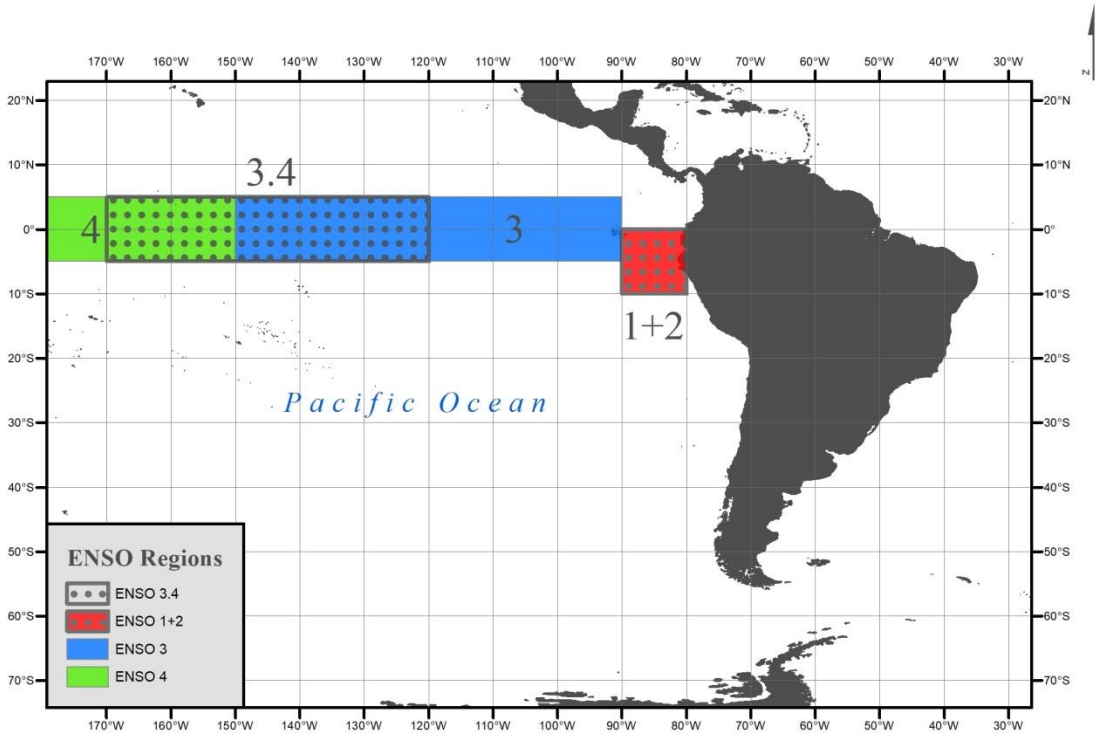

Supplementary Material – Figure 2. ENSO regions distribution map.

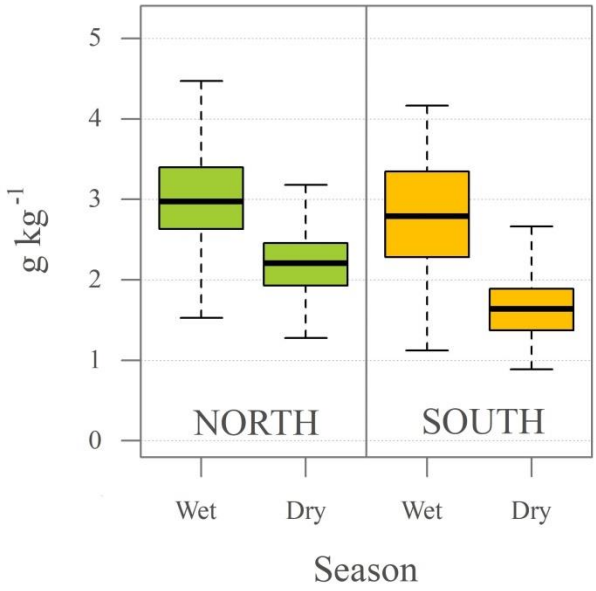

Supplementary Material – Figure 3. 500 hPa specific atmospheric humidity (in g kg-1) as a function of seasons and subregions. The median (black line) and the interquartile range (boxes; Y-axis) are plotted.

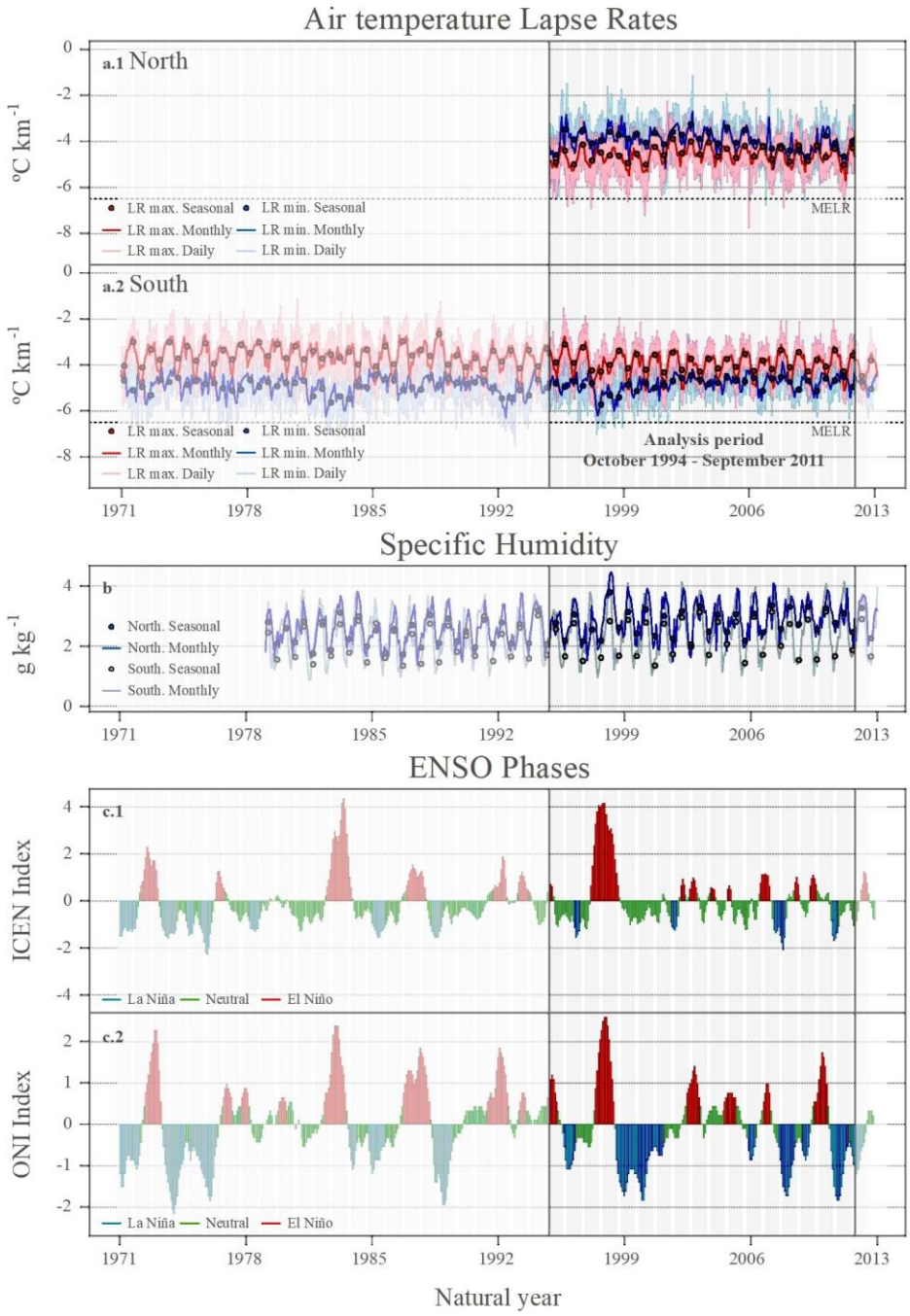

Supplementary Material – Figure 4. (a) Daily, monthly and seasonal North (a.1) and South (a.2) series of LRmax and LRmin. Mean Environmental Lapse-Rate (MELR -6.5 ºC km^{-1}) was represented by dashed grey line; (b) Available monthly and seasonal 500 hPa specific atmospheric humidity (in g kg^{-1}); (c) ENSO El Niño (red), Neutral (green) and La Niña (blue) phases based on the ICEN index (c.1) and the ONI index (c.2). All available data from 1971.

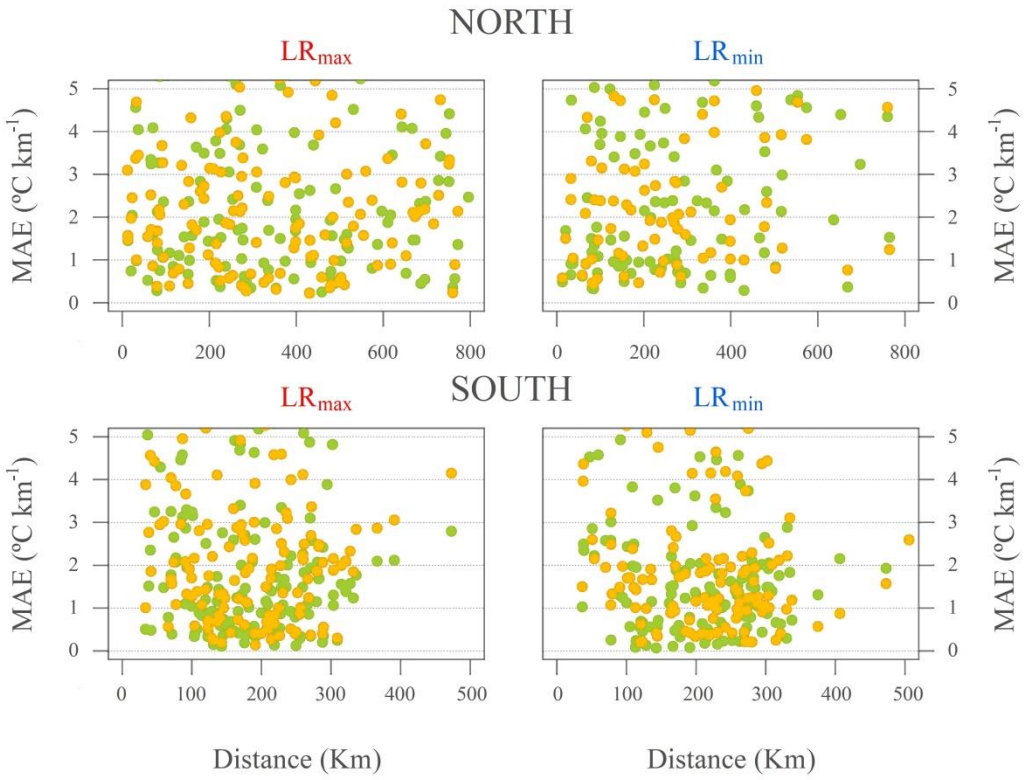

Supplementary Material – Figure 5. Seasonal LRmax and LRmin MAE (in ºC km^{-1}) distribution by wet (green) – dry (orange) seasons, and distance between pairs (in kilometers) for both the northern and southern subregions. Only pairs with MAE < 5 ºC km^{-1} were represented.

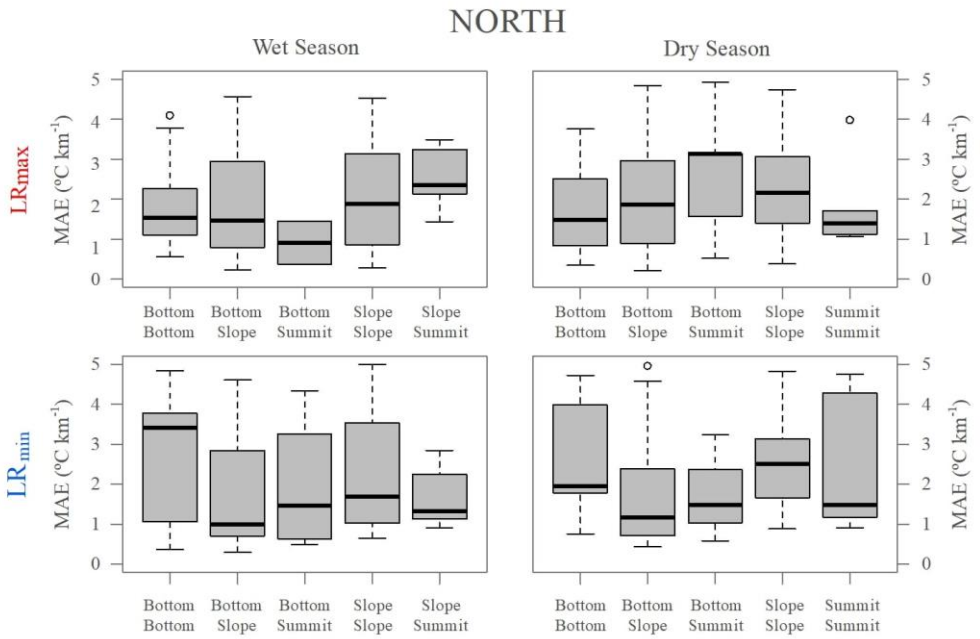

Supplementary Material – Figure 6.a. MAE distribution by season (i.e. wet and dry) and topographic position between pairs for both the northern subregion. MAE only covers the pairs with <5ºC km-1 to focusing on the better pairs.

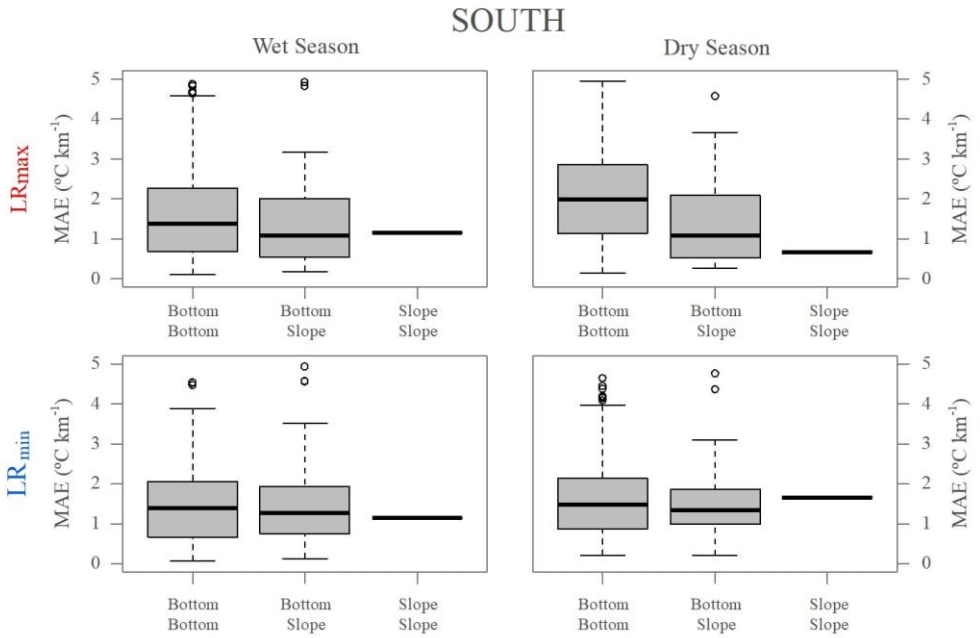

Supplementary Material – Figure 6.b. As for Fig. 6.a, but for the southern subregion.

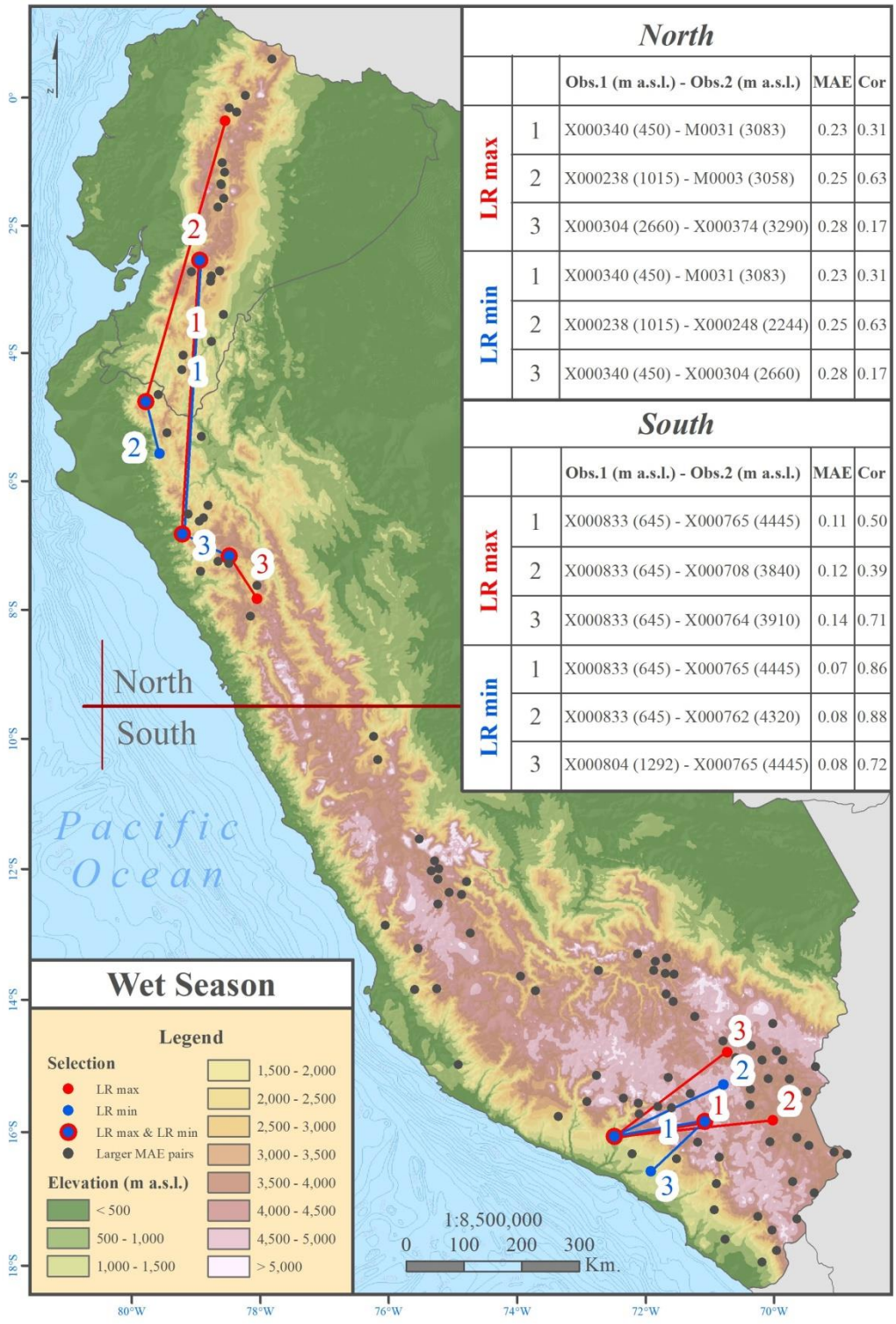

North

		Obs.1 (m a.s.l.) - Obs.2 (m a.s.l.)	MAE	Cor
LR max	1	X000340 (450) - M0031 (3083)	0.23	0.31
	2	X000238 (1015) - M0003 (3058)	0.25	0.63
	3	X000304 (2660) - X000374 (3290)	0.28	0.17
LR min	1	X000340 (450) - M0031 (3083)	0.23	0.31
	2	X000238 (1015) - X000248 (2244)	0.25	0.63
	3	X000340 (450) - X000304 (2660)	0.28	0.17

South

		Obs.1 (m a.s.l.) - Obs.2 (m a.s.l.)	MAE	Cor
LR max	1	X000833 (645) - X000765 (4445)	0.11	0.50
	2	X000833 (645) - X000708 (3840)	0.12	0.39
	3	X000833 (645) - X000764 (3910)	0.14	0.71
LR min	1	X000833 (645) - X000765 (4445)	0.07	0.86
	2	X000833 (645) - X000762 (4320)	0.08	0.88
	3	X000804 (1292) - X000765 (4445)	0.08	0.72

Supplementary Material – Figure 7.a. Location of the most representative station pairs in the wet season. LRmax pairs are shown in red, while LRmin are plotted in blue. Station codes and elevation (in m a.s.l.) are listed in the corresponding table.

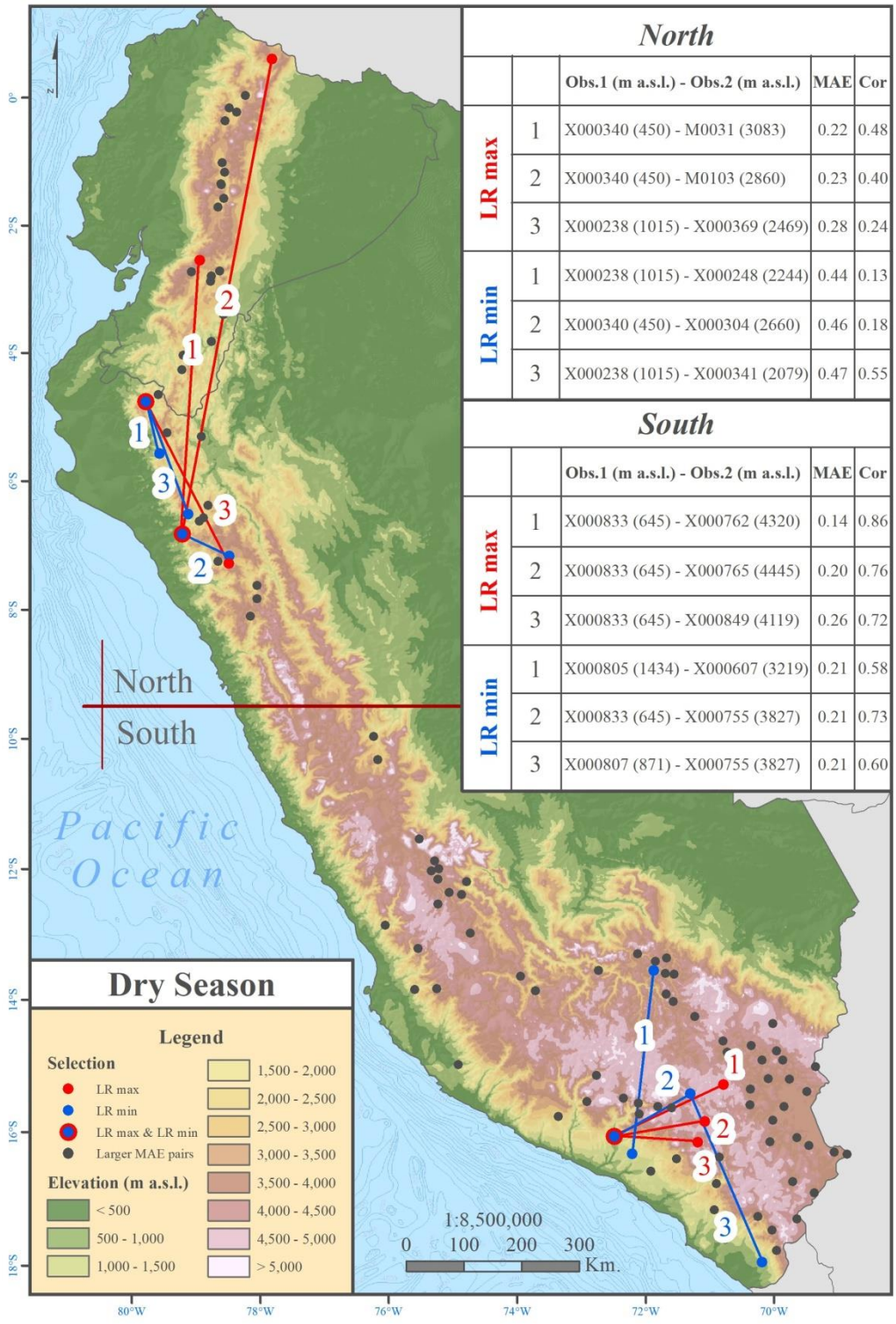

North

		Obs.1 (m a.s.l.) - Obs.2 (m a.s.l.)	MAE	Cor
LR max	1	X000340 (450) - M0031 (3083)	0.22	0.48
	2	X000340 (450) - M0103 (2860)	0.23	0.40
	3	X000238 (1015) - X000369 (2469)	0.28	0.24
LR min	1	X000238 (1015) - X000248 (2244)	0.44	0.13
	2	X000340 (450) - X000304 (2660)	0.46	0.18
	3	X000238 (1015) - X000341 (2079)	0.47	0.55

South

		Obs.1 (m a.s.l.) - Obs.2 (m a.s.l.)	MAE	Cor
LR max	1	X000833 (645) - X000762 (4320)	0.14	0.86
	2	X000833 (645) - X000765 (4445)	0.20	0.76
	3	X000833 (645) - X000849 (4119)	0.26	0.72
LR min	1	X000805 (1434) - X000607 (3219)	0.21	0.58
	2	X000833 (645) - X000755 (3827)	0.21	0.73
	3	X000807 (871) - X000755 (3827)	0.21	0.60

Supplementary Material – Figure 7.b. As for Fig. 7.a., but for the dry season.

Supplementary Material – Table 1. The main characteristics of the weather stations used in this study. Percentage (%) data are referred to definitive analyzed period (1 October 1994 – 30 September 2011).

CODE	Subregion	Category	Name	Country	Country Region	LAT. (decimal °)	LON. (decimal °)	ELE. a.s.l. (m)	N (%) Tmax	N (%) Tmin
M0002	NORTH	Selected	La Tola	Ecuador	Distrito Metropolitano de Quito	-0.23	-78.37	2480	6053 (97.5%)	6050 (97.4%)
M0003	NORTH	Selected	Izobamba	Ecuador	Centro Norte	-0.37	-78.55	3058	6053 (97.5%)	6062 (97.6%)
M0004	NORTH	Selected	Rumipamba-Salcedo	Ecuador	Centro	-1.02	-78.59	2685	6026 (97.1%)	6040 (97.3%)
M0005	NORTH	Fog Reject	Portoviejo-UTM	Ecuador	Pacifico	-1.04	-80.46	59	5972 (96.2%)	5186 (83.5%)
M0006	NORTH	Fog Reject	Pichilingue	Ecuador	Litoral	-1.07	-79.49	81	6093 (98.1%)	4658 (75%)
M0024	NORTH	Selected	Quito Inamhi-Innaquito	Ecuador	Distrito Metropolitano de Quito	-0.17	-78.48	2789	5835 (94%)	5775 (93%)
M0025	NORTH	Fog Reject	La Concordia	Ecuador	Norte	-0.02	-79.38	244	6083 (98%)	3192 (51.4%)
M0026	NORTH	Fog Reject	Puerto Ila	Ecuador	Pacifico	-0.48	-79.34	319	6069 (97.7%)	3995 (64.3%)
M0031	NORTH	Selected	Cañar	Ecuador	Austro	-2.55	-78.95	3083	5620 (90.5%)	5771 (92.9%)
M0033	NORTH	Selected	La Argelia-Loja	Ecuador	Sur	-4.04	-79.20	2160	6001 (96.7%)	6044 (97.3%)
M0037	NORTH	Fog Reject	Milagro (Ingenio Valdez)	Ecuador	Litoral	-2.12	-79.60	23	6042 (97.3%)	4450 (71.7%)
M0045	NORTH	Selected	Palmas-Azuay	Ecuador	Austro	-2.72	-78.63	2400	4585 (73.8%)	4624 (74.5%)
M0051	NORTH	Fog Reject	Babahoyo-UTB	Ecuador	Litoral	-1.80	-79.53	7	5972 (96.2%)	3624 (58.4%)
M0103	NORTH	Selected	San Gabriel	Ecuador	Norte	0.60	-77.82	2860	6027 (97.1%)	6025 (97%)
M0127	NORTH	Selected	Pillaro	Ecuador	Centro	-1.17	-78.56	2793	1015 (16.3%)	929 (15%)
M0128	NORTH	Selected	Pedro Fermin Cevallos (Colegio)	Ecuador	Centro	-1.35	-78.62	2910	5447 (87.7%)	5244 (84.5%)
M0129	NORTH	Fog Reject	Caluma	Ecuador	Litoral	-1.62	-79.29	350	2455 (39.5%)	2096 (33.8%)
M0133	NORTH	Selected	Guaslan	Ecuador	Centro	-1.72	-78.66	2850	3630 (58.5%)	3694 (59.5%)
M0138	NORTH	Selected	Paute	Ecuador	Austro	-2.80	-78.76	2194	5917 (95.3%)	5909 (95.2%)
M0139	NORTH	Selected	Gualaceo	Ecuador	Austro	-2.88	-78.78	2230	5017 (80.8%)	5407 (87.1%)
M0141	NORTH	Selected	El Labrado	Ecuador	Austro	-2.73	-79.07	3335	4998 (80.5%)	4837 (77.9%)
M0144	NORTH	Selected	Vilcabamba	Ecuador	Sur	-4.26	-79.22	1563	1905 (30.7%)	1938 (31.2%)
M0160	NORTH	Fog Reject	El Carmen	Ecuador	Pacifico	-0.26	-79.43	260	3219 (51.8%)	1810 (29.2%)
M0162	NORTH	Fog Reject	Chone-U.Catolica	Ecuador	Pacifico	-0.66	-80.04	36	5932 (95.5%)	3993 (64.3%)
M0165	NORTH	Fog Reject	Rocafuerte	Ecuador	Pacifico	-0.92	-80.45	20	5831 (93.9%)	4411 (71%)
M0166	NORTH	Fog Reject	Olmedo-Manabi	Ecuador	Pacifico	-1.40	-80.21	67	4815 (77.5%)	4709 (75.8%)
M0172	NORTH	Fog Reject	Pueblo Viejo	Ecuador	Litoral	-1.52	-79.54	19	5749 (92.6%)	3403 (54.8%)
M0176	NORTH	Fog Reject	Naranjal	Ecuador	Litoral	-2.66	-79.62	25	5209 (83.9%)	3770 (60.7%)
M0179	NORTH	Fog Reject	Arenillas	Ecuador	Sur	-3.54	-80.05	26	1520 (24.5%)	1688 (27.2%)
M0184	NORTH	Fog Reject	Pagua	Ecuador	Sur	-3.08	-79.76	8	713 (11.5%)	1037 (16.7%)
M0185	NORTH	Fog Reject	Machala-Utm-Pagua	Ecuador	Sur	-3.10	-79.73	13	3806 (61.3%)	1915 (30.8%)
M0189	NORTH	Selected	Gualaquiza Inamhi	Ecuador	Austro	-3.40	-78.58	851	5714 (92%)	5512 (88.8%)
M0190	NORTH	Selected	Yanzatza	Ecuador	Sur	-3.82	-78.76	830	1800 (29%)	1802 (29%)
M0218	NORTH	Fog Reject	Ingenio San Carlos (Batey)	Ecuador	Litoral	-2.22	-79.41	63	5312 (85.6%)	2931 (47.2%)
M0243	NORTH	Selected	Pungales	Ecuador	Centro	-1.58	-78.57	2550	1467 (23.6%)	1601 (25.8%)
M0258	NORTH	Selected	Querochaca (UTA)	Ecuador	Centro	-1.37	-78.61	2865	6057 (97.6%)	6080 (97.9%)
M0283	NORTH	Fog Reject	Inmoriec-El Vergel	Ecuador	Litoral	-0.78	-79.35	151	1791 (28.8%)	949 (15.3%)
M0292	NORTH	Fog Reject	Granja Santa Ines (UTM)	Ecuador	Sur	-3.29	-79.90	5	4822 (77.7%)	3191 (51.4%)
M0482	NORTH	Fog Reject	Chacras	Ecuador	Sur	-3.54	-80.20	60	5260 (84.7%)	3835 (61.8%)
M1094	NORTH	Selected	Tomalon-Tabacundo	Ecuador	Centro Norte	0.03	-78.23	2790	6022 (97%)	6086 (98%)
M1095	NORTH	Fog Reject	Ingenio Aztra (La Troncal)	Ecuador	Austro	-2.44	-79.35	89	5888 (94.8%)	3948 (63.6%)
M1096	NORTH	Fog Reject	Guayaquil U. Estatal (Radio Sonda)	Ecuador	Guayaquil - Samborondon - Duran	-2.18	-79.90	6	5872 (94.6%)	4359 (70.2%)
M1208	NORTH	Fog Reject	La Teodomira	Ecuador	Pacifico	-1.16	-80.39	60	3134 (50.5%)	2958 (47.6%)
X000132	NORTH	Fog Reject	Puerto Pizarro	Perú	Tumbes	-3.51	-80.46	7	5864 (94.4%)	5230 (84.2%)
X000134	NORTH	Fog Reject	Papayal	Perú	Zarumilla	-3.58	-80.24	45	6027 (97.1%)	5161 (83.1%)
X000135	NORTH	Fog Reject	El Salto	Perú	Zarumilla	-3.44	-80.32	6	5705 (91.9%)	5612 (90.4%)
X000207	NORTH	Fog Reject	Miraflores	Perú	Piura	-5.17	-80.63	30	5930 (95.5%)	5803 (93.5%)
X000208	NORTH	Fog Reject	Mallares	Perú	Chira	-4.86	-80.75	29	6013 (96.8%)	5879 (94.7%)
X000230	NORTH	Fog Reject	La Esperanza	Perú	Chira	-4.93	-81.07	6	6069 (97.7%)	5657 (91.1%)
X000231	NORTH	Fog Reject	Chusis	Perú	Piura	-5.53	-80.85	6	5991 (96.5%)	5557 (89.5%)
X000235	NORTH	Fog Reject	Morropon	Perú	Piura	-5.18	-79.98	109	6053 (97.5%)	5921 (95.4%)
X000237	NORTH	Selected	Ayabaca	Perú	Chira	-4.64	-79.73	2830	6005 (96.7%)	4908 (79%)
X000238	NORTH	Selected	Sausal De Culucan	Perú	Chira	-4.76	-79.78	1015	6048 (97.4%)	4962 (79.9%)
X000239	NORTH	Selected	Huancabamba	Perú	Chamaya	-5.25	-79.45	1950	6066 (97.7%)	6096 (98.2%)
X000247	NORTH	Fog Reject	San Miguel	Perú	Piura	-5.30	-80.68	20	6026 (97.1%)	6005 (96.7%)
X000248	NORTH	Selected	Huarmaca	Perú	Chamaya	-5.56	-79.52	2244	6024 (97%)	5851 (94.2%)
X000255	NORTH	Fog Reject	Chulucanas	Perú	Piura	-5.10	-80.17	87	5349 (86.1%)	5308 (85.5%)
X000260	NORTH	Selected	Chirinos	Perú	Chinchipe	-5.30	-78.91	1528	6082 (98%)	4911 (79.1%)
X000301	NORTH	Fog Reject	Lambayeque	Perú	Chancay - Lambayeque	-6.70	-79.92	12	5435 (87.5%)	4993 (80.4%)
X000304	NORTH	Selected	Augusto Weberbauer	Perú	Crisnejas	-7.17	-78.48	2660	6051 (97.5%)	6061 (97.6%)
X000320	NORTH	Fog Reject	Cayalti	Perú	Saña	-6.90	-79.56	70	5960 (96%)	6034 (97.2%)
X000325	NORTH	Fog Reject	Talla (Guadalupe)	Perú	Jequetepeque	-7.27	-79.42	105	5886 (94.8%)	5444 (87.7%)
X000332	NORTH	Fog Reject	Reque	Perú	Chancay - Lambayeque	-6.90	-79.85	15	5800 (93.4%)	4764 (76.7%)
X000333	NORTH	Fog Reject	Jayanca (La Viña)	Perú	Motupe	-6.32	-79.78	65	5756 (92.7%)	5358 (86.3%)
X000340	NORTH	Selected	El Espinal	Perú	Saña	-6.83	-79.22	450	6015 (96.9%)	5329 (85.8%)
X000341	NORTH	Selected	Llama	Perú	Chancay - Lambayeque	-6.51	-79.12	2079	6016 (96.9%)	5937 (95.6%)
X000351	NORTH	Selected	Santa Cruz	Perú	Chancay - Lambayeque	-6.63	-78.95	2039	6008 (96.8%)	6029 (97.1%)
X000352	NORTH	Selected	Cutervo	Perú	Llaucano	-6.38	-78.82	2616	5957 (95.9%)	5693 (91.7%)
X000369	NORTH	Selected	San Juan	Perú	Jequetepeque	-7.29	-78.49	2469	4532 (73%)	5753 (92.7%)
X000373	NORTH	Selected	Cajabamba	Perú	Crisnejas	-7.63	-78.05	2612	6102 (98.3%)	6107 (98.4%)
X000374	NORTH	Selected	Huamachuco	Perú	Crisnejas	-7.83	-78.05	3290	6053 (97.5%)	6098 (98.2%)
X000392	NORTH	Selected	Magdalena	Perú	Jequetepeque	-7.25	-78.66	1257	6099 (98.2%)	5750 (92.6%)
X000395	NORTH	Selected	Chancay Baños	Perú	Chancay - Lambayeque	-6.58	-78.88	1575	6051 (97.5%)	6005 (96.7%)
X000404	SOUTH	Selected	Huanuco	Perú	Alto Huallaga	-9.97	-76.24	2090	6052 (97.5%)	5958 (96%)
X000435	NORTH	Fog Reject	Buena Vista	Perú	Casma	-9.43	-78.20	216	6072 (97.8%)	5039 (81.2%)
X000477	SOUTH	Selected	Santa Ana	Perú	Mantaro	-12.00	-75.22	3302	6047 (97.4%)	6082 (98%)
X000508	SOUTH	Selected	Pampas	Perú	Mantaro	-12.39	-74.87	3240	6052 (97.5%)	5739 (92.4%)
X000534	SOUTH	Fog Reject	Lomas De Lachay	Perú	Intercuenca del Pacifico	-11.37	-77.37	300	4555 (73.4%)	3339 (53.8%)
X000539	SOUTH	Fog Reject	Huayan	Perú	Chancay - Huaral	-11.45	-77.12	350	5436 (87.6%)	4508 (72.6%)
X000543	SOUTH	Fog Reject	Ñaña	Perú	Rimac	-11.99	-76.84	523	5451 (87.8%)	2778 (44.7%)
X000546	SOUTH	Fog Reject	Donoso	Perú	Chancay - Huaral	-11.47	-77.23	180	6057 (97.6%)	5289 (85.2%)
X000552	SOUTH	Selected	San Rafael	Perú	Alto Huallaga	-10.32	-76.17	3060	5984 (96.4%)	5780 (93.1%)
X000607	SOUTH	Selected	Granja Kcayra	Perú	Urubamba	-13.56	-71.88	3219	5845 (94.1%)	5867 (94.5%)

X000608	SOUTH	Selected	Viques	Perú	Mantaro	-12.16	-75.23	3186	3777 (60.8%)	4694 (75.6%)
X000625	SOUTH	Selected	Acostambo	Perú	Mantaro	-12.37	-75.06	3675	6052 (97.5%)	6083 (98%)
X000635	SOUTH	Selected	Huayao	Perú	Mantaro	-12.03	-75.34	3360	5993 (96.5%)	6037 (97.2%)
X000638	SOUTH	Selected	Pacaran	Perú	Cañete	-12.86	-76.06	721	5929 (95.5%)	5683 (91.5%)
X000640	SOUTH	Selected	Huamani	Perú	Ica	-13.85	-75.59	1060	5871 (94.6%)	5700 (91.8%)
X000650	SOUTH	Fog Reject	Hacienda Bernales	Perú	Pisco	-13.76	-75.97	294	5444 (87.7%)	5443 (87.7%)
X000657	SOUTH	Selected	Lircay	Perú	Mantaro	-12.98	-74.73	3513	6040 (97.3%)	6042 (97.3%)
X000677	SOUTH	Selected	Curahuasi	Perú	Apurimac	-13.55	-72.74	2737	4447 (71.6%)	5577 (89.8%)
X000683	SOUTH	Selected	Urubamba	Perú	Urubamba	-13.30	-72.13	3071	6057 (97.6%)	6058 (97.6%)
X000687	SOUTH	Selected	Acomayo	Perú	Apurimac	-13.92	-71.68	3227	6099 (98.2%)	6061 (97.6%)
X000690	SOUTH	Selected	Ccatcca	Perú	Yavero	-13.61	-71.56	3693	5973 (96.2%)	5959 (96%)
X000698	SOUTH	Fog Reject	Rio Grande	Perú	Grande	-14.54	-75.22	317	4337 (69.9%)	4388 (70.7%)
X000700	SOUTH	Fog Reject	San Camilo	Perú	Ica	-14.07	-75.73	398	5538 (89.2%)	5569 (89.7%)
X000708	SOUTH	Selected	Puno	Perú	Ilave	-15.82	-70.02	3840	6069 (97.7%)	6032 (97.1%)
X000727	SOUTH	Selected	Copara	Perú	Grande	-14.98	-74.92	600	6018 (96.9%)	6034 (97.2%)
X000730	SOUTH	Fog Reject	Ocucaje	Perú	Ica	-14.38	-75.68	313	5659 (91.1%)	5886 (94.8%)
X000746	SOUTH	Selected	Caraveli	Perú	Caraveli	-15.77	-73.36	1779	6009 (96.8%)	5547 (89.3%)
X000754	SOUTH	Selected	La Angostura	Perú	Apurimac	-15.18	-71.65	4256	5838 (94%)	5963 (96%)
X000755	SOUTH	Selected	Sibayo	Perú	Camana	-15.49	-71.45	3827	5806 (93.5%)	6059 (97.6%)
X000758	SOUTH	Selected	Chivay	Perú	Camana	-15.64	-71.60	3661	6076 (97.9%)	6057 (97.6%)
X000759	SOUTH	Selected	Sicuani	Perú	Urubamba	-14.25	-71.24	3574	6071 (97.8%)	6045 (97.4%)
X000762	SOUTH	Selected	Pampahuta	Perú	Cabanillas	-15.49	-70.68	4320	6112 (98.4%)	6097 (98.2%)
X000764	SOUTH	Selected	Chuquibambilla	Perú	Ramis	-14.80	-70.73	3910	6071 (97.8%)	6049 (97.4%)
X000765	SOUTH	Selected	Imata	Perú	Quilca	-15.84	-71.09	4445	6042 (97.3%)	6028 (97.1%)
X000776	SOUTH	Selected	Ayaviri	Perú	Ramis	-14.88	-70.59	3920	6048 (97.4%)	6077 (97.9%)
X000778	SOUTH	Selected	Progreso	Perú	Ramis	-14.69	-70.36	3905	6105 (98.3%)	3287 (52.9%)
X000779	SOUTH	Selected	Lampa	Perú	Cabanillas	-15.36	-70.37	3900	6037 (97.2%)	6077 (97.9%)
X000780	SOUTH	Selected	Cabanillas	Perú	Cabanillas	-15.64	-70.35	3890	6079 (97.9%)	6011 (96.8%)
X000781	SOUTH	Selected	Azangaro	Perú	Ramis	-14.91	-70.19	3863	5980 (96.3%)	6082 (98%)
X000783	SOUTH	Selected	Arapa	Perú	Ramis	-15.14	-70.12	3920	6003 (96.7%)	6063 (97.6%)
X000785	SOUTH	Selected	Muñani	Perú	Huancane	-14.78	-69.97	4119	5977 (96.3%)	6146 (99%)
X000786	SOUTH	Selected	Huancane	Perú	Huancane	-15.20	-69.76	3860	6086 (98%)	6088 (98.1%)
X000787	SOUTH	Selected	Huaraya Moho	Perú	Intercuenca del Titicaca	-15.39	-69.49	3890	6073 (97.8%)	6076 (97.9%)
X000788	SOUTH	Selected	Capachica	Perú	Intercuenca del Titicaca	-15.62	-69.84	3819	6099 (98.2%)	6119 (98.6%)
X000791	SOUTH	Fog Reject	Fonagro (Chincha)	Perú	San Juan	-13.47	-76.14	60	5979 (96.3%)	5906 (95.1%)
X000804	SOUTH	Selected	La Joya	Perú	Intercuenca del Pacifico	-16.59	-71.92	1292	6071 (97.8%)	6063 (97.6%)
X000805	SOUTH	Selected	Pampa De Majes	Perú	Camana	-16.33	-72.21	1434	6130 (98.7%)	6137 (98.8%)
X000806	SOUTH	Selected	Moquegua	Perú	Ilo - Moquegua	-17.17	-70.93	1450	5988 (96.4%)	6094 (98.1%)
X000807	SOUTH	Selected	Calana	Perú	Caplina	-17.95	-70.19	871	5845 (94.1%)	6092 (98.1%)
X000809	SOUTH	Selected	Cay Cay	Perú	Urubamba	-13.60	-71.70	3150	4381 (70.6%)	4380 (70.5%)
X000812	SOUTH	Selected	Pomacanchi	Perú	Urubamba	-14.03	-71.57	3686	6029 (97.1%)	5928 (95.5%)
X000822	SOUTH	Selected	Isla Suana	Perú	Intercuenca del Titicaca	-16.34	-68.86	3845	6050 (97.4%)	6064 (97.7%)
X000823	SOUTH	Selected	Santa Rosa	Perú	Ramis	-14.63	-70.80	3940	4171 (67.2%)	5003 (80.6%)
X000827	SOUTH	Selected	Cojata	Perú	Intercuenca del Titicaca	-15.02	-69.36	4344	3968 (63.9%)	4018 (64.7%)
X000830	SOUTH	Fog Reject	Punta Atico	Perú	Intercuenca del Pacifico	-16.23	-73.69	20	6019 (96.9%)	3336 (53.7%)
X000833	SOUTH	Selected	Aplao	Perú	Camana	-16.07	-72.49	645	6078 (97.9%)	6078 (97.9%)
X000837	SOUTH	Fog Reject	Pampa Blanca	Perú	Tambo	-17.07	-71.72	100	5794 (93.3%)	5782 (93.1%)
X000839	SOUTH	Selected	La Pampilla	Perú	Quilca	-16.40	-71.52	2400	6069 (97.7%)	6040 (97.3%)
X000840	SOUTH	Fog Reject	Ilo	Perú	Ilo - Moquegua	-17.63	-71.29	75	6039 (97.3%)	6077 (97.9%)
X000844	SOUTH	Selected	Pisac	Perú	Urubamba	-13.42	-71.85	3147	5191 (83.6%)	5203 (83.8%)
X000846	SOUTH	Fog Reject	Punta Coles	Perú	Intercuenca del Pacifico	-17.70	-71.37	25	5413 (87.2%)	5309 (85.5%)
X000849	SOUTH	Selected	El Frayle	Perú	Quilca	-16.15	-71.19	4119	6056 (97.5%)	5556 (89.5%)
X000851	SOUTH	Selected	Ubinas	Perú	Tambo	-16.38	-70.86	3491	5929 (95.5%)	5940 (95.7%)
X000853	SOUTH	Selected	Locumba	Perú	Locumba	-17.61	-70.76	641	4880 (78.6%)	4108 (66.2%)
X000860	SOUTH	Selected	Chuapalca	Perú	Maure	-17.31	-69.64	4177	4690 (75.5%)	4681 (75.4%)
X000875	SOUTH	Fog Reject	Sama Grande	Perú	Sama	-17.78	-70.49	534	5817 (93.7%)	6035 (97.2%)
X000876	SOUTH	Selected	Candarave	Perú	Locumba	-17.27	-70.25	3435	5412 (87.2%)	5848 (94.2%)
X000877	SOUTH	Selected	Tarata	Perú	Sama	-17.47	-70.03	3050	6122 (98.6%)	4780 (77%)
X000878	SOUTH	Selected	Mazo Cruz	Perú	Ilave	-16.75	-69.71	3970	5859 (94.4%)	5871 (94.6%)
X000879	SOUTH	Selected	Ilave	Perú	Zapatilla	-16.08	-69.64	3850	5657 (91.1%)	5894 (94.9%)
X000880	SOUTH	Selected	Juli	Perú	Callacame	-16.20	-69.46	3825	6021 (97%)	6075 (97.8%)
X000881	SOUTH	Selected	Pizacoma	Perú	Maure Chico	-16.92	-69.37	3940	5928 (95.5%)	5826 (93.8%)
X000882	SOUTH	Selected	Tahuaco-Yunguyo	Perú	Intercuenca del Titicaca	-16.31	-69.07	3860	5823 (93.8%)	5861 (94.4%)
X000889	SOUTH	Selected	Laraqueri	Perú	Ilave	-16.15	-70.07	3970	5694 (91.7%)	3636 (58.6%)
X000901	SOUTH	Fog Reject	Jorge Basadre	Perú	Caplina	-18.03	-70.25	545	6093 (98.1%)	5984 (96.4%)
X006200	SOUTH	Selected	Salcabamba	Perú	Mantaro	-12.20	-74.79	3275	3505 (56.5%)	3449 (55.5%)
X007415	SOUTH	Selected	Crucero	Perú	Ramis	-14.36	-70.02	4130	4350 (70.1%)	4359 (70.2%)
X151503	SOUTH	Selected	Huachos	Perú	San Juan	-13.22	-75.54	2598	3523 (56.7%)	3490 (56.2%)
X153201	NORTH	Selected	San Benito	Perú	Chicama	-7.41	-78.93	1600	3122 (50.3%)	3343 (53.8%)
X154103	NORTH	Selected	Cachicadan	Perú	Santa	-8.10	-78.15	2890	3802 (61.2%)	3134 (50.5%)
X155229	SOUTH	Selected	Ricran	Perú	Perene	-11.54	-75.53	3687	3207 (51.7%)	3214 (51.8%)
X155231	SOUTH	Selected	Ingenio	Perú	Mantaro	-11.88	-75.29	3422	3723 (60%)	3609 (58.1%)
X156123	SOUTH	Selected	Santiago De Chocorvos	Perú	Ica	-13.83	-75.25	2794	3647 (58.7%)	3531 (56.9%)
X156126	SOUTH	Selected	Huancalpi	Perú	Mantaro	-12.54	-75.24	4450	3114 (50.2%)	3114 (50.2%)
X156211	SOUTH	Selected	Vilcashuaman	Perú	Pampas	-13.64	-73.95	3394	3236 (52.1%)	3250 (52.3%)
X156212	SOUTH	Selected	Chilcayoc	Perú	Pampas	-13.87	-73.72	3441	2661 (42.9%)	2682 (43.2%)
X156306	SOUTH	Selected	Colquepata	Perú	Yavero	-13.36	-71.67	3699	3870 (62.3%)	3828 (61.7%)
X157300	SOUTH	Selected	Chichas	Perú	Ocoña	-15.54	-72.92	2120	3313 (53.4%)	3121 (50.3%)
X157309	SOUTH	Selected	Pullhuay (Ayahuasi)	Perú	Ocoña	-15.15	-72.77	3113	2919 (47%)	2857 (46%)
X157310	SOUTH	Selected	Andahua	Perú	Camana	-15.49	-72.35	3528	3817 (61.5%)	3854 (62.1%)
X157314	SOUTH	Selected	Choco	Perú	Camana	-15.57	-72.12	3192	4241 (68.3%)	3805 (61.3%)
X157315	SOUTH	Selected	Huambo	Perú	Camana	-15.73	-72.10	3500	3450 (55.6%)	3548 (57.1%)
X157317	SOUTH	Selected	Madrigal	Perú	Camana	-15.62	-71.81	3262	2956 (47.6%)	2994 (48.2%)
X157414	SOUTH	Selected	Putina	Perú	Huancane	-14.91	-69.87	3878	2867 (46.2%)	3071 (49.5%)
X158301	SOUTH	Selected	Quinistaquillas	Perú	Tambo	-16.78	-70.90	1590	3487 (56.2%)	3380 (54.4%)
X158321	SOUTH	Selected	Palca	Perú	Caplina	-17.78	-69.97	2953	4039 (65.1%)	4046 (65.2%)

Supplementary Material – Table 2. Monthly non-absolute mean residuals of estimated-observed air temperature (i.e. Tmax and Tmin) for the northern and southern subregions.

VARIABLE	Jan	Feb	Mar	Apr	May	Jun	Jul	Aug	Sep	Oct	Nov	Dec
NORTH – Tmax	0.05	0.11	0.09	0.08	0.11	0.05	0.07	0.05	0.00	-0.04	0.03	0.10
NORTH – Tmin	0.16	-0.07	0.07	0.21	0.09	0.21	0.13	0.15	0.35	0.00	-0.12	0.32
SOUTH – Tmax	0.02	0.01	0.06	-0.06	-0.03	0.00	0.03	-0.01	0.03	0.05	-0.04	0.02
SOUTH – Tmin	-0.01	-0.02	-0.02	-0.03	0.02	0.04	-0.03	-0.03	-0.05	0.00	0.00	0.03
	WET SEASON					DRY SEASON				WET SEASON		

Capítulo 5

MEDICIONES DE TEMPERATURA EN AMBIENTES NEVADOS DE MONTAÑA

Publicado como:

Navarro-Serrano, F., López-Moreno, J.I., Azorin-Molina, C., Buisán, S., Domínguez-Castro, F., Sanmiguel-Vallelado, A., Alonso-González, E., Khorchani, M. 2019. Air temperature measurements using autonomous seld-recording dataloggers in mountainous and snow covered areas. *Atmospheric Research* 224: 168-179. DOI: https://doi.org/10.1016/j.atmosres.2019.03.034.

Los autores agradecen a ELSEVIER el permiso para publicar de manera íntegra el contenido de la publicación, que puede encontrarse en https://www.sciencedirect.com/science/article/pii/S0169809518316144.

Atmospheric Research 224 (2019) 168–179

Contents lists available at ScienceDirect

Atmospheric Research

journal homepage: www.elsevier.com/locate/atmosres

Air temperature measurements using autonomous self-recording dataloggers in mountainous and snow covered areas

F. Navarro-Serrano[a,b,*], J.I. López-Moreno[a], C. Azorin-Molina[c], S. Buisán[d], F. Domínguez-Castro[a], A. Sanmiguel-Vallelado[a], E. Alonso-González[a], M. Khorchani[a]

[a] Department of Geoenvironmental Processes and Global Change, Pyrenean Institute of Ecology, CSIC, Campus de Aula Dei, Avenida de Montañana, P.O. Box 202, 50080 Zaragoza, Spain
[b] Department of Geography, University of Zaragoza, San Juan Bosco, 7, 50009 Zaragoza, Spain
[c] Regional Climate Group, Department of Earth Sciences, University of Gothenburg, Box 460, 405 30 Gothenburg, Sweden
[d] Regional AEMET (Spanish Meteorological Agency) Office in Aragón, Paseo del Canal, 17, 50009 Zaragoza, Spain

ARTICLE INFO

Keywords:
Air temperature
Temperature logger
Radiation shield
Snow
Complex terrain
SPICE (Solid Precipitation Intercomparison Experiment)

ABSTRACT

High mountain areas are poorly represented by official weather observatories. It implies that new instruments must be evaluated over snow-covered and strongly insolated environments (i.e. mid-latitude mountain areas). We analyzed uncertainty sources over snow covered areas including: 1) temperature logger accuracy and bias of two widely used temperature sensors (Tinytag and iButton); 2) radiation shield performance under various radiation, snow, and wind conditions; 3) appropriate measurement height over snow covered ground; and 4) differences in air temperature measured among nearby devices over a horizontal band.

The major results showed the following. 1) Tinytag performance device (mean absolute error: MAE ≈ 0.1–0.2 °C in relation to the reference thermistor) was superior to the iButton (MAE ≈ 0.7 °C), which was subject to operating errors. 2) Multi-plate radiation shield showed the best performance under all conditions (> 90% samples has bias between ± 0.5 °C). The tube shield required wind (> 2.5 m s^{-1}) for adequate performance, while the funnel shield required limited radiation (< 400 W m^{-2}). Snow cover causes certain overheating. 3) Air temperatures were found to stabilize at 75–100 cm above the snow surface. Air temperature profile was more constant at night, showing a considerable cooling on near surface at midday. 4) Horizontal air temperature differences were larger at midday (0.5 °C). These findings indicate that to minimize errors air temperature measurements over snow surfaces should be carried out using multi-plate radiation shields with high-end thermistors such as Tinytags, and be made at a minimum height above the snow covered ground.

1. Introduction

Air temperature affects many environmental and technical processes, and has been measured since the 17th century (Camuffo and Bertolin, 2012). Air temperature data are necessary for a variety of purposes, including to analyze crop yields, hydrological regimes, energy efficiency, biological processes (Hubbart, 2011) or to evaluate the impact of global change on economy of mountain areas (López-Moreno et al., 2018). Air temperature varies temporally and spatially, so well distributed measurement networks are needed. However, high mountain areas are usually poorly represented in official networks because of the complex topography, snow cover, and the low population density, all of which affect the installation and maintenance of stations (Alonso-González et al., 2018; Barry, 1992). Moreover, the periodic presence of snow cover modifies the spatial distribution of air temperature (Navarro-Serrano et al., 2018; Rolland, 2003), and therefore the typical location of measurement stations, in valley bottoms, is inadequate. For these reasons the guidelines provided by the World Meteorological Organization (WMO, 2014) concerning the location, devices, shielding, and height above the ground for temperature measurement are very difficult to meet in mountainous areas. Thus, the absence of official measurement stations necessitates the use of portable, autonomous, easily installed, and self-recording temperature measurement devices (Nakamura and Mahrt, 2005), and their use for scientific and applied purposes has increased markedly in recent years (Bonnardot et al., 2012; Lundquist and Lott, 2008). However, a number of uncertainties need to be adequately quantified prior to analyzing data collected using such devices.

* Corresponding author at: Pyrenean Institute of Ecology, Campus de Aula Dei, Avenida de Montañana, P.O. Box 202, Zaragoza 50080, Spain.
E-mail address: fnavarro@ipe.csic.es (F. Navarro-Serrano).

https://doi.org/10.1016/j.atmosres.2019.03.034
Received 15 December 2018; Received in revised form 21 March 2019; Accepted 22 March 2019
Available online 23 March 2019

In terms of accuracy, temperature logger miniaturization is a positive development because of the associated reduction in shortwave radiative heating, as the small size favors convective flux (Fritschen and Gay, 1979; Richardson et al., 1999). Nevertheless, problems including bias and device failure and data loss for no apparent reason should be addressed by the comparison with reference measurements (Roznik and Alford, 2012; Wolaver and Sharp, 2007). Calibration process is common for scientific purposes (Shedekar et al., 2016). Several studies have analyzed and calibrated miniature temperature loggers in ice baths or other laboratory-controlled conditions (Hubbart et al., 2005; Imholt et al., 2013; Johnson et al., 2005; Yang et al., 2012), but rarely has this been done under field conditions (Lundquist and Huggett, 2008; Pagès et al., 2017).

Regardless of the device accuracy and quality, to obtain accurate measurements it is necessary to protect the device from shortwave and longwave radiation fluxes (Harrison, 2010; WMO, 2014), especially in environments having strong insolation, high albedo rates, and weak winds (Huwald et al., 2009; Nakamura and Mahrt, 2005). Direct exposure of devices to sunlight causes an increase in the measured air temperature (Nordli et al., 1997). The opposite occurs at night because of the effect of outgoing longwave radiation (Azorin-Molina and Azorin-Molina, 2008). Radiative heating problems increase in snow covered environments because of reflection of shortwave radiation from the snow (Arck and Scherer, 2001; Huwald et al., 2009), especially in areas having temporary snow cover, where nonsystematic heating occurs (Georges and Kaser, 2002; Lundquist and Huggett, 2008). The design of radiation shields, and their construction materials and geometry are not trivial factors, as they determine the protection from radiation and internal air flow efficiency. To ensure correct internal airflow, forced fan-aspirated radiation shields claim to provide continuous and regular airflow, and are preferred (Georges and Kaser, 2002; Nakamura and Mahrt, 2005). However, the energy requirements of the fan-aspirated system prevent its use in remote mountain areas. Thus, since the 19th century the Stevenson wooden double-louvre naturally-ventilated screen has generally been used by meteorological agencies (Brunet et al., 2006). Device miniaturization has occurred concurrently with the development of radiation shields and their design. The most commercialized small shield is the plastic multi-plate radiation shield, based on the design of Gill (1983), and has been generally used in official automatic weather station networks since the mid-1980s. A major disadvantage is that miniaturization of radiation shields has not resulted in a reduction in price, and generally the shields are more expensive than the miniature air temperature loggers. This is particularly serious for dense air temperature monitoring networks, because it drastically increases costs. Consequently, there has been a concerted search for non-commercial and cheaper radiation shields that achieve equilibrium between ventilation and radiation protection. These alternatives have usually been homemade, and generally have not been designed for snow covered and high-albedo environments, and as a result have produced measurements having substantial uncertainties (Hubbard et al., 2001). Although there have been studies of the performance of alternative radiation shields above grass ground or bare soil (Holden et al., 2013; Kurzeja, 2010; Richardson et al., 1999; Tarara and Hoheisel, 2007), few have been carried out above simulated high-albedo (Georges and Kaser, 2002; Hubbard et al., 2001) and snow covered surfaces (Huwald et al., 2009; Lundquist and Huggett, 2008). To avoid uncertainties associated with inappropriate uses of radiation shields, it is essential that shelter performance be analyzed.

Another uncertainty source that has rarely been taken into account in the miniature temperature logger network setting is the height of the device above the surface. The vertical temperature in the near-surface boundary layer is dependent on turbulent energy fluxes between the ground and the atmosphere (Anderson and Neff, 2008; Helgason and Pomeroy, 2012; Sokol et al., 2017), which cause significant variations over distances of a few meters or centimeters, and even greater variations in snow covered environments (Halberstam and Schieldge, 1981). Temperature extremes occur in the bottom air layer, near the exchange surface (Campbell and Norman, 1998), but the amplitude decreases as the measurement height increases. It has been reported (WMO, 2014) that the optimal air temperature measurement height is between 125 and 200 cm above bare ground or natural vegetation. However, no guideline has been reported for snow covered environments, except that it should be constant among observatories, and studies of this issue are rare and limited (Anderson and Neff, 2008; Halberstam and Schieldge, 1981; Hanna et al., 2017). In addition, snow depth varies among seasons, introducing seasonal measurement uncertainty. Thus, it is important to analyze the height of the stabilization layer above snow covered ground. In this regard, Lundquist and Huggett (2008) installed devices at different heights, in function of the snow depth variability, from 2 to 10 m above the ground with the aim of to measure comparable air temperature. Thus, installation of a measurement device at an inappropriate height can cause inconsistencies among measurements, and horizontal and vertical air temperature differences can be mixed (Nakamura and Mahrt, 2005).

In addition to the uncertainty sources noted above, there are others that could affect the measurement reliability but are not so evident. The distribution of horizontal air temperature locally and regionally is mainly determined by elevation, orography, orientation, and land use (Lundquist and Cayan, 2007). However, other environmental factors can affect the air temperature, including sunshine, the presence of trees or buildings (Kurzeja, 2010), shrub height (Nakamura and Mahrt, 2005), the presence of water, and plant density. Consequently, it is extremely difficult to account for all the factors influencing temperature in designing a miniature temperature logger network, so device measurement differences in part result from interferences, and not just because of real horizontal differences in temperature. All these issues mean that chosen measurement points are rarely fully representative of the entire experimental plot. Thus, it is necessary to include a certain measure of uncertainty for mountainous areas that, in principle, we consider homogeneous as, in this case, an evergreen mountain forest.

The aim of this study was to analyze uncertainty sources that could affect air temperature measurements in mountainous and snow covered areas. Users of naturally-ventilated shielded miniature temperature loggers in snow covered and forested areas need to be aware of the magnitude and the effects of such uncertainties on air temperature measurements, particularly associated with inappropriate design of observational networks, and choice of measuring device and radiation shields. It is necessary to obtain precise and accurate measurements of air temperature, because these are indispensable in environmental applications. This is particularly the case in the context of global change, which seems to affect high mountain areas more rapidly (Morán-Tejeda et al., 2016). We undertook four experiments to assess uncertainty sources, using autonomous and commonly used temperature loggers and radiation shields:

- Experiment 1 assessed temperature logger accuracy in terms of consistency among several sensors, and bias compared with a reference air temperature device.
- Experiment 2 assessed the performance of different types of radiation shield over snow covered ground.
- Experiment 3 assessed the influence of measurement height above a snow covered surface.
- Experiment 4 assessed variation in air temperature measured by nearby devices in a similar elevation band.

The results of this study will improve the quality of temperature data for disciplines that depend on accurate information on snow covered and mountainous environments.

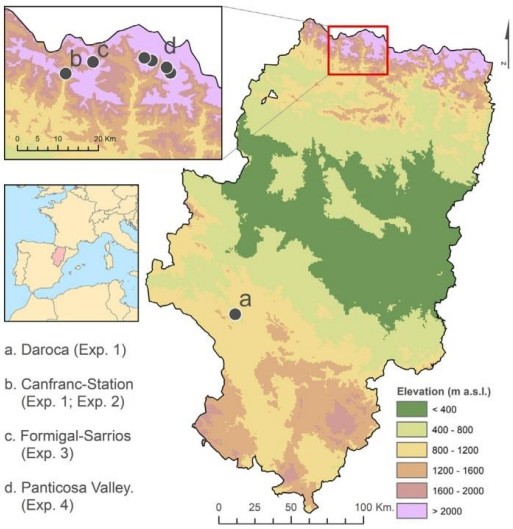

Fig. 1. Aragón (Spain) terrain map showing the location of the four experimental sites. Elevation is expressed in meters above sea level (m a.s.l.).

2. Study areas and material

2.1. Study areas

All experiments were carried out in Aragon (Spain). Experiment 1 was undertaken at Daroca and Canfranc-Station (Fig. 1). Daroca is a small town located on a high continental plateau (779 m a.s.l.; 41.11°N, 1.41°W). The climate in Daroca is cold and dry (average temperature: 6.5 °C; precipitation: 65 mm from January to March), and snowfalls are occasional (12 snowfall days yr^{-1}). Canfranc-Station is a valley-bottom town in the Spanish Pyrenees (1170 m a.s.l., 42.75°N, 0.52°W), near the French border. Its climate is cold and humid (average temperature: 3.7 °C; precipitation: 417 mm from January to March), and snowfalls are common in winter (25 snowfall days yr^{-1}), and snow cover is typical throughout winter and early spring. These locations facilitated the analysis under cold conditions of different climate impacts on measurement accuracy, and the influence of seasonal snowpack (more common at Canfranc-Station). Daroca and Canfranc-Station have meteorological stations managed by the Spanish Meteorological Agency (AEMET), and served as the reference temperature measurement for analyzing the accuracy and performance of miniature dataloggers.

Experiment 2 was carried out at Canfranc-Station (Fig. 1) because of the availability of a reference Stevenson screen, in addition to wind speed measures and the occurrence of contrasting continuous snow cover during winter and grass cover during spring. Canfranc-Station is relatively sheltered from the winds, but as a mountainous location, it can suffer strong winds in certain conditions.

Experiment 3 was carried out at Formigal-Sarrios (Fig. 1). Formigal-Sarrios is an experimental plot located in the high elevation Formigal Pyrenees ski resort (1820 m a.s.l.; 42.76°N, 0.39°W), near the French border. This plot is integrated within the SPICE Project (WMO Solid Precipitation Intercomparison Experiment). It is exposed to cold and humid air flows from the north, snowfalls are common and regular, and the snow depth can reach 2–3 m in optimal years (Buisán et al., 2017). The climatic conditions result in continuous snow cover from late autumn to early summer. Formigal-Sarrios was chosen for this experiment because the main objective was to assess the vertical distribution of air temperature over snow covered areas. At this location the snow cover is continuous, and the snow depth enables assessment of temperature at various heights above the snow surface.

Experiment 4 was undertaken in Panticosa Valley (Fig. 1), which is a high Pyrenees valley (from 1600 to 3064 m a.s.l.; 42.76°N, 0.23°W) on the Gállego River. The valley is covered with a dense evergreen forest of *Pinus mugo* subsp. *uncinata*. Four experimental plots were established in various combinations of north-south slope and high-low elevation bands (Upper-North: 2195–2213 m a.s.l.; Bottom-North: 1742–1757 m a.s.l.; Upper-South: 2039–2053 m a.s.l.; Bottom-South: 1854–1882 m a.s.l.). Panticosa-Valley was chosen because its evergreen forest and the presence of snow during several months of the year. The potential to analyze the horizontal air temperature at four sites enabled comparison based on different exposures and elevational environments. These four sites had an approximate area of 1500–2000 square meters each.

2.2. Thermistors

Autonomous self-recording and price competitive temperature loggers are widely used in research in areas involving building construction (Fang et al., 2014), animal biology (Schofield et al., 2009), and vegetation (Brabyn et al., 2014; Measham et al., 2017), and also in climatic-meteorological applications (Domínguez-Villar et al., 2015; Imholt et al., 2013; Juliussen and Humlum, 2007; Lundquist and Lott, 2008; O'Neill and Christiansen, 2018). In the present study temperature measurements were made using three thermistor types: Thies PT100, Tinytag-Plus-2 (Tinytag), and Thermochron iButton (iButton).

The accuracy of the Thies PT100 thermistor is ± 0.2 °C for high and low temperature daily extremes (Buisán et al., 2015), and its resolution is 0.1 °C within the measurement range of −30° to +70 °C (https://www.thiesclima.com/pdf/en/Products/Temperature-Electrical-sensors/?art=965; last accessed 20 March 2019). In Spain the Thies PT100 thermistors are managed by AEMET, and their use follows all WMO guidelines. Price range is $600–700 (Thies Clima representative contact in Spain).

The Tinytag autonomous miniature and waterproof temperature logger model TGP-4017 (produced by Gemini DataLoggers UK Ltd.; Chichester, West Sussex, UK) is equipped with a 10 K NTC thermistor. The manufacturer reports a precision error of < ± 0.5 °C over a measurement range of −40 °C to +85 °C (http://gemini2.assets.d3r.com/pdfs/original/3239-tgp-4017.pdf; last accessed 20 March 2019) and a resolution of 0.01 °C. It offers high storage capacity (up to 32,000 measurements) and is powered by a replaceable battery (≈ 3 years of service). The Tinytag price range is $150–200.

The iButton autonomous miniature temperature logger models DS-1922L and DS-1921G are produced by Dallas Semiconductors, Texas, USA (https://datasheets.maximintegrated.com/en/ds/DS1922L-DS1922T.pdf; last accessed 20 March 2019). The manufacturer reports an accuracy of < ± 0.5 °C over a measurement range − 10 °C to +65 °C, and a resolution of 0.5 °C. The clock calendar is accurate to ± 2 min per month within a 0–40 °C range (Gasvoda et al., 2002). It is powered by a non-replaceable internal battery (≈ 10 years of device service), and the price range is $50–80 per device.

2.3. Radiation shields

In recent years, commercial naturally-ventilated plastic multi-plate radiation shields based on the design of Gill (1983) have been widely used (Hanna et al., 2017; Hofer et al., 2017; Makgose and Phillipus, 2015; Quénol and Bonnardot, 2014; Richardson et al., 1999). Because of the high price of commercial shields, non-commercial naturally-ventilated alternative radiation shields (e.g. cones, tubes, funnels, pagodas) have also been used in environmental research (Hubbart et al., 2007; Lundquist and Huggett, 2008; Pagès et al., 2017; Pepin and Kidd, 2006; Tarara and Hoheisel, 2007). In this study we used four naturally-

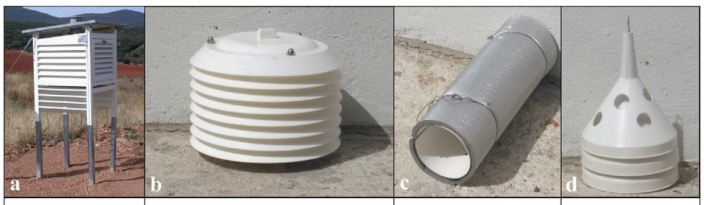

Stevenson	Datamate	Tube	Funnel
78,660 cm^3	4,461 cm^3	2,317 cm^3	1,150 cm^3

Fig. 2. The Stevenson, Datamate ACS-5050, tube and funnel radiation shields. Total volume is expressed in cubic centimeters (cm^3).

ventilated radiation shields including the Stevenson and Datamate ACS-5050 shields, and a tube and a funnel shield.

The Stevenson double-louvered wooden screen (Fig. 2a) is the shield typically used by official meteorological agencies. It is made from wood that is painted white, to reflect direct solar radiation. The standard dimensions, colour, and materials for this screen have been published (WMO, 2014).

The Datamate ACS-5050 Weather Shield (Fig. 2b; http://gemini2.assets.d3r.com/pdfs/original/1684-acs-5050.pdf; last accessed 20 March 2019) is produced by Gemini DataLoggers UK Ltd. (Chichester, West Sussex, UK). It is an 8-plate PVC radiation shield having 15 mm spaces between the plates, to enable air to circulate freely. Its dimensions (142 mm height × 198 mm diameter) provide space for two miniature dataloggers.

The tube shield (Fig. 2c) is a non-commercial radiation shield. It was built from white PVC tube (295 mm long × 100 mm diameter), following the design of Pepin and Kidd (2006), and was covered by reflective aluminum foil duct tape, based on the reports of Fuchs and Tanner (1965) and Holden et al. (2013). Based on the suggestion of Pepin et al. (2010), to avoid direct solar radiation it was oriented towards the north and sloped K degrees from the vertical (K = 90° minus latitude, in degrees).

The funnel shield (Fig. 2d) is also a non-commercial bottom-opening radiation shield. Following the design of Hubbart (2011), it was built from two perforated and one non-perforated white PVC funnels (diameter: 130 mm) assembled vertically with a 10 mm gap between the funnels, providing a perforated area equivalent to 20% of the total.

2.4. Environmental variables

Downwelling radiation was measured at Formigal-Sarrios using a Kipp & Zonen model CM11 pyranometer (http://www.kippzonen.com/Product/13/CMP11-Pyranometer, last accessed 20 March 2019). Wind speed was measured at a standard height of 10 m using a heated anemometer (Thies Clima; Göttingen, Germany) managed by AEMET at Canfranc-Station and Formigal-Sarrios. Snow surface presence information in Canfranc-Station and Daroca was derived from AEMET snow data, measured by manual operators by traditional poles. Snow depth was measured at Formigal-Sarrios using a SR50A acoustic snow depth measurement sensor (https://www.eoas.ubc.ca/courses/atsc303/Instruments/manuals/TBC_sonic_ranger.pdf; last accessed 20 March 2019). Precipitation was measured at Formigal-Sarrios using an automatic weighing gauge (OTT Pluvio2 gauge; OTT Hydromet, Kempten, Germany) with a 200 cm^2 orifice area and 1500 mm capacity. The gauge was used in reference configuration, and was shielded inside a DFIR (*Double Fence Intercomparison Reference*, single Alter, SA) fence (Buisán et al., 2017). For analysis, each day was separated into four periods from solar incoming radiation cycle, following the procedure of Tarara and Hoheisel (2007). The four periods were generated from downwelling global solar radiation hourly averages measured at the Formigal-Sarrios reference location during the entire 2017–2018 (November to May) snow season, and included: Period 1 "Night": 20:01–04:00 UTC; Period 2 "Sunrise-Evening": 04:01–07:00 and 17:01–20:00 UTC; Period 3 "Morning-Afternoon": 07:01–10:00 and 14:01–17:00 UTC; Period 4 "Midday": 10:01–14:00 UTC.

3. Experimental design and methods

3.1. Experiment 1. Temperature logger accuracy, consistency among simultaneous measurements, and bias relative to a reference temperature

The Tinytag and iButton temperature loggers were compared with the Thies PT100 reference logger (calibrated annually at the AEMET calibration laboratory). The measurement periods were during winter, when snow can occur: 22 December 2016 to 13 February 2017 at Daroca, and 20 January 2017 to 1 March 2017 at Canfranc-Station. In total, 14 Tinytag (Daroca: 8; Canfranc-Station: 6) and 14 iButton (Daroca: 6; Canfranc-Station: 8) autonomous temperature loggers having 10-min sampling intervals were installed. The loggers were placed near the PT100 reference sensor, and shared a double-louvered Stevenson screen at a height of 150 cm.

Measurement differences (ΔT, in °C) between the Tinytag and iButton temperature loggers and the Thies PT100 reference thermistor within the Stevenson reference radiation shield were calculated. Mean absolute error (MAE) from reference were calculated. Hourly and snow effects were analyzed and confidence intervals (0.95) were calculated, and the range between the coolest and hottest temperatures measured by the loggers were determined.

3.2. Experiment 2. Performance of the tested radiation shields

It involved measurements made in the absence of a shield (no shield), and using the tube and funnel radiation shields and a commercial white multi-plate Datamate ACS-5050 shield. Comparisons were made with reference to measurements made using the Stevenson reference shield. The shields were mounted at 150 cm above the ground, and all measurements were logged using 5 autonomous Tinytag devices (10-min sampling interval) within each shielding situation. The paired data measurement period was from 11 January 2018 to 30 May 2018. Snow cover was present for 33% of days (n = 33,150 samples). Solar radiation was measured at Formigal-Sarrios in a location comparable to that at Canfranc-Station in terms of orientation, exposure, and topography.

Differences (bias) in relation to measurement data derived using the Stevenson screen were expressed in degrees Celsius (ΔT). Wind speed was aggregated based on hourly averaged speeds. Downwelling global solar radiation ($W\,m^{-2}$), wind speed ($m\,s^{-1}$) and snow depth (cm) effects on ΔT were summarized and analyzed in relation to bias. The Wilcoxon-Mann-Whitney (Wilcoxon, 1945) test was used to analyze differences among shields and between snow- and grass-covered

Table 1
MAE (°C) and confidence interval (0.95) for Tinytag and iButton bias relative to the Thies PT100 reference thermistor. Mean range (°C) between devices by hourly periods and location.

Hourly period (UTC h)	Tinytags	iButtons	Location
1. Night (21–04)	MAE: 0.223 ± 0.009 Range: 0.19 (n: 11520)	MAE: 0.703 ± 0.106 Range: 1.21 (n: 10244)	Canfranc-Station
2. Sunrise-Evening (05–07 & 18–20)	MAE: 0.226 ± 0.009 Range: 0.20 (n: 8640)	MAE: 0.687 ± 0.100 Range: 1.22 (n: 7668)	
3. Morning-Afternoon (08–10 & 15–17)	MAE: 0.196 ± 0.011 Range: 0.27 (n: 8640)	MAE: 0.669 ± 0.090 Range: 1.16 (n: 7668)	
4. Midday (11–14)	MAE: 0.146 ± 0.011 Range: 0.40 (n: 5760)	MAE: 0.631 ± 0.056 Range: 1.00 (n: 5112)	
1. Night (21–04)	MAE: 0.085 ± 0.005 Range: 0.18 (n: 20352)	MAE: 0.767 ± 0.074 Range: 0.77 (n: 17808)	Daroca
2. Sunrise-Evening (05–07 & 18–20)	MAE: 0.090 ± 0.006 Range: 0.21 (n: 15264)	MAE: 0.653 ± 0.062 Range: 0.75 (n: 13356)	
3. Morning-Afternoon (08–10 & 15–17)	MAE: 0.096 ± 0.008 Range: 0.25 (n: 15243)	MAE: 0.633 ± 0.053 Range: 0.71 (n: 13335)	
4. Midday (11–14)	MAE: 0.166 ± 0.015 Range: 0.29 (n: 10176)	MAE: 0.530 ± 0.037 Range: 0.64 (n: 8904)	

ground.

3.3. Experiment 3. Effect of sensor height above the snowpack on temperature measurements

This experiment was conducted at Formigal-Sarrios and involved comparison of hourly air temperature measurements made from 15 November 2017 to 30 May 2018 (during the snow season) at 6 heights above the land surface (100, 150, 200, 250, 300, and 350 cm) using Tinytags within naturally-aspirated Datamate ACS-5050 radiation shields mounted on north-facing wooden poles. Snow depth was measured simultaneously. Hourly mean wind speed was measured at a height of 10 m above bare ground. The mean hourly incident global solar radiation was measured 1 m away Tinytags. The 2017–2018 snow season at Formigal-Sarrios station lasted approximately 170 days (n = 24,510, 86.8% samples), from 30 November 2017 until 20 May 2018. The snow depth was > 100 cm for 54.3% of the time, > 150 cm for 32.4% of the time, > 200 cm for 21.0% of the time, and > 250 cm for 1.9% of the time; the greatest snow depth was 275 cm, on 11 April 2018 (18:00 UTC). No failures in measurement were detected. Measurements recorded from sensors completely covered by snow were not included in the analysis (n = 5134; 18.2% samples).

Vertical air temperature profiles were analyzed and assessed in relation to environmental data (global solar radiation, wind speed, and precipitation). Vertical temperature stabilization was calculated from the lowest device height above the snow (not bare ground); the temperature difference relative to the highest device (always snow-free) was < ± 0.1 °C.

3.4. Experiment 4. Horizontal variability

The main objective of this experiment was to assess the horizontal variability of temperature over relatively homogeneous terrain (mountain forest), to determine the potential impact of random selection of the location used to characterize the temperature regimen for a given area, in this case within the 1742–2213 m elevation band. Air temperature was measured in four homogeneous plots (two north-facing and two south-facing) in terms of latitude, longitude, land use, slope, and elevation. In these cases, air temperature differences may be determined by non-identified factors, which have been wanted to quantify (e.g. specific-site sun hours, water presence, shrub height, proximity to sources of longwave transmission including rocks). Hourly paired data were logged from 5 September 2017 to 22 January 2018; at the end of the experiment the plots were covered by snow. Because of the very steep slopes it was difficult to find suitable measurement locations at equivalent elevations, but all were within a maximum difference of 28 m, imply a difference of 0.13 °C assuming a seasonal lapse rate of -0.47 °C 100 m^{-1} (Navarro-Serrano et al., 2018). Measurements were made using Tinytags (5 in each plot, with a distance between loggers of around 15–20 m; 10 in each altitudinal band; 20 total) in Datamate ACS-5050 radiation shields. To avoid snow effects the loggers were installed at a height of 250–300 cm above the ground, and within an evergreen forested area.

Hourly absolute bias between the mean plot air temperature and specific devices was calculated and analyzed to determine the variations involved. ANOVA, Scheffe Post-Hoc test, and descriptive statistical analyses were made using the original absolute temperature data to determine variability, and the confidence intervals (0.95) in relation to the mean were calculated.

4. Results

4.1. Temperature logger accuracy and consistency

Eight (6) Tinytag and six (8) iButton devices were originally installed at the Canfranc-Station (Daroca). However, two of the iButtons (one each at Daroca and Canfranc-Station) failed and were discarded, and three additional iButtons at Canfranc-Station failed to save data during the last month of the experiment, reducing the expected number of measurements. The remaining data were analyzed.

Based on analysis of MAE and confidence intervals, Table 1 shows that Tinytags had less bias than iButtons (especially at morning-afternoon and midday), and there was less bias at Daroca than at Canfranc-Station. Radiation effects were not equal between device types and locations. Thus, the MAE for Tinytags decreased and the confidence interval increased with increasing radiation, while for the iButtons there was only a decrease in the confidence interval at morning-afternoon and midday. Fig. 3 shows the variation between the Tinytag and iButton data and the reference Thies PT100 data. This indicates that bias for almost all Tinytag measurements was ± 0.3 to ± 0.4 °C, especially at Daroca, while for the iButtons > 20% of measurements showed ± 1 °C deviation.

Fig. 3 presents that was no clear effect of the presence of snowpack on the observed bias. However, differences were found between the biases of the Tinytags and iButtons, as shown on Table 1. iButton records below 0 °C shows a noticeable scattering. There was a slight and negative Pearson correlation (non-significant) between the bias and the observed temperature (for temperatures > 0 °C the bias rarely exceeded +0.5 °C for the Tinytags and + 2 °C for the iButtons). At Canfranc-Station there was an extreme and short negative bias when one iButton

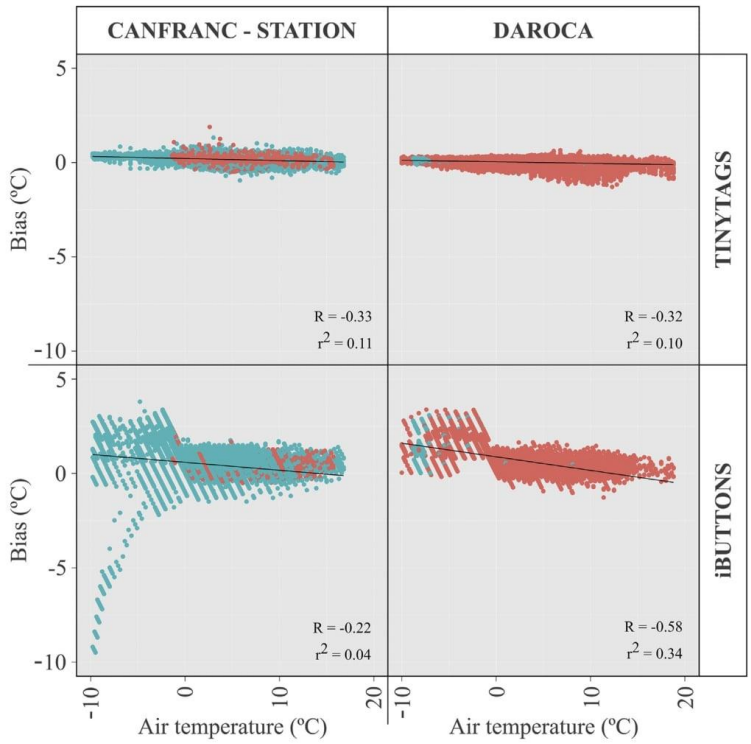

Location / Device		± 0.1ºC	± 0.2ºC	± 0.3ºC	± 0.4ºC	± 0.5ºC	± 1ºC
Canfranc Station	Tinytags	16.6 %	49.0 %	83.8 %	96.9 %	99.3 %	100 %
	iButtons	9.0 %	19.1 %	28.6 %	36.9 %	46.0 %	82.7 %
Daroca	Tinytags	59.7 %	89.4 %	96.4 %	98.2 %	99.1 %	100 %
	iButtons	9.2 %	18.9 %	30.9 %	42.9 %	54.2 %	79.2 %

Fig. 3. Tinytag and iButton bias relative to the Thies PT100 reference air temperature. Days with snow on the ground (turquoise) and snow-free days (red) are distinguished for the two locations. Global linear fit is expressed by black line. The table shows the % device bias relative to the reference Thies PT100 data. (For interpretation of the references to colour in this figure legend, the reader is referred to the web version of this article.)

DS-1921G device measured −19 °C while the Thies reference thermistor measured −9.7 °C, although the device returned to normal functioning 4 h later (Fig. 4).

4.2. Performance of radiation shields

Table 2 shows temperature bias in relation to a Stevenson-shielded Tinytag. All snow-grass and radiation shield combinations were found to differ significantly ($p < .05$; Wilcoxon-Mann-Whitney test). Under all conditions the Datamate radiation shield showed the smallest ΔT, with > 90% of measurements between ± 0.5 ΔT ($Percentile_{10}$–0.33 and P_{90} 0.18), indistinctly over snow and grass. As expected, measurements made in the absence of a shield were the worst in all situations (P_{10}–1.37 and P_{90} 1.64), with < 40% and < 25% of samples between ± 0.5 ΔT over snow and grass, respectively; however, the percentage of samples between ± 2 ΔT were similar between the tube and funnel shields. In all situations the funnel shield showed less uncertainty than the tube shield, reaching approximately 70% of samples between ± 0.5 ΔT (P_{10}–0.65; and P_{90} 0.82), while the tube shield (P_{10}–0.94 and P_{90} 1.16) was 10% and 20% of samples below in the snow and grass situations, respectively. The slightly better whole shield performances over snow than grass indicates the need for specific radiation-wind analysis.

Fig. 5 shows the mean ΔT for combinations of ground surface, radiation, and wind speed for each shielding condition. An increase in ΔT was common under high solar radiation levels and with weak winds. Nevertheless, the magnitude of ΔT varied among shielding conditions and the cover type/radiation/wind speed combinations. However, the Datamate ΔT was almost equilibrate between all combinations (generally between ± 0.5 of the mean ΔT), although there was general

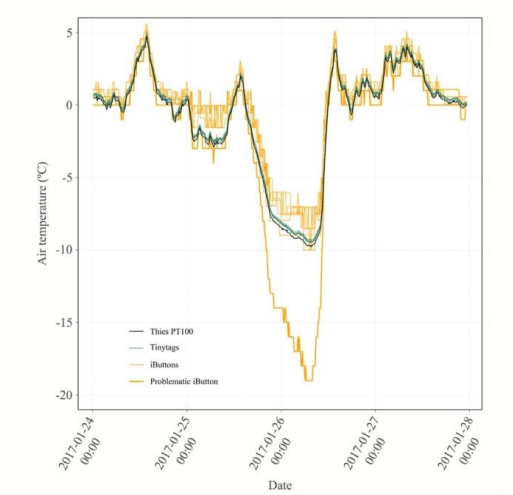

Fig. 4. Episode (between 24 January 2017 and 27 January 2017) of extreme decoupling of temperature measurement between one iButton device (thick orange) and the Thies PT100 reference thermistor (black), Tinytags (green), and other iButtons (orange). (For interpretation of the references to colour in this figure legend, the reader is referred to the web version of this article.)

slightly overcooling with grass cover conditions. In the absence of a shield (no shield) the ΔT was extremely positively correlated with radiation (Pearson's correlation; $r = 0.72$). The tube and funnel shields behaved differently. The tube shield performance was more related to wind speed, while for the funnel it was more related to radiation. Above snow cover (Fig. 5, right side) the environmental effects were variable. The mean no shield ΔT suffers a relevant overcooling under null radiation conditions (night), and extreme overheating in strong radiation conditions, almost independent of wind speed. The tube shield performance was more related to wind speed than to radiation, and performed well under strong radiation conditions if the wind speed was $> 2.5\ m\ s^{-1}$. The funnel shield performance was more correlated with radiation, and performed well under zero to weak wind conditions if radiation was $< 400\ W\ m^{-2}$. The Datamate performance was constant below different conditions, and no significant differences were found between snow and grass ground cover situations (always between ± 0.5 ΔT). Above grass cover (Fig. 5, left side), environmental effects were similar, but some differences were found. The performance of the funnel improved significantly, with a generalized decrease in ΔT for the majority of combinations, except under null radiation. The performance of the tube shield was slightly worse, especially under weak wind conditions. Frequency distribution of wind-radiation combinations is shown in Supplementary Material (Fig. 1).

4.3. Effect of sensor height above the snowpack

Fig. 6 shows the most representative hour of each hourly period. It shows that there was a cooling effect on sensors located near the snow surface (< 100 cm above the surface) that followed a near logarithmic function, especially at 12 and 16 UTC. This pattern weakened between late 19 and 2 UTC, when the vertical temperature distribution was more stable and homogeneous. Moreover, the variation decreased with time from midday to night. Maximum cooling generally occurred under calm or weak wind conditions (red colour in Fig. 6), indicating an influence of wind on the vertical temperature profile. Generally, temperature stabilized at ≈ 75–100 cm above the snow surface, with clear stabilization above this height, particularly between 12 and 16 UTC. A more constant air temperature profile was found under rainy/snowy conditions (Supplementary Material. Fig. 2), and greater differences occurred when the weather was stable. To analyze the height at which stabilization occurred (representing the temperature stabilization height above snow cover), we used the lowest device height above snow cover where a difference < ± 0.1 °C in relation to the highest device was found (Fig. 7).

4.4. Horizontal variability

Fig. 8a shows an evident reduction in bias at night (≈ 0.2 °C), while at midday the mean absolute bias increased to produce the largest differences (peaks of 0.6–0.8 °C). Differences during the night (22–04 UTC) were small and constant (< ± 0.5 °C for 89.6% of the cases). Fig. 8b shows the mean hourly confidence interval (0.95) in each site, derived by averaging the confidence interval for specific devices. This figure shows an evident decrease in the confidence interval at night, and maximum rates between 8 and 17 UTC, particularly at midday. The general behavior approximated the daily global radiation curve. The Upper-South site showed less uncertainty than the other sites, especially at night. Similar behavior among the other sites was found, despite a slight increase in uncertainty for the Upper-North site during the night. The maximum mean hourly confidence interval was small (± 0.10 °C). ANOVA and Scheffe Post-hoc test analysis of the original absolute temperature data enabled identification of those devices that behaved differently relative to the sensors in the same plot ($p < .05$), including: Upper-North, 1 case; Bottom-North: 1 case; Upper-South: No cases; Bottom-South: 1 case. The ANOVA results were consistent with Fig. 8b, which shows both night-day phases.

5. Discussion

Experimental results (in particular Experiment 1) showed that Thermochron iButton devices were subject to read/load measurement problems that lead to total data loss. This issue has been reported in previous studies (Roznik and Alford, 2012; Wolaver and Sharp, 2007), and can be attributed to occasional operational problems resulting from poor water protection, despite iButton devices being submerged in water in some studies (Angilletta and Krochmal, 2003). In addition, we found some isolated measurements made using iButtons produced

Table 2
Temperature bias (% of total observations) under different shielding conditions for snow and grass ground covers.

Condition		± 0.1 °C	± 0.2 °C	± 0.3 °C	± 0.4 °C	± 0.5 °C	± 1 °C	± 2 °C
Snow	No-shield	5.9	13.8	23.2	32.6	39.9	68.9	95.3
	Tube	8.4	21.3	36.3	47.6	58.7	87.0	98.4
	Funnel	17.9	37.0	52.3	61.3	68.5	87.4	97.9
	Datamate	50.0	74.3	85.7	91.3	94.5	99.5	99.8
Grass	No-shield	3.1	7.1	12.2	18.7	25.4	56.7	89.4
	Tube	5.7	12.7	23.0	35.3	46.2	77.8	94.1
	Funnel	11.8	26.6	42.0	55.5	66.9	90.9	98.0
	Datamate	39.8	64.0	79.5	87.0	91.6	98.7	99.9

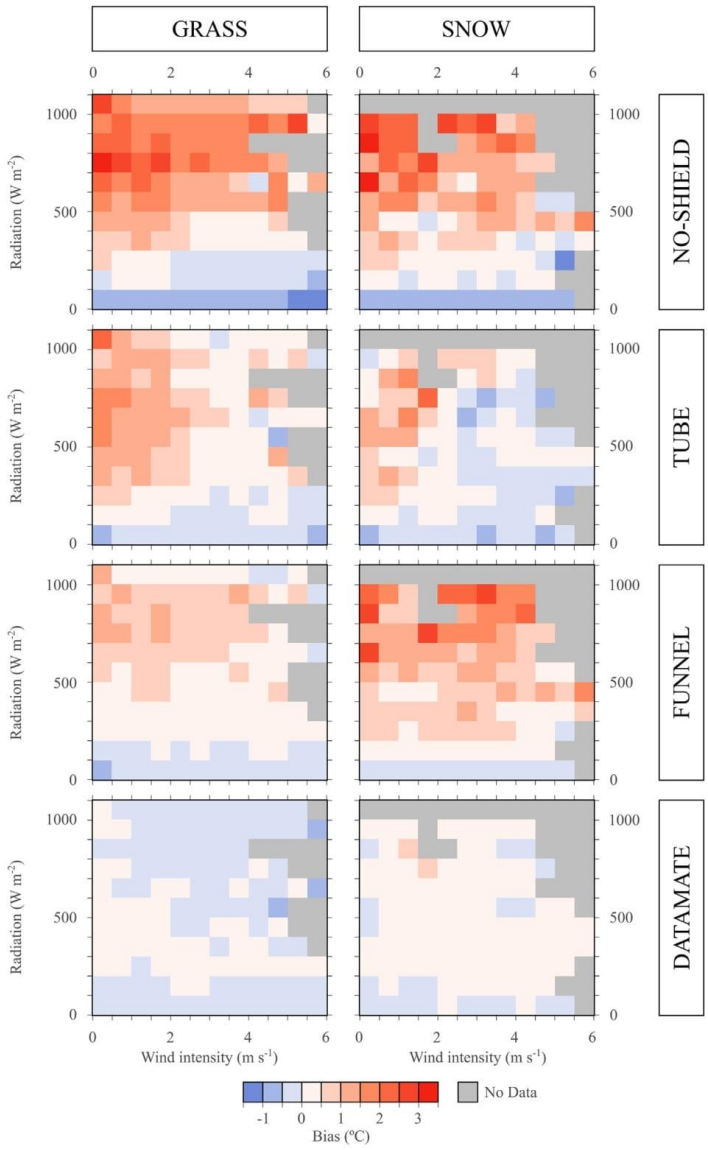

Fig. 5. Performance of radiation shields under grass (left) and snow (right) cover, and under differing wind speed ($m\,s^{-1}$) and shortwave radiation ($W\,m^{-2}$) conditions. 1) No shield, 2) Tube Shield, 3) Funnel Shield, 4) Datamate ACS-5050 shield. Bias is expressed in °C, calculated in relation to measurements made using the Stevenson shield. Positive values imply a relative overheating effect, and negative values indicate a cooling effect.

biases of up to 10 °C compared with the reference thermistor. The Tinytag devices were not subject to data loss, and provided reliable air temperature estimates compared with the reference over the temperature range. This is consistent with the results of Imholt et al. (2013), Yang et al. (2012), and the manufacturer's specifications. Substantial biases (bias > ± 0.5 °C; defined by Hubbart et al., 2005) in measurements using Tinytag sensors only affected 0.9% of measurements at Daroca and 0.7% at Canfranc-Station (compared with 45.8% and 54% using iButton devices, respectively). The performance of the iButton devices in the present study are consistent with those reported by Hubbart et al. (2005), who noted that these devices worked properly at air temperatures > 0 °C, but bias and uncertainty increased below this temperature. In previous studies (Hubbart et al., 2005; Lundquist and Huggett, 2008) iButton devices were calibrated in ice baths, so the problematic frozen conditions were not checked. This issue is clearly relevant for applications involving use of these sensors in sub-zero

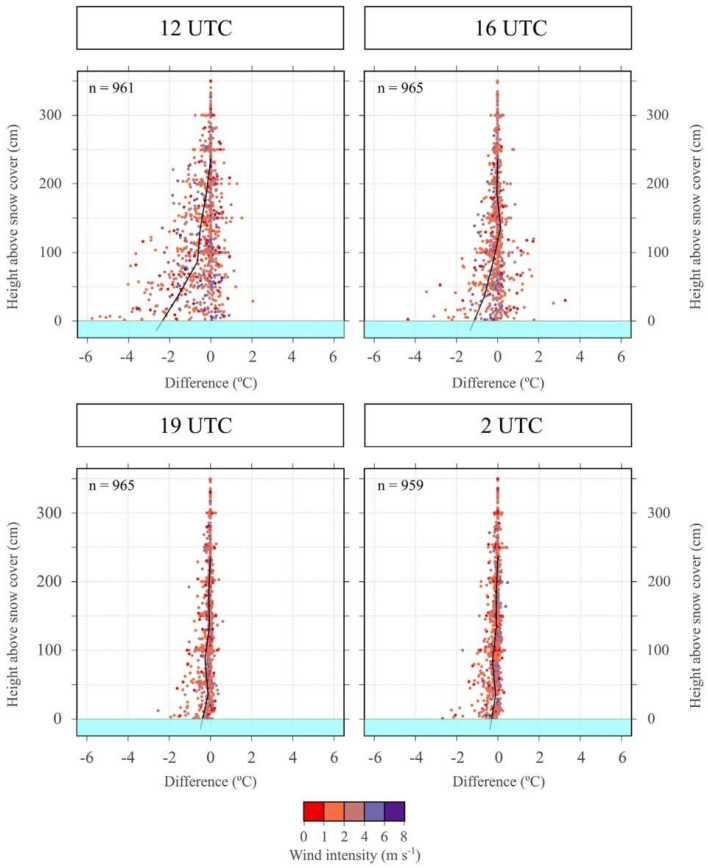

Fig. 6. Vertical temperature profile at 12, 16, 19, and 02 UTC. The black line shows the mean for the 6 devices. Bias (X axis) was calculated in relation to the highest device (no. 6). The height (Y axis) was calculated dynamically in relation to the snow depth present. Wind speed is represented from strong (purple) to weak (red) winds. (For interpretation of the references to colour in this figure legend, the reader is referred to the web version of this article.)

environments. A slight negative correlation was found between bias and observed air temperature for both the Tinytag and iButton sensors, in agreement with the findings of Johnson et al. (2005).

Experiment 2 shows that air temperature variation relative to measurements made using the Stevenson screen was less above snow than above grass. However, this does not show that snow was the factor responsible, as analysis of radiation-wind effects showed that variations were larger above snow covered surfaces than above grass when radiation and wind conditions were constant. Therefore, radiation and wind are the major factors influencing the performance of radiation shields, as reported previously (Buisán et al., 2015; Georges and Kaser, 2002; Holden et al., 2013; Huwald et al., 2009). The results showed that under varying radiation, wind, and snow conditions the commercial multi-plate Datamate ACS5050 shield provided the best performance compared with the other simpler and more economic alternatives. The Datamate radiation shield is based on Gill's multi-plate models (Gill, 1983), but has been substantially improved over the intervening years. The outstanding performance of multi-plate radiation shields has been previously reported. For example, Payne (1987) indicated a bias range from +0.2 to +0.3 °C for winds > 2 m s^{-1}, Hubbart et al. (2005) reported a bias generally ranging from +0.5 to +1.0 °C, and Martínez-Ibarra et al. (2010) showed that these radiation shields provide greater protection than the Stevenson screen with less temperature variation, which is consistent with our findings. Our results showed that the bias was ± 0.5 °C above grass, and 0–0.5 °C above snow. The non-commercial tube and funnel shields, and the absence of a shield, provided variable results depending on the environmental conditions, as the measurements were differently affected by radiation and wind speed. Generally, the tube, funnel, and no shield results were consistent with those of Georges and Kaser (2002), who reported a significant decrease in bias for wind speeds > 3.5–4 m s^{-1}. Based on the ± 1 °C threshold proposed by Tarara and Hoheisel (2007), the no shield data were only slightly valid at mean night temperatures (zero radiation). Tube shield data were when wind intensity was > 3 ms^{-1}, funnel shield data were when radiation was < 700 W m^{-2} (400–500 W m^{-2} with snow presence), and Datamate data were in all situations. The absence of a shield provided the worst conditions, with 95% measurements showing variation of ± 2 °C, although the bias was relatively low at night (slight cooling). Unshielded devices (no protection and maximum ventilation) were influenced mainly by incident radiation and snow albedo effects. Thus, unshielded devices used in previous studies (e.g., Shine et al., 2003; Sternberg et al., 2011) may have been affected by daytime

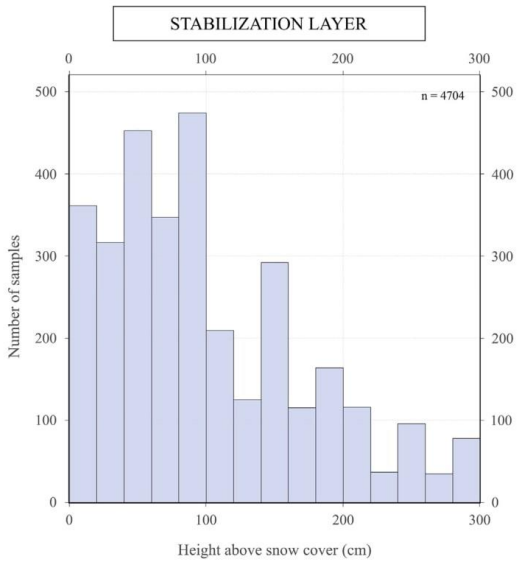

Fig. 7. Stabilization layer frequency calculated as the lowest device height where a bias < ± 0.1 °C in relation to device no. 6 was measured. The height (X axis) was calculated dynamically in relation to snow depth.

overheating and underestimation at night (Azorin-Molina and Azorin-Molina, 2008). The funnel design provided little protection from incident radiation (large positive bias even with strong winds). Because of its open bottom design, the performance of devices using the funnel shield was similar to that where no shield was used above high albedo snow surfaces, consistent with the findings of Nakamura and Mahrt (2005) and Tarara and Hoheisel (2007), and better above grass. The funnel design causes overheating that cannot be dissipated by natural ventilation, so better results have been found at low radiation levels (Ribeiro da Cunha, 2015) or avoiding the central hour of the day or in little insolated slopes or forest areas (Lundquist and Huggett, 2008). The tube shield does not favor internal ventilation, so large positive biases occurred even at low radiation levels, with a deficient performance for wind speeds < 4 m s^{-1} above grass and snow. However, the performance for wind speeds > 4 m s^{-1} was much better than for the funnel design, especially above snow covered surfaces. In any case, the performance of tube shield is partially dependent on the latitude of measurements, since the inclination depends on it and ventilation is easier when the tube is horizontal, and because albedo effect is more effective overheating when tube is vertical. This implies that its performance would be better in low latitudes than in high ones.

The results of Experiment 3 showed a radiation effect on vertical hourly temperature profiles, with an increasing of variability at midday and a progressive decreasing at night. In addition, this increasing of variability for measurements made close to the snow surface; extreme examples involved deviations of −6 °C in relation to highest measurement, especially at midday. Hanna et al. (2017) indicated that ± 4 °C differences can occur at midday at heights of 1–2 m above the snow surface. Midday results showed generalized cooling with decreasing height of devices above the snow, which can be explained by heat exchange between air and the frozen snow surface during daylight hours. Gustavsson (1995) also found that snow can cause cooling of the near surface layer air, and that this is more pronounced at low wind speeds. We found small differences among measurements recorded at night at different heights above the snow. On an hourly basis our results were not always consistent with those of previous studies. For example, Halberstam and Schieldge (1981) proposed that night generally favors air stabilization and near surface air cooling relative to higher air layers, because of air subduction and stratification caused by the cold snow surface. That study also reported a constant diurnal air temperature profile, in contrast with our measurements. However, differences may be determined by differences in climatic conditions, where Pyrenees generally rounds isotherm 0 °C during winter. In addition, Experiment 3 encompassed a complete snow season of 7 months, compared with 3 days in the study of Halberstam and Schieldge (1981) and 1 week in the study of Hanna et al. (2017). Although the optimal is to measure temperature data at a constant height above the snow surface along snow season, remote areas and autonomous self-recording dataloggers make it difficult to carry it out. For this, Experiment 3 analyzes temperature stabilization. Stabilization boundary analysis has showed that stabilization occurs at 75–100 cm above the snow surface.

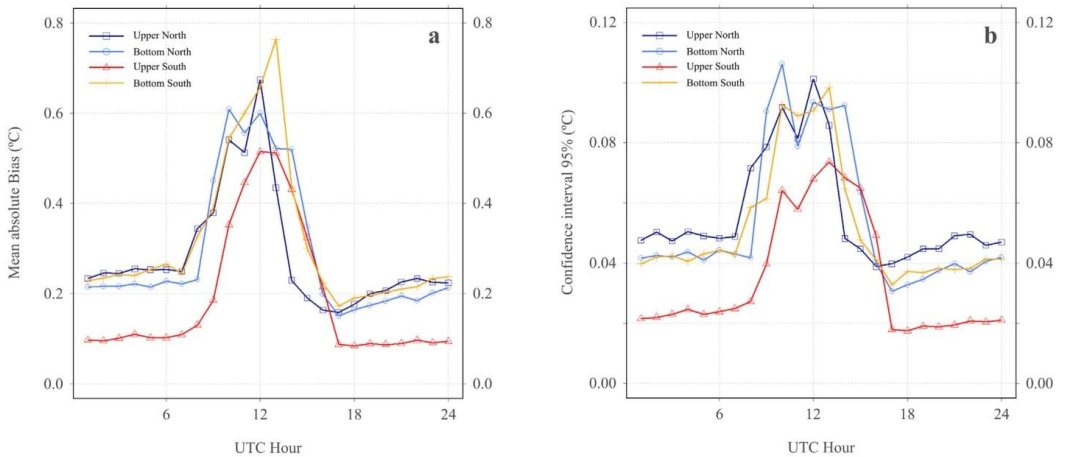

Fig. 8. a) Mean hourly absolute temperature bias for the four sites. b) Experimental plots hourly air temperature confidence interval (0.95), based on temperature differences between devices and plot average.

This suggests that devices should be placed at heights > 100 cm above the maximum expected snow depth. Lundquist and Cayan (2007), Lundquist and Huggett (2008) and Hubbart et al. (2007) anticipated this issue and overcame the problem by installing their devices at varying heights (2–10 m) above the snow surface. Parallel snow depth measurements during field studies can be very useful for estimating data quality.

Experiment 4 showed that there was a significant radiative effect on the horizontal variability of air temperature within forested mountain plots, with two clear temporal periods (daytime and night). Uncertainty was similar among all plots, with uncertainty constant during the night and increasing during daylight hours, especially at midday. The temperature at random selected locations showed a temporal behavior related to shortwave radiation (early morning-late afternoon, morning, afternoon, midday). However, individual devices occasionally produced significantly different measurements. The largest divergences among sensors took place at midday, when solar radiation fluxes were stronger. Thus, despite the use of radiation shields in this experiment, when strong shortwave radiation fluxes occurred, other environmental factors including the presence of rocks, water, or trees produced longwave radiation (Gustavsson, 1995; Holden et al., 2013; Lundquist and Huggett, 2008) that could have affected the measurements made by individual devices. The smallest variations were recorded in the Upper-South site, in agreement with ANOVA analysis, which indicated that measurements made by devices in this plot were consistent. However, in the other plots there were always some devices producing significantly different measurements, and so increased uncertainty. The more dense forest in the Upper-South plot may have reduced measurement variability, because of reduced downwelling of shortwave radiation. In conclusion, diurnal variations may have been because of different shortwave radiation exposures (i.e. forest vs. cleared land; local topographic shadowing) or the proximity to longwave transmitters (i.e. rock surfaces). Night variations were probably mainly to because of the proximity of longwave transmitters (i.e. forest vs. cleared land; rock surfaces; Lundquist and Huggett, 2008). These results suggest the need for analysis of horizontal temperature variability on flat and open areas in future investigations.

6. Conclussions

The major findings of this research can be summarized as follows:

- Autonomous self-recording dataloggers are an appropriate and easy option for measuring air temperature in snow-covered and mountainous areas. Tinytag devices showed a robust and constant performance in relation to a reference sensor, whereas the iButton devices showed unstable biases (especially at temperatures < 0 °C), and were subject to unexpected read-save errors. Thus, the use of Tinytag devices is recommended. In the event that iButton devices are used, it is necessary to place multiple devices (2 or more) in parallel.
- Protection of temperature measuring devices from solar radiation is necessary to ensure the quality of air temperature data. Use of the traditional double-louvre naturally-ventilated Stevenson screen is not necessary, as there are other reliable screens available. The commercial multi-plate Datamate ACS5050 shield provided the best protection over all radiation, wind, and snow conditions. The tube and funnel shields showed variable performance, and their limitations must be considered: the tube shield is more useful in snowy and windy environments, while the funnel shield is more useful in the snow-free and low wind areas). Overall, use of commercial plate radiation shields, as the Datamate ACS5050, provide much better results than other more inexpensive alternatives. Only low radiation and windy conditions seemed to be favorable for use of the inexpensive shielding alternatives.
- The air temperature vertical profile showed stabilization at 75–100 cm above the snow cover surface. Thus, prior to device installation it is important to know the expected snow depth, and to install devices above this level by > 100 cm. Different temporal performances were found including: i) intense superficial air cooling during daylight hours, especially at midday, possibly because of energy fluxes from air to cold snow surfaces; ii) stabilization at night, when all devices involved in the experiment were within (always < 350 cm) the zone of environmental cooling, favored by topography.
- Horizontal air temperature variability analysis showed that measurement variation increased at midday, simultaneously with the increase in solar radiation. Solar radiation enhances physical characteristics of the materials (absorption, emission, reflection), so affecting the temperature measurements.

More research is needed to assess the performance of other devices (dataloggers and radiation shields) used in mountain environments. However, our horizontal variability analysis is novel, and can help explain the “noise” effect found when measuring air temperatures in mountain and snowy environments.

Acknowledgments

This study was funded by the research projects “El papel de la nieve en la hidrología de la peninsula ibérica y su respuesta a procesos de cambio global-HIDROIBERNIEVE-CGL2017-82216-R” and CLIMPY “Characterization of the evolution of climate and provision of information for adaptation in the Pyrenees” (FEDER-POCTEFA). We thank the Spanish Meteorological Agency (AEMET) and observers Y. Jimenez and S. Campo for the permissions to use official observatories and for the meteorological data used in this study. Navarro-Serrano, F. and Sanmiguel-Vallelado, A. are granted with a pre-doctoral FPU grant (Spanish Ministry of Education, Culture and Sports). Alonso-González, E. and Khorchani, M. are granted with a pre-doctoral FPI grant (Spanish Ministry of Economy and Competitiveness). The authors thank all colleagues who helped in the development of the experiments. Raw data is freely downloadable at https://zenodo.org/record/1495572. The authors wish to acknowledge anonymous reviewers for their detailed and helpful comments to the original manuscript.

Appendix A. Supplementary data

Supplementary data to this article can be found online at https://doi.org/10.1016/j.atmosres.2019.03.034.

References

Alonso-González, E., Ignacio López-Moreno, J., Gascoin, S., García-Valdecasas Ojeda, M., Sanmiguel-Vallelado, A., Navarro-Serrano, F., Revuelto, J., Ceballos, A., Esteban-Parra, M.J., Essery, R., 2018. Daily gridded datasets of snow depth and snow water equivalent for the Iberian Peninsula from 1980 to 2014. Earth Syst. Sci. Data 10. https://doi.org/10.5194/essd-10-303-2018.

Anderson, P., Neff, W., 2008. Boundary layer physics over snow and ice. Atmos. Chem. Phys. 8, 3563–3582. https://doi.org/10.5194/acp-8-3563-2008.

Angilletta, M., Krochmal, A., 2003. The thermochron: a truly miniature and inexpensive temperature-logger. Herpetol. Rev. 34 (1), 31–32.

Arck, M., Scherer, D., 2001. A physically based method for correcting temperature data measured by naturally ventilated sensors over snow. J. Glaciol. 47, 665–670. https://doi.org/10.3189/172756501781831774.

Azorin-Molina, C., Azorin-Molina, J.C., 2008. Estudio experimental del efecto artificial introducido por la garita meteorológica en la temperatura mínima del aire. In: Sigro, J., Brunet, M., Aguilar, E. (Eds.), Cambio Climático Regional y Sus Impactos. 2. Spanish Climatological Society (AEC), Tarragona (Spain), pp. 25–35.

Barry, R., 1992. Mountain Weather and Climate, 2nd ed. Psychology Press.

Bonnardot, V., Carey, V., Madelin, M., Cautenet, S., Coetzee, Z., Quénol, H., 2012. Spatial variability of Night temperatures at a fine scale over the Stellenbosch Wine District, South Africa. J. Int. Sci. Vigne Vin 46, 1–13.

Brabyn, L., Zawar-Reza, P., Stichbury, G., Cary, C., Storey, B., Laughlin, D., Katurji, M., 2014. Accuracy assessment of land surface temperature retrievals from Landsat 7 ETM + in the Dry Valleys of Antarctica using iButton temperature loggers and weather station data. Environ. Monit. Assess. 186, 2619–2628. https://doi.org/10.1007/s10661-013-3565-9.

Brunet, M., Saladié, O., Jones, P., Sigró, J., Aguilar, E., Moberg, A., Lister, D., Walther, A., Lopez, D., Almarza, C., 2006. The development of a new dataset of Spanish Daily Adjusted Temperature Series (SDATS) (1850–2003). Int. J. Climatol. 26, 1777–1802. https://doi.org/10.1002/joc.1338.

Buisán, S., Azorin-Molina, C., Jimenez, Y., 2015. Impact of two different sized Stevenson screens on air temperature measurements. Int. J. Climatol. 35, 4408–4416. https://doi.org/10.1002/joc.4287.

Buisán, S., Earle, M.E., Collado, J.L., Kochendorfer, J., Alastrué, J., Wolff, M., Smith, C.D., López-Moreno, J.I., 2017. Assessment of snowfall accumulation underestimation by tipping bucket gauges in the Spanish operational network. Atmos. Meas. Tech. 10, 1079–1091. https://doi.org/10.5194/amt-10-1079-2017.

Campbell, G., Norman, J., 1998. Introduction to Environmental Biophysics. Springer.

Camuffo, D., Bertolin, C., 2012. The earliest temperature observations in the world: the Medici Network (1654–1670). Clim. Chang. 111, 335–363. https://doi.org/10.1007/s10584-011-0142-5.

Domínguez-Villar, D., Lojen, S., Krklec, K., Baker, A., Fairchild, I., 2015. Is global warming affecting cave temperatures? Experimental and model data from a paradigmatic case study. Clim. Dyn. 45, 569–581. https://doi.org/10.1007/s00382-014-2226-1.

Fang, Z., Li, N., Li, B., Luo, G., Huang, Y., 2014. The effect of building envelope insulation on cooling energy consumption in summer. Energy Build. 77, 197–205. https://doi.org/10.1016/J.ENBUILD.2014.03.030.

Fritschen, L., Gay, L., 1979. Environmental Instrumentation. Springer, New York.

Fuchs, M., Tanner, C., 1965. Radiation shields for air temperature thermometers. J. Appl. Meteorol. 4, 544–547.

Gasvoda, D., Tinus, R., Burr, K., Trent, A., 2002. Monitoring the temperature of tree seedlings with the thermochron iButton data logger. In: USDA For. Serv. Technol. Dev. Program, Timber Tech Tips, 2400, March 2002.

Georges, C., Kaser, G., 2002. Ventilated and unventilated air temperature measurements for glacier-climate studies on a tropical high mountain site. J. Geophys. Res. 107, 4775. https://doi.org/10.1029/2002JD002503.

Gill, G., 1983. Comparison Testing of Selected Naturally Ventilated Solar Radiation Shields. NOAA, Bay St. Louis.

Gustavsson, T., 1995. A study of air and road-surface temperature variations during clear windy nights. Int. J. Climatol. 15, 919–932. https://doi.org/10.1002/joc.3370150806.

Halberstam, I., Schieldge, J., 1981. Anomalous behavior of the atmospheric surface layer over a melting snowpack. J. Appl. Meteorol. 20, 255–265. https://doi.org/10.1175/1520-0450(1981)020<0255:ABOTAS>2.0.CO;2.

Hanna, E., Mernild, S., Yde, J., Villiers, S., 2017. Surface Air temperature fluctuations and lapse rates on Olivares Gamma Glacier, Rio Olivares Basin, Central Chile, from a novel meteorological sensor network. Adv. Meteorol. 2017, 1–15. https://doi.org/10.1155/2017/6581537.

Harrison, R.G., 2010. Natural ventilation effects on temperatures within Stevenson screens. Q. J. R. Meteorol. Soc. 136, 253–259. https://doi.org/10.1002/qj.537.

Helgason, W., Pomeroy, J., 2012. Characteristics of the near-surface boundary layer within a mountain valley during winter. J. Appl. Meteorol. Climatol. 51, 583–597. https://doi.org/10.1175/JAMC-D-11-058.1.

Hofer, I., Hart, A., Martín-Vega, D., Hall, M., 2017. Optimising crime scene temperature collection for forensic entomology casework. Forensic Sci. Int. 270, 129–138. https://doi.org/10.1016/J.FORSCIINT.2016.11.019.

Holden, Z., Klene, A., Keefe, R., Moisen, G., 2013. Design and evaluation of an inexpensive radiation shield for monitoring surface air temperatures. Agric. For. Meteorol. 180, 281–286. https://doi.org/10.1016/J.AGRFORMET.2013.06.011.

Hubbard, K., Lin, X., Walter-Shea, E., 2001. The effectiveness of the ASOS, MMTS, Gill, and CRS air temperature radiation shields*. J. Atmos. Ocean. Technol. 18, 851–864. https://doi.org/10.1175/1520-0426(2001)018<0851:TEOTAM>2.0.CO;2.

Hubbart, J., 2011. An inexpensive alternative solar radiation shield for ambient air temperature micro-sensors. J. Nat. Environ. Sci. 2, 9–14.

Hubbart, J., Link, T., Campbell, C., Cobos, D., 2005. Evaluation of a low-cost temperature measurement system for environmental applications. Hydrol. Process. 19, 1517–1523. https://doi.org/10.1002/hyp.5861.

Hubbart, J., Kavanagh, K., Pangle, R., Link, T., Schotzko, A., 2007. Cold air drainage and modeled nocturnal leaf water potential in complex forested terrain. Tree Physiol. 27, 631–639. https://doi.org/10.1093/treephys/27.4.631.

Huwald, H., Higgins, C., Boldi, M., Bou-Zeid, E., Lehning, M., Parlange, M., 2009. Albedo effect on radiative errors in air temperature measurements. Water Resour. Res. 45. https://doi.org/10.1029/2008WR007600.

Imholt, C., Soulsby, C., Malcolm, I., Hrachowitz, M., Gibbins, C., Langan, S., Tetzlaff, D., 2013. Influence of scale on thermal characteristics in a large montane River Basin. River Res. Appl. 29, 403–419. https://doi.org/10.1002/rra.1608.

Johnson, A., Boer, B., Woessner, W., Stanford, J., Poole, G., Thomas, S., O'Daniel, S., 2005. Evaluation of an inexpensive small-diameter temperature logger for documenting ground water-river interactions. Groundw. Monit. Remediat. 25, 68–74. https://doi.org/10.1111/j.1745-6592.2005.00049.x.

Juliussen, H., Humlum, O., 2007. Towards a TTOP ground temperature model for mountainous terrain in central-eastern Norway. Permafr. Periglac. Process. 18, 161–184. https://doi.org/10.1002/ppp.586.

Kurzeja, R., 2010. Accurate temperature measurements in a naturally-aspirated radiation shield. Bound. Layer Meteorol. 134, 181–193. https://doi.org/10.1007/s10546-009-9430-2.

López-Moreno, J.I., Navarro-Serrano, F., Azorín-Molina, C., Sánchez-Navarrete, P., Alonso-González, E., Rico, I., Morán-Tejeda, E., Buisán, S., Revuelto, J., Pons, M., Vicente-Serrano, S.M., 2018. Air and wet bulb temperature lapse rates and their impact on snowmaking in a Pyrenean ski resort. Theor. Appl. Climatol. https://doi.org/10.1007/s00704-018-2448-y.

Lundquist, J., Cayan, D., 2007. Surface temperature patterns in complex terrain: Daily variations and long-term change in the Central Sierra Nevada, California. J. Geophys. Res. 112, D11124. https://doi.org/10.1029/2006JD007561.

Lundquist, J., Huggett, B., 2008. Evergreen trees as inexpensive radiation shields for temperature sensors. Water Resour. Res. 44. https://doi.org/10.1029/2008WR006979.

Lundquist, J., Lott, F., 2008. Using inexpensive temperature sensors to monitor the duration and heterogeneity of snow-covered areas. Water Resour. Res. 44. https://doi.org/10.1029/2008WR007035.

Makgose, M., Phillipus, C., 2015. Effect of plant growth regulators on growth, yield, and quality of sweet pepper plants grown hydroponically. Hort Sci. 50, 383–386.

Martínez-Ibarra, E., Azorin-Molina, C., Bañón, M., Olcina Cantos, J., Estrela, M.J., Gil-Olcina, A., 2010. Intercomparación de las temperaturas extremas en tres tipos de garita meteorológica: Montsouris, Stevenson y Young.

Measham, P., Darbyshire, R., Turpin, S., Murphy-White, S., 2017. Complexity in chill calculations: a case study in cherries. Sci. Hortic. (Amsterdam) 216, 134–140. https://doi.org/10.1016/J.SCIENTA.2017.01.006.

Morán-Tejeda, E., Bazo, J., López-Moreno, J.I., Aguilar, E., Azorín-Molina, C., Sanchez-Lorenzo, A., Martínez, R., Nieto, J.J., Mejía, R., Martín-Hernández, N., Vicente-Serrano, S.M., 2016. Climate trends and variability in Ecuador (1966-2011). Int. J. Climatol. 36, 3839–3855. https://doi.org/10.1002/joc.4597.

Nakamura, R., Mahrt, L., 2005. Air temperature measurement errors in naturally ventilated radiation shields. J. Atmos. Ocean. Technol. 22, 1046–1058. https://doi.org/10.1175/JTECH1762.1.

Navarro-Serrano, F., López-Moreno, J.I., Azorin-Molina, C., Alonso-González, E., Tomás-Burguera, M., Sanmiguel-Vallelado, A., Revuelto, J., Vicente-Serrano, S.M., 2018. Estimation of near-surface air temperature lapse rates over continental Spain and its mountain areas. Int. J. Climatol. https://doi.org/10.1002/joc.5497.

Nordli, P., Alexandersson, H., Frich, P., Førland, E., Heino, R., Jónsson, T., Tuomenvirta, H., Tveito, O., 1997. The effect of radiation screens on Nordic time series of mean temperature. Int. J. Climatol. 17, 1667–1681. https://doi.org/10.1002/(SICI)1097-0088(199712)17:15<1667::AID-JOC221>3.0.CO;2-D.

O'Neill, H., Christiansen, H., 2018. Detection of ice wedge cracking in permafrost using miniature accelerometers. J. Geophys. Res. Earth Surf. 123, 642–657. https://doi.org/10.1002/2017JF004343.

Pagès, M., Pepin, N., Miró, J.R., 2017. Measurement and modelling of temperature cold pools in the Cerdanya valley (Pyrenees), Spain. Meteorol. Appl. 24, 290–302. https://doi.org/10.1002/met.1630.

Payne, R.E., 1987. Technical Report: Air Temperature Shield Test.

Pepin, N., Kidd, D., 2006. Spatial temperature variation in the Eastern Pyrenees. Weather 61, 300–310. https://doi.org/10.1256/wea.106.06.

Pepin, N., Duane, W., Hardy, D., 2010. The montane circulation on Kilimanjaro, Tanzania and its relevance for the summit ice fields: comparison of surface mountain climate with equivalent reanalysis parameters. Glob. Planet. Change 74, 61–75. https://doi.org/10.1016/J.GLOPLACHA.2010.08.001.

Quénol, H., Bonnardot, V., 2014. A multi-scale climatic analysis of viticultural terroirs in the context of climate change: the TERADCLIM project. J. Int. Sci. Vigne Vin 25–34.

Ribeiro da Cunha, A., 2015. Evaluation of measurement errors of temperature and relative humidity from HOBO data logger under different conditions of exposure to solar radiation. Environ. Monit. Assess. 187, 236. https://doi.org/10.1007/s10661-015-4458-x.

Richardson, S., Brock, F., Semmer, S., Jirak, C., 1999. Minimizing errors associated with multiplate radiation shields. J. Atmos. Ocean. Technol. 16, 1862–1872. https://doi.org/10.1175/1520-0426(1999)016<1862:MEAWMR>2.0.CO;2.

Rolland, C., 2003. Spatial and seasonal variations of air temperature lapse rates in alpine regions. J. Clim. 16, 1032–1046. https://doi.org/10.1175/1520-0442(2003)016<1032:SASVOA>2.0.CO;2.

Roznik, E., Alford, R., 2012. Does waterproofing Thermochron iButton dataloggers influence temperature readings? J. Therm. Biol. 37, 260–264. https://doi.org/10.1016/J.JTHERBIO.2012.02.004.

Schofield, G., Bishop, C., Katselidis, K., Dimopoulos, P., Pantis, J., Hays, G., 2009. Microhabitat selection by sea turtles in a dynamic thermal marine environment. J. Anim. Ecol. 78, 14–21. https://doi.org/10.1111/j.1365-2656.2008.01454.x.

Shedekar, V.S., King, K.W., Fausey, N.R., Soboyejo, A.B.O., Harmel, R.D., Brown, L.C., 2016. Assessment of measurement errors and dynamic calibration methods for three different tipping bucket rain gauges. Atmos. Res. 178–179, 445–458. https://doi.org/10.1016/J.ATMOSRES.2016.04.016.

Shine, R., Elphick, M.J., Barrott, E.G., 2003. Sunny side up: lethally high, not low, nest temperatures may prevent oviparous reptiles from reproducing at high elevations. Biol. J. Linn. Soc. 78, 325–334. https://doi.org/10.1046/j.1095-8312.2003.00140.x.

Sokol, Z., Bližňák, V., Sedlák, P., Zacharov, P., Pešice, P., Škuthan, M., 2017. Ensemble forecasts of road surface temperatures. Atmos. Res. 187, 33–41. https://doi.org/10.1016/J.ATMOSRES.2016.12.010.

Sternberg, T., Viles, H., Cathersides, A., 2011. Evaluating the role of ivy (Hedera helix) in moderating wall surface microclimates and contributing to the bioprotection of historic buildings. Building and Environment 46, 293e297.

Tarara, J., Hoheisel, G., 2007. Low-cost shielding to minimize radiation errors of temperature sensors in the field. Hort Sci. 42, 1372–1379.

Wilcoxon, F., 1945. Individual comparisons by ranking methods. Biom. Bull. 1, 80. https://doi.org/10.2307/3001968.

WMO, 2014. Guide to Meteorological Instruments and Methods of Observation. (Geneva, Switzerland).

Wolaver, B., Sharp, J., 2007. Thermochron iButton: limitation of this inexpensive and small-diameter temperature logger. Ground Water Monit. Remediat. 27 (3), 127–128.

Yang, Z., Hanna, E., Callaghan, T., Jonasson, C., 2012. How can meteorological observations and microclimate simulations improve understanding of 1913–2010 climate change around Abisko, Swedish Lapland? Meteorol. Appl. 19, 454–463. https://doi.org/10.1002/met.276.

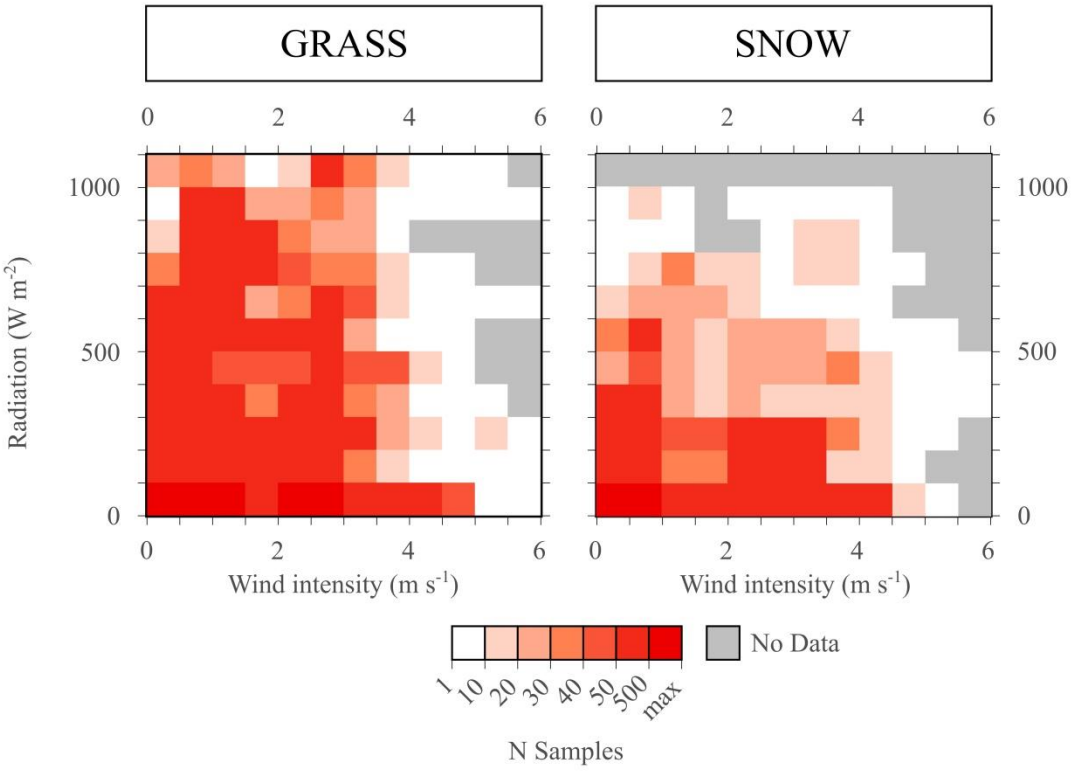

SM. Figure 1. Number of ten-minute samples under grass (left) and snow (right) cover, and under differing wind speed (m s^{-1}) and shortwave radiation (W m^{-2}) conditions.

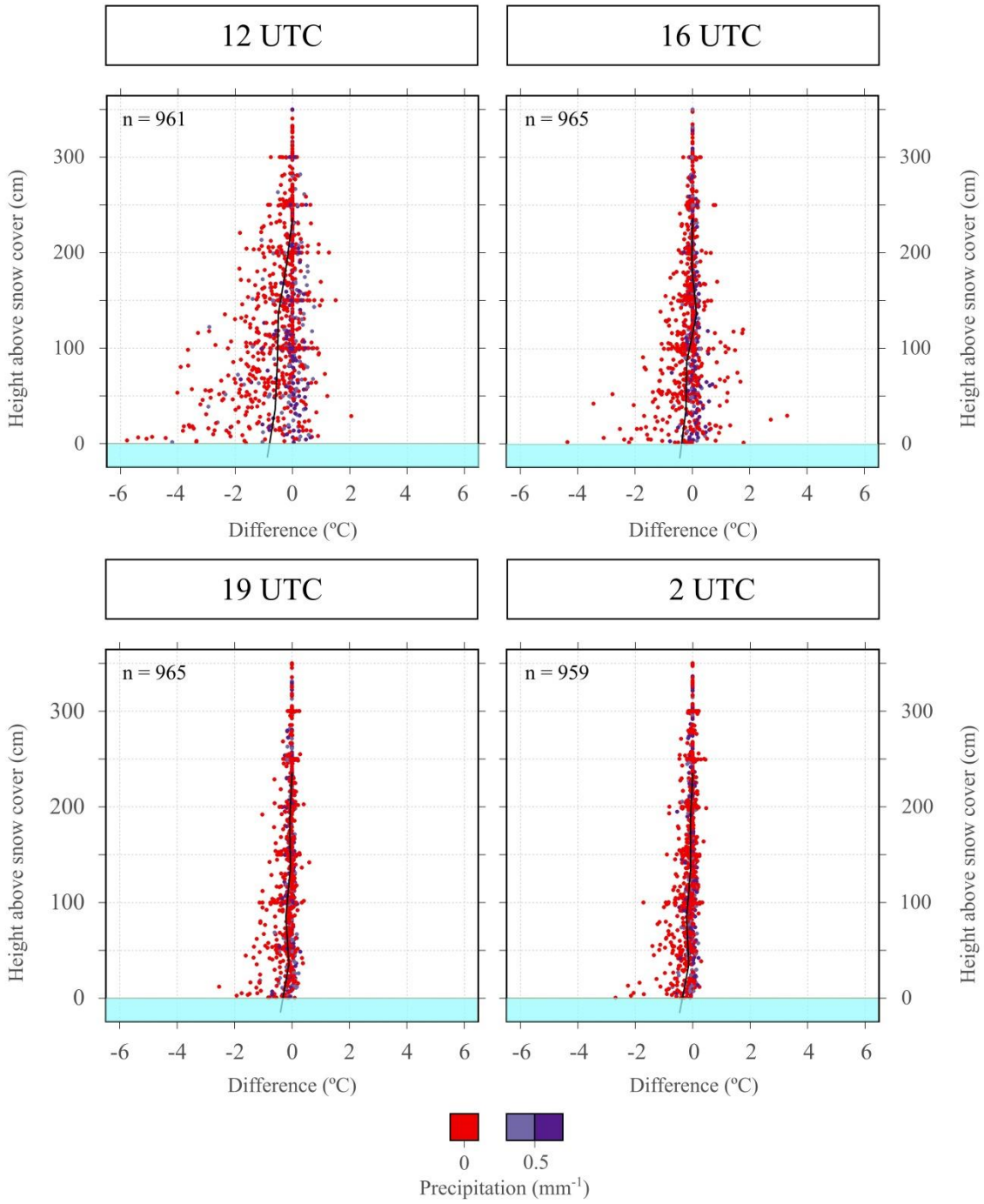

SM. Figure 2. Vertical temperature profile at 12, 16, 19, and 02 UTC. The black line shows the mean for the 6 devices. Bias (X axis) was calculated in relation to the highest device (no. 6). The height (Y axis) was calculated dynamically in relation to the snow depth present. Precipitation is represented from null (red) to intense (blue) rain rates.

Capítulo 6

EFECTOS DE LA ELEVACIÓN SOBRE LA TEMPERATURA EN UN VALLE DE LOS PIRINEOS ESPAÑOLES

Publicado como:

Navarro-Serrano, F., López-Moreno, J.I., Azorin-Molina, C., Alonso-González, E., Aznárez-Balta, M., Buisán, S., Revuelto, J. 2020. Elevation effects on air temperature in a topographically complex mountain valley in the Spanish Pyrenees. *Atmosphere* 11(6): 656. DOI: https://doi.org/10.3390/atmos11060656.

atmosphere

MDPI

Article

Elevation Effects on Air Temperature in a Topographically Complex Mountain Valley in the Spanish Pyrenees

Francisco Navarro-Serrano [1,2,*], Juan Ignacio López-Moreno [1], Cesar Azorin-Molina [3], Esteban Alonso-González [1], Marina Aznarez-Balta [1], Samuel T. Buisán [4] and Jesús Revuelto [1]

[1] Department of Geoenvironmental Process and Global Change, Pyrenean Institute of Ecology, CSIC, Campus de Aula Dei, Avenida de Montañana, P.O. Box 202, 50059 Zaragoza, Spain; nlopez@ipe.csic.es (J.I.L.-M.); e.alonso@ipe.csic.es (E.A.-G.); maznarez@ipe.csic.es (M.A.-B.); jrevuelto@ipe.csic.es (J.R.)

[2] Department of Geography, University of Zaragoza, San Juan Bosco, 7, 50009 Zaragoza, Spain

[3] Centro de Investigaciones sobre Desertificación, CIDE-CSIC, Montcada, 46113 Valencia, Spain; cesar.azorin@uv.es

[4] Regional AEMET (Spanish Meteorological Agency) Office in Aragón, Paseo del Canal, 17, 50009 Zaragoza, Spain; sbuisans@aemet.es

* Correspondence: fnavarro@ipe.csic.es

Received: 29 May 2020; Accepted: 17 June 2020; Published: 19 June 2020

check for updates

Abstract: Air temperature changes as a function of elevation were analyzed in a valley of the Spanish Pyrenees. We analyzed insolation, topography and meteorological conditions in order to understand how complex topoclimatic environments develop. Clustering techniques were used to define vertical patterns of air temperature covering more than 1000 m of vertical elevation change. Ten locations from the bottom of the valley to the summits were monitored from September 2016 to June 2019. The results show that (i) night-time lapse rates were between −4 and −2 °C km^{-1}, while in the daytime they were from −6 to −4 °C km^{-1}, due to temperature inversions and topography. Daily maximum temperature lapse rates were steeper from March to July, and daily minimum temperatures were weaker from June to August, and in December. (ii) Different insolation exposure within and between the two analyzed slopes strongly influenced diurnal air temperatures, creating deviations from the general lapse rates. (iii) Usually, two cluster patterns were found (i.e., weak and steep), which were associated with stable and unstable weather conditions, respectively, in addition to high-low atmospheric pressure and low-high relative humidity. The results will have direct applications in disciplines that depend on air temperature estimations (e.g., snow studies, water resources and sky tourism, among others).

Keywords: air temperature; complex terrain; cluster analysis; lapse rates; weather types

1. Introduction

Near-surface air temperature (i.e., ≈2.0 m above the ground) is a key variable to understanding a multitude of environmental processes, also influencing human activities that are analyzed in agronomy [1,2], ecology [3], the tourism industry [4,5] and health [6]. In high-elevation mountain areas, the study of surface air temperature behavior is vital to understand and manage the available water resources [7,8], for forecasting weather [9], studying climatic refuges for flora species [10] or for snowmaking in ski resorts [11].

Therefore, studying regional and local spatiotemporal air temperature patterns has been common for decades. The main objective is to create regional climates, using datasets from a wide area but sparsely populated with station networks, which generally poorly represent high-elevation mountain

areas. Studies like those of Ackerman [12] in North America, Villmow [13] in Europe and Capel Molina [14] in the Iberian peninsula are a few examples of this approach. However, regional and local factors and the complex climate of mountain regions are rather underrepresented as a heterogeneous mountain climate.

The study of air temperature distribution implies a different approach in topographically complex and small-scale environments. Specific factors such as elevation, topography, aspect and steepness, radiation, land cover, etc., cause highly complex spatiotemporal weather conditions and air temperature patterns [15,16]. Thus, air temperature modeling in mountain areas is a challenging task and, despite the advances in the field associated with high resolution numerical modelling [17,18] and remote sensing techniques [19,20], there is still a long way to go in improving temporal and spatial resolution.

Conventional networks of meteorological stations lack an appropriate density to capture the small-scale climate variability of mountain areas [21]. Therefore, detailed in situ monitoring of air temperature enables knowledge of these complex environments to advance. Some precursors were Geiger [22] and Whiteman, who, through his studies of cold air pools, investigated their formation and explanatory factors [15,23–25]. More recently, air temperature studies in mountain areas, made from self-recording and autonomous datalogger data, have been developing rapidly, as shown in the works of Lundquist and Lott [26], Hubbart et al. [27] and Minder et al. [28] in the United States; Pepin et al. [29] in Africa; Kattel et al. [30] in the Himalayas; Hanna et al. [31] in the Andes; Braun and Hock [32] in Antarctica; and also in the Iberian peninsula [33–35], to name but a few. The use of this type of measures has been previously tested, as Navarro-Serrano et al. [36] described. These devices allow the monitoring of a large number of new locations, due to their good performance and relative low cost.

Although there are different possible approaches, the use of elevational air temperature lapse rates is a method widely used in the literature as it easy to calculate and can be applied to various disciplines to model air temperature [8,37]. The elevational lapse rate (hereinafter, LR) is defined as the air temperature change for each elevation unit change (usually measured in °C km^{-1}). This approach is based on the fact that in most situations, air temperatures change mainly due to elevation, a mechanism that has been widely demonstrated [16,38]. Atmospheric conditions and topography can even reverse its behavior, generating cold air pools and downwelling cold air to low elevation valleys, especially under stable weather conditions and at night. Despite being aware of this dynamic relationship between air temperature and elevation, it is usual to use fixed LRs to roughly estimate temperature. For instance, the most well-known LR in the free atmosphere is the mean environmental lapse rate (MELR, −6.5 °C km^{-1}), not calculated for near-surface air temperature, but for the air column in the free atmosphere. Thus, these fixed LRs have been proved to be insufficient and inaccurate in estimating near-surface air temperature, since they are not able to represent the spatiotemporal variability of air temperature. Despite this evidence, this type of fixed LR is commonly used to estimate near-surface air temperature in different applications. The reality of near-surface air temperature is more complex, and this has been confirmed in several regions across the globe, such as the Rocky Mountains [28], the Himalayas [38], the Alps [39] and the Polar areas [40], as well as in the Iberian peninsula [9,41]. In fact, the ratio between elevation and near-surface air temperature is different between the summer and winter months [42], or between day and night [43,44]. Along with elevation, other local factors (such as insolation, topographic shading and vegetation cover, among others) play a key role in modifying fixed LRs [45], even in environments with smooth topography [46,47].

Air temperature is the result of an input (solar radiation) and the way in which that energy is distributed spatiotemporally throughout the territory [48]. Therefore, in complex environments such as a high-elevation mountain valley, the exchange of energy in vegetated versus bare ground areas can strongly modify the maximum and minimum air temperatures, mainly driven by long-wave emissions [49]. In addition, permanent shadows at the valley bottoms usually strengthen the persistence of cold air pools [50]. Moreover, air temperature patterns also vary depending on the atmospheric conditions, as e.g., Moron et al. [51] and Kirchner et al. [52] reported.

The Mediterranean mountains and basins are highly sensitive to climate change and the increase in air temperatures [53–55], since snow-ice melting is of major importance in water resource management [56]. This is due to the fact that the mid-latitude and elevation (<3500 m above sea level [a.s.l.]) of these mountains create very sensitive precipitation phase thresholds, as well as the presence of strong melting events, even in winter [57]. These events heavily affect water availability and the economy, which are directly dependent on winter and spring snowpacks [58]. Therefore, over complex mountain areas, assessing spatiotemporal air temperature patterns with high resolution is of great socioeconomic and environmental importance. There are some previous studies on this subject, such as López-Moreno et al. [11], Pagès et al. [33] and Miró et al. [34], focusing on the detection and analysis of cold air pools in the Spanish Pyrenees.

With this background, this study analyzes air temperature behavior in relation to elevation in the high mountains and steep valleys of the Spanish Pyrenees. Thus, we assess its relationship with seasonality, the time of day, the incidence of insolation and weather conditions (circulation weather type, atmospheric pressure, relative humidity and wind speed). In particular, we analyze (i) hourly and seasonal LRs in very steep south-southeast (SSE, sunny) and north-northwest (NNW, shady) facing slopes; (ii) the effect of differential insolation generated by the complex topography, which results in sheltered and exposed locations along the same slopes; and (iii) air temperature patterns along the slopes as a function of different environmental factors such as circulation weather types, wind speed, atmospheric pressure and relative humidity. This work advances the knowledge of air temperature distribution in mid-latitude and Mediterranean environments. The few local-scale works developed in this area have focused on the interesting night behavior. However, this work also aims to advance the knowledge of daytime patterns, where topographically complex terrains tend to present notable spatial differences.

2. Study Area

The Pyrenees are a mountain range in southwestern Europe, separating the Iberian peninsula from the rest of the continent (Figure 1a). Its longitudinal distribution along more than 400 km from west to east causes large differences between the northern French and southern Spanish basins [59], and between the maritime western and Mediterranean eastern side. The highest summits are situated in the axial central Pyrenees (Aneto, 3404 m ASL) with large areas lying over 2000 m ASL, leading to a persistent annual snowpack [57,60]. The Pyrenees host the headwaters of the main tributaries of the Ebro River, contributing to more than 60% of the Ebro River's total runoff [61]. The Ebro River basin covers areas of scant annual precipitation [62,63], so the water resources generated in the Pyrenees are essential for the entire Ebro basin [64,65].

The Aragón River valley, a tributary of the Ebro River, is located in the headwater zone of the river with the same name, in the western Spanish Pyrenees (Figure 1b). In this region, the climate lies in a transitional area from Mediterranean to Atlantic influence, with abundant rainfall (1500–2000 mm average annual precipitation) throughout the year [66]. The snow season begins at the end of autumn (October–November) and can last until late spring (May–June), disappearing from the summits at the end of summer (August). The most common weather types in absolute terms are anticyclonic, although during winter and autumn the general circulation patterns are more unstable with common frontal passages from the north-west, west and north, usually causing snowfall in cold seasons [67], as well as from the south-west. These atmospheric conditions give rise to significant ski-tourism and hydroelectric generation industries across the region. Moreover, an irregular forest canopy (adjusting to the steep topography and avalanche zones) covers most of the slopes up to 1800 m ASL, with a dominance of evergreen *Pinus* species with interspersed with diverse deciduous species in the most humid areas [68,69]. Above this treeline, the forest gradually opens and gives way to subalpine meadows and periglacial environments in the summits. Urban areas are very scarce with just a few small villages located at the valley bottom.

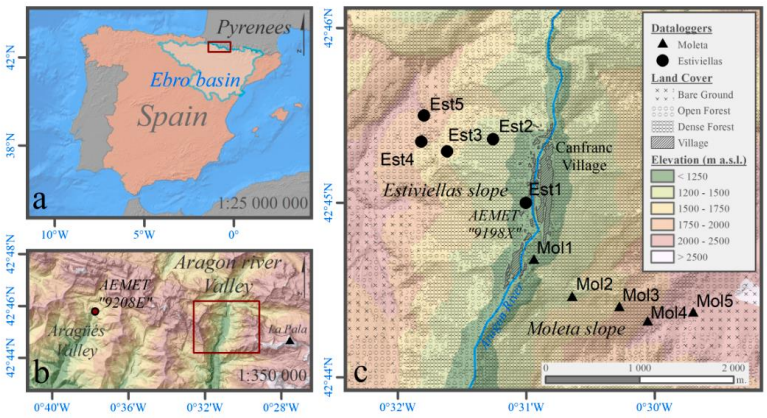

Figure 1. Geographical approximation of the local area: (**a**) represents the Iberian peninsula, in the southwest of Europe, (**b**) represents the location of the river valley in the Pyrenean context and (**c**) shows the terrain map of the local study domain, showing the Estiviellas and Moleta slopes and dataloggers located west and east of the Aragón River, respectively. Land cover is represented by textures as shown in the legend, and retrieved from the photointerpretation of a Sentinel-2B summer image (11 September 2019) and the help of the normalized difference vegetation index band. Canfranc-Station village is located in the center of the valley.

The study area is a sector of the Aragon River valley located in the vicinity of the Canfranc-Station village (1100 m a.s.l., 42.75° N, 0.52° W). In this area, the altimetric range covers from 1100 m a.s.l. (river level) to 2573 m a.s.l. (Moleta Peak) in a 2 km transect. This valley section is enclosed to the north (upstream), the east (2500 m mountains) and the west (2350 m mountains), while towards the south (downstream) it is not entirely enclosed, although the river passes through a narrow canyon. The topography is favorable for the generation of cold air pools, although the valley bottom is narrow, so they would not be very extensive. The river crosses the study area from north to south, generating two slopes at opposite sides. The two selected slopes rise to the summit of the Estiviellas and Moleta peaks, facing to the SSE (sunny) and NNW (shady), respectively (Figure 1c).

3. Data and Methods

3.1. Experimental Designs

Ten locations were monitored in this work, 9 of which were installed for this study (Table 1). The tenth was the Spanish Meteorological Agency (AEMET) weather station (id. 9198X), located in Canfranc-Station village (Figure 1c). Nine autonomous, self-recording and waterproof Tinytag temperature data loggers (http://gemini2.assets.d3r.com/pdfs/original/3239-tgp-4017.pdf) were installed within Datamate radiation shields. The widely used Tinytag dataloggers have a precision error of <0.5 °C, and a resolution of 0.01 °C, while the deviation of the Datamate radiation shield never exceeds 0.5 °C under high solar radiation conditions when compared to the operative AEMET Stevenson radiation screen [36]. The air temperature sensor used in Canfranc-Station corresponds to a Thies PT100 model located in a naturally ventilated medium-sized wooden Stevenson screen [70]. The correspondence and validity of the Tinytag and Thies PT100 sensors and the radiation protection have been previously tested [71,72], and also checked in Canfranc-Station weather station [36], with satisfactory results.

Table 1. Main characteristics of the monitored locations. Elevation is expressed in meters above sea level (m a.s.l.). Latitude and Longitude are expressed in geographical degrees.

Slope	Name	Installation	Elev. m a.s.l.	Land Use	Facing Slope	Lat (°)	Lon (°)
Estiviellas (Sunny)	Est-5	TGP4017 and Datamate	1948	Open Forest	S	42.758	−0.529
	Est-4	TGP4017 and Datamate	1789	Dense Forest	S	42.756	−0.529
	Est-3	TGP4017 and Datamate	1602	Open Forest	SE	42.755	−0.526
	Est-2	TGP4017 and Datamate	1269	Dense Forest	SE	42.756	−0.520
	Est-1	Th. PT100 and Stevenson Sc.	1170	Village	SE	42.749	−0.516
Moleta (Shady)	Mol-5	TGP4017 and Datamate	2255	Open Forest	W	42.738	−0.494
	Mol-4	TGP4017 and Datamate	2026	Open Forest	NW	42.736	−0.502
	Mol-3	TGP4017 and Datamate	1808	Dense Forest	W	42.738	−0.504
	Mol-2	TGP4017 and Datamate	1464	Dense Forest	N	42.740	−0.510
	Mol-1	TGP4017 and Datamate	1234	Dense Forest	N	42.743	−0.515

Tinytag dataloggers were placed within radiation shields and hung from tree branches (Figure S1) at a height of ≈2.5 m above the bare ground, which is enough to avoid winter snowpack, according to Navarro-Serrano et al. [36], and >50 cm distant from the main trunk. The evergreen character of the forest ensures an equal canopy cover all year around. To prevent the dataloggers from being affected by excess moisture or condensation, silica bags were placed inside them, and batteries were replaced yearly. Furthermore, our experiment consisted of measuring air temperatures on two opposite slopes (i.e., Estiviellas and Moleta, Figure 1c) to verify the differences between sunny and shady conditions, following the procedures described by Pepin and Kidd [73]. The locations on Estiviellas faced southeast (Est-1, 2 and 3 loggers) and south (Est-4 and 5), while those on Moleta faced north (Mol-1 and 2), west (Mol-3 and 5) and northwest (Mol-4), derived from a 5 m digital elevation model. Thus, the dataloggers were placed at different elevations, from the valley bottom to the highest areas. The aim of the experimental design was to cover, in a homogeneous way, the two slopes, with regular elevational intervals between locations. However, due to the limited number of trees above the timber-line, the dataloggers were placed in scattered trees. This situation, together with the rugged topography, the necessity to follow the only path existing in both slopes, and the need to select suitable trees to ensure an optimal location of the sensors, prevented a fully symmetric placement of elevations between the two slopes. Data were collected by an instantaneous hourly value at LT (local time = UTC + 2 h, Central European Summer Time) during the period between 11 September 2016 and 22 June 2019, generating 24,357 samples for each data series.

Relative humidity and 10-m wind speed data were measured at Canfranc-Station (Figure 1c) by Thies Clima operative instruments, and the atmospheric pressure in the weather station of Aragués del Puerto (AEMET "9208E", located at 10 km, Figure 1b) by the operative instrument Vaisala PMT, at 10-min measuring intervals. In addition, to better evaluate the results, land cover was classified into the different land covers presented in the study area cartography.

3.2. Climate Data and Quality Control Checks

Air temperature data were checked by applying a quality control that ensured that the dataloggers were not buried under snow. For this, daily air temperature ranges were analyzed, discarding those days with hourly standard deviation < 0.1 °C and an average air temperature < 2 °C. The air temperature in snow-burial conditions was constant at a value close to 0 °C [74], so it was relatively easy to filter out this issue. The 10 locations passed this filter and 0 samples were discarded. However, the raw experimental design had 11 locations, of which one (Est-6, at 2067 m a.s.l.) had to be removed in this quality control check. This location suffered problems from December to May, affecting 5422 hourly samples (22.3% of the study period). Furthermore, a total amount of 60 hourly samples (0.02% of the total) were discarded due to annual battery changes. Of these, 23 were gaps of less than two continuous samples, so they were filled by a regression model based on the best neighboring air temperature series for that month. The remaining data were maintained as Not Available (NA) data.

Next, the hourly samples were summarized by day using the air maximum (*Tmax*), minimum (*Tmin*) and average (*Tavg*) temperature of the raw 24-hourly samples for each location. It was verified that more than 90% of hourly samples were available each day. Raw weather data measured at Canfranc-Station and Aragués del Puerto were summarized according to the daily mean atmospheric air pressure (in hPa), the daily mean relative humidity (in %) and the daily mean 10-min wind speed (in m s^{-1}).

3.3. Lapse Rate Calculation

Air temperature LRs were calculated for both the Estiviellas and Moleta slopes at hourly time steps (LR_h), and for daily maximum (*LRmax*), minimum (*LRmin*) and average (*LRavg*) air temperatures. Following procedures outlined by Rolland [75], Du et al. [76] and Navarro-Serrano et al. [41], regressions were used to determinate LRs, formulated in Equation (1) as:

$$T' = a_1 \text{ Elev} + e, \quad (1)$$

where T′ is the estimated air temperature (in °C), Elev is the elevation above sea level (m a.s.l.), e is the regression error and a_1 is the regression coefficient, which corresponds to the air temperature elevational LR. Latitude and longitude variables can be included in the model, but the effect in such a small study area is usually negligible due to the short distances between locations. The regression model approach has been used by other authors [42,44,77], and provides an appropriate way to analyze the effects of elevation on air temperature distribution. The influence of synoptic conditions can be analyzed subsequently. All these LRs were also calculated among all the combinations for the locations. To clarify the interpretation of the LR values, when in the following paragraphs we refer to a "steeper" LR and a "weaker" LR, we refer to a larger change in air temperature with elevation, and a smaller change, respectively (e.g., −7.2 °C km^{-1} is steeper than −4.3 °C km^{-1}).

3.4. Estimated Solar Radiation

The amount of solar radiation received by the terrain [16,45], topographic shadows and surface orientation are crucial to better understand the spatiotemporal distribution of air temperature, especially during daylight hours [78]. To obtain this information, we used a digital elevation model (DEM5) with 5 m spatial resolution purchased from the PNOA-LiDAR program [79]. The instantaneous solar radiation estimation under clear sky conditions by hour was estimated by applying the insolation function of the R package "insol" [80], developed for R language version 3.5.0 [81]. This function takes into account diffuse radiation, in addition to air temperature, humidity, date and location, to estimate instantaneous insolation (in W m^{-2} s^{-1}). The solar radiation estimated in each monitored location throughout the year and summarized by seasonal (i.e., winter: December–February; spring: March–May; summer: June–August; autumn: September–November) hourly means (Figure 2) shows variability due to topographic conditions and differences between the Estiviellas and Moleta slopes (sunny and shady, respectively). In addition, this dataset clearly displays the topographic shadows

occurring in the bottom location of the study area, mainly on the Moleta slope, and during winter. This estimated information allows the identification of the characteristics of the monitored locations, which allow discussion of the results keeping in mind the effect of topography on solar radiation reception.

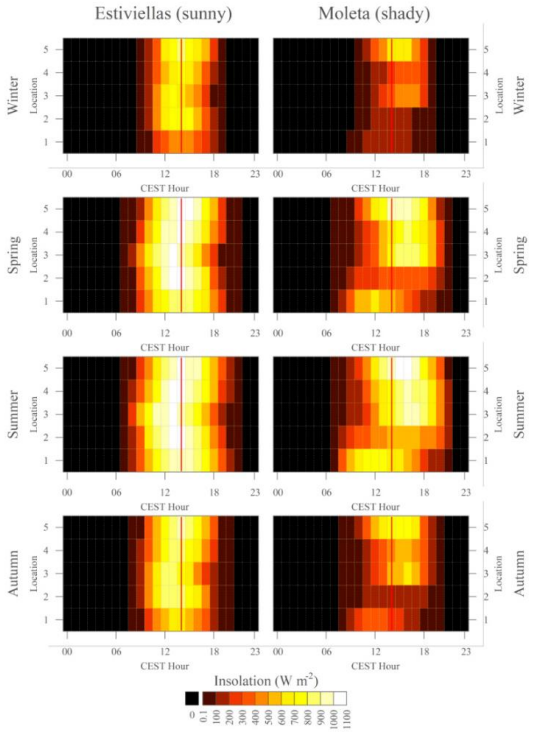

Figure 2. Mean seasonal estimated hourly insolation in the ten monitored locations of the Estiviellas and Moleta slopes. Black represents null insolation (night), and red to white ramp color represents intensity (in W m^2). Red lines represent the solar noon (at 14 h UTC + 2, local time).

3.5. Circulation Weather Types Classification

Circulation weather types (CWTs) at daily scale over the Pyrenees were calculated using Jenkinson and Collison's [82] classification method, based on Lamb's weather types [83] and simplified satisfactorily by Rasilla Álvarez et al. [84] and Navarro-Serrano et al. [41] for the Iberian peninsula. This version classifies the raw CWTs into two pure (anticyclonic-A and cyclonic-C), eight directional (north-N, northeast-NE, east-E, southeast-SE, south-S, southwest-SW, west-W and northwest-NW) and one unclassifiable (U) CWT, prioritizing directional flows in hybrids. The method is based on the distribution of sea-level atmospheric pressure in a 16-point grid covering an area of 30 × 20° (longitude × latitude) centered on the study area. This information was obtained from the NCEP-NCAR reanalysis (5 × 5° longitude-latitude) dataset [85]. To simplify the analysis, U days were not represented, but were computed in the total amount of days. The frequency of CWTs is shown in Figure S2.

3.6. Cluster Analysis

To analyze different patterns in the daily elevational distribution of maximum (*Tmax*), minimum (*Tmin*) and average (*Tavg*) air temperature, a cluster analysis was applied. Cluster analysis is a multivariate statistical technique, that is, it analyzes the behavior of three or more variables

simultaneously, aiming for the creation of clusters or groups that have large internal homogeneity and maximum difference in relation to the other groups. This process is carried out automatically, based on the study of daily temperatures in relation to highest location of each slope and the creation of clusters based on the distances between them. Daily air temperature differences between the *Tmax*, *Tmin* and *Tavg* of each location and the reference datalogger of its slope (i.e., the highest: the Est-5 [1948 m] and Mol-5 [2255 m] loggers on the Estiviellas and Moleta slopes, respectively) were computed. These new series were employed as input variables for the cluster analysis, which, in function of the air temperature difference of each location in relation to the highest one, generated groups or clusters of days with similar behavior. In this way, similar (close) days were classified in the same cluster, while distant days were classified in different clusters.

The number of clusters was determined by executing the NbClust function of the R package "NbClust" [86], which analyzes 30 different indices to determine the most appropriate number of groups using Euclidean distance and the hierarchical Ward.D2 method [87], minimizing the total within-cluster variance. After determining the appropriate number for each combination (*Tmax*/*Tmin*/*Tavg* and the Estiviellas and Moleta slopes), a cluster analysis was run using the Ward.D2 and Euclidean distance parameters. This classified each day according to the nearest cluster centroid. Differences between pairs of clusters were compared by the Wilcoxon–Mann–Whitney test [88] to identify statistically significant differences among groups. In cases of 3 clusters, these were compared between pairs (i.e., 1 and 2, 1 and 3, 2 and 3). This nonparametric statistical test allows the similarities/differences between two independent samples to be tested. Differences were tested at a 0.05 significance level.

4. Results

4.1. Air Temperature

The daily mean maximum (*Tmax*), minimum (*Tmin*) and average (*Tavg*) air temperatures for each of the ten locations are shown in Figure 3. Although an inverse relationship between air temperature and elevation exits, this is not linear. Moreover, there were differences between the behaviors of *Tmax*/*Tmin*/*Tavg*, and between the two opposing slopes. The air temperature across the study area varied from a mean *Tmax* around 15 °C at the valley bottom to 10 °C at 2000 m a.s.l. *Tmax* differences are noticeable between the slopes, showing a decoupling between the two faces at mid-slope locations, mainly due to the variable behavior of Est-1 and Est-2 and heating at the Mol-4 location. *Tmin* shows a more complex relationship with elevation, especially at the valley bottom. Above the slopes, *Tmin* was around 5 °C at 1500 m ASL and 2 °C at 2000 m a.s.l. Unlike *Tmax*, *Tmin* shows similar patterns between both the Estiviellas and Moleta slopes, except for at Est-1, i.e., the location at the valley bottom.

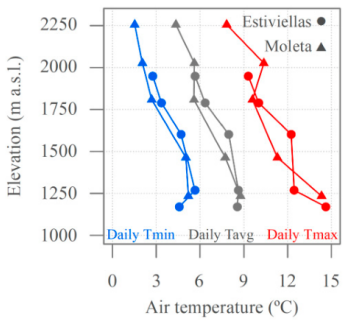

Figure 3. Mean daily maximum (*Tmax*), minimum (*Tmin*) ares in the ten locations during the study pnd average (*Tavg*) air temperatueriod.

The monthly air temperature patterns for *Tmax* and *Tmin* among the ten locations are shown in Figure 4. The Estiviellas slope presented the expected inverse relationship between elevation and *Tmax* for most of the year, although it presented some nuances during August and December between the Est-2 and Est-3 locations, which had similar *Tmax* values. However, the Moleta slope returned an irregular elevation–*Tmax* relationship throughout the year (except from June to August). *Tmax* differences between the lower and higher locations increased during June and July, decreasing from September to November. Furthermore, the elevation–*Tmin* relationship was less evident. The Estiviellas location with the warmest *Tmin* throughout the year was Est-2, while Est-1 and Est-3 had similar values, but were cooler than Est-2. On Moleta, a decoupling between its three highest and its two lowest locations was found (probably as a result of the larger elevational distance between them). For instance, Mol-1 and Mol-2 had similar *Tmin* values throughout the year, with Mol-1 being slightly colder than Mol-2 in December. Mol-3, Mol-4 and Mol-5 kept their positions, but presented similar air temperature values from July to September.

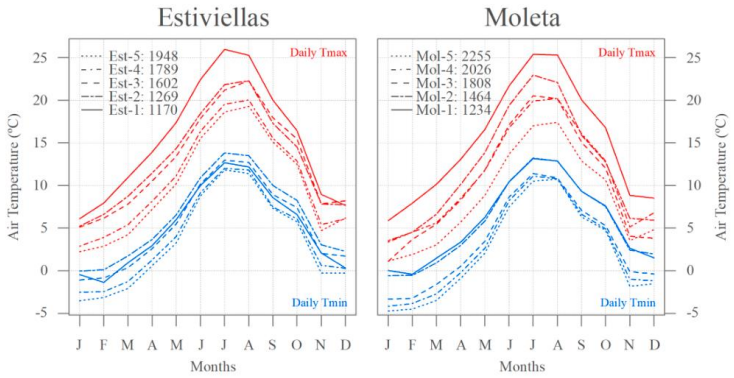

Figure 4. Monthly means of daily maximum (*Tmax*, red lines) and minimum (*Tmin*, blue lines) air temperatures for the ten locations during the study period.

4.2. Hourly Air Temperature Lapse Rates (LR_h)

In Figure 5, both the Estiviellas and Moleta slopes show weak LR_h (local time UTC + 2) during the night (especially at sunrise, calculated by the methodology explained in Section 3.4), and high LR_h in the afternoon. This pattern occurred every month, although with a time shift caused by the expansion of weak LR_h during the winter months, and narrowing during the spring and summer months. In absolute terms, LR_h was around −4 and −2 °C km^{-1} at night and sunrise (even weaker on Estiviellas at 9 h UTC + 2), and around −6 and −4 °C km^{-1} in the afternoon (even steeper on the Estiviellas slope from 15 to 17 h UTC + 2). These hours showed a slight seasonal shift, with weaker LR_h delayed during the winter months, and occurring earlier during the spring and summer (e.g., the weaker LR_h in Estiviellas occurred at 9 h UTC + 2 during August and at noon during December), so the LR_h was steeper in June than in December.

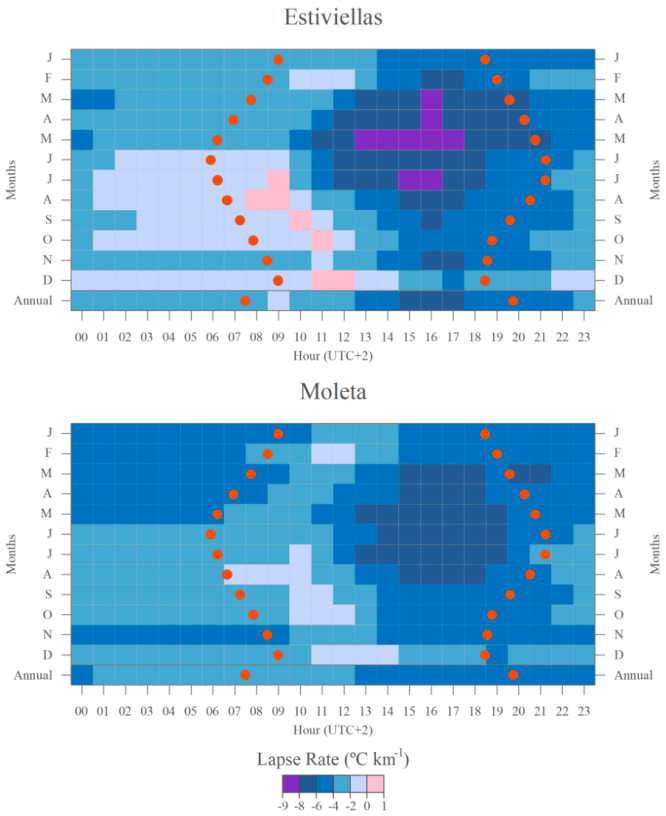

Figure 5. Mean hourly lapse rates (LRs, measured in °C km^{-1}) for the Estiviellas and Moleta slopes by month. Red dots represent the sunrise/sunset time without topography effects, calculated for the 15th day of each month, and for equinoctial day in the Annual row.

Both the Estiviellas and Moleta slopes had a similar seasonal pattern at the hourly resolution, since steepness of LR_h occurred from May to July in mid-afternoon, while the weakest LR_h occurred in December at night. LR_h was weaker during the night from June to October than from January to May, and steeper during the afternoon from March to August than from September to February. However, we found significant ($p < 0.05$) differences in the slope of the LRs between the two slopes, since in Estiviellas they ranged from −8.90 (May at 16 h UTC + 2) to +0.80 °C km^{-1} (December at 12 h UTC + 2), and in Moleta from −7.46 (July at 17 h UTC + 2) to −1.01 °C km^{-1} (August at 10 h UTC + 2). The coefficients of variation were calculated and shown in Figure S3. This figure shows that the most favorable hours for thermal inversion were those that generated the largest variability (early morning and night).

4.3. Monthly Maximum (LRmax), Minimum (LRmin) and Average (LRavg) Air Temperature Lapse Rates

Figure 6a shows that, generally, *LRmax* was steeper than *LRmin* on both the Estiviellas and Moleta slopes ($p < 0.05$). *LRavg* returned mixed behavior between *LRmax* and *LRmin*. The annual data support this fact, through an annual average *LRmax*, in °C km^{-1}, of −6.0 (−5.5), and a *LRmin* annual average of −2.8 (−4.0) for the Estiviellas (Moleta) slope. This pattern was present during most of the year, although it intensified during the summer (e.g., July). The differences in winter were smaller and even reversed from November to January on the Moleta slope. *LRmax* weakened from October to February

and became steeper from March to July. *LRmin* was also steeper from March to May, but weakened from June to August (and December). In any case, although there were seasonal differences, *LRmin* showed low variation in absolute terms (−4.4 to −1.7 on Estiviellas; −5.3 to −2.5 on Moleta) compared to *LRmax* (−8.1 to −2.1 on Estiviellas; −7.6 to −2.6 on Moleta). *LRavg* returned mixed behavior between *LRmax* and *LRmin*, but was much closer to *LRmin*. The comparison between the two slopes showed that the *LRmax* was similar from June to December, with a steepening on Estiviellas from January to May. *LRmin* was similar between both slopes throughout the year, although steeper on Moleta.

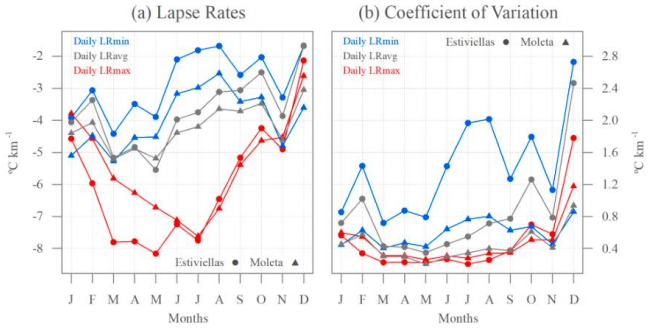

Figure 6. (**a**) Monthly maximum (*LRmax*), minimum (*LRmin*), and average (*LRavg*) air temperature lapse rates (measured in °C km^{-1}) from the Estiviellas and Moleta slopes; and (**b**) monthly *LRmax*, *LRmin* and *LRavg* coefficient of variation (in °C km^{-1}) from the Estiviellas and Moleta slopes.

Figure 6b shows monthly variability based on LRs by the coefficient of variation. In general terms, *LRmin* had larger variability than *LRmax*, especially on Estiviellas. Seasonally, the *LRmin* coefficients increased during the summer (e.g., June to August) and December. On the contrary, in spring (March–May) and autumn (September–November) the coefficients were the lowest of the year. *LRmax* had reduced coefficients throughout the year (generally <0.8 °C km^{-1}), which increased gradually during autumn, with the highest value in December (>1 °C km^{-1}). The *LRmax*, *LRmin*, and *LRavg* calculated between partial sections on each slope are not shown, but their behavior was extremely variable and wide-ranging, demanding the use of all available datalogger series to calculate the LRs on each slope.

4.4. Cluster Analysis

4.4.1. Cluster Classification

Figure 7 shows the air temperature differences from each monitored location to the highest measured level on each slope (i.e., 1948 m a.s.l. in Estiviellas, and 2255 m a.s.l. in Moleta), with a noticeable daily variability in air temperature profiles. The figure shows a dynamic and continuous relationship between air temperature and elevation, where it is difficult to visually establish linear patterns along the entire slopes. However, cluster analysis allows daily profile types to be established with a statistical approach. For maximum air temperatures, bottom locations were usually warmer, but the profiles throughout the entire slope were not completely linear. For minimum air temperatures, the lowest Estiviellas location (1170 m a.s.l.) had an inverse relationship with the rest of the slope, less evident on Moleta. In this way, cluster analysis generated the optimal number of profile typologies, with the mean values given in Table 2. Other than the air average temperatures on Moleta (three clusters), the remaining combinations each generated two clusters. The clusters were ordered from weak to steep lapse rates (i.e., Cluster 1 represents the group of weakest lapse rates).

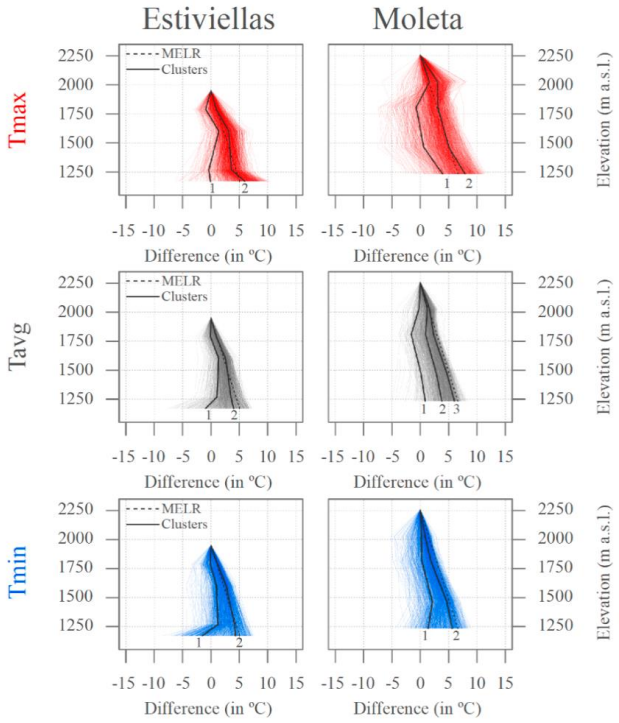

Figure 7. Daily maximum, minimum and average air temperature profiles (measured as the difference from the highest slope location) of the Estiviellas and Moleta slopes are represented by colored lines. Centroids of the generated clusters are represented by solid grey lines. The mean environmental lapse rate (MELR, −6.5 °C km^{-1}) from the top location is represented by dashed grey lines.

Table 2. *Tmax*, *Tmin*, and *Tavg* cluster centroid values for the Estiviellas and Moleta slopes. Loc = location order, from bottom (1st) to top (5th).

	Estiviellas			Moleta		
	Loc.	**Cluster 1**	**Cluster 2**	**Loc.**	**Cluster 1**	**Cluster 2**
Tmax	5th	0	0	5th	0	0
	4th	−0.92	+0.94	4th	+1.62	+3.04
	3rd	+1.41	+3.15	3rd	−0.73	+3.11
	2nd	−0.38	+3.62	2nd	+0.60	+5.02
	1st	−0.09	+5.96	1st	+3.93	+7.89
	Loc.	**Cluster 1**	**Cluster 2**	**Loc.**	**Cluster 1**	**Cluster 2**	**Cluster 3**
Tavg	5th	0	0	5th	0	0	0
	4th	−0.10	+0.94	4th	−0.25	+1.24	+1.64
	3rd	+1.37	+2.58	3rd	−1.61	+0.91	+2.32
	2nd	+1.08	+3.53	2nd	+0.14	+2.87	+4.74
	1st	−0.96	+4.00	1st	+0.87	+3.78	+6.01

Table 2. *Cont.*

	Estiviellas			Moleta		
	Loc.	**Cluster 1**	**Cluster 2**	**Loc.**	**Cluster 1**	**Cluster 2**
Tmin	5th	0	0	5th	0	0
	4th	−0.14	+1.16	4th	+1.38	+0.82
	3rd	+0.97	+2.69	3rd	+2.14	+1.92
	2nd	+1.25	+4.15	2nd	+0.30	+4.67
	1st	−1.57	+4.31	1st	+0.18	+5.62

Clusters generated from maximum air temperatures were similar in form, but differences arose from the degree of difference to the reference highest locations. The *LRmax* values for Cluster 2 from Estiviellas and Moleta were close to the MELR, with much warmer bottom location values. The contrasting behavior between Cluster 1 and Cluster 2 was more clearly present in air minimum temperatures, where *LRmin* values for Cluster 1 from Estiviellas and Moleta were decoupled from those for Cluster 2, especially in the bottom locations. In the average air temperatures, a more linear behavior can be observed along the slopes, especially on Moleta, where three clusters were generated. However, Cluster 1 from Estiviellas was inverted in its bottom location.

4.4.2. Monthly Distribution of Clusters

Figure 8 shows the monthly distribution (% of days) of each cluster throughout the year. On the one hand, the cluster associated with steep *LRmax* (Cluster 2) was more common than the weak *LRmax* cluster (Cluster 1), especially from March to August (>80% of "steep" days). On the other hand, the days classified with weak LRs increased in frequency from September to January, becoming as frequent as those with steep LRs, especially along the Moleta slope (≈50%). *LRmin* cluster frequency was more equal on the two slopes. However, Cluster 2, associated with steep *LRmin*, was more common from January to May (>50% of days), and Cluster 1 from July to December. On Estiviellas, the frequency of *LRavg* Cluster 1 was higher during the summer and December and lower/null in spring. On Moleta, despite having three *LRavg* clusters, the same pattern was repeated, although less frequently for Cluster 1. On Moleta, in any case, *LRavg* was dominated by medium and steep clusters (Clusters 2 and 3, in most months generally >80%) over the weak Cluster 1, although the latter increased in frequency from August to February.

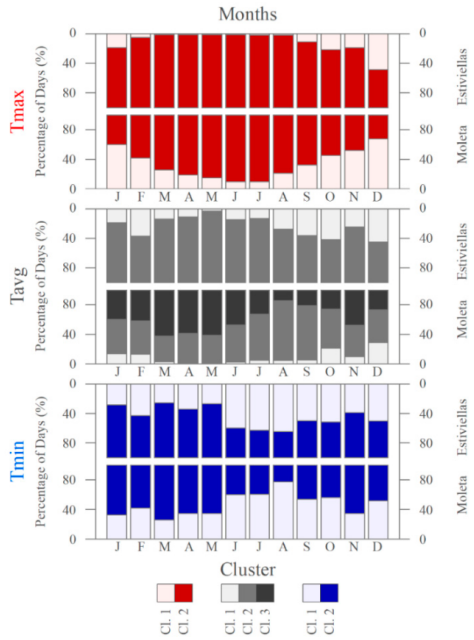

Figure 8. *Tmax*, *Tmin* and *Tavg* cluster monthly frequency (measured as daily percentage for the month).

4.4.3. Clusters, Circulation Weather Types and Weather Conditions

To analyze the synoptic and weather patterns found during each cluster day, Figure 9 shows the circulation weather type (CWT) distribution. Atmospheric pressure (Figure S4), relative humidity (Figure S5) and wind speed (Figure S6) variability for each cluster are also presented.

Days classified within the *Tmax* Cluster 1 (associated with weak *LRmax*) were dominated by anticyclonic (A) and NE and E circulations (Figure 9), accompanied by higher atmospheric pressures (≈1026 hPa) and lower relative humidity (≈69.4%), although no clear wind speed pattern was found on those days. On the contrary, when analyzing the *Tmax* Cluster 2 (associated with steep *LRmax*) no particular CWTs prevailed, except for some westerly and northerly circulations, and also the anticyclonic-A and cyclonic-C types. However, atmospheric pressure values were lower (≈1.019 hPa), relative humidity values were higher (≈75.1%) and wind speed was variable. Wind speed daily values between *Tmax* clusters in Estiviellas were compared and were significantly different ($p < 0.05$). The same occurred when comparing the values of atmospheric pressure and relative humidity (also on the Moleta slope). Thus, days associated with each cluster differed not only in the behavior of the air temperature, but also in other meteorological variables measured.

For *Tmin*, days classified within Cluster 1 (associated with weak *LRmin*) were marked by a clear dominance of the A weather type, weaker winds (≈2.1 m s^{-1}, especially on Estiviellas), higher atmospheric pressure (≈1023 hPa) and lower relative humidity (≈70.9%). *Tmin* Cluster 2 (associated with steep *LRmin*) was represented by different circulation types (e.g., northerly, westerly and C, among others), moderate to strong winds (≈3.9 m s^{-1}), lower atmospheric pressure (≈1019 hPa) and higher relative humidity (≈76.2%). The same pattern occurred for *Tavg* values, although the three *Tavg* clusters on Moleta showed the anticyclonic dominance of weak lapse rates more clearly. As with *Tmax* clusters, the differences between *Tmin* clusters were statistically significant ($p < 0.05$) for wind, relative humidity and atmospheric pressure, again on both slopes. The air temperatures from bottom-summit locations during the extreme period from 3 December 2017 and 5 December 2017 are presented in

Figure S7 to show the transition between unstable and stable weather types, together with atmospheric pressure and wind speed. The moment at which wind speed fell coincided with the beginning of thermal inversion between Est-1 and Est-2 (and almost between Mol-1 and Mol-5). Similarly, the lowest atmospheric pressure values coincided with the largest differences between the locations, and vice versa.

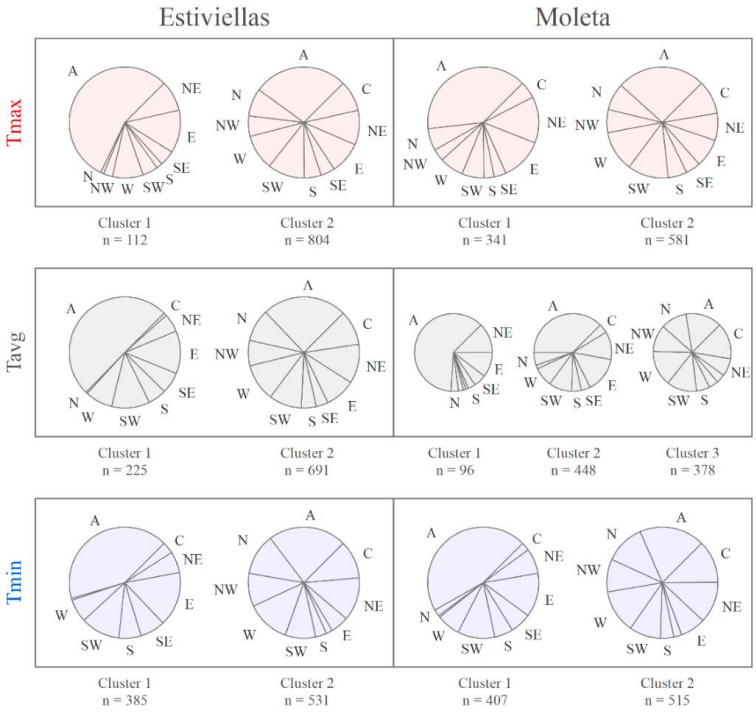

Figure 9. Circulation weather type (CWT) frequency for the *Tmax*, *Tmin* and *Tavg* clusters. n indicates the number of days in each cluster. The unclassifiable (U) type was not computed.

5. Discussion

The air temperature and lapse rates in two opposite steep and complex slopes (i.e., sunny Estiviellas and shady Moleta) of the upper Aragon river valley (Spanish Pyrenees) were analyzed in ten locations (elevations ranging from 1170 to 2255 m a.s.l.) for 1015 consecutive days from September 2016 to June 2019. Following previous studies, such as Barry [16] and Lookingbill and Urban [45] for North America, this one analyzed the relationship between air temperature and local terrain characteristics (e.g., facing slope, insolation, land cover, weather types and atmospheric parameters such as air pressure, relative humidity and wind speed). This study focused on a single Pyrenean valley, complementing previous regional work on the Iberian peninsula [41,89,90]. Also, the study of diurnal lapse rates at this local scale provided new information for this region of Europe, which has mainly been investigated for its night-time cold air pools [33,34,73].

The results show variable insolation values within and between slopes, as in Lookingbill and Urban [45]. The differential insolation has a direct effect on air temperature distribution and variability [31,91,92]. The lesser insolation at the valley bottom, more significant in the lower locations on the shady Moleta slope, especially around December, was consistent with the complex topography. Direct insolation on the Moleta slope is very limited during the autumn and winter months, as we can

see in Figures 1 and 2. On the other hand, in higher locations on Moleta, more insolation was estimated due to the increasing sky view factor, reducing the differences in relation to the sunny Estiviellas slope. At this point, the use of digital elevation models of high spatial resolution is essential to represent the terrain reliably. Other local differences could be explained by land cover, such as the diurnal overheating of the Est-1 (village) location in comparison with Est-2 (dense forest), or the combined effect of the low insolated and dense forested locations (e.g., Mol-3 and Mol-4), according to the buffering effect of the forest canopy [49]. Therefore, the results show that elevation is not a factor with a linear effect, but that there are local variables that can alter the diurnal air temperature distribution [76]. At night, the topography also exerts an effect, as the valley bottom locations demonstrated by capturing thermal inversion phenomena, according to papers on cold air pools [17,23,93]. Partial *LRmin* between Est-1 and Est-2 were close to +20 °C km^{-1} of thermal inversion, which agrees with the extreme values registered by Pepin and Kidd [73] and Pagès et al. [33] in the Cerdanya valley in the eastern Pyrenees. More variance was detected in *Tmax* than *Tmin* both between and within slopes, showing a strong influence of land cover on *Tmax*, which caused inversions between the Est2/Est3 and Mol3/Mol4 locations, due to the correspondence with the treeline ecotone. To summarize, air temperatures registered at each location were not only the result of elevation, but also of effects caused by insolation, topography and land cover.

In terms of lapse rates, the hourly analysis in Section 4.2 allowed the continuous identification of the behavior throughout the 24 h sections and the months of the year. In this way, the analysis has a larger wealth than analysis of the daily max and min air temperature moments exclusively, being able to show other nuances between the slopes. Thus, this analysis showed the influence of insolation on thermal mechanisms, with a weakening of the night-time lapse rates due to cold air subsidence from the summits to the valley bottom [77,94,95]. Thus, the weakest hourly lapse rates occurred in the morning (+0.81 °C km^{-1} in December at 12 h in Estiviellas, and −1.02 °C km^{-1} in August at 10 h in Moleta, *Central European Summer Time* time zone). This is because that is the time when insolation reaches the highest locations, while the lower ones remain shady, according to insolation data, and with an accumulation of cold night air. However, insolation is seasonally variable (later in December, and earlier in July). These results are in agreement with Pagès et al. [33]. Moreover, the steepest lapse rates took place in the early afternoon and were explained by high insolation in the lower locations, especially on Estiviellas, which broke up the cold layers and steepened the relationship between elevation and air temperature (on Moleta the lapse rates were less intense). Later, the sun begins to descend and the topographic shadows reach the low locations first, reiterating the process [50].

The results show that *LRmin* were generally weaker than *LRmax* (total mean of −2.8 vs. −6.0 °C km^{-1} on Estiviellas, and −4.0 vs. −5.5 °C km^{-1} on Moleta), as in most similar studies around the globe [8,94,96], which attribute it to the previously mentioned nocturnal cold air subsidence toward the bottom areas. However, this behavior changed through the year, since the differences were larger in summer (diurnal steepening along the slope in addition to nocturnal weakening), and smaller in winter (diurnal weakening due to topographic shadows in addition to nocturnal weakening). This supports the hypothesis that topographic shadows affect air temperature distribution during the daytime [10,78]. This process was also corroborated by decoupling between the Estiviellas and Moleta *LRmax* from March to May when the Estiviellas slope was completely insolated. However, on Moleta, the insolation did not yet reach lower locations. This comparison between sunny and shady slopes can only be observed where the topography is abrupt enough to generate permanent topographic shadows that alter air temperatures, and not in open valleys. The existence of snow cover in higher locations has also been mentioned as a reason for the steepening of *LRmax* [31], due to the albedo effect in elevated areas, in which snow cover persists during the spring months. This could explain the peak delay between the *LRmax* in Estiviellas (June) and Moleta (July), due to the longer snow season on the northern Moleta slope [97]. It would be very useful to advance the study of this issue in the future, and analyze the importance of this factor.

However, the study of the monthly coefficients of variation has confirmed that the monthly LR values derived from a linear fit are not entirely representative, since they hide different internal behaviors, especially in the *LRmin*. To deepen the study of LR patterns from a global (and non-linear) perspective, a cluster analysis was performed. In this respect, the cluster analysis showed that, regardless of the month, there were usually two distinct profile patterns (weak vs. steep), and that these could occur at any time of the year, although there were more propitious moments. In general terms, the steep clusters were close to the MELR (−6.5 °C km^{-1}). This method was proposed by Barringer [98] to classify days based on air temperature profiles. The merged analysis between clusters, insolation, circulation weather types and weather conditions supports the hypotheses, since it shows a broadly weak *LRmin* with stable conditions, high atmospheric pressure, low relative humidity and weak winds, according to the majority of studies on Cold Air Pools [34,40,44,73], and the regional results of Navarro-Serrano et al. [41] in the Pyrenees. On the other hand, steep *LRmin* occurs under conditions of instability, dynamic weather types, low atmospheric pressure, high relative humidity and strong winds, which explains the breakup of cold layers and the prevalence of the free-air lapse rate [1,27,33,77,99,100].

However, *Tmax* clusters were more complex than expected prior to beginning this research, unlike claims by other authors on a regional scale [41,101]. This is due to the previously explained complex topographic conditions of the study area, which are more influential during the winter months. The results show that the *Tmax* clusters associated with steep *LRmax* were more frequent than those associated with weak ones, especially during spring and summer, according to Minder et al. [28]. As mentioned above, *LRmax* intensified during the summer due to the insolation reaching the lower locations, and in spring also due to more frequent cloudy days under unstable meteorological conditions. Therefore, these *Tmax* clusters associated with steep *LRmax* were accompanied by varied CWTs and wind speed conditions, since they occurred under diverse synoptic situations (e.g., sunny summer days and rainy March days) [34,94]. Furthermore, *Tmax* clusters associated with weak *LRmax* only occurred under topographic shadows (i.e., more frequently in winter, anticyclonic situations, high atmospheric pressure and low relative humidity). This is because *LRmax* returned a high coefficient of variation in winter (e.g., a sunny stable winter day weakens *LRmax*, and a cloudy one steepens it; and yet in summer, both unstable and stable sunny days steepen *LRmax*). In any case, the limitations of the use of humidity and wind speed valley bottom measurements should be taken into account. Although we think that it can be representative of the timings of higher or lower humidity/wind speed in the whole valley, we cannot assume that this is absolutely right, and it should be analyzed in the future with more information. To summarize, local terrain factors must be taken into account, especially in study areas with complex terrain [102]. In these cases, the same synoptic conditions could generate different effects on lapse rates, depending on the position of the sun and azimuth. This is an approach that has been recognized in some studies on persistent cold air pools [50,103].

Therefore, although previous work has tried to analyze the variability of LRs based solely on synoptic conditions, this analysis reveals that insolation, heavily affected by topographic shadows, has noticeable impact on diurnal air temperature variability. Thus, terrain factors such as sky view factor, aspect, forest canopy must be taken into account when designing experimental measurement networks in mountain terrain, so that these factors are not underestimated when analyzing *LRmax*. *LRmin* analysis has corroborated findings from previous studies on the influence of synoptic conditions and topography [104]. Future research should carry out in-depth analysis of the variability of the air temperature along a slope. Factors such as weather conditions, insolation, aspect, and topography have been shown to be explanatory variables for air temperature distribution in topographically complex areas, although they have often been underestimated in favor of elevation above sea level. Future work may also specifically analyze the effect of snow cover on air temperature, as well as the effects caused by forest density. These factors actively influence diurnal air temperature distribution.

6. Conclusions

This work advances the knowledge of small-scale variability of air temperature in mountain areas. The few local-scale works developed in the Pyrenees to date have focused on nocturnal patterns, while this work includes daytime patterns that are very influenced by topography, land cover and snow presence. The main findings of this spatiotemporal study of air temperature lapse rates in a complex Spanish Pyrenees study area are:

1. Nighttime lapse rates were weaker than diurnal ones due to air cold subsidence processes and topography. Daily maximum air temperature lapse rates (*LRmax*) were steeper from March to July, although on the shady slope this only occurred around July. *LRmax* was weaker in winter. Daily minimum air temperature lapse rates (*LRmin*) were weaker from June to August (and December), and steeper from March to May.
2. Different insolation values within and between the analyzed slopes were found, due to the facing slope and elevation of the locations, which directly influence diurnal air temperatures because of the topographic shadows in the valley bottom. This causes the retention of cold night air during the short days.
3. Steep and weak lapse rate patterns were found, explained by various factors (slope insolation, daytime, topography, season and weather conditions). On clear winter days, the lower insolation of lower locations weakened *LRmax*. However, at this time, *LRmax* was steep under unstable atmospheric conditions. During the summer, *LRmax* was almost always steep (with few topographic shadows and mainly clear). *LRmin* was weak under stable atmospheric conditions, and steep under unstable ones, regardless of the month and season.

Our results support the fact that elevation is not a linear factor, as there are local variables that can alter the spatial and temporal distribution of air temperatures, so the selection of the measurement sites is crucial. This implies a need for rethinking when modeling air temperature at detailed scale, since it is important to analyze insolation, as well as vegetation cover, in addition to the effect of weather conditions. This work shows the need to analyze air temperature on a local scale when our applications need high spatial resolution.

Supplementary Materials: The following are available online at http://www.mdpi.com/2073-4433/11/6/656/s1, Figure S1: (a) The Tinytag-Plus-2 TGP4017 datalogger; and (b) Tinytag datalogger field installation within radiation shield. Figure S2: Daily frequency (in % of monthly days) of circulation weather types (CWTs) by month. The unclassified (U) CWT is not shown in the plot. Figure S3: Hourly coefficient of variation (measured in $^{\circ}C\ km^{-1}$) for the Estiviellas and Moleta slopes by month. Red dots represent the sunrise/sunset time without topography effects, calculated for the 15th day of each month, and for equinoctial day in the Annual row. Figure S4: Boxplots of daily mean atmospheric pressure (in hPa) by *LRmax*, *LRmin* and *LRavg* cluster. The median (black line), interquartile range (boxes) and whiskers are shown. Figure S5: Boxplots of daily mean relative humidity (in %) by *LRmax*, *LRmin* and *LRavg* cluster. The median (black line), interquartile range (boxes) and whiskers are shown. Figure S6: Boxplots of daily mean wind speed (in $m\ s^{-1}$) by *LRmax*, *LRmin* and *LRavg* cluster. The median (black line), interquartile range (boxes) and whiskers are shown. Figure S7: Air temperatures of the lower and higher slope locations. Dates from 3 December 2017 to 5 December 2017. The wind speed (purple) and atmospheric pressure (red), measured at AEMET Canfranc-Station "9198X" operative weather station, are represented.

Author Contributions: Data collection, F.N.-S., J.I.L.-M., E.A.-G., J.R. and S.T.B.; Supervision, J.I.L.-M. and C.A.-M.; Analysis and investigation, F.N.-S., J.I.L.-M., C.A.-M. and M.A.-B.; Writing—original draft preparation, F.N.-S.; Writing—review and editing, all authors; Funding acquisition, J.I.L.-M. All authors have read and agreed to the published version of the manuscript.

Funding: This study was funded by the Spanish Ministry of Economy and Competitiveness project CGL2017-82216-R (HIDROIBERNIEVE). Navarro-Serrano, F. is the recipient of a pre-doctoral FPU grant (Spanish Ministry of Education, Culture and Sports, FPU15/00742). Revuelto, J. is supported by the INDECIS project, which is part of ERA4CS, and by ERA-NET, initiated by JPI Climate, and funded by FORMAS (SE), DLR (DE), BMWFW (AT), IFD (DK), MINECO (SP), ANR (FR) with co-funding by the European Union (Grant 690462). Alonso-González, E. and Aznárez-Balta, M. are beneficiaries of a pre-doctoral FPI grant (Spanish Ministry of Economy and Competitiveness, BES-2015-071466 and PRE2018-084295), and Azorin-Molina, C. of the Ramon y Cajal fellowship (RYC-2017-22830).

Acknowledgments: The authors thank all colleagues who helped in the development of the study. Raw data is freely downloadable at https://zenodo.org/record/3860564. The authors wish to acknowledge the anonymous reviewers for their detailed and helpful comments on the original manuscript.

Conflicts of Interest: The authors declare no conflict of interest.

References

1. Bonnardot, V.; Carey, V.; Madelin, M.; Cautenet, S.; Coetzee, Z.; Quénol, H. Spatial variability of Night temperatures at a fine scale over the Stellenbosch Wine District, South Africa. *J. Int. Sci. Vigne Vin* **2012**, *46*, 1–13. [CrossRef]
2. Hatfield, J.L.; Prueger, J.H. Temperature extremes: Effect on plant growth and development. *Weather Clim. Extrem.* **2015**, *10*, 4–10. [CrossRef]
3. Tang, Z.; Fang, J. Temperature variation along the northern and southern slopes of Mt. Taibai, China. *Agric. For. Meteorol.* **2006**, *139*, 200–207. [CrossRef]
4. Gilaberte-Búrdalo, M.; López-Martín, F.; Pino-Otín, M.R.; López-Moreno, J.I. Impacts of climate change on ski industry. *Environ. Sci. Policy* **2014**, *44*, 51–61. [CrossRef]
5. Pons, M.; Johnson, P.; Rosas-Casals, M.; Sureda, B.; Jover, È. Modeling climate change effects on winter ski tourism in Andorra. *Clim. Res.* **2012**, *54*, 197–207. [CrossRef]
6. Harlan, S.; Chowell, G.; Yang, S.; Petitti, D.; Morales Butler, E.; Ruddell, B.; Ruddell, D. Heat-Related Deaths in Hot Cities: Estimates of Human Tolerance to High Temperature Thresholds. *Int. J. Environ. Res. Public Health* **2014**, *11*, 3304–3326. [CrossRef]
7. Barnett, T.P.; Adam, J.C.; Lettenmaier, D.P. Potential impacts of a warming climate on water availability in snow-dominated regions. *Nature* **2005**, *438*, 303–309. [CrossRef]
8. Immerzeel, W.W.; Petersen, L.; Ragettli, S.; Pellicciotti, F. The importance of observed gradients of air temperature and precipitation for modeling runoff from a glacierized watershed in the Nepalese Himalayas. *Water Resour. Res.* **2014**, *50*, 2212–2226. [CrossRef]
9. Pagès, M.; Miró, J.R. Determining temperature lapse rates over mountain slopes using vertically weighted regression: A case study from the Pyrenees. *Meteorol. Appl.* **2010**, *17*, 53–63. [CrossRef]
10. García, M.B.; Domingo, D.; Pizarro, M.; Font, X.; Gómez, D.; Ehrlén, J. Rocky habitats as microclimatic refuges for biodiversity. A close-up thermal approach. *Environ. Exp. Bot.* **2019**, *170*, 1–10. [CrossRef]
11. López-Moreno, J.I.; Navarro-Serrano, F.; Azorín-Molina, C.; Sánchez-Navarrete, P.; Alonso-González, E.; Rico, I.; Morán-Tejeda, E.; Buisán, S.; Revuelto, J.; Pons, M.; et al. Air and wet bulb temperature lapse rates and their impact on snowmaking in a Pyrenean ski resort. *Theor. Appl. Climatol.* **2019**, *135*, 1361–1373. [CrossRef]
12. Ackerman, E.A. The Koppen Classification of Climates in North America. *Geogr. Rev.* **1941**, *31*, 105. [CrossRef]
13. Villmow, J.R. Regional patterns of Climates in Europe according to the Thornthwaite Classification. *Ohio J. Sci.* **1962**, *62*, 39–53.
14. Capel Molina, J.J. *El Clima de la Península Ibérica*; Ariel: Barcelona, Spain, 2000; p. 197.
15. Whiteman, C.D.; Bian, X.; Zhong, S.; Whiteman, C.D.; Bian, X.; Zhong, S. Wintertime Evolution of the Temperature Inversion in the Colorado Plateau Basin. *J. Appl. Meteorol.* **1999**, *38*, 1103–1117. [CrossRef]
16. Barry, R. *Mountain Weather and Climate*, 3rd ed.; Cambridge University Press: Cambridge, UK, 2008; ISBN 978-0-521-68158-2.
17. Karki, R.; ul Hasson, S.; Schickhoff, U.; Scholten, T.; Böhner, J.; Gerlitz, L. Near surface air temperature lapse rates over complex terrain: A WRF based analysis of controlling factors and processes for the central Himalayas. *Clim. Dyn.* **2020**, *54*, 329–349. [CrossRef]
18. Mahrt, L. Stratified atmospheric boundary layers and breakdown of models. *Theor. Comput. Fluid Dyn.* **1998**, *11*, 263–279. [CrossRef]
19. Jiménez-Muñoz, J.C.; Sobrino, J.A. A generalized single-channel method for retrieving land surface temperature from remote sensing data. *J. Geophys. Res. D Atmos.* **2003**, *108*, 4688. [CrossRef]
20. Khorchani, M.; Martin-Hernandez, N.; Vicente-Serrano, S.M.; Azorin-Molina, C.; Garcia, M.; Domínguez-Duran, M.A.; Reig, F.; Peña-Gallardo, M.; Domínguez-Castro, F. Average annual and seasonal Land Surface Temperature, Spanish Peninsular. *J. Maps* **2018**, *14*, 465–475. [CrossRef]

21. Navarro-Serrano, F.; López-Moreno, J.I.; Domínguez-Castro, F.; Alonso-González, E.; Azorin-Molina, C.; El-Kenawy, A.; Vicente-Serrano, S.M. Maximum and minimum air temperature lapse rates in the Andean region of Ecuador and Peru. *Int. J. Clim.* **2020**. [CrossRef]
22. Geiger, R. *The Climate near the Ground*; Rowman & Littlefield Publishers: Lanham, MD, USA, 1965; ISBN 0742518574.
23. Whiteman, C.D. Breakup of temperature inversions in deep mountain valleys: Part I. Observations. *J. Appl. Meteorol. Clim.* **1982**, *21*, 270–289. [CrossRef]
24. Whiteman, C.D.; McKee, T.B. Breakup of temperature inversions in deep mountain valleys: Part II. Thermodynamic model. *J. Appl. Meteorol. Clim.* **1982**, *21*, 290–302. [CrossRef]
25. Whiteman, C.D.; Zhong, S.; Shaw, W.J.; Hubbe, J.M.; Bian, X.; Mittelstadt, J. Cold Pools in the Columbia Basin. *Weather* **2001**, *16*, 432–447. [CrossRef]
26. Lundquist, J.; Lott, F. Using inexpensive temperature sensors to monitor the duration and heterogeneity of snow-covered areas. *Water Resour. Res.* **2008**, *44*, 1–6. [CrossRef]
27. Hubbart, J.; Kavanagh, K.; Pangle, R.; Link, T.; Schotzko, A. Cold air drainage and modeled nocturnal leaf water potential in complex forested terrain. *Tree Physiol.* **2007**, *27*, 631–639. [CrossRef] [PubMed]
28. Minder, J.R.; Mote, P.W.; Lundquist, J.D. Surface temperature lapse rates over complex terrain: Lessons from the Cascade Mountains. *J. Geophys. Res. Atmos.* **2010**, *115*, 1–13. [CrossRef]
29. Pepin, N.; Maeda, E.E.; Williams, R. Use of remotely sensed land surface temperature as a proxy for air temperatures at high elevations: Findings from a 5000 m elevational transect across Kilimanjaro. *J. Geophys. Res. Atmos.* **2016**, *121*, 9998–10015. [CrossRef]
30. Kattel, D.B.; Yao, T.; Yang, W.; Gao, Y.; Tian, L. Comparison of temperature lapse rates from the northern to the southern slopes of the Himalayas. *Int. J. Clim.* **2015**, *35*, 4431–4443. [CrossRef]
31. Hanna, E.; Mernild, S.; Yde, J.; Villiers, S. Surface Air Temperature Fluctuations and Lapse Rates on Olivares Gamma Glacier, Rio Olivares Basin, Central Chile, from a Novel Meteorological Sensor Network. *Adv. Meteorol.* **2017**, *2017*, 6581537. [CrossRef]
32. Braun, M.; Hock, R. Spatially distributed surface energy balance and ablation modelling on the ice cap of King George Island (Antarctica). *Glob. Planet. Chang.* **2004**, *42*, 45–58. [CrossRef]
33. Pagès, M.; Pepin, N.; Miró, J. Measurement and modelling of temperature cold pools in the Cerdanya valley (Pyrenees), Spain. *Meteorol. Appl.* **2017**, *24*, 290–302. [CrossRef]
34. Miró, J.R.; Peña, J.C.; Pepin, N.; Sairouni, A.; Aran, M. Key features of cold-air pool episodes in the northeast of the Iberian Peninsula (Cerdanya, eastern Pyrenees). *Int. J. Clim.* **2017**, *38*, 1105–1115. [CrossRef]
35. Benavides, R.; Montes, F.; Rubio, A.; Osoro, K. Geostatistical modelling of air temperature in a mountainous region of Northern Spain. *Agric. For. Meteorol.* **2007**, *146*, 173–188. [CrossRef]
36. Navarro-Serrano, F.; López-Moreno, J.I.; Azorin-Molina, C.; Buisán, S.; Domínguez-Castro, F.; Sanmiguel-Vallelado, A.; Alonso-González, E.; Khorchani, M. Air temperature measurements using autonomous self-recording dataloggers in mountainous and snow covered areas. *Atmos. Res.* **2019**, *224*, 168–179. [CrossRef]
37. Kulshrestha, S.; Ramsankaran, R. Investigating the performance of snowmelt runoff model using temporally varying near-surface lapse rate in Western Himalayas. *Curr. Sci.* **2018**, *114*, 808–813. [CrossRef]
38. Heynen, M.; Miles, E.; Ragettli, S.; Buri, P.; Immerzeel, W.W.; Pellicciotti, F. Air temperature variability in a high-elevation Himalayan catchment. *Ann. Glaciol.* **2016**, *57*, 212–222. [CrossRef]
39. Nigrelli, G.; Fratianni, S.; Zampollo, A.; Turconi, L.; Chiarle, M. The altitudinal temperature lapse rates applied to high elevation rockfalls studies in the Western European Alps. *Theor. Appl. Climatol.* **2017**, *131*, 1479–1491. [CrossRef]
40. Marshall, S.J.; Sharp, M.J.; Burgess, D.O.; Anslow, F.S. Near-surface-temperature lapse rates on the Prince of Wales Icefield, Ellesmere Island, Canada: Implications for regional downscaling of temperature. *Int. J. Clim.* **2007**, *27*, 385–398. [CrossRef]
41. Navarro-Serrano, F.; López-Moreno, J.; Azorin-Molina, C.; Alonso-González, E.; Tomás-Burguera, M.; Sanmiguel-Vallelado, A.; Revuelto, J.; Vicente-Serrano, S.M. Estimation of near-surface air temperature lapse rates over continental Spain and its mountain areas. *Int. J. Clim.* **2018**, *38*, 3233–3249. [CrossRef]
42. Ojha, R. Identification of homogeneous regions of near surface air temperature lapse rates across India. *Int. J. Clim.* **2019**, *39*, 4288–4304. [CrossRef]

43. Romshoo, S.A.; Rafiq, M.; Rashid, I. Spatio-temporal variation of land surface temperature and temperature lapse rate over mountainous Kashmir Himalaya. *J. Mt. Sci.* **2018**, *15*, 563–576. [CrossRef]
44. Gardner, A.S.; Sharp, M.J.; Koerner, R.M.; Labine, C.; Boon, S.; Marshall, S.J.; Burgess, D.O.; Lewis, D. Near-Surface Temperature Lapse Rates over Arctic Glaciers and Their Implications for Temperature Downscaling. *J. Clim.* **2009**, *22*, 4281–4298. [CrossRef]
45. Lookingbill, T.R.; Urban, D.L. Spatial estimation of air temperature differences for landscape-scale studies in montane environments. *Agric. For. Meteorol.* **2003**, *114*, 141–151. [CrossRef]
46. Mahrt, L.; Vickers, D.; Nakamura, R.; Soler, M.R.; Sun, J.; Burns, S.; Lenschow, D.H. Shallow Drainage Flows. *Bound. Layer Meteorol.* **2001**, *101*, 243–260. [CrossRef]
47. Soler, M.R.; Infante, C.; Buenestado, P.; Mahrt, L. Observations of Nocturnal Drainage Flow in a Shallow Gully. *Bound. Layer Meteorol.* **2002**, *105*, 253–273. [CrossRef]
48. Barry, R.; Chorley, R. *Atmosphere, Weather and Climate*, 1st ed.; Taylor & Francis: Abingdon, UK, 1987; p. 536.
49. Von Arx, G.; Dobbertin, M.; Rebetez, M. Spatio-temporal effects of forest canopy on understory microclimate in a long-term experiment in Switzerland. *Agric. For. Meteorol.* **2012**, *166–167*, 144–155. [CrossRef]
50. Lareau, N.P.; Horel, J.D. Dynamically Induced Displacements of a Persistent Cold-Air Pool. *Bound. Layer Meteorol.* **2014**, *154*, 291–316. [CrossRef]
51. Moron, V.; Oueslati, B.; Pohl, B.; Janicot, S. Daily Weather Types in February–June (1979–2016) and Temperature Variations in Tropical North Africa. *J. Appl. Meteorol. Clim.* **2018**, *57*, 1171–1195. [CrossRef]
52. Kirchner, M.; Faus-Kessler, T.; Jakobi, G.; Leuchner, M.; Ries, L.; Scheel, H.-E.; Suppan, P. Altitudinal temperature lapse rates in an Alpine valley: Trends and the influence of season and weather patterns. *Int. J. Clim.* **2013**, *33*, 539–555. [CrossRef]
53. García-Ruiz, J.M.; López-Moreno, J.I.; Vicente-Serrano, S.M.; Lasanta–Martínez, T.; Beguería, S. Mediterranean water resources in a global change scenario. *Earth Sci. Rev.* **2011**, *105*, 121–139. [CrossRef]
54. Lasanta, T.; Laguna, M.; Vicente-Serrano, S.M. Do tourism-based ski resorts contribute to the homogeneous development of the Mediterranean mountains? A case study in the Central Spanish Pyrenees. *Tour. Manag.* **2007**, *28*, 1326–1339. [CrossRef]
55. Morán-Tejeda, E.; Herrera, S.; López-Moreno, J.I.; Revuelto, J.; Lehmann, A.; Beniston, M. Evolution and frequency (1970–2007) of combined temperature–precipitation modes in the Spanish mountains and sensitivity of snow cover. *Reg. Environ. Chang.* **2013**, *13*, 873–885. [CrossRef]
56. López-Moreno, J.I.; García-Ruiz, J.M. Influence of snow accumulation and snowmelt on streamflow in the central Spanish Pyrenees. *Hydrol. Sci. J.* **2004**, *49*, 787–801. [CrossRef]
57. López-Moreno, J.I.; Gascoin, S.; Herrero, J.; Sproles, E.A.; Pons, M.; Alonso-González, E.; Hanich, L.; Boudhar, A.; Musselman, K.N.; Molotch, N.P.; et al. Different sensitivities of snowpacks to warming in Mediterranean climate mountain areas. *Environ. Res. Lett.* **2017**, *12*, 074006. [CrossRef]
58. Esteban, P.; Ninyerola, M.; Prohom, M. Spatial modelling of air temperature and precipitation for Andorra (Pyrenees) from daily circulation patterns. *Theor. Appl. Climatol.* **2009**, *96*, 43–56. [CrossRef]
59. Buisán, S.; Saz, M.A.; López-Moreno, J.I.; López-Moreno, J.I. Spatial and temporal variability of winter snow and precipitation days in the western and central Spanish Pyrenees. *Int. J. Clim.* **2015**, *35*, 259–274. [CrossRef]
60. Alonso-González, E.; López-Moreno, J.I.; Navarro-Serrano, F.; Sanmiguel-Vallelado, A.; Revuelto, J.; Domínguez-Castro, F.; Ceballos, A. Snow climatology for the mountains in the Iberian Peninsula using satellite imagery and simulations with dynamically downscaled reanalysis data. *Int. J. Clim.* **2020**, *40*, 477–491. [CrossRef]
61. López-Moreno, J.I.; Vicente-Serrano, S.M.; Moran-Tejeda, E.; Zabalza, J.; Lorenzo-Lacruz, J.; García-Ruiz, J.M. Impact of climate evolution and land use changes on water yield in the ebro basin. *Hydrol. Earth Syst. Sci.* **2011**, *15*, 311–322. [CrossRef]
62. Esteban-Parra, M.J.; Rodrigo, F.S.; Castro-Diez, Y. Spatial and temporal patterns of precipitation in Spain for the period 1880–1992. *Int. J. Clim.* **1998**, *18*, 1557–1574. [CrossRef]
63. Agencia Estatal de Meteorología (AEMET); Ministerio de Medio Ambiente y Medio Rural y Marino; Instituto de Meteorología de Portugal. *Atlas Climático Ibérico*, 1st ed.; Closas-Orcoyen, S.L.: Madrid, Spain, 2011.
64. Crespo, D.; Albiac, J.; Kahil, T.; Esteban, E.; Baccour, S. Tradeoffs between Water Uses and Environmental Flows: A Hydroeconomic Analysis in the Ebro Basin. *Water Resour. Manag.* **2019**, *33*, 2301–2317. [CrossRef]
65. García-Garizábal, I.; Causapé, J.; Merchán, D. Evaluation of alternatives for flood irrigation and water usage in Spain under Mediterranean climate. *Catena* **2017**, *155*, 127–134. [CrossRef]

66. Buisán, S.; López-Moreno, J.; Saz, M.; Kochendorfer, J. Impact of weather type variability on winter precipitation, temperature and annual snowpack in the Spanish Pyrenees. *Clim. Res.* **2016**, *69*, 79–92. [CrossRef]
67. Navarro-Serrano, F.; López-Moreno, J.I. Spatio-temporal analysis of snowfall events in the Spanish Pyrenees and ther relationship to atmospheric circulation. *Cuad. Investig. Geográfica* **2017**, *43*, 233–254. [CrossRef]
68. Nadal-Romero, E.; Cammeraat, E.; Pérez-Cardiel, E.; Lasanta, T. Effects of secondary succession and afforestation practices on soil properties after cropland abandonment in humid Mediterranean mountain areas. *Agric. Ecosyst. Environ.* **2016**, *228*, 91–100. [CrossRef]
69. Pueyo, Y.; Beguería, S. Modelling the rate of secondary succession after farmland abandonment in a Mediterranean mountain area. *Landsc. Urban Plan.* **2007**, *83*, 245–254. [CrossRef]
70. Buisán, S.; Azorin-Molina, C.; Jimenez, Y. Impact of two different sized Stevenson screens on air temperature measurements. *Int. J. Clim.* **2015**, *35*, 4408–4416. [CrossRef]
71. Imholt, C.; Soulsby, C.; Malcolm, I.; Hrachowitz, M.; Gibbins, C.; Langan, S.; Tetzlaff, D. Influence of Scale on Thermal characteristics in a large montane River Basin. *River Res. Appl.* **2013**, *29*, 403–419. [CrossRef]
72. Yang, Z.; Hanna, E.; Callaghan, T.; Jonasson, C. How can meteorological observations and microclimate simulations improve understanding of 1913–2010 climate change around Abisko, Swedish Lapland? *Meteorol. Appl.* **2012**, *19*, 454–463. [CrossRef]
73. Pepin, N.; Kidd, D. Spatial temperature variation in the Eastern Pyrenees. *Weather* **2006**, *61*, 300–310. [CrossRef]
74. Serrano, E.; Sanjosé-Blasco, J.J.; Gómez-Lende, M.; López-Moreno, J.I.; Pisabarro, A.; Martínez-Fernández, A. Periglacial environments and frozen ground in the central Pyrenean high mountain area: Ground thermal regime and distribution of landforms and processes. *Permafr. Periglac. Process.* **2019**, *30*, 292–309. [CrossRef]
75. Rolland, C. Spatial and Seasonal Variations of Air Temperature Lapse Rates in Alpine Regions. *J. Clim.* **2003**, *16*, 1032–1046. [CrossRef]
76. Du, M.; Liu, J.; Zhang, X.; Li, Y.; Tang, Y. Changes of spatial patterns of surface-air-temperature on the Tibetan Plateau. *Latest Trends Theor. Appl. Mech. Fluid Mech. Heat Mass Transf.* **2010**, *47*, 42–47.
77. Blandford, T.R.; Humes, K.S.; Harshburger, B.J.; Moore, B.C.; Walden, V.P.; Ye, H. Seasonal and Synoptic Variations in Near-Surface Air Temperature Lapse Rates in a Mountainous Basin. *J. Appl. Meteorol. Clim.* **2008**, *47*, 249–261. [CrossRef]
78. Florinsky, I.V.; Kulagina, T.B.; Meshalkina, J.L. Influence of topography on landscape radiation temperature distribution. *Int. J. Remote Sens.* **1994**, *15*, 3147–3153. [CrossRef]
79. IGN Plan Nacional de Ortofotografía Aérea. Available online: https://pnoa.ign.es/presentacion-y-objetivo (accessed on 27 January 2020).
80. Corripio, J.G. Insol: Solar Radiation. R Package Version 1.2.1. Available online: https://CRAN.R-project.org/package=insol. (accessed on 20 May 2020).
81. R Core-Team. *R: A Language and Environment for Statistical Computing 2013*; R Foundation for Statistical Computing: Vienna, Austria, 2013.
82. Jenkinson, A.F.; Collison, P. An initial climatology of Wales over the North Sea. In *Synoptic Climatology Branch Memorandum*; Meteorological Office: Bracknell, UK, 1997; p. 62.
83. Lamb, H.H. British Isles weather types and a register of daily sequence of circulation patterns, 1861–1971. *Geophys. Mem.* **1972**, *116*, 85.
84. Rasilla Álvarez, D.F.; García-Codrón, J.C.; Garmendia Pedraja, C. Los temporales de viento: Propuesta metodológica para el análisis de un fenómeno infravalorado. In Proceedings of the 7th Reunión Nacional de Climatología, Albarracin, Spain, 27–29 June 2002; pp. 129–136.
85. Basnett, T.A.; Parker, D.E. Development of the global mean sea level pressure data set GMSLP2. In *Climatic Research Technical Note*; Hadley Centre, Meteorological Office: Bracknell, UK, 1997; Volume 79.
86. Charrad, M.; Ghazaali, N.; Boiteau, V.; Niknafs, A. NbClust: An R package for determining the relevant number of clusters in a data Set. *J. Stat. Softw.* **2014**, *61*, 1–36. [CrossRef]
87. Murtagh, F.; Legendre, P. Ward's Hierarchical Agglomerative Clustering Method: Which Algorithms Implement Ward's Criterion? *J. Classif.* **2014**, *31*, 274–295. [CrossRef]
88. Wilcoxon, F. Individual Comparisons by Ranking Methods. *Biom. Bull.* **1945**, *1*, 80. [CrossRef]
89. Ninyerola, M.; Pons, X.; Roure, J.M. A methodological approach of climatological modelling of air temperature and precipitation through GIS techniques. *Int. J. Clim.* **2000**, *20*, 1823–1841. [CrossRef]

90. Espín-Sánchez, E.; Ruiz-Álvarez, V.; Martí-Talavera, J.; García-Marín, R. Estudio preliminar de las inversiones térmicas en el sureste de la Península Ibérica: El caso de los campos de Hernán Perea. *Pirin. Rev. Ecol. Montaña.* **2018**, *173*, 1–18.
91. Daly, C.; Gibson, W.; Taylor, G.; Johnson, G.; Pasteris, P. A knowledge-based approach to the statistical mapping of climate. *Clim. Res.* **2002**, *22*, 99–113. [CrossRef]
92. Sadoti, G.; McAfee, S.A.; Roland, C.A.; Fleur Nicklen, E.; Sousanes, P.J. Modelling high-latitude summer temperature patterns using physiographic variables. *Int. J. Clim.* **2018**, *38*, 4033–4042. [CrossRef]
93. Lundquist, J.D.; Pepin, N.; Rochford, C. Automated algorithm for mapping regions of cold-air pooling in complex terrain. *J. Geophys. Res.* **2008**, *113*, 1–15. [CrossRef]
94. Pepin, N. Lapse rate changes in northern England. *Theor. Appl. Climatol.* **2001**, *68*, 1–16. [CrossRef]
95. Price, J.D.; Vosper, S.; Brown, A.; Ross, A.; Clark, P.; Davies, F.; Horlacher, V.; Claxton, B.; McGregor, J.R.; Hoare, J.S.; et al. Colpex: Field and numerical studies over a region of small hills. *Bull. Am. Meteorol. Soc.* **2011**, *92*, 1636–1650. [CrossRef]
96. Du, M.; Zhang, M.; Wang, S.; Zhu, X.; Che, Y. Near-surface air temperature lapse rates in Xinjiang, northwestern China. *Theor. Appl. Climatol.* **2017**, *131*, 1–14. [CrossRef]
97. Sanmiguel-Vallelado, A.; López-Moreno, J.I.; Morán-Tejeda, E.; Alonso-González, E.; Navarro-Serrano, F.; Rico, I.; Camarero, J.J. Variable effects of forest canopies on snow processes in a valley of the central Spanish Pyrenees. *Hydrol. Process.* **2020**, *34*, 2247–2262. [CrossRef]
98. Barringer, J.R.F. A variable lapse rate snowline model for the Remarkables, Central Otago, New Zealand. *J. Hydrol.* **1989**, *28*, 32–46.
99. Duane, W.J.; Pepin, N.C.; Losleben, M.L.; Hardy, D.R. General characteristics of Temperature and Humidity Variability on Kilimanjaro, Tanzania. *Arct. Antarct. Alp. Res.* **2008**, *40*, 323–334. [CrossRef]
100. Dumas, M.D. Changes in temperature and temperature gradients in the French Northern Alps during the last century. *Theor. Appl. Climatol.* **2013**, *111*, 223–233. [CrossRef]
101. Dodson, R.; Marks, D. Daily air temperature interpolated at high spatial resolution over a large mountainous region. *Clim. Res.* **1997**, *8*, 1–20. [CrossRef]
102. Joshi, R.; Sambhav, K. Near surface temperature lapse rate for treeline environment in western Himalaya and possible impacts on ecotone vegetation. *Trop. Ecol.* **2018**, *59*, 197–209. [CrossRef]
103. Lareau, N.P.; Crosman, E.; Whiteman, C.D.; Horel, J.D.; Hoch, S.W.; Brown, W.O.J.; Horst, T.W. The Persistent Cold-Air Pool Study. *Bull. Am. Meteorol. Soc.* **2013**, *94*, 51–63. [CrossRef]
104. Bolstad, P.V.; Swift, L.; Collins, F.; Régnière, J. Measured and predicted air temperatures at basin to regional scales in the southern Appalachian mountains. *Agric. For. Meteorol.* **1998**, *91*, 161–176. [CrossRef]

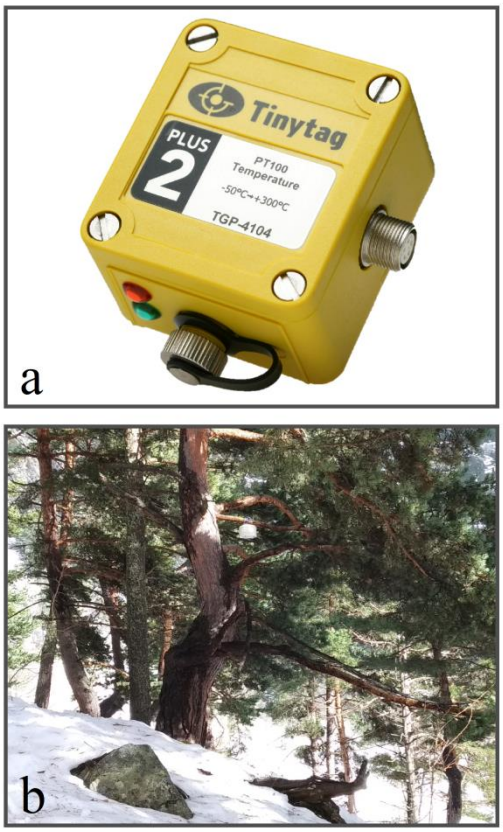

Figure S1. (a) The Tinytag-Plus-2 TGP4017 datalogger; and **(b)** Tinytag datalogger within radiation shield field installation.

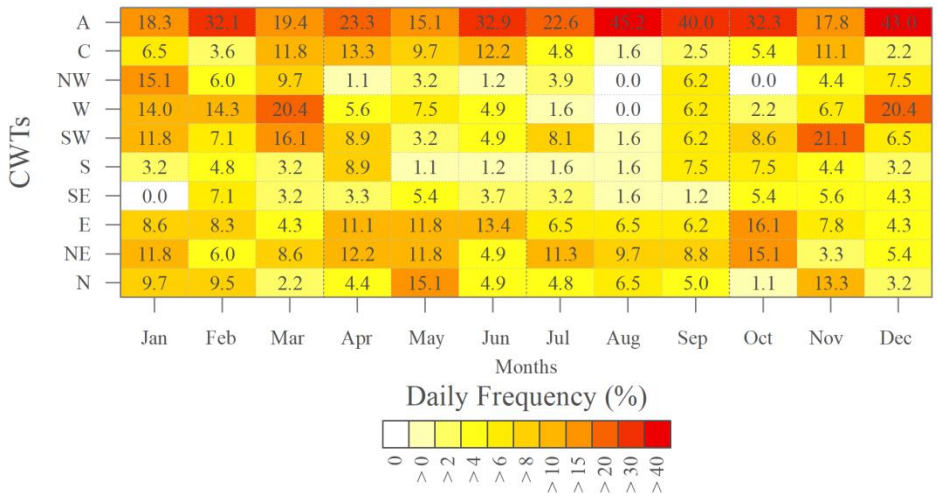

Figure S2. Daily frequency (in % of the monthly days) of the Circulation Weather Types (CWTs) by months. The unclassified (U) CWT is not shown in the plot.

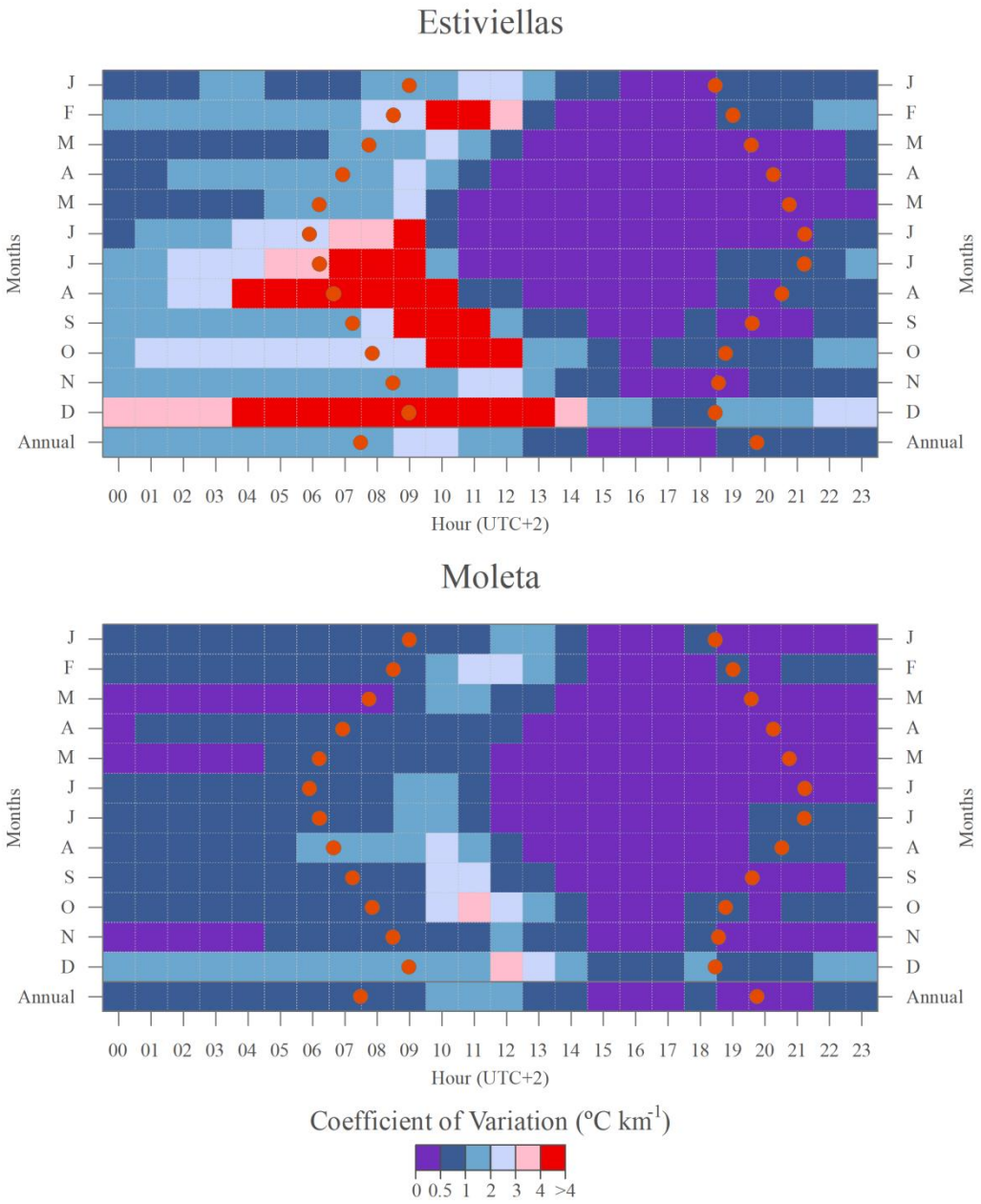

Figure S3. Hourly Coefficient of variation (measured in ºC km^{-1}) for Estiviellas and Moleta slopes by months. Red dots represent the sunrise/sunset time without topography effects, calculated for 15th day of each month, and for equinoctial day to Annual row.

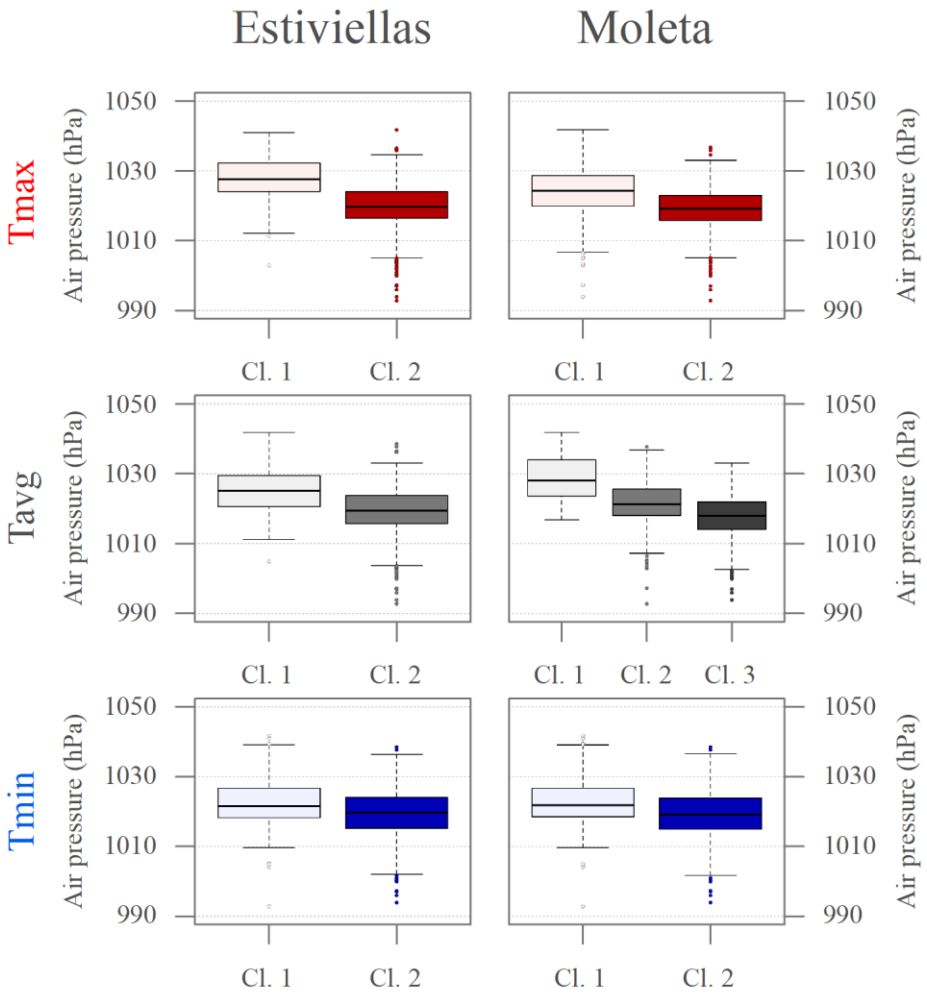

Figure S4. Boxplots of Daily mean atmospheric pressure (in hPa) by Tmax, Tmin, and Tavg clusters. The median (black line), the interquartile range (boxes), and whiskers are shown.

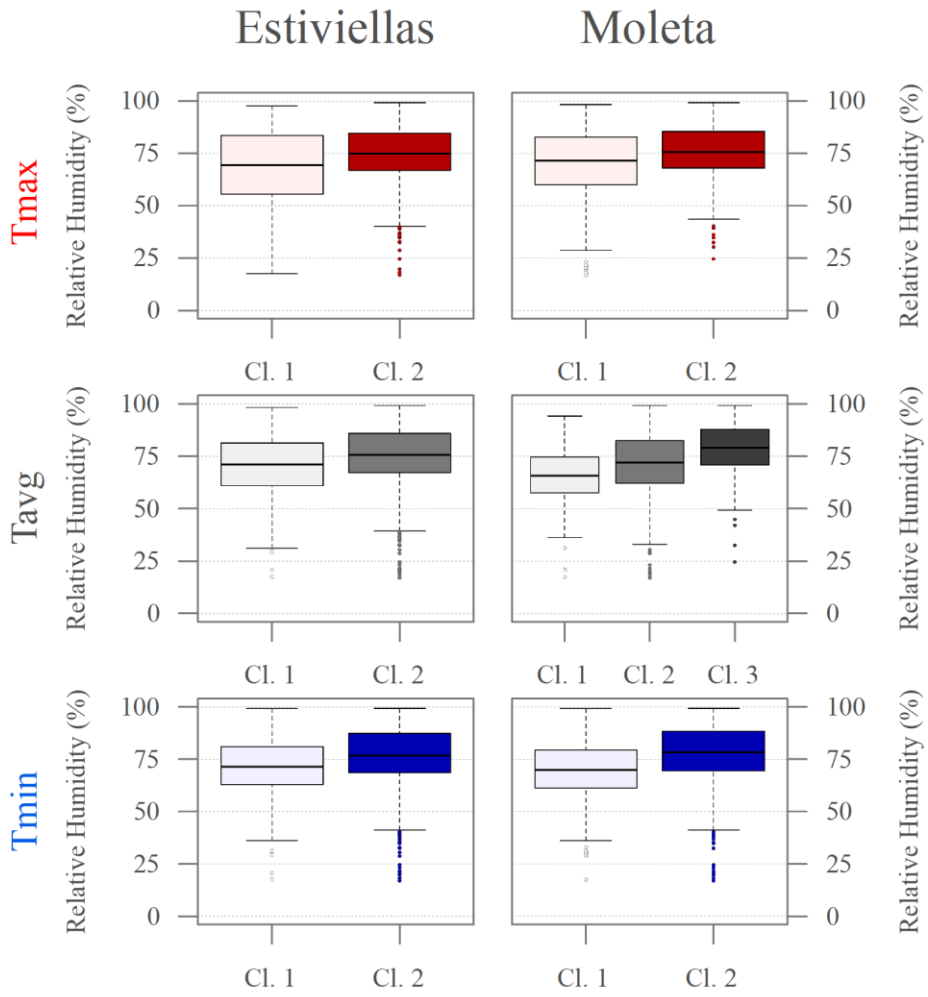

Figure S5. Boxplots of Daily mean relative humidity (in %) by Tmax, Tmin, and Tavg clusters. The median (black line), the interquartile range (boxes), and whiskers are shown.

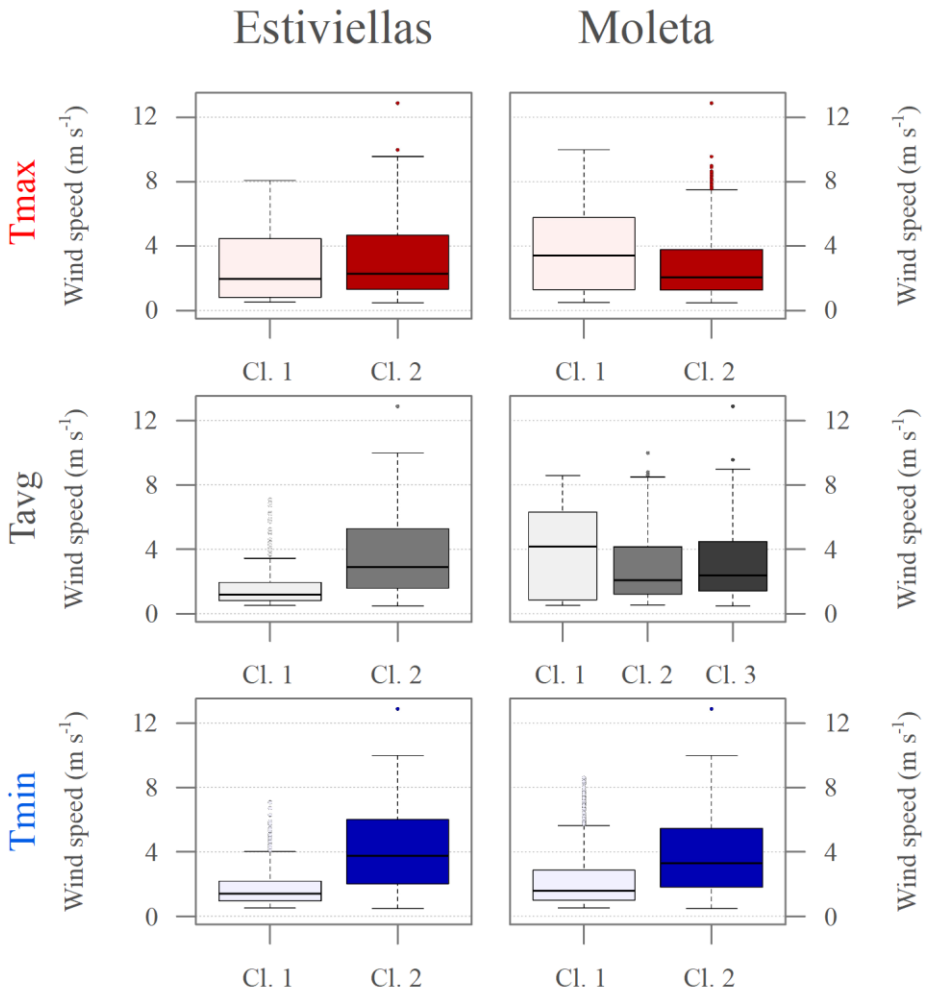

Figure S6. Boxplots of Daily mean wind speed (in m s^{-1}) by Tmax, Tmin, and Tavg clusters. The median (black line), the interquartile range (boxes), and whiskers are shown.

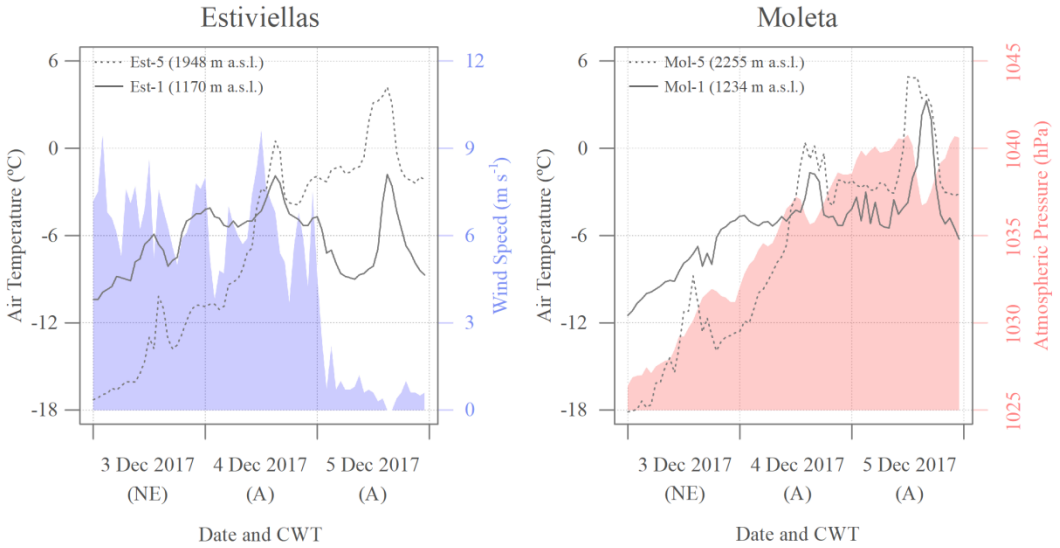

Figure S7. Air temperatures of the lower and higher slope locations. Dates from 3 Dec 2017 to 5 Dec 2017. The Wind speed (purple) and Atmospheric Pressure (red), measured at AEMET Canfranc-Station "9198X" operative weather station, were represented.

Capítulo 7

GRADIENTES DE TEMPERATURA SECA Y HÚMEDA Y SU IMPACTO EN LA PRODUCCIÓN DE NIEVE

Publicado como:

López-Moreno, J.I., **Navarro-Serrano, F.**, Azorin-Molina, C., Sánchez-Navarrete, P., Alonso-González, E., Rico, I., Morán-Tejeda, E., Buisán, S., Revuelto, J., Pons, M., Vicente-Serrano, S.M. 2019. Air and wet bulb temperature lapse rates and their impact on snowmaking in a Pyrenean ski resort. *Theoretical and Applied Climatology* 135: 1361-1373. DOI: https://doi.org/10.1007/s00704-018-2448-y.

Theoretical and Applied Climatology (2019) 135:1361–1373
https://doi.org/10.1007/s00704-018-2448-y

ORIGINAL PAPER

Air and wet bulb temperature lapse rates and their impact on snowmaking in a Pyrenean ski resort

Juan Ignacio López-Moreno[1] · F. Navarro-Serrano[1] · C. Azorín-Molina[2] · P. Sánchez-Navarrete[1] · E. Alonso-González[1] · I. Rico[1,3] · E. Morán-Tejeda[7] · S. Buisan[4] · J. Revuelto[5] · M. Pons[6] · S.M. Vicente-Serrano[1]

Received: 3 December 2017 / Accepted: 1 March 2018 / Published online: 9 March 2018

Abstract
A set of 17 air temperature and relative humidity sensors were used to analyze the temporal variability of surface air temperature (Tair), wet bulb temperature (Twb), and daily snowmaking hours (SM, number of hours per day with Twb < − 2 °C), lapse rates, and the occurrence of thermal inversions at the Formigal ski resort (Spanish Pyrenees) from December to March during three consecutive ski seasons (2012–2013, 2013–2014, and 2014–2015). The Tair and Twb lapse rates showed strong hourly and daily variability, with both exhibiting almost identical temporal fluctuations.

The Twb exhibited average lapse rates that were slightly steeper (− 5.2 °C/km) than those observed for Tair (− 4.9 °C/km). The less steep lapse rates and most thermal inversions were observed in December. Days having less (more) steep Tair and Twb lapse rates were observed under low (high) wind speeds and high (low) relative humidity and air pressure. The temporal dynamics of the SM lapse rates was more complex, as this involved consideration of the average Tair in the ski resort, in addition to the driving factors of the spatio-temporal variability of Twb. Thus, on a number of cold (warm) days, snowmaking was feasible at all elevations at the ski resort, independently of the slopes of the lapse rates. The SM exhibited an average daily lapse rate of 8.2 h/km, with a progressive trend of increase from December to March.

Weather types over the Iberian Peninsula tightly control the driving factors of the Tair, Twb, and SM lapse rates (wind speed, relative humidity, and Tair), so the slopes of the lapse rates and the frequency of inversions in relation to elevation for the three variables are very dependent on the occurrence of specific weather types. The less steep lapse rates occurred associated with advections from the southeast, although low lapse rates also occurred during advections from the east and south, and under anticyclonic conditions. The steepest Tair and Twb lapse rates were observed during north and northwest advections, while the steepest rates for SM were observed during days of cyclonic circulation and advections from the northeast.

✉ Juan Ignacio López-Moreno
nlopez@ipe.csic.es

[1] Campus de Aula Dei, Instituto Pirenaico de Ecología, CSIC, Avda Montañana 1005, 50059 Zaragoza, Spain

[2] Regional Climate Group, Department of Earth Sciences, University of Gothenburg, Gothenburg, Sweden

[3] Departamento de Geografía, Prehistoria y Arqueología, Universidad del País Vasco, Vitoria-Gasteiz, Spain

[4] AEMET, Spanish Meteorological Service, Zaragoza, Spain

[5] Centre d'Etudes de la Neige, Météo-France—CNRS, CNRM UMR3589, Grenoble, France

[6] Snow and Mountain Research Center of Andorra, Andorran Research Institute, Sant Julià, Andorra

[7] Department of Geography, University of the Balearic Islands, Palma, Majorca, Spain

1 Introduction

In recent decades, ski tourism has become one of the most important sources of income for many mountain regions worldwide (Gilaberte et al. 2014). Despite their obvious environmental impacts, ski developments provide for economic and income diversification, and are associated with improvements to services and infrastructure (Lindberg et al. 2001; Lasanta et al. 2007). However, the economic viability of ski-based tourism relies on the presence of adequate snow depths during the ski season (Steiger and Mayer 2008; Scott et al. 2012; Pons et al. 2015). This is a major challenge for winter sport destinations (Rixen et al. 2011), especially those located at mid-latitudes or in low elevation areas, where the snowpack is characterized by strong interannual fluctuations, and global warming is acting to diminish the snowpack (López-Moreno et al. 2009).

In low elevation ski areas, snowmaking represents a key technology to buffer the impact of interannual variability of snow conditions, and is increasingly considered to be the most reliable adaptation measure for alpine ski resorts facing the consequences of climate change (Uhlmann et al. 2009; Spandre et al. 2017). However, for successful and efficient production of machine-made snow, particular air temperature and humidity conditions need to be met, generally defined by a wet bulb temperature (Twb) threshold. This threshold is not always met, especially at lower elevation sites where the natural snowpack is less abundant (López-Moreno et al. 2017). For this reason, the use of snowmaking is questioned, and discouraged in those areas where the potential for regular snow production is uncertain under short-term climate projection scenarios that indicate declining conditions for skiing and snow production in coming decades (Gilaberte et al. 2017). Thus, to assess the potential for snowmaking to overcome the large spatial and temporal variability of natural snowpacks, it is imperative to understand the spatial and temporal dynamics of Twb within ski resorts. No such studies have yet been reported.

The Twb is the temperature of a particular volume of air cooled to saturation (100% relative humidity) by the evaporation of water into it, and is always less than or equal to dry Tair. The more moisture in a parcel of air, the less moisture it can absorb, and the colder it must become to form snow crystals from the fine droplets of water. Depending on the snowmaking technology, Twb values colder than − 1 to − 4 °C are commonly used as thresholds for snow production. At the local scale (i.e., within a ski resort), the spatial variability of relative humidity (RH) is mostly determined by Tair because the specific humidity (the water content of air) tends to be highly spatially homogeneous (Brutsaert 1998). At local scales, most of the variability in Tair is because of vertical changes described by the so-called environmental lapse rate (ELR), which is assumed to be − 6.5 °C/km under neutral conditions in free atmosphere (Frederick 2008); this value is commonly used to spatially interpolate and extrapolate air temperature (López-Moreno et al. 2017). However, many studies have indicated that numerous factors make air temperature gradients very site-specific, including topography (slope, aspect, sky view factor), the presence of snow and ice, and vegetation and soil types (Nunez and Calhoun 1986; Roland 2003; Marshall et al. 2007; Blandford et al. 2008; Pepin and Lundquist 2008, Pagès and Miró 2010; Kattel et al. 2013). In addition, Tair lapse rates are highly dependent on surface processes (Minder et al. 2010) including air moisture, wind speed, atmospheric pressure, and solar radiation, and this explains the very strong temporal variability in the slope of ELR at sub-daily to seasonal and interannual scales (Thayyen et al. 2005, Tang and Fang 2006; Gardner et al. 2009, Heynen et al. 2016). The various meteorological conditions affecting ELRs are generally associated with the passage of air masses having differing characteristics (Kirchner et al. 2013), providing the potential to establish the relationships of various weather types and synoptic conditions to the slopes of the ELRs (Pepin 2001; Blandford et al. 2008; Holden and Rose 2011).

Thus, knowledge of the spatio-temporal evolution of Tair and Twb temperatures is essential for mountain areas where artificial snow production is important in the management of ski resorts. In this study, based on the ski resort of Formigal (Spanish Pyrenees), we used hourly data from 17 sensors measuring temperature and relative humidity over three consecutive ski seasons (2013–14, 2014–15, and 2015–16) to assess the temporal variability of the Tair and Twb lapse rates, and their impacts on the production of artificial snow. The effects of meteorological factors and the weather types on the slope of the lapse rates were also analyzed.

2 Study area

This study was carried out at the Formigal Ski Resort (Central Pyrenees; 42.5° N 0.25° W; Fig. 1), which is the largest ski area in the Spanish Pyrenees, comprising 137 km of ski runs. Elevations at Formigal range from 1550 to 2300 m a.s.l., and the lifts have a maximum capacity of 35,920 skiers per hour. The ski season generally starts in early December and finishes in early April.

Data from the automatic weather stations at Izas (2056 m a.s.l.), which is located in the vicinity of this ski area, indicates a mean annual Tair of 3 °C and an average of 130 days each year when the daily mean Tair is < 0 °C (Revuelto et al. 2017). The mean annual precipitation is approximately 2000 mm, of which more than 50% falls as snow (López-Moreno et al. 2013). Although the mean winter Tair is < 0 °C, the area is subject to temperate or rainy spells during winter, which trigger melting events and major metamorphosis of the snowpack throughout the snow season (Fassnacht et al. 2010). The wind direction is predominantly from northwest and southeast (Revuelto et al. 2014, 2017; Navarro-Serrano and López-Moreno 2017).

3 Data and methods

One measurement per hour of Tair and RH was obtained from 17 Tinytag TGP-4500 data loggers (www.geminidataloggers.com/data-loggers/tinytag-plus-2/tgp-4500) evenly placed in an area of 12 km^2 within the Formigal ski resort (Fig. 1); these provided data for 331 days during the three seasons of the

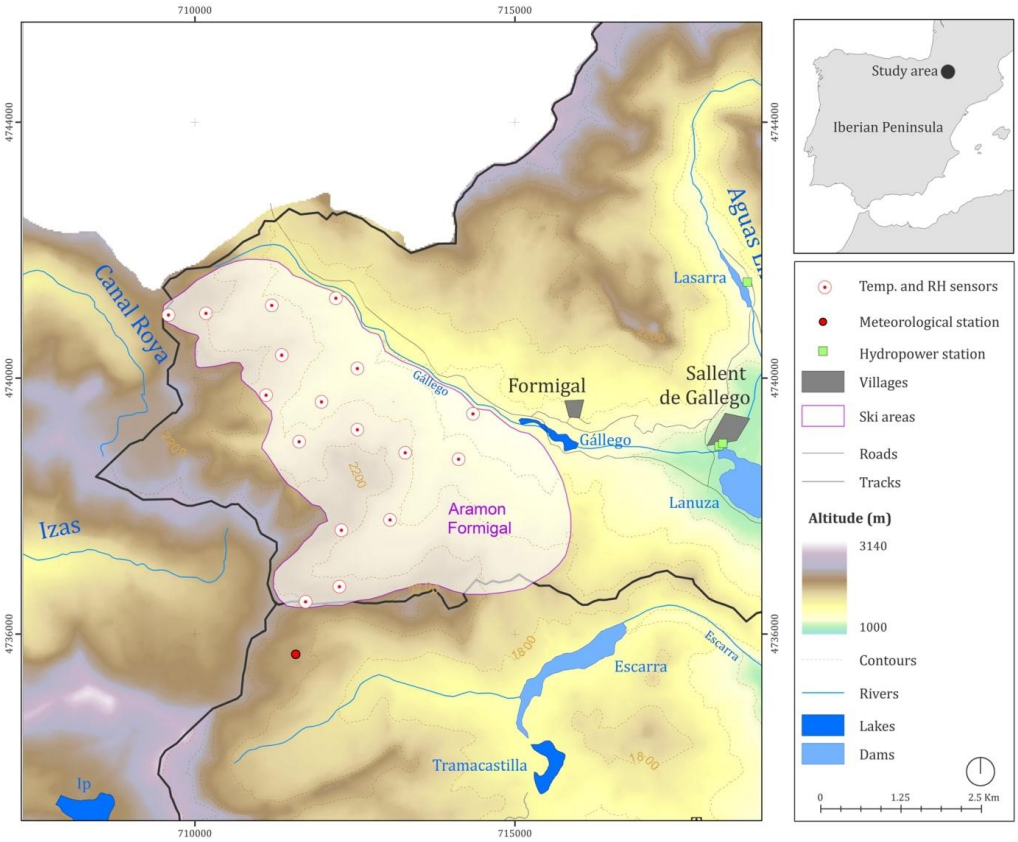

Fig. 1 Study area. Location of the temperature (Temp.) and relative humidity (RH) sensors, and the meteorological station. Contour lines are drawn for every 200 m of elevation

study. The manufacturer's stated accuracy for the sensors is ± 0.01 °C for Tair and ± 0.3% for RH. The data loggers were hung from the eaves of the roofs of chair lift sheds, at approximately 2.5 m height above the bare ground, and were protected by radiation shields (DataMate™). The lowest sensor was at 1554 m a.s.l. and the highest was at 2305 m a.s.l., at the top of the ski area. At least one sensor was placed in each 100-m elevation band in the two main valleys of the ski area. There is also an automatic weather station at 2056 m a.s.l. in the study area; this records temperature (Tair), wind speed (WS), RH, and air pressure (Pat) every 10 min. Table 1 shows a list of variables used and evaluated in this study. The data for Tair and RH from this station provided an extra sensor for the study (i.e., total = 18). The WS, RH, and Pat parameters were used as explanatory variables for temporal fluctuations of the lapse rates for Tair, Twb, and the snowmaking hours (SM, Twb < − 2 °C).

The Twb was calculated from Tair and RH using the equation of Stull (2011), which presented a mean absolute error < 0.3 °C:

$$Twb = Tair \times \tan\left[0.151977(RH + 8.313659)^{1/2}\right] + \operatorname{atan}(Tair + RH) - \operatorname{atan}(RH - 1.676331) + 0.00391838(RH)^{3/2} \operatorname{atan}(0.023101RH\%) - 4.686035$$

From the hourly Twb series, it was set the daily number of hours of snowmaking (SM hours) summing all hours per day with Twb < − 2 °C at each sensor. This threshold was based on the technical specifications of the 440 snow guns (Technoalpin TL6 and M18) installed in the ski area. The slopes of the linear regressions of Tair, Twb, and SM hours as a function of elevation were used as measures of the lapse rates, and the Pearson's r coefficient was used to assess the strength of the correlations. A threshold of $p < 0.05$ was used to assess whether the relationships were statistically significant. Significant correlations for data

Table 1 List of variables used in the study

Variable	Name and units	Calculation
Tair	Air temperature (°C)	
RH	Relative humidity (%)	
Twb	Wet bulb temperature (°C)	From Tair and RH (Stull 2011)
SM	Snowmaking hours (hours per day)	N° hours per day with Twb < 2 °C
WS	Wind speed (m/s)	
Pat	Atmospheric pressure (hPa)	

from the 17 data loggers corresponded to *r* values less than and greater than − 0.41 and + 0.41, respectively.

The relationships of the Twb and SM daily lapse rates to average daily WS, RH, Pat, and Tair were assessed. The interactions among variables were explored using regression tree classification models (Breiman et al. 1984); these are non-parametric methods based on recursive splitting of the information from the predictor variables to minimize the sum of the squared residuals obtained in each group. The complexity of the final tree is generally based on the tree size that minimizes model deviance from cross-validation measures, and maximizes the coefficient of determination (Molotch et al. 2005). Similarly, the tree size was fitted based on a 1% threshold for the relationship of reduced variance to complexity for a sequence in the pruned tree, and assignment of a minimum node size (at least 20 observations per node).

To explore the dependence of the Tair, Twb, and SM lapse rates on the passage of air masses having different characteristics and trajectories, a classification of weather types over the Iberian Peninsula was conducted. Daily weather types for the Iberian Peninsula were classified as described by Jenkinson and Collison (1977). The method is based on an index obtained from the direction and vorticity of geostrophic wind, calculated from daily sea level pressure data at 16 points that form a grid of 5° latitude encompassing the Iberian Peninsula. This method has been fully explained and discussed by Jones et al. (1993) and Trigo and DaCamara (2000), and successfully applied to the Iberian Peninsula (Goodess and Palutikof 1998; Spellman 2000; Trigo and Dacamara 2000; López-Moreno and Vicente-Serrano 2007). This classification generates 26 circulation weather types (CWTs): anticyclonic (A), cyclonic (C), 8 directional and 16 hybrid CWTs. The number of types was reduced by assigning the 16 hybrid CWTs according to their directional flow; for example, ANE (anticyclonic–northeast) was classified as NE (northeast). This enabled interpretation of the results to be simplified to 2 pure (A, C) and 8 directional (N, NE, E, SE, S, SW, W, NW) CWTs. Following a modified version of the procedure of Rasilla et al. (2002), unclassified (U) days were reclassified using two rules based on the sea level pressure at point 8 on the grid (p8; located approximately over Lisbon, on the west Iberian Peninsula), plus a third rule introduced for this analysis:

- p8 < 1020 mb: Cyclonic (C)
- 1020 < p8 < 1030 mb: Anticyclonic (A)
- p8 > 1030 mb: Severe anticyclonic (A+)

The selection of p8 was based on it being closest to a center in the Iberian Peninsula grid. We added the severe anticyclonic (A+) type because we detected a much stronger relationship between the near surface temperature lapse rate (NSLR) and A+ days compared with generic anticyclonic situations.

4 Results

Figure 2 shows the daily fluctuations in the Tair and Twb lapse rates during the three ski seasons in the study (Fig. 2a), the frequency distribution of the lapse rates, and the coefficient of correlation between elevation and Tair, Twb, and daily SM hours during each ski season and in each month for the period December–March (Fig. 2b–c). The plots show that there were very large daily fluctuations in the lapse rates and very similar values for Tair and Twb, which averaged − 4.9 and − 5.2 °C km^{-1} (respectively) over the entire study period. During December, the average lapse rates were the least steep (− 2.9 and − 3.1 °C/km, respectively) and the coefficients of correlation were lower than during the other periods of the snow season. January had the most variable lapse rates and coefficients of variation, but the average and median values (approximately − 5 and – 6 °C km^{-1}, respectively) were similar to the values for February and March. The relationship between elevation and snowmaking hours is on average 8.2 h km^{-1}, and the correlations exhibit much lower values compared to Tair and Twb. Both the lapse rates and the correlation coefficients tended to increase during each ski season.

Figure 3 shows the daily number of hours having a Twb value below – 2 °C (bottom plot), calculated from the daily Twb lapse rates at three different elevations in the ski resort (1550, 1900, and 2250 m a.s.l.), and illustrates the effect of average Tair on the lapse rates for SM. This figure also shows that during cold periods, there are no lapse rates because there are conditions for SM throughout the day at the three

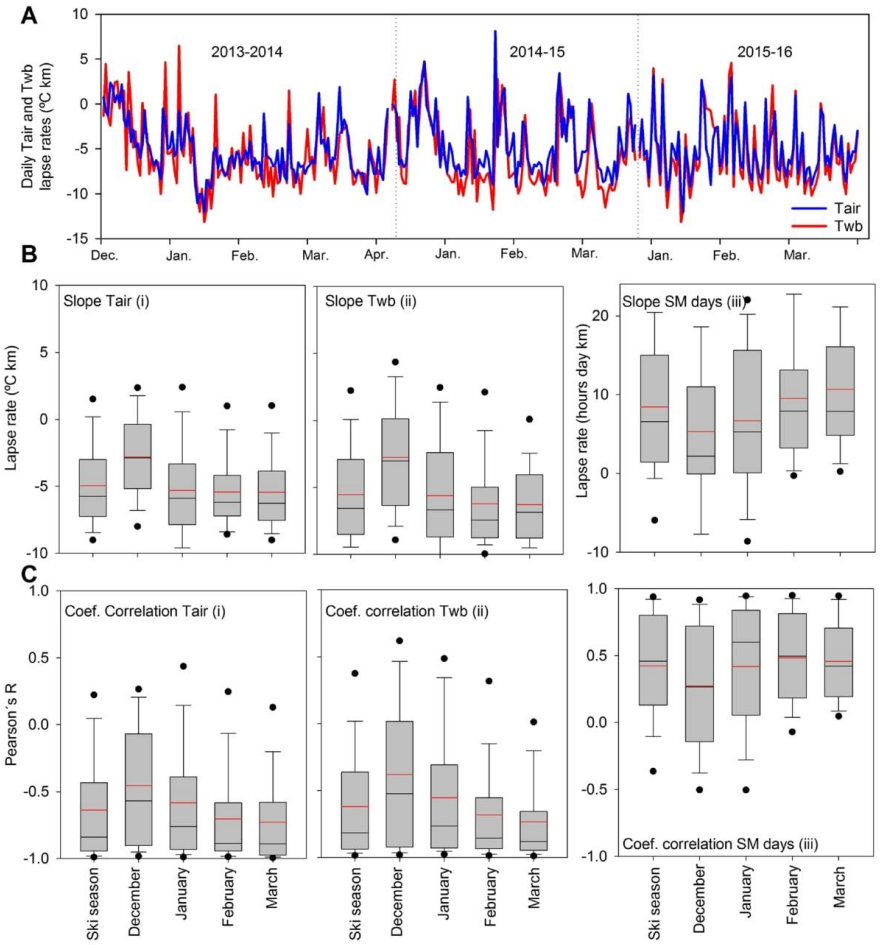

Fig. 2 Average daily Tair and Twb lapse rates for the three ski seasons in the study (**a**); and the frequency distribution of lapse rates (**b**) and the coefficients of correlation (**c**) between elevation and Tair (i), Twb (ii) and SM hours (iii). Horizontal lines indicate the interannual mean (red) and median (black) values, the boxes indicate the 25th and 75th percentiles, the bars indicate the 10th and 90th percentile, and the dots indicate the 5th and 95th percentiles

elevations. However, under warmer Tair conditions, the lapse rates in Twb caused marked differences, with several days having 24 h of SM conditions at 2250 m a.s.l. but only 10–15 h at the lowest elevation. Thus, during warmer days when it was only possible to produce snow for a few hours at the highest elevation, the conditions for snowmaking at lower elevations did not exist. For only a few days during the three snow seasons was snowmaking not possible at any time of the day at 2250 m a.s.l.

Figure 3 also shows that there were a number of days when there were more hours of potential SM at lower elevations than at higher elevations, as a consequence of thermal inversions. On these days, the low Twb temperatures enabled SM at the three elevations. However, on other days, the Twb was more than 2 °C lower in the valleys bottoms compared with the upper slopes. This explains the mismatch between the number of inversion days in Twb and SM shown in Fig. 3.

Table 2 shows the total and monthly frequencies of days when cooling of the snowpack was not significantly ($p < 0.05$) correlated with elevation, and the days when the slope of the linear fit of Tair and Twb (SM) as a function of elevation was positive (negative). For 24 and 28% of the days, respectively, there was no statistically significant correlation of Tair and Twb with elevation. In

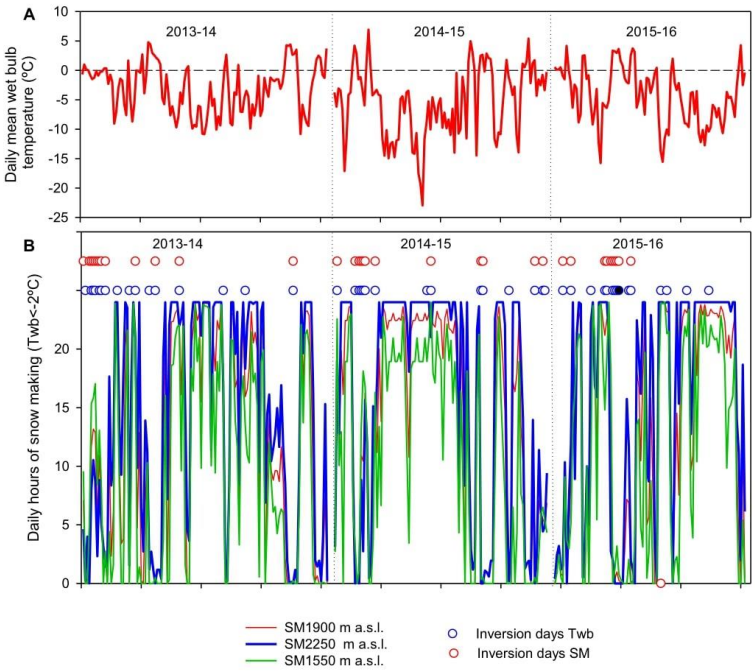

Fig. 3 **a** Daily mean Twb in the ski resort based on data from the 17 installed sensors. **b** Daily number of SM hours (daily hours when Twb < − 2 °C) at 1550 m (green), 1900 m (red), and 2250 m (blue), calculated from the linear relationships between SM and elevation. Blue and red circles indicate days having inverted lapse rates for Twb and SM, respectively

December, the proportion of days (40 and 46%, respectively) when this relationship pertained was greater than during the period from January to March (16–24% for Tair, and 17–18% for Twb). Among those days, only on 11.1 and 11.7% of the days were there inverted elevation lapse rates for Tair and Twb, respectively, with December again having a higher proportion of days (20 and 24%, respectively) having inverted lapse rates for Tair and Twb relative to the period from January to March (< 10% of days having thermal inversions). As noted above, the result for the numbers for SM hours was very different from the cases for Tair and Twb. Thus, for > 50% of the days, there was no statistically significant linear relationship of SM with elevation, but the proportion of those days having inverted lapse rates (9.4%) was less than for Tair and Twb. For SM daily hours, there was a clear reduction in the inverted lapse rate with time during the ski season, with average values of 22, 8.3, 4.7, and 2.2 days per month per year for December, January, February, and March, respectively.

Figure 4 shows the average hourly lapse rates for Tair and Twb calculated for the entire dataset. This shows clear sub-daily variability, with steeper lapse rates during the hours in the middle of the day (from 11:00 a.m. to 15:00 p.m.), when lapse rates were similar to the standard ELR (− 5.9 and − 6.6 °C/km for Tair and Twb, respectively). Furthermore, the lapse rates tended to moderate in the evening and during the night, followed by a steep reduction in the lapse rates from 4:00 a.m. to 8:00 a.m., when the lowest lapse rates during the day were recorded (− 3.6 and − 3.9 °C/km for Tair and Twb, respectively).

Table 2 Total and monthly frequency of days when snowpack does not cool following a statistically significant ($p < 0.05$) relationship with elevation, and the days when the slope of the linear fit of Tair and Twb (SM) is positive (negative)

	% days with no significant correlation with elevation			% days with inverted elevation lapse rate		
	Ta	Twb	SM days	Ta	Twb	SM days
Dec.	40	46	57	20	24.4	22
Jan	24	28	53	8.6	9.6	8.3
Feb.	16	17	49	8.23	7.3	4.7
Mar.	17	20	53	7.8	5.5	2.2
Average	24	28	53	11.1	11.7	9.4

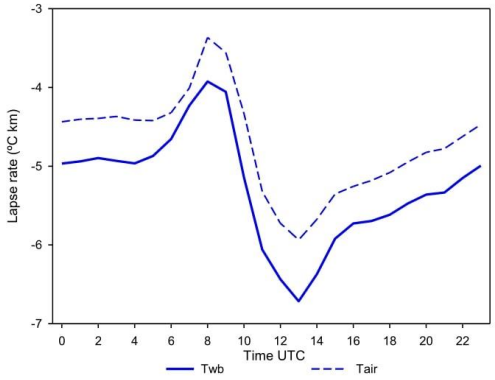

Fig. 4 Total average hourly lapse rates for Tair and Twb. The study area is in zone UTC + 1

Figure 5 shows the correlation of Twb and SM lapse rates with daily WS, RH, and Pat. Statistically significant linear correlations were found for WS, RH, and Pat with Twb ($p < 0.05$), and were clearer for RH ($r = -0.57$) and Pat ($r = 0.48$). Thus, days having lower RH and higher Pat were associated with the lowest Twb lapse rates, and vice versa. The correlation coefficient for WS ($r = -0.37$) indicated that the Twb lapse rate decreased with decreasing WS. The Tair and Twb lapse rates were not correlated ($r = 0.03$). The SM lapse rates showed similar relationships with WS, RH, and Pat as those found for Twb, but because of the many days when the SM lapse rate was 0, the correlation coefficients were lower, resulting in only the correlation with RH being statistically significant ($p < 0.05$; $r = -0.38$).

Figure 6 shows the classification trees for predicting the Twb and SM lapse rates using WS, RH, Tair, and Pat as predictor variables, although Pat was not included in either of the two models. Mean absolute errors (MAEs) of 1.51 °C km^{-1} and 0.0021 h km^{-1} were obtained for Twb and SM, respectively. For the Twb lapse rates, the first classification was based on three classes of WS (≤ 3.8, 3.8–4.7, and > 4.7 m s^{-1}). The days of lowest wind speed were classified into three classes of RH; those having RH < 56.7%, those having the lowest lapse rate (− 2 °C km^{-1}), and those where the lapse rates increased with increasing RH. Those days in the windiest class (WS > 4.7 m s^{-1}) and having high RH (> 84%) were associated with the highest predicted Twb lapse rates (mean value 9 °C km^{-1}).

The classification tree for SM hours also presents the first split based on WS, but with a lower threshold than for Twb (classifying days having WS values less than and greater than 2.9 m s^{-1}). The days having very low WS and low RH (≤ 44.5%) values had a low lapse rate (1 h km^{-1}), with the slope of the SM lapse rate increasing as RH increased (up to 14 h km^{-1} for RH > 85.4%). For days having low WS (< 2.9 m s^{-1}) and medium RH (44.5–84.5%), those having Tair > 0.6 °C had very low lapse rates, so it is unlikely that snow could be made at any elevation. For days having WS > 2.9 m s^{-1} and RH > 85.4%, the SM lapse rate average was 16 h km^{-1}. For days having high WS but low RH (≤ 30.7%), the average lapse rate was 3 h km^{-1}. Days having intermediate RH (30.7–85.4%) were highly dependent on Tair; very low SM lapse rates were found for the coldest days (Tair < − 3.4; 1 h km^{-1}), intermediate SM lapse rates were found when Tair ranged from − 3.4 to − 1.5 °C (6 h km^{-1}), and very high lapse rates were found for days warmer than − 1.5 °C (14 h km^{-1}).

Figure 7a–c shows the averages and standard deviations for the three main explanatory variables (WS, RH, and Tair) identified in the tree models, and the Tair, Twb, and SM lapse rates associated with the various circulation weather types (CWTs) for the Iberian Peninsula during the study period (Fig. 7d). This shows that the CWTs strongly influenced the lapse rates in the ski area. Thus, the lowest WS (2.5–3 m s^{-1}) and RH (40–45%) conditions occurred under the E, SE, and S CWTs. During A weather type conditions, the WS was also very low (2.9 m s^{-1}), increasing to 3.9 m s^{-1} during A+ conditions; but low RH (45%) was associated with the A+ type, and mean RH of 59% was associated with the A type. This explains why the days on which SE, E, S, A+, and A CWTs occurred had (in increasing order of importance) the lowest Tair and Twb lapse rates. In addition, these CWTs were also associated with the warmest daily mean Tair values (Fig. 7c), all of which were > 0 °C; this also explains the lowest lapse rates for SM. The SE weather type was associated with the most moderate lapse rates for Tair, Twb, and SM. In contrast, in descending order the highest mean WSs (3.8–4.7 m s^{-1}) occurred during N, NW, NE, W, and C CWTs, while the W, NW, C, N, and NE types were associated the highest RH conditions (from 81 to 62%, in descending order). The combination of these two variables resulted in the N, NW, and NE CWTs being associated with the steepest Tair and Twb lapse rates (with values very similar to the standard ELR of − 6.5 °C km^{-1}); high but slightly lower lapse rates also occurred during W and C conditions. The lowest Tair in the ski area occurred during advections from the N and NW, but the standard deviations indicated large variability. The Tair values (> or approximately 0 °C) during C, W, and NE weather types were considerably higher than those associated with N and NW CWTs, resulting in the steepest SM lapse rates occurring during C days, followed by days under W, NW, and NE weather types.

Figure 8a shows the percentage of days for each weather type when Tair, Twb, and SM lapse rates exhibited inversions. A 25–40% of the days under SE, E, and S weather types, and almost 20% of the days under A and A+ types, there was warming and reduced potential for artificial snow production with increasing elevation. However, as the A and A+ weather types were much more common than the E, SE, and S types

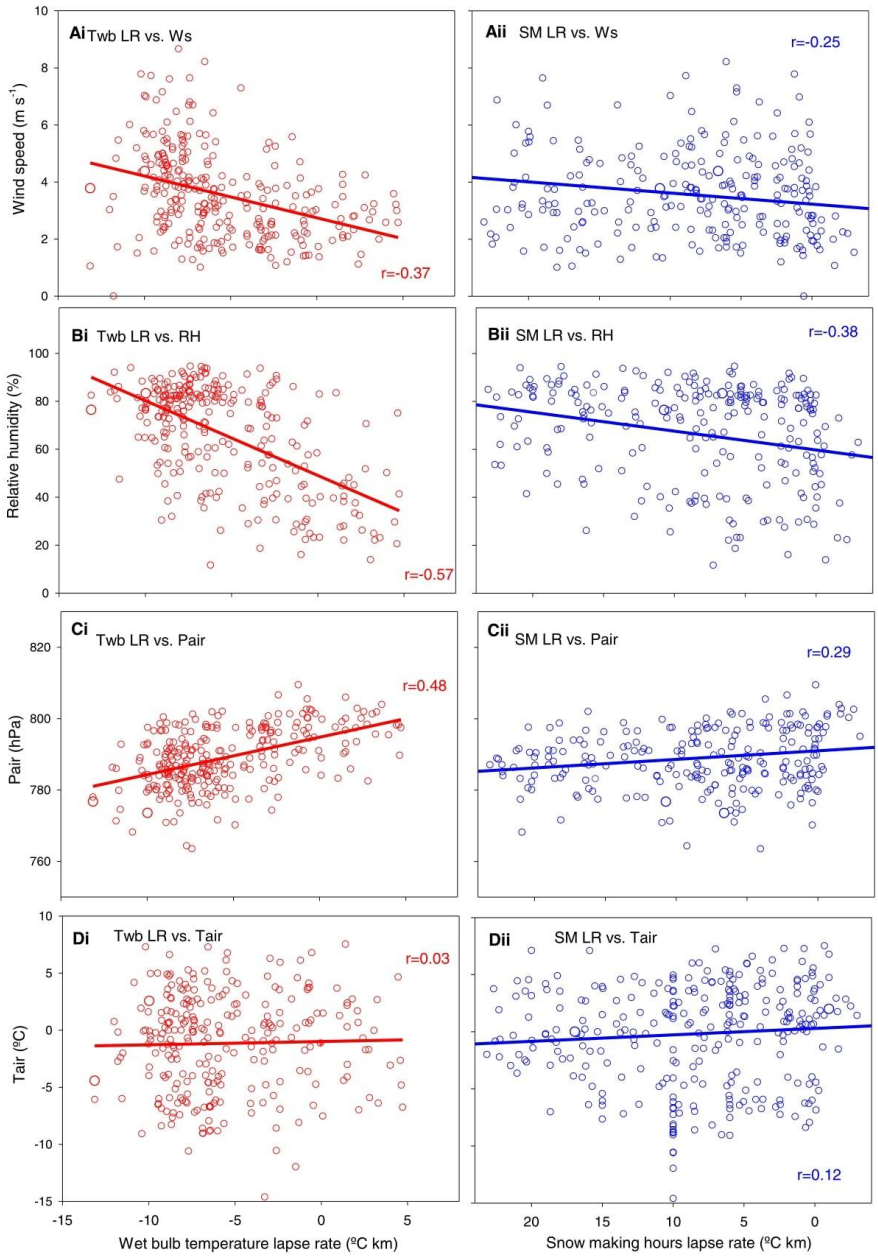

Fig. 5 Correlations of wet bulb temperature (Twb; i) and daily snowmaking hours (SM; ii) lapse rates with daily (A) wind speed (Ws), (B) relative humidity (RH), (C) atmospheric pressure (Pair), and (D) air temperature (Tair)

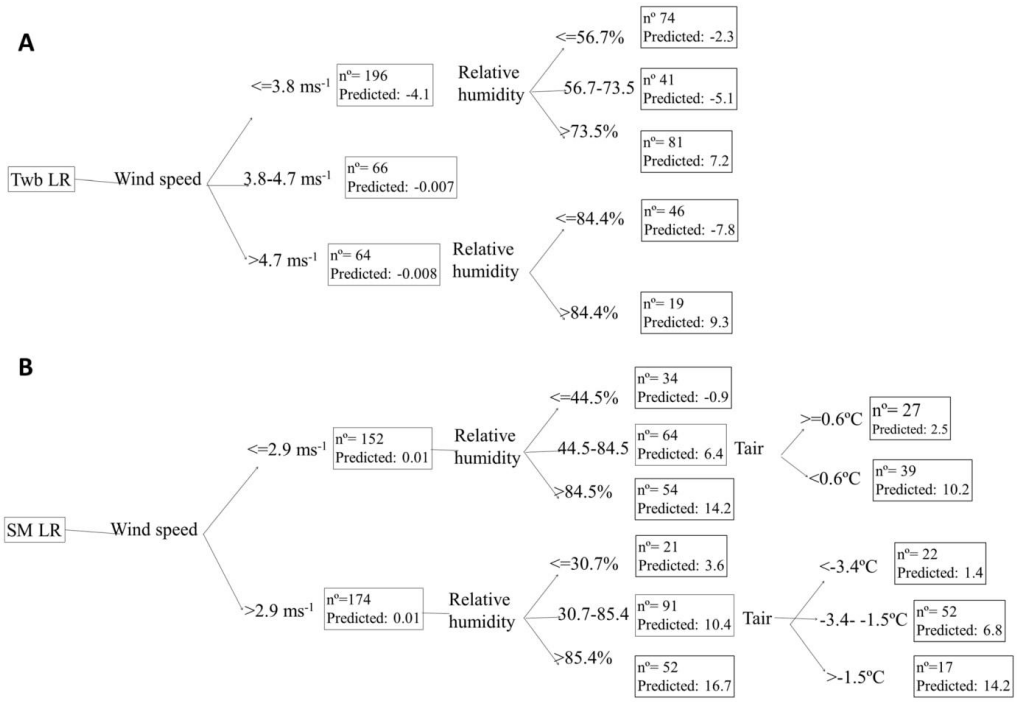

Fig. 6 Tree classification models for predicting the Twb and SM lapse rates (Twb LR and SM LR, respectively), based on the variables WS, RH, and Pat. N° is the number of data points at each node. Terminal nodes are framed in a thick line

(Fig. 8b), by far, the majority of the thermal (Tair and Twb) and SM inversions were associated with A and A+ weather types. Thus, 35 and 23% of the SM inversions were observed under A and A+ weather types, respectively, whereas the SE, S, SW, E, and W types were associated with only 16, 12, 9, and 5%, respectively, of the total SM inversions during the three ski seasons in the study.

5 Discussion

This study showed that Tair and Twb lapse rates were subject to strong sub-daily and daily variability in the Formigal ski area from December to March during the 2012–13, 2013–14, and 2014–15 ski seasons. The Tair and Twb lapse rates showed almost the same daily fluctuations, and the long-term average for both was well below the average standard environmental lapse rate for dry temperature (− 6.5 °C km^{-1}), with the Twb lapse rate (− 5.2 °C km^{-1}) being slightly steeper than the Tair lapse rate (− 4.9 °C km^{-1}). The Twb lapse rate controlled the elevation dependence of SM, but SM was also strongly controlled by Tair because for very cold and very warms days the SM lapse rate was close to 0 independently of the Twb lapse rate. For this reason, the correlation coefficients between elevation and SM were considerably lower than those for Tair and Twb. The average SM lapse rate was 8 h km^{-1}, reflecting marked differences in the potential for production of artificial snow within the ski resort. The study also identified that there were a number of days where an inversion in the lapse rate occurred with increasing Tair and Twb (11.1 and 11.7% of the studied days, respectively), and a decrease of SM occurred with elevation (9.4% of the days).

Because this study focused only on the ski season (from December to March), it did not identify clear monthly variability in the Tair and Twb lapse rates, as has been reported in many studies based on the entire year (Roland et al. 2002; Tang and Fang 2006); these studies have generally shown that the weakest gradients occur in winter (Blanford et al. 2008; Kirchner et al. 2013; Kattel et al. 2015). Nonetheless, December had by far the least steep air temperature lapse rate and the highest number of thermal inversions. The SM lapse rate is closely related to Tair, but showed more marked monthly changes than the Tair and Twb lapse rates, and increased continuously from December to March as Tair progressively increased. The strong SM lapse rates that occurred in March (10.3 h km^{-1}) suggest that at the end of the snow season, this

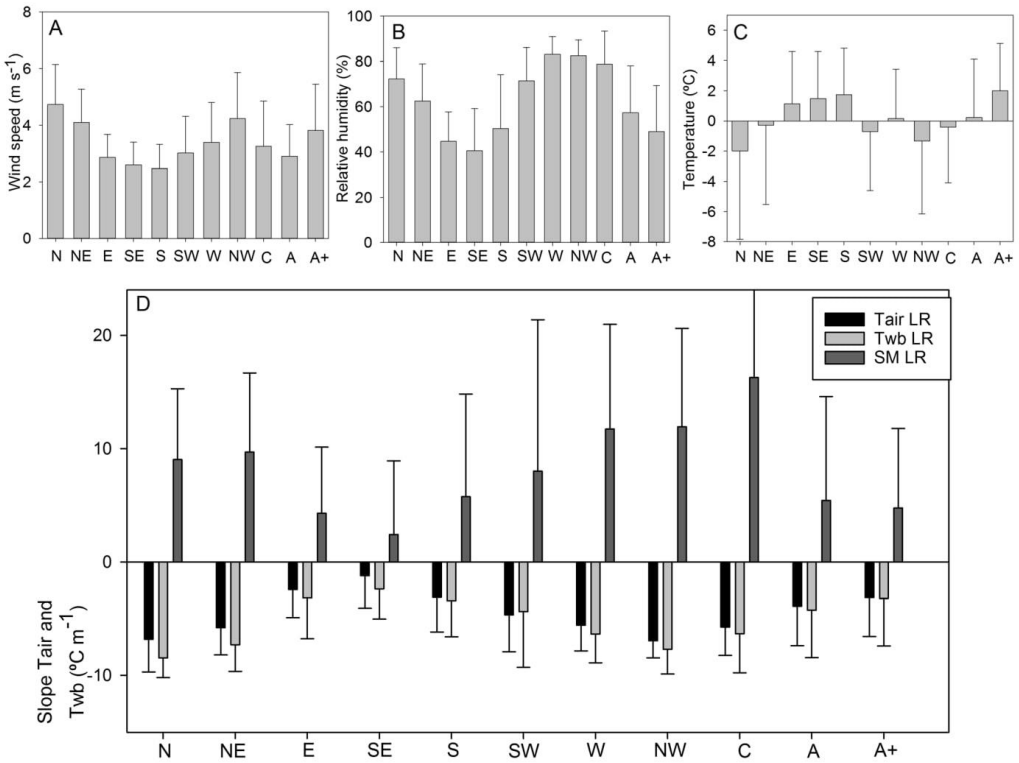

Fig. 7 Average (bars) and standard deviation (whiskers) for WS (**a**), RH (**b**), Tair (**c**), and the Tair, Twb, and SM lapse rates (**d**) for various weather types over the Iberian Peninsula

measure is useful at high elevations, but of very limited value for lower parts of the ski area, which are the most problematical for skiing because of the shallow snowpack (Gilaberte et al. 2017). We also found considerable diurnal variability in the Tair and Twb lapse rates; this needs to be taken into consideration when estimating SM productivity, as the weakest lapse rates occurred during the midnight to early morning period, when usually more artificial snow is produced.

The marked daily variability of the Tair and Twb lapse rates showed strong negative linear correlations with relative air humidity and wind speed, with the most humid and windiest days exhibiting the steepest rates. Similar relationships have been found for Tair lapse rates in other geographic areas. Thus, Kattel et al. (2013, 2015) reported that the difference between wet and dry air conditions was the most important factor controlling the near-surface lapse rates in the Himalayas. Pepin et al. (1999) and Li et al. (2013) also reported a negative relationship between lapse rates and relative humidity in northern England and China, respectively. Negative relationships between WS and Tair lapse rates have been reported for the Swiss Alps (Kirchner et al. 2013) and the Pyrenees (Pages and Miro 2010). Atmospheric pressure (Pat) was also strongly positively correlated with the Tair and Twb lapse rates. This variable also exhibited high collinearity with RH and WS, so seems to be redundant in explaining the temporal dynamics of lapse rates when information on RH and WS is available. However, it may be a useful indicator of temporal fluctuations in lapse rates in regions where limited meteorological information is available, as Pat tends to exhibit a relatively homogeneous behavior over large areas, including in complex topography, and where reliable gridded datasets covering long-term periods are available (Allan and Ansell 2006). The temporal dynamics of the SM lapse rates was more complex. Thus, correlations with meteorological variables were lower than Twb because the average Tair in the ski resort led to 0 or 24 SM hours independently of the magnitude of the atmospheric variables.

A regression tree model enabled reliable classification of days into groups (nodes) according to various thresholds of RH and WS that had similar Twb lapse rates. This type of

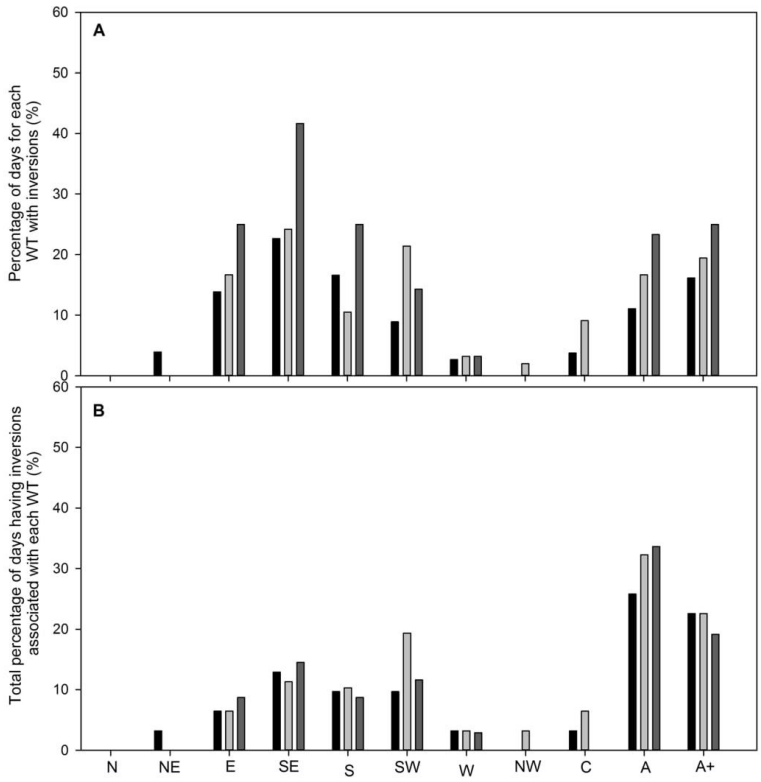

Fig. 8 Percentage of days for each weather type with inversions in the Tair, Twb, and SM relationship with elevation (**a**); and the total percentage of days having inversions associated with each weather type (**b**)

classification may be useful for managers of ski areas in estimating the spatial distribution of SM effectiveness, based on short-term weather forecasts.

Tair was a good predictor of the temporal fluctuation of SM hours lapse rates. The regressions tree models used Tair to identify which days having steep Twb lapse rates led to strong elevational differences in SM hours, and which days had an SM lapse rate of 0 as a consequence of sufficiently cold or warm conditions, ensuring successful SM throughout the ski area.

This study also confirmed that weather types (CWTs) tightly control RH, WS, and Tair at the Formigal ski resort. Thus, major differences in the Tair, Twb, and SM lapse rates occurred in the study area, depending on the CWTs. Knowledge of the characteristics of the air masses associated with different CWTs has previously been identified as useful in understanding the temporal dynamics of air temperature lapse rates (Blanford et al. 2008; Holden and Rose 2011; Kirchner et al. 2013).

We found that the SE weather type was associated with the lowest RH and WS, and high temperature explained the most moderate Tair, Twb, and SM lapse rates. The E, SE, S, A, and A+ weather types shared the same conditions, with obvious shadings, mentioned for SE. The A and A+ types are among the most common weather types over the Iberian Peninsula during the winter months (López-Moreno and Vicente-Serrano 2007; Navarro-Serrano and López-Moreno 2017), which explains why winter lapse rates are much less than the standard average ELR (−6.5 °C km^{-1}), and that the majority of thermal inversions at Formigal (and in the Pyrenees) are because of the occurrence of anticyclonic periods (Pepin and Kidd 2006), which are particularly persistent in December and early January (Pages and Miró 2010). Cyclonic systems and advections from the N, NW, NE cause the windiest, most humid, and coldest conditions. Thus, the steepest Tair and Twb lapse rates were observed during N and NW weather types, followed by NE and cyclonic conditions, while the steepest lapse rates for SM occurred during C, W, NE, and NW weather types, when Tair was higher than during the N weather type, or the lapse rates exhibited large variability associated with marked elevational differences in SM production.

As the occurrence of CWTs over a given area is normally controlled by hemispheric-scale atmosphere circulation, strong interannual differences occur for the most common CWTs (Buisan et al. 2015). This may be one of the main explanations for the significant differences reported in year to year Tair lapse rates (Holden and Rose 2011). Thus, the availability of multi-year detailed datasets is necessary to fully understand the dynamics of regional-based lapse rates.

6 Conclusions

This study shows that the dynamics of Tair lapse rates must be understood to enable analysis of Twb lapse rates and assessment of spatial differences in the potential for snowmaking within a ski resort. At the Formigal ski resort, an increase in elevation of 1000 m caused average cooling of 4.9 and 5.2 °C for Tair and Twb, respectively, equating to 8-h difference in artificial snow production per day. The lapse rates for Tair, Twb, and SM showed strong diurnal, daily, and monthly variability, mostly driven by variability in relative humidity and wind speed (both negatively correlated with lapse rates); these parameters were closely related to the weather types dominating at the synoptic scale. The smoothest lapse rates occurred under advections from the southeast, and to a lesser extent from the east and south and under anticyclonic conditions. The steepest Tair and Twb lapse rates were observed during north and northwest advections, while the steepest rates for SM were observed during days involving cyclonic circulation and advections from the northeast. Identification of the relationships of meteorological and synoptic conditions to the magnitude of the lapse rates provides useful information enabling ski area managers to forecast the short-term potential for production of artificial snow. Decadal variability in atmospheric circulation patterns may impact on the magnitude of Tair and Twb. In addition, the lapse rates for snowmaking are also dependent on air temperature. Thus, the climate warming projected for the majority of mountain areas is likely to have a major effect on the overall capacity to produce artificial snow, but will also increase the spatial heterogeneity for potential snowmaking.

Acknowledgements We thank the ski resort of Formigal for its support in this research.

Funding information This study was funded by the research project CGL2014-52599-P "Estudio del manto de nieve en la montaña española y su respuesta a la variabilidad y cambio climatico" (Ministry of Economy and Development, MINECO).

References

Allan R, Ansell T (2006) A new globally complete monthly gridded mean sea level pressure dataset (HadSLP2): 1850-2004. J Clim 19:5816–5842

Blandford TR, Humes KS, Harshburger BJ, Moore BC, Walden VP, Ye H (2008) Seasonal and synoptic variations in near-surface air temperature lapse rates in a mountainous basin. J Appl Meteorol Climatol 47(1):249–261

Breiman L, Friedman JH, Olshen RA, Stone CJ (1984) Classification and regression trees. Chapman and hall, New York

Brutsaert W (1998) Land-surface water vapor and sensible heat flux: spatial variability, homogeneity, and measurement scales. Water Resour Res 34(10):2433–2442. https://doi.org/10.1029/98WR01340

Buisan S, Saz MA, López-Moreno JI (2015) Spatial and temporal variability of winter snow and precipitation days in the western and central Spanish Pyrenees. Int J Climatol 35:259–274

Fassnacht SR, Heun CM, López-Moreno JI, Latron J (2010) Variability of snow density measurements in the Esera valley, Pyrenees mountains, Spain. Cuadernos de Investigación Geográfica 36(1):59–72

Frederick JE (2008) Principles of atmospheric Science. Ed. Jones and Bartlett. Massachusets, 199 p

Gardner AS, Sharp MJ, Koerner RM, Labine C, Boon S, Marshall SJ, Burgess DO, Lewis D, Gardner AS, Sharp MJ, Koerner RM, Labine C, Boon S, Marshall SJ, Burgess DO, Lewis D (2009) Near-surface temperature lapse rates over Arctic glaciers and their implications for temperature downscaling. J Clim 22(16):4281–4298

Gilaberte M, Pino MR, López F, López-Moreno JI (2014) Impacts of climate change on ski industry. Environ Sci Policy 44:51–66

Gilaberte M, López-Moreno JI, Morán-Tejeda E, Jerez S, Alonso-González E, López-Martín F, Pino-Otín MR (2017) Assessment of ski condition reliability in the Spanish and Andorran Pyrenees for the second half of the 20th century. Appl Geogr 70:127–142

Goodess CM, Palutikof JP (1998) Development of daily rainfall scenarios for southeast Spain using a circulation—type approach to downscaling. Int J Climatol 18(10):1051–1083

Heynen M, Miles E, Ragettli S, Buri P, Immerzeel W, Pellicciotti F (2016) Air temperature variability in a high-elevation Himalayan catchment. Ann Glaciol 57(71):212–222

Holden J, Rose R (2011) Temperature and surface lapse rate change: a study of the UK's longest upland instrumental record. Int J Climatol 31(6):907–919

Jenkinson AF, Collison P (1977) An initial climatology of Wales over the North Sea. In synoptic climatology branch Memorandum, 62

Jones PD, Hulme M, Briffa KR (1993) A comparison of Lamb circulation types with an objective classification scheme. Int J Climatol 13(6):655–663

Kattel DB, Yao T, Yang K, Tian L, Yang G, Joswiak D (2013) Temperature lapse rate in complex mountain terrain on the southern slope of the central Himalayas. Theor Appl Climatol 113(3–4):671–682

Kirchner M, Faus-Kessler T, Jakobi G, Leuchner M, Ries L, Scheel H-E, Suppan P (2013) Altitudinal temperature lapse rates in an Alpine valley: trends and the influence of season and weather patterns. Int J Climatol 33(3):539–555

Lasanta T, Laguna M, Vicente-Serrano SM (2007) Do tourism-based ski resorts contribute to the homogeneous development of the mediterranean mountains? A case study in the Central Spanish Pyrenees. Tour Manag 28:1326–1339

Lindberg K, Andersson TD, Dellaert BGC (2001) Tourism development: assessing social gains and losses. Ann Tour Res 28:1010–1030

López-Moreno JI, Vicente-Serrano SM (2007) Atmospheric circulation influence on the interannual variability of snow pack in the Spanish Pyrenees during the second half of the 20th century. Hydrol Res 38(1):33–44

López-Moreno JI, Goyette S, Beniston M (2009) Impact of climate change on snowpack in the Pyrenees: horizontal spatial variability and vertical gradients. J Hydrol 374(3–4):384–396

López-Moreno JI, Pomeroy J, Revuelto J, Vicente-Serrano SM (2013) Response of snow processes to climate change: spatial variability in

a small basin in the Spanish Pyrenees. Hydrol Process 27(18):2637–2650

López-Moreno JI, Gascoin S, Herrero J, Sproles EA, Pons M, Hanich L, Boudhar A, Musselman KN, Molotch NP, Sickman J, Pomeroy J (2017) Different sensitivities of snowpack to warming in Mediterranean climate mountain areas. Environ Res Lett 12:074006

Marshall SJ, Sharp MJ, Burgess DO, Anslow FS (2007) Near-surface-temperature lapse rates on the Prince of Wales Icefield, Ellesmere Island, Canada: implications for regional downscaling of temperature. Int J Climatol 27(3):385–398

Minder JR, Mote PW, Lundquist JD (2010) Surface temperature lapse rates over complex terrain: lessons from the Cascade Mountains. J Geophys Res 115(D14):D14122

Molotch NP, Colee MT, Bales RC, Dozier J (2005) Estimating the spatial distribution of snow water equivalent in an alpine basing using binary regression tree models: the impact of digital elevation data and independent variable selection. Hydrol Process 19:1459–1479

Navarro-Serrano FM, López-Moreno JI (2017) Spatio-temporal analysis of snowfall events in the Spanish Pyrenees and their relationship to atmospheric circulation. Cuadernos de Investigación Geográfica/geographical Res Lett 43(1):233–254

Nunez M, Calhoun EA (1986) A note on air temperature lapse rates on Mount Wellington, Tasmania. Pap Proc R Soc Tasm 12012(120): 11–15

Pagès M, Miró JR (2010) Determining temperature lapse rates over mountain slopes using vertically weighted regression: a case study from the Pyrenees. Meteorol Appl 17(1):53–63

Pepin N (2001) Lapse rate changes in northern England. Theor Appl Climatol 68:1–2), 1–16

Pepin N, Kidd D (2006) Spatial temperature variation in the Eastern Pyrenees. Weather 61(11):300–310

Pepin NC, Lundquist JD (2008) Temperature trends at high elevations: patterns across the globe. Geophys Res Lett 35:L14701

Pons M, López-Moreno JI, Rosas-Casals M, Jover E (2015) The vulnerability of Pyrenean ski resorts to climate-induced changes in the snowpack. Clim Chang 131(4):591–605. https://doi.org/10.1007/s10584-015-1400-8

Revuelto J, López-Moreno JI, Azorin-Molina C, Vicente-Serrano SM (2014) Topographic control on snowpack distribution in a small catchment in the central Pyrenees: intra- and inter-annual persistence. Cryosphere 8(5):1889–2006

Revuelto J, Azorin-Molina C, Alonso-González E, Sanmiguel-Vallelado A, Navarro-Serrano F, Rico I, López-Moreno JI (2017) In situ observations of meteorological variables and snowpack distribution at the Izas Experimental Catchment (Spanish Pyrenees): the importance of high quality data in sub-alpine ambients. Earth Syst Sci Data 9:993–1005. https://doi.org/10.5194/essd-9-993-2017

Rixen C, Teich M, Lardelli C, Gallati D, Pohl M, Pütz M, Bebi P (2011) Winter tourism and climate change in the Alps: an assessment of resource consumption, snow reliability, and future snowmaking potential source. Mt Res Dev 31(3):229–236

Roland C (2003) Spatial and seasonal variations of air temperature lapse rates in Alpine regions. J Clim 16(7):1032–1046

Scott D, Hall CM, Gössling S (2012) Tourism and climate change: impacts, adaptation and mitigation. Routledge, London

Spandre P, François H, Thibert E, Morin S, George-Marcelpoil E (2017) Determination of snowmaking efficiency on a ski slope from observations and modelling of snowmaking events and seasonal snow accumulation. Cryosphere 11:891–909. https://doi.org/10.5194/tc-11-891-2017

Steiger R, Mayer M (2008) Snowmaking and climate change: future options for snow production in Tyrolean ski resorts. Mt Res Dev 28(3–4):292–298

Stull R (2011) Wet-bulb temperature from relative humidity and air temperature. J Appl Meteorol Climatol 50:2257–2269

Tang ZY, Fang JY (2006) Temperature variation along the northern and southern slopes of Mt. Taibai, China. Agric For Meteorol 139(3–4): 200–207

Thayyen RJ, Gergan JT, Dobhal DP (2005) Lapse rate of slope air temperature in a Himalayan catchment—a study from Dingad (Dokriani Glacier) basin, Garhwal Himalaya, India. Bull Glaciol Res 22:19–25

Trigo RM, Dacamara CC (2000) Circulation weather types and their influence on the precipitation regime in Portugal. Int J Climatol 20:1559–1581

Uhlmann B, Goyette S, Beniston M (2009) Sensitivity analysis of snow patterns in Swiss ski resorts to shifts in temperature, precipitation and humidity under conditions of climate change. Int J Climatol 29: 1048–1055

Capítulo 8

CONCLUSIONES Y TRABAJOS FUTUROS

En último lugar, este capítulo trata de dar sentido explicativo al conjunto de la Tesis Doctoral, armonizando coherentemente las diferentes conclusiones obtenidas, procediendo a realizar una valoración general de las aportaciones realizadas sobre el comportamiento de la temperatura del aire superficial en áreas de montaña. Los resultados de las diferentes investigaciones han permitido sintetizar una serie de conclusiones generales y específicas, discutidas previamente en cada uno de los capítulos correspondientes. De la misma forma, se plantean líneas futuras de investigación, que estarán dirigidas a profundizar en el conocimiento de esta variable, y a aplicarlo posteriormente en las actividades humanas.

8.1. Conclusiones generales

La Ordenación del Territorio y el Medio Ambiente, recordemos, implican el conocimiento exhaustivo del Medio que nos rodea y determina como sociedad, influyendo activamente en las actividades humanas. De esta forma, mediante el conocimiento del Medio podremos analizar de forma integral las debilidades, amenazas, fortalezas y oportunidades que nos marca el territorio.

En este sentido, el sistema climático es uno de los principales elementos que incide en el territorio y en las actividades que en él llevamos a cabo los seres humanos. Variables como la temperatura del aire, las precipitaciones, la intensidad y dirección de los vientos, o la mayor o menor frecuencia de inundaciones, sequías o temporales, tienen una influencia directa sobre las actividades que se dan en el territorio y, por tanto, deberían tenerla sobre la ordenación territorial realizada con un prisma medioambiental. Entre estas variables, la presente Tesis Doctoral ha analizado una de ellas, como es la temperatura del aire superficial, que hemos presentado como una variable influyente sobre la gestión de los recursos hídricos, las demandas agrícolas, la producción hidroeléctrica o las actividades económicas basadas en el clima (estaciones de esquí, turismo de sol y playa, deportes de aventura, etc.). La temperatura del aire es, a su vez, influyente sobre cuestiones indirectas como el consumo energético, los desplazamientos estacionales hacia zonas más benévolas meteorológicamente o la presión urbanística generada en zonas muy concretas del territorio peninsular.

La presente Tesis Doctoral pretende analizar, bajo diferentes miradas o escalas espaciales, los factores explicativos de la distribución espacio-temporal de la temperatura del aire superficial, así como su compleja relación con la altitud, que no es tan fija como la literatura tradicional ha presentado. Estas pretensiones se han intentado cumplir mediante el uso de diferentes fuentes de información, desde las procedentes de Redes Oficiales de Observación Meteorológica (gestionadas por organismos estatales como AEMET, INAMHI y SENAMHI), hasta las fuentes producidas por el propio Grupo de Investigación de Hidrología Ambiental (IPE – CSIC) mediante trabajo de campo e instrumental propio.

Sin embargo, pese a la necesidad de datos para llegar a conclusiones rigurosas, estos no siempre son suficientes ni de la calidad y representatividad exigida, con lo que es posible que, debido a la complejidad topográfica de los ámbitos montañosos, no se haya podido captar toda la variabilidad espacial posible, por lo que será necesario seguir profundizando en esta cuestión en el futuro. A pesar de ello, las diferentes metodologías y técnicas empleadas, así como las distintas variables que han sido analizadas, han permitido avanzar y profundizar en el conocimiento del

comportamiento de la temperatura del aire superficial en áreas montañosas, de tal forma que es posible asegurar que este trabajo ha contribuido activamente a dicha profundización, especialmente sobre la España Peninsular y, en cierta medida, sobre los Andes de Ecuador y Perú.

En este sentido, una de las principales conclusiones generales que se han obtenido por la presente Tesis Doctoral es que los factores que explican el comportamiento de la temperatura del aire superficial en estos ámbitos son múltiples, y su peso varía en función de la escala de trabajo analizada, lo cual era una de las hipótesis de trabajo originales, y por la cual se planteó una Tesis Doctoral con la estructura presentada: estudios regionales frente a estudios locales.

De este modo, a escala regional, además de la altitud, son la latitud, la continentalidad o la distancia al mar los factores que influyen activamente en la distribución espacio-temporal de las temperaturas. Sin embargo, los ambientes montañosos son complejos, y aunque el enfoque con el que los analicemos sea de escala regional, eso no va a impedir que sigan existiendo procesos y fenómenos locales que siguen afectando a las localizaciones concretas de los observatorios, pudiendo generar ciertos artefactos o ruidos si analizamos únicamente a una escala regional. Un ejemplo de esta situación se ha obtenido en el trabajo regional sobre la región andina de Ecuador y Perú, en la que se han medido gradientes nocturnos más intensos que los diurnos, algo difícilmente explicable a no ser que realicemos un estudio local de las características topográficas de los observatorios más elevados. Por eso ha sido necesaria la inclusión de estudios a escala local, que permitieran analizar en profundidad zonas topográficamente complejas y huir así de la infrarrepresentación de las zonas montañosas, aspecto detectado con claridad en las redes oficiales de observación meteorológica.

A escalas locales, los factores explicativos regionales citados anteriormente pierden fuerza, puesto que estos se mueven en rangos espaciales más amplios que las zonas de estudio analizadas, con lo que no generan diferencias entre los observatorios. Sin embargo, aparecen activamente otros factores como las posiciones topográficas (en fondos de valle, en cumbre o en ladera), la insolación diferencial entre laderas de solana o de umbría, las horas diarias de sol, el tipo de superficie (bosque, suelo desnudo o nieve), o la cercanía a edificaciones, que determinan las diferencias térmicas en distancias muy reducidas, pudiendo establecerse diferencias de temperatura casi aberrantes en escasos metros en función de algunos de estos factores explicativos.

Sin embargo, también se han encontrado factores transversales, que influyen en la distribución espacio-temporal de la temperatura del aire superficial a lo largo de las diferentes escalas

espaciales. Uno de estos factores transversales es la estacionalidad, la cual determina multitud de aspectos, como la mayor o menor cantidad de insolación recibida, la importancia de la orientación y la exposición solar, o su posición topográfica, pero también afecta en otro factor transversal como son las situaciones sinópticas. Este último es un factor dependiente de la circulación atmosférica, y se plasma en los diferentes tipos de tiempo atmosférico que afectan a un territorio, los cuales generan diferencias entre observatorios potenciando unos fenómenos u otros. De esta forma, la estabilidad anticiclónica va a propiciar el debilitamiento de los gradientes nocturnos, mientras que la inestabilidad y las precipitaciones provocarán el efecto contrario. La clasificación de tipos de tiempo se ha presentado como una síntesis muy válida del estado de la atmósfera, ya que permiten clasificar una gran cantidad de variables meteorológicas en una única categoría que, eso sí, debe ser correctamente discutida. Por tanto, las interrelaciones entre factores explicativos dan como resultado que la temperatura del aire superficial sea una variable de compleja distribución espacio-temporal en los ámbitos de montaña, y que exige un estudio concienzudo en función de cada área de estudio, no pudiendo establecer reglas y normas genéricas obtenidas en otra región diferente.

Esto da como resultado que aquellas actividades humanas que dependan de la distribución espacio-temporal de las temperaturas deban profundizar intensamente en el conocimiento de esta variable para poder conocer su propia vulnerabilidad, y poderse adaptar a condiciones futuras. Es el caso de las estaciones de esquí de las montañas pirenaicas, que debido a la variabilidad del clima mediterráneo, así como a su escasa altitud, se encuentran a expensas de la variabilidad meteorológica, que puede obligar a cerrar completamente complejos invernales debido a la falta de nieve. Para afrontar esa situación, la gran mayoría de estos establecimientos de buena parte del mundo han tratado de producir nieve artificial, pero esta tecnología depende al completo de la temperatura del aire, así como de otras variables. Esta tecnología permite reducir el riesgo producido por la falta de precipitaciones, pero no aleja el riesgo de la subida de las temperaturas, tal y como se ha mostrado en el trabajo de Formigal (Capítulo 7), donde las pistas a menor altitud podrían sufrir las consecuencias si se dieran los peores escenarios de cambio climático, situación que afectaría a muchas otras estaciones de latitudes medias. Todo este conocimiento permitirá al sector del esquí conocer con cuánta urgencia deben adaptarse a escenarios futuros, ya sea mediante la modernización tecnológica, o por el desplazamiento de las zonas de explotación.

La conclusión general que podemos obtener de todo esto es que la temperatura del aire superficial no es una variable tan sencilla como podríamos creer en las primeras fases del trabajo de Tesis Doctoral, tal y como pudimos incluso publicar en la introducción del primer artículo del

compendio (Capítulo 3), y mucho menos en áreas de topografía compleja. De este modo, no se recomienda la histórica simplificación del "clima de montaña", ni tampoco la común relación entre temperatura y altitud de -6.5º C km^{-1}, que lleva a una idea confusa de que la interpolación y extrapolación de observaciones temperatura no tiene mucha complicación. La temperatura del aire superficial es una variable crucial y extremadamente compleja, tal y como se ha demostrado. Además, debemos tener en cuenta un aspecto añadido como es la forma de medición de la temperatura en estos ámbitos, ya que la falta de observatorios oficiales nos ha obligado a instalar nuestros propios dispositivos para poder aumentar la representatividad de nuestra red de observación. De este modo, es posible que se hubieran producido errores en la forma de medición, por lo que los resultados experimentales obtenidos pueden arrojar algo de luz a la hora de los diseños experimentales de trabajos futuros sobre ámbitos montañosos.

8.2. Conclusiones específicas

En las siguientes líneas quedan recogidas las conclusiones derivadas de los objetivos específicos que se indicaron previamente en el Capítulo 1 (véase Sección 1.4.2 Objetivos):

Analizar el comportamiento espacio-temporal de la temperatura del aire superficial a escala regional sobre la España Peninsular, prestando especial atención a las principales regiones montañosas y a factores como la circulación atmosférica y la continentalidad (Capítulo 3).

- Los gradientes basados en temperaturas medias diarias fueron más débiles que el gradiente ambiental promedio (MELR) de -6.5º C km^{-1}, que es el empleado tradicionalmente en el modelado de temperatura del aire. Además, estos gradientes variaron espacio-temporalmente, teniendo una estrecha relación con las condiciones sinópticas, sintetizadas mediante la clasificación de tipos de tiempo. Los valores promedio de todas las subregiones montañosas de la España Peninsular fueron más débiles que el MELR, oscilando entre los -4.83º C km^{-1} de los Sistemas Béticos a los -5.79º C km^{-1} del Ibérico. El valor para el conjunto de la España Peninsular fue de -5.28º C km^{-1}. Los gradientes más intensos tuvieron lugar en primavera y otoño para la España Peninsular; en primavera y primeros de verano en los Pirineos, Sistema Central e Ibérico; y en otoño y primeros de invierno para el Cantábrico y los Sistemas Béticos.
- La clasificación de tipos de tiempo ha permitido detectar que los tiempos anticiclónicos y del sur-sureste favorecen las inversiones térmicas y el debilitamiento de los gradientes, mientras que los tipos de norte llevan a una intensificación de los mismos. Este comportamiento fue observado en todas las subregiones montañosas analizadas, aunque

con algunos matices. Una de las excepciones se dio en las subregiones montañosas cercanas al mar (Cordillera Cantábrica y Sistemas Béticos), en las que los tipos anticiclónicos no llegaban a debilitar demasiado los gradientes.

- Los gradientes fijos y de referencia, como el MELR o los gradientes promedios específicos para cada subregión montañosas (Zonales) no son los más recomendables, habiendo mostrando la mayor incertidumbre. En este sentido, se recomienda el uso de gradientes específicos adaptados a la estacionalidad y a los tipos de tiempo existentes.

Analizar el comportamiento espacio-temporal de la temperatura del aire superficial a escala regional sobre áreas de montaña de latitudes tropicales y los posibles efectos de factores de teleconexión como el fenómeno de El Niño (Capítulo 4).

- Se observó una mayor incertidumbre en la estimación de las temperaturas mínimas que en las temperaturas máximas, algo achacado a que las temperaturas nocturnas están sujetas a factores propios de la escala local, como la topografía, que no se detectan adecuadamente con redes de observación de escala regional.
- Al igual que en el caso de la España Peninsular, los gradientes obtenidos suelen ser más débiles que el gradiente ambiental promedio (MELR) de -6.5º C km^{-1}. De igual modo, se recomienda la sub-regionalización del área de estudio para poder focalizar el análisis y poder obtener cifras de gradientes más representativas y específicas de cada una de estas subregiones, teniendo en cuenta la estacionalidad y la heterogeneidad territorial.
- Tanto los gradientes de temperaturas máximas como los de temperaturas mínimas fueron más intensos durante la estación húmeda (octubre a mayo), que durante la estación seca (junio a septiembre). La única excepción para este comportamiento fueron los gradientes de temperaturas mínimas obtenidos en la subregión sur, en los que la continentalidad, la topografía local y la humedad específica que afecta a una parte de los observatorios pudieron llevar al conjunto a mostrar una intensificación inesperada a escala regional.
- El fenómeno ENSO influye significativamente en la variabilidad de los gradientes en la subregión sur, mientras que su impacto es más variable en la subregión norte. En algunos eventos excepcionales correspondientes a eventos fuertes y muy fuertes de El Niño (como 1997-1998), los gradientes pueden sufrir una fuerte intensificación. Sin embargo, los episodios débiles parecen no interactuar demasiado con la región andina.
- Se recomienda que, en caso de calcular gradientes con únicamente pares de observatorios, estos deban mantener un desnivel de, al menos, 1500 metros.

La falta de información espacial requirió de la instalación de redes de observación propias, con lo que otro objetivo específico fue establecer una serie de criterios metodológicos que permitan el diseño de redes experimentales sobre ámbitos de montaña en cuanto a la elección de los sensores, protecciones contra la radiación solar y elevación sobre el manto de nieve (Capítulo 5).

- Los sensores de temperatura autónomos son una buena y fácil opción de medir la temperatura del aire en áreas cubiertas de nieve y de montaña. Los modelos Tinytag mostraron un rendimiento robusto y constante en relación al sensor de referencia, mientras que los modelos iButton mostraron un comportamiento inestable (especialmente en temperaturas bajo 0º C), y están además sujetos a errores inesperados operativos. Así, es recomendable el uso de los Tinytag. En el caso de que se use el modelo de iButton, estos dispositivos deben instalarse siempre en paralelo (dos o más) para asegurar la medición.
- La protección de la radiación solar de los dispositivos es necesaria para asegurar la calidad de los datos de temperatura del aire. El uso de las garitas tradicionales Stevenson no es obligatorio, ya que existen otras opciones con unos costes más reducidos y logísticamente mejores. Las garitas comerciales modelo Datamate ACS-5050 dan la mejor protección en todas las condiciones de radiación, intensidad de viento y existencia de nieve. Las opciones caseras realizadas mediante tubos y embudos de PVC mostraron un comportamiento variable, y sus limitaciones deben tenerse en cuenta: el tubo es más útil en ámbitos nevados y ventosos, mientras que el modelo de embudos funciona mejor en áreas sin nieve y con poco viento. En cualquier caso, el uso de las garitas comerciales como la Datamate ACS5050 da resultados significativamente mejores que cualquier otra alternativa no comercial. Únicamente en condiciones de escasa radiación y vientos fuertes las opciones no comerciales y pueden tener un rendimiento aceptable.
- El perfil vertical de temperatura del aire muestra una estabilización a los 75 – 100 cm sobre la superficie de nieve. De esta forma, antes de instalar los dispositivos es importante conocer la nieve que se puede esperar en ese lugar, e instalar los sensores al menos 1 metro por encima de esa altura. Además, se han detectado algunos comportamientos específicos: 1) un intenso enfriamiento cerca de la superficie de la nieve durante las horas de día, especialmente a mediodía, posiblemente debido a los flujos de energía que van desde el aire frío a la superficie de nieve; 2) estabilización por la noche, cuando todos los dispositivos pueden estar situados dentro de la capa de enfriamiento topográfico.

- El análisis de la variabilidad horizontal mostró que la variabilidad se incrementa a mediodía, simultáneamente al incremento de radiación solar, que potencia las características físicas de los materiales, afectando a las mediciones de temperatura del aire.

Analizar el comportamiento espacio-temporal de la temperatura del aire superficial a escala local sobre un área montañosa topográficamente compleja del Pirineo Aragonés con especial atención a factores locales como la topografía o el efecto de las condiciones meteorológicas (Capítulo 6).

- Los gradientes nocturnos son más débiles que los diurnos debido a la subsidencia de aire frío y a la topografía. Por otro lado, los gradientes de máximas (LRmax) fueron más intensos de marzo a julio, aunque en la ladera de umbría esto se restringe únicamente al mes de julio; mientras que LRmax se debilita durante el invierno. Los gradientes de mínimas (LRmin) fueron más débiles de junio a agosto (y diciembre), intensificándose desde marzo a mayo.
- Se han encontrado valores diferentes de insolación entre localizaciones de una misma ladera y entre las dos laderas, debido a la exposición de las mismas y a la elevación de las localizaciones. Esto influye directamente en la temperatura del aire, debido a las sombras topográficas del fondo del valle, causando la retención del aire frío nocturno durante los días más cortos en estas partes bajas del valle.
- Se han encontrado patrones diferenciados de gradientes más intensos y más débiles, explicándose por diversos factores (insolación de la ladera, duración del día, topografía, estacionalidad y condiciones meteorológicas). En un día despejado de invierno, la menor insolación de las localizaciones más bajas debilita el LRmax. Sin embargo, también en invierno, LRmax se intensifica bajo condiciones de inestabilidad. Durante el verano, LRmax es casi siempre intenso (con pocas sombras topográficas y generalmente con tiempo despejado). LRmin es más débil bajo condiciones de estabilidad atmosférica, y más intenso bajo condiciones de inestabilidad, independientemente del mes y la estación.

Aplicar estos análisis en el estudio de la fragilidad de determinadas actividades económicas de ámbitos de montaña del Pirineo Aragonés, tales como la industria del esquí (Capítulo 7).

- En la estación de esquí de Aramón – Formigal, el gradiente de temperatura media (seca) del aire observado ha sido de -4.9º C km^{-1}, mientras que el gradiente de temperatura húmeda fue de -5.2º C km^{-1}. Por otro lado, el gradiente de horas diarias de producción de nieve artificial es de 8h km^{-1}. Es decir, la temperatura húmeda es más variable verticalmente a lo largo de la estación de esquí que la temperatura seca, con lo que se

producirán importantes diferencias en el potencial de producción de nieve artificial entre las cotas bajas y altas.

- Los gradientes de temperatura del aire, temperatura húmeda y horas de producción de nieve artificial mostraron gran variabilidad horaria, diaria y mensual, que estuvo principalmente controlada por la variabilidad de la humedad relativa y de la velocidad del viento, estando ambas correlacionadas con los gradientes (a más viento y humedad relativa, gradientes más intensos).
- La clasificación de tipos de tiempo se presentó como una síntesis adecuada de estas variables meteorológicas. De este modo, los gradientes más débiles estuvieron relacionados con tipos de tiempo de sureste y, en menor medida, del este y del sur, además de los tipos anticiclónicos. Los gradientes más intensos de temperatura seca y húmeda se observaron durante los tipos de tiempo del noroeste, mientras que los más intensos en horas de producción de nieve fueron los tipos ciclónicos o del noreste.
- La identificación de las relaciones de las condiciones meteorológicas y sinópticas en la magnitud de los gradientes nos da una información muy útil a la hora de permitir a los gestores de una estación de esquí predecir el potencial de producción de nieve a corto plazo. La variabilidad decadal de los patrones de circulación atmosférica podría impactar en la magnitud de la temperatura húmeda y seca del aire y, por tanto, en la viabilidad de la producción de nieve artificial en algunas localizaciones más vulnerables.

8.3. Trabajos futuros

El presente trabajo supone el inicio, dentro del Grupo de Investigación de Hidrología Ambiental (IPE – CSIC), de los análisis de la distribución espacio-temporal de la temperatura del aire superficial en las áreas montañosas que llevan estudiando desde distintos enfoques (principalmente hidrológicos) desde hace más de quince años. Con respecto a esto, el sentido multiescalar de artículos de investigación que han compuesto la Tesis Doctoral, así como la incorporación de gran cantidad de datos propios mediante extensas temporadas de trabajo de campo, ha permitido que sea una línea novedosa dentro del Grupo, y que se une a una creciente corriente investigadora que está tratando de mejorar en el conocimiento de la temperatura del aire en estos medios complejos.

La necesidad de datos de temperatura del aire que permitieran un análisis a escala local ha exigido un intenso aprendizaje en los criterios para hacer correctos diseños experimentales en materia de dispositivos de medición, protecciones contra la radiación, ubicación de los sensores,

etc. En este sentido, las recomendaciones propuestas en la Tesis Doctoral pueden suponer un punto de inicio y de referencia a la hora de establecer nuevos diseños experimentales, no sólo dentro del Grupo de Investigación, sino de cualquier investigador que necesite analizar la temperatura del aire en un medio montañoso con dispositivos propios, pudiendo así lograr la comparabilidad de los datos. De todo lo analizado, una de las conclusiones principales ha sido que la escala espacial más adecuada para el estudio de la temperatura del aire en áreas de montaña es la escala local, ya que en la que se observa mayor variabilidad, existiendo por tanto un amplio camino por delante para avanzar en su conocimiento. Para ello, no existen redes oficiales de observación meteorológica capaces de cumplir con los requisitos de representatividad, por lo que será el desarrollo de redes propias el que permitirá avanzar. Esta será una de las líneas principales de trabajo futuro: la monitorización de más áreas montañosas para poder comparar resultados y observar posibles nuevos factores explicativos, o poder cuantificar de mejor manera los ya conocidos, como el efecto de los cambios en el tipo de superficie, o el efecto de las distintas coberturas forestales.

En la misma dirección, será necesario también profundizar en otras técnicas como la teledetección, que pueden hacer aumentar de forma notable la información disponible en estas áreas. Para ello será necesario avanzar en el conocimiento del acoplamiento entre esta información y la tomada en campo. La correcta adaptación entre ambas medidas permitiría la masificación de la información disponible, estando esta además generada de forma continua por el territorio. Esta línea ya ha sido trabajada con anterioridad por otros grupos de investigación, con lo que sería positiva la realización de estancias de investigación en estos grupos.

Por otro lado, otro de los campos a desarrollar la aplicabilidad de estos resultados va en relación con la existencia de refugios climáticos en un contexto de calentamiento. La complejidad térmica de las laderas provoca que, en determinadas ocasiones, las especies vegetales puedan encontrar, mediante desplazamiento horizontal, un nuevo hábitat en el que desarrollarse. Sin embargo, si estos medios son eminentemente verticales (como los riscos o acantilados de montaña), los desplazamientos horizontales no pueden llevarse a cabo, existiendo la única (y difícil) vía del desplazamiento vertical, que es más restrictivo.

En distinto orden de ideas, la otra de las grandes líneas de trabajo futuro que se presenta a partir de ahora es la profundización en el intercambio de conocimiento con la sociedad. De esta forma, planteamos dos líneas de trabajo principales: la viabilidad de los complejos invernales y la gestión de los recursos hídricos:

- Elaboración de planes de acción y viabilidad específicos para estaciones de esquí en los que se determine el grado de vulnerabilidad existente y las principales zonas de riesgo de viabilidad del modelo, estableciendo calendarios de actuación y posibles puntos de no retorno. Consideración de medidas a tomar, desde la mejora tecnológica en la producción de nieve artificial, hasta el abandono de la actividad por falta de viabilidad.
- Profundización en los efectos que supone alterar los gradientes térmicos habituales (-6.5º C km^{-1}) en la modelización hidrológica, estableciendo medidas de incertidumbre derivadas del uso de estos gradientes. El objetivo es mejorar en la modelización hidrológica y poder así estimar mejor los recursos hídricos disponibles, y la posible evolución de los mismos a lo largo de las temporadas. En este sentido, la instalación de redes de observación locales se presenta fundamental para lograr la correcta modelización térmica de las cuencas hidrográficas, por lo que se podrá seguir profundizando en los diseños experimentales mediante la proposición de densidades idóneas de sensores en función de las características de las cuencas, entre otros aspectos.

Paralelamente, otra de las líneas que se presentan de trabajo futuro es avanzar en la clasificación de tipos de tiempo mediante la incorporación de más variables, además de la presión atmosférica a nivel superficial, pudiendo incorporar información de otras capas altimétricas mejorando así la clasificación final.

En conclusión, las líneas de trabajo futuras continúan en la dirección de unir el estudio del medio que nos rodea con la incorporación de este conocimiento en la sociedad, mediante su aplicación en actividades humanas como la gestión de los recursos hídricos o el estudio de la viabilidad de determinados modelos turísticos en las áreas de montaña. Es el sentido de la Geografía el conseguir unir este conocimiento científico y su aplicación en la sociedad. Únicamente de esta forma será posible que la ordenación territorial no esté únicamente al servicio de las necesidades económicas, sino que también incorpore el conocimiento del medio, que es el que determinará las viabilidades presentes y futuras y, por tanto, la sostenibilidad de nuestro modelo como sociedad.

Referencias (Capítulos 1 y 2)

Ackerman, E.A. 1941. The Koppen Classification of Climates in North America. *Geographical Review* 31: 105.

Alonso-González, E., López-Moreno, J.I., Gascoin, S., García-Valdecasas Ojeda, M., Sanmiguel-Vallelado, A., Navarro-Serrano, F., Revuelto, J. et al. 2018. Daily gridded datasets of snow depth and snow water equivalent for the Iberian Peninsula from 1980 to 2014. *Earth System Science Data* 10: 303-315.

Alonso-González, E., López-Moreno, J.I., Navarro-Serrano, F., Sanmiguel-Vallelado, A., Revuelto, J., Domínguez-Castro, F., Ceballos, A. 2020. Snow climatology for the mountains in the Iberian Peninsula using satellite imagery and simulations with dynamically downscaled reanalysis data. *International Journal of Climatology* 40: 477-491.

ARCE. 2018. *Estadística Anual y Multianual del Sector Eléctrico Ecuatoriano*. ARCE (Agencia de Regulación y Control de Electricidad), Quito.

Barry, R. 2008. *Mountain weather and Climate*. 3.ª ed. Cambridge University Press, Cambridge.

Barry, R., Chorley, R. 2003. *Atmosphere, Weather and Climate*. 8.ª ed. Routledge, Londres.

Basnett, T.A., Parker, D.E. 1997. Development of the global mean sea level pressure data set GMSLP2. En Office, H. C.-M. (ed.), *Climatic Research Technical Note*, Bracknell.

Bayona, E. 2012. El Cielo enfurece a los ríos. *El Periódico de Aragón*.

Benavides, R., Montes, F., Rubio, A., Osoro, K. 2007. Geostatistical modelling of air temperature in a mountainous region of Northern Spain. *Agricultural and Forest Meteorology* 146: 173-188.

Bennett, M., New, M., Marino, J., Sillero-Zubiri, C. 2016. Climate complexity in the Central Andes: A study case on empirically-based local variations in the Dry Puna. *Journal of Arid Environments* 128: 40-49.

Berrisford, P., Dee, D., Poli, P., Brugge, R., Fielding, K., Fuentes, M., Kallberg, P. et al. 2011. The ERA-Interim archive, version 2.0. *ERA report series.* 1: 23.

Blandford, T.R., Humes, K.S., Harshburger, B.J., Moore, B.C., Walden, V.P., Ye, H. 2008. Seasonal and Synoptic Variations in Near-Surface Air Temperature Lapse Rates in a Mountainous Basin. *Journal of Applied Meteorology and Climatology* 47: 249-261.

Bolstad, P. V., Swift, L., Collins, F., Régnière, J. 1998. Measured and predicted air temperatures at basin to regional scales in the southern Appalachian mountains. *Agricultural and Forest Meteorology* 91: 161-176.

Bonnardot, V., Carey, V., Madelin, M., Cautenet, S., Coetzee, Z., Quénol, H. 2012. Spatial variability of Night temperatures at a fine scale over the Stellenbosch Wine District, South Africa. *J. Int. Sci. Vigne Vin* 46: 1-13.

Braun, M., Hock, R. 2004. Spatially distributed surface energy balance and ablation modelling on the ice cap of King George Island (Antarctica). *Global and Planetary Change* 42: 45-58.

Breiman, L., Friedman, J.H., Olsen, R.A., Stone, C.J. 1984. *Classification and regression trees*. Chapman and Hall, Nueva York.

Brooks, C.F. 1947. Recommended climatological networks based on the representativeness of climatic stations for different elements. *Transactions, American Geophysical Union* 28: 845.

Bryant, E. 2005. *Natural Hazards*. 2.ª ed. Cambridge University Press, New York.

Buisán, S., Azorin-Molina, C., Jimenez, Y. 2015. Impact of two different sized Stevenson screens on air temperature measurements. *International Journal of Climatology* 35: 4408-4416.

Buisán, S., Earle, M.E., Collado, J.L., Kochendorfer, J., Alastrué, J., Wolff, M., Smith, C.D., López-Moreno, J.I. 2017. Assessment of snowfall accumulation underestimation by tipping bucket gauges in the Spanish operational network. *Atmospheric Measurement Techniques* 10: 1079-1091.

Buishand, T.A., Brandsma, T. 1997. Comparison of circulation classification schemes for predicting temperature and precipitation in the Netherlands. *International Journal of Climatology* 17: 875-889.

Bumke, K. 2016. Validation of ERA-Interim Precipitation Estimates over the Baltic Sea. *Atmosphere* 7: 82.

Camuffo, D., Bertolin, C. 2012. The earliest temperature observations in the world: the Medici Network (1654–1670). *Climatic Change* 111: 335-363.

Capel Molina, J.J. 2000. *El clima de la Península Ibérica*. Ariel, Barcelona.

Charrad, M., Ghazaali, N., Boiteau, V., Niknafs, A. 2014. NbClust: an R package for determining the relevant number of clusters in a data Set. *Journal of Statistical Software* 61: 1-36.

CHE. 2020. SAIH: Sistema Automático de Información Hidrológica de la Cuenca Hidrográfica del Ebro. Disponible en: http://www.saihebro.com/.

Corripio, J.G. 2019. insol: Solar Radiation. R package version 1.2. https://CRAN.R-project.org/package=insol.

Cortesi, N., Gonzalez-Hidalgo, J.C., Trigo, R.M., Ramos, A.M. 2014. Weather types and spatial variability of precipitation in the Iberian Peninsula. *International Journal of Climatology* 34: 2661-2677.

Cuadrat Prats, J.M., Pita López, M.F. 2006. *Climatología*. Ediciones Cátedra, Madrid.

Daly, C., Gibson, W., Taylor, G., Johnson, G., Pasteris, P. 2002. A knowledge-based approach to the statistical mapping of climate. *Climate Research* 22: 99-113.

Dávila, G., Olazával, H. 2006. *De la mediación al a movilización social: Análisis de algunos conflictos por el agua en Chimborazo*. Ediciones ABYA-YALA, Quito.

Dijkstra, H.A. 2006. The ENSO phenomenon: theory and mechanisms. *Advances in Geosciences* 6: 3-15.

Du, M., Liu, J., Zhang, X., Li, Y., Tang, Y. 2010. Changes of spatial patterns of surface-air-temperature on the Tibetan Plateau. *Latest Trends on Theoretical and Applied Mechanics, Fluid Mechanics and Heat & Mass Transfer*.

Duane, W.J., Pepin, N.C., Losleben, M.L., Hardy, D.R. 2008. General characteristics of Temperature and Humidity Variability on Kilimanjaro, Tanzania. *Arctic, Antarctic, and Alpine Research* 40: 323-334.

Dumas, M.D. 2013. Changes in temperature and temperature gradients in the French Northern Alps during the last century. *Theoretical and Applied Climatology* 111: 223-233.

Durre, I., Menne, M.J., Gleason, B.E., Houston, T.G., Vose, R.S. 2010. Comprehensive Automated Quality Assurance of Daily Surface Observations. *Journal of Applied Meteorology and Climatology* 49: 1615-1633.

ENFEN. 2012. *Definición operacional de los eventos El Niño y La Niña y sus magnitudes en la costa del Perú*. Lima.

Espín-Sánchez, E., Ruiz-Álvarez, V., Martí-Talavera, J., García-Marín, R. 2018. Estudio preliminar de las inversiones térmicas en el sureste de la Península Ibérica: el caso de los campos de Hernán Perea. *Pirineos: Revista de Ecología de Montaña.* 173: 1-18.

Fang, J.-Y., Yoda, K. 1988. Climate and vegetation in China (I). Changes in the altitudinal lapse rate of temperature and distribution of sea level temperature. *Ecological Research* 3: 37-51.

Farr, T.G., Rosen, P.A., Caro, E., Crippen, R., Duren, R., Hensley, S., Kobrick, M. et al. 2007. The Shuttle Radar Topography Mission. *Reviews of Geophysics* 45: 1-33.

Florinsky, I. V., Kulagina, T.B., Meshalkina, J.L. 1994. Influence of topography on landscape radiation temperature distribution. *International Journal of Remote Sensing* 15: 3147-3153.

Gao, L., Bernhardt, M., Schulz, K., Chen, X. 2017. Elevation correction of ERA-Interim temperature data in the Tibetan Plateau. *International Journal of Climatology* 37: 3540-3552.

García-Ruiz, J.M., Beguería-Portugués, S., López-Moreno, J.I., Lorente, A., Seeger, M. 2001. *Los recursos hídricos superficiales del Pirineo aragonés y su evolución reciente.* Editorial Geoforma, Logroño.

García-Ruiz, J.M., López-Moreno, J.I., Vicente-Serrano, S.M., Lasanta–Martínez, T., Beguería, S. 2011. Mediterranean water resources in a global change scenario. *Earth-Science Reviews* 105: 121-139.

García-Ruiz, J.M., White, S.M., Martí, C., Valero-Garcés, B., Errea, M.P., Gómez-Villar, A. 1996. *La catástrofe del barranco de Arás (Biescas, Pirineo aragonés) y su contexto espacio-temporal.* Instituto Pirenaico de Ecología (IPE - CSIC), Zaragoza.

García, D., Santiago Ochoa, W. 2012. Relación entre crecimiento económico y medio ambiente en Ecuador a nivel provincial (Promedio 2010-2015). *Revista Amazónica Ciencia y Tecnología* 6: 99-112.

García, M.B., Domingo, D., Pizarro, M., Font, X., Gómez, D., Ehrlén, J. 2019. Rocky habitats as microclimatic refuges for biodiversity. A close-up thermal approach. *Environmental and Experimental Botany* 170: 1-10.

Gardner, A.S., Sharp, M.J., Koerner, R.M., Labine, C., Boon, S., Marshall, S.J., Burgess, D.O., Lewis, D. 2009. Near-Surface Temperature Lapse Rates over Arctic Glaciers and Their Implications for Temperature Downscaling. *Journal of Climate* 22: 4281-4298.

Geiger, R., Pohl, W. 1953. Revision of Koeppen-Geiger climate maps of the Earth.

Gesch, D.B., Verdin, K.L., Greenlee, S.K. 1999. New land surface digital elevation model covers the Earth. *Eos, Transactions American Geophysical Union* 80: 69.

Gilaberte-Búrdalo, M., López-Martín, F., Pino-Otín, M.R., López-Moreno, J.I. 2014. Impacts of climate change on ski industry. *Environmental Science and Policy* 44: 51-61.

Gilaberte-Búrdalo, M., López-Moreno, J.I., Morán-Tejeda, E., Jerez, S., Alonso-González, E., López-Martín, F., Pino-Otín, M.R. 2017. Assessment of ski condition reliability in the Spanish and Andorran Pyrenees for the second half of the 20th century. *Applied Geography* 79: 127-142.

Gill, G. 1983. *Comparison testing of selected naturally ventilated solar radiation shields*. NOAA, Bay St. Louis.

Goerlich, F.J., Cantarino, I. 2013. A population density grid for Spain. *International Journal of Geographical Information Science* 27: 2247-2263.

Gómez Martín, B. 1999. La relación clima-turismo: consideraciones básicas en los fundamentos teóricos y prácticos. *Investigaciones Geográficas* 21: 21-34.

Greenland, D., Burbank, J., Key, J., Klinger, L., Moorhouse, J., Oaks, S., Shankman, D. 1985. The bioclimates of the Colorado Front Range. *Mountain Research & Development* 5: 251-262.

Grimm, A.M., Tedeschi, R.G., Grimm, A.M., Tedeschi, R.G. 2009. ENSO and Extreme Rainfall Events in South America. *Journal of Climate* 22: 1589-1609.

Hanna, E., Mernild, S., Yde, J., Villiers, S. 2017. Surface Air Temperature Fluctuations and Lapse Rates on Olivares Gamma Glacier, Rio Olivares Basin, Central Chile, from a Novel Meteorological Sensor Network. *Advances in Meteorology* 2017: 1-15.

Hatfield, J.L., Prueger, J.H. 2015. Temperature extremes: Effect on plant growth and development. *Weather and Climate Extremes* 10: 4-10.

Heynen, M., Miles, E., Ragettli, S., Buri, P., Immerzeel, W.W., Pellicciotti, F. 2016. Air temperature variability in a

high-elevation Himalayan catchment. *Annals of Glaciology* 57: 212-222.
Huang, B., Thorne, P.W., Banzon, V.F., Boyer, T., Chepurin, G., Lawrimore, J.H., Menne, M.J. et al. 2017. Extended Reconstructed Sea Surface Temperature, Version 5 (ERSSTv5): Upgrades, Validations, and Intercomparisons. *Journal of Climate* 30: 8179-8205.
Hubbart, J. 2011. An Inexpensive Alternative Solar Radiation Shield for Ambient Air Temperature Micro-Sensors. *Journal of Natural and Environmental Sciences* 2: 9-14.
Hubbart, J., Kavanagh, K., Pangle, R., Link, T., Schotzko, A. 2007. Cold air drainage and modeled nocturnal leaf water potential in complex forested terrain. *Tree Physiology* 27: 631-639.
IGME. 1994. *Mapa Geológico de España a escala 1:50.000. Hojas del MAGNA*.
IGN. 2020. Plan Nacional de Ortofotografía Aérea. Disponible en: https://pnoa.ign.es/presentacion-y-objetivo [Accedido 27 de enero de 2020].
Immerzeel, W.W., Petersen, L., Ragettli, S., Pellicciotti, F. 2014. The importance of observed gradients of air temperature and precipitation for modeling runoff from a glacierized watershed in the Nepalese Himalayas. *Water Resources Research* 50: 2212-2226.
INE. 2019a. *España en Cifras*. Instituto Nacional de Estadística, Madrid.
INE. 2019b. Padrón Municipal del año 2019.
INEC. 2012. *Proyecciones de la Población de la República del Ecuador (2010-2020)*. Quito.
INEI. 2018. *Principales Indicadores Macroeconómicos*. Lima.
INEI. 2017. *XII Censo de Población*. Lima.
Jenkinson, A.F., Collison, P. 1977. An initial climatology of Wales over the North Sea. En *Synoptic Climatology Branch memorandum, 62.*,
Jensen, A.H. 1992. *Geografía. Historia y conceptos*. 1.ª ed. Majoral, R., Majoral, L. (eds.),. Ediciones Vicens-Vives, S.A., Barcelona.
Jiménez-Muñoz, J.C., Sobrino, J.A. 2003. A generalized single-channel method for retrieving land surface temperature from remote sensing data. *Journal of Geophysical Research D: Atmospheres* 108: 4688.
Jones, P.D., Hulme, M., Briffa, K.R. 1993. A comparison of Lamb circulation types with an objective classification scheme. *International Journal of Climatology* 13: 655-663.
Joshi, R., Sambhav, K. 2018. Near surface temperature lapse rate for treeline environment in western Himalaya and possible impacts on ecotone vegetation. *Tropical Ecology* 59: 197-209.
Kaiser, D.P. 2002. Decreasing trends in sunshine duration over China for 1954–1998: Indication of increased haze pollution? *Geophysical Research Letters* 29: 2042.
Karki, R., Hasson, S. ul, Schickhoff, U., Scholten, T., Böhner, J., Gerlitz, L. 2020. Near surface air temperature lapse rates over complex terrain: a WRF based analysis of controlling factors and processes for the central Himalayas. *Climate Dynamics* 54: 329-349.
Kass, G. V. 1980. An Exploratory Technique for Investigating Large Quantities of Categorical Data. *Applied Statistics* 29: 119.
Kattel, D.B., Yao, T., Panday, P.K. 2018. Near-surface air temperature lapse rate in a humid mountainous terrain on the southern slopes of the eastern Himalayas. *Theoretical and Applied Climatology* 132: 1129-1141.
Kattel, D.B., Yao, T., Yang, W., Gao, Y., Tian, L. 2015. Comparison of temperature lapse rates from the northern to the southern slopes of the Himalayas. *International Journal of Climatology* 35: 4431-4443.
Khorchani, M., Martin-Hernandez, N., Vicente-Serrano, S.M., Azorin-Molina, C., Garcia, M., Domínguez-Duran, M.A., Reig, F. et al. 2018. Average annual and seasonal Land Surface Temperature, Spanish Peninsular. *Journal of Maps* 14: 465-475.
Kiehl, J.T., Trenberth, K.E. 1997. Earth's Annual Global Mean Energy Budget. *Bulletin of the American Meteorological Society* 78: 197-208.
Lamb, H.H. 1972. British Isles weather types and a register of daily sequence of circulation patterns, 1861 - 1971. *Geophysical Memoires* 116: 85.
Lareau, N.P., Crosman, E., Whiteman, C.D., Horel, J.D., Hoch, S.W., Brown, W.O.J., Horst, T.W. 2013. The Persistent Cold-Air Pool Study. *Bulletin of the American Meteorological Society* 94: 51-63.
Lareau, N.P., Horel, J.D. 2014. Dynamically Induced Displacements of a Persistent Cold-Air Pool. *Boundary-Layer Meteorology* 154: 291-316.
Li, X., Wang, L., Chen, D., Yang, K., Xue, B., Sun, L. 2013. Near-surface air temperature lapse rates in the mainland China during 1962-2011. *Journal of Geophysical Research: Atmospheres* 118: 7505-7515.
Lookingbill, T.R., Urban, D.L. 2003. Spatial estimation of air temperature differences for landscape-scale studies in montane environments. *Agricultural and Forest Meteorology* 114: 141-151.
López-Moreno, J.I. 2006. *Cambio ambiental y gestión de embalses en el Pirineo Central español*. Universidad de Zaragoza.
López-Moreno, J.I., Beguería, S., García-Ruiz, J.M. 2002. Influence of the Yesa reservoir on floods of the Aragón River, central Spanish Pyrenees. *Hydrology and Earth System Sciences Discussions* 6: 753-762.
López-Moreno, J.I., Beguería, S., García-Ruiz, J.M. 2004. The management of a large Mediterranean reservoir: Storage regimens of the Yesa Reservoir, Upper Aragon River basin, Central Spanish Pyrenees. *Environmental*

Management 34: 508-515.
López-Moreno, J.I., Goyette, S., Beniston, M. 2009. Impact of climate change on snowpack in the Pyrenees: Horizontal spatial variability and vertical gradients. *Journal of Hydrology* 374: 384-396.
López-Moreno, J.I., Navarro-Serrano, F., Azorín-Molina, C., Sánchez-Navarrete, P., Alonso-González, E., Rico, I., Morán-Tejeda, E. et al. 2019. Air and wet bulb temperature lapse rates and their impact on snowmaking in a Pyrenean ski resort. *Theoretical and Applied Climatology* 135: 1361-1373.
López-Moreno, J.I., Vicente-Serrano, S.M. 2007. Atmospheric circulation influence on the interannual variability of snow pack in the Spanish Pyrenees during the second half of the 20th century. *Hydrology Research* 38: 33-44.
López-Moreno, J.I., Pomeroy, J.W., Revuelto, J., Vicente-Serrano, S.M. 2013. Response of snow processes to climate change: spatial variability in a small basin in the Spanish Pyrenees. *Hydrological Processes* 27: 2637-2650.
Lundquist, J., Cayan, D. 2007. Surface temperature patterns in complex terrain: Daily variations and long-term change in the central Sierra Nevada, California. *Journal of Geophysical Research* 112: 1-15.
Lundquist, J., Lott, F. 2008. Using inexpensive temperature sensors to monitor the duration and heterogeneity of snow-covered areas. *Water Resources Research* 44: 1-6.
Lundquist, J.D., Pepin, N., Rochford, C. 2008. Automated algorithm for mapping regions of cold-air pooling in complex terrain. *Journal of Geophysical Research* 113: 1-15.
Marshall, S.J., Sharp, M.J., Burgess, D.O., Anslow, F.S. 2007. Near-surface-temperature lapse rates on the Prince of Wales Icefield, Ellesmere Island, Canada: implications for regional downscaling of temperature. *International Journal of Climatology* 27: 385-398.
Martinec, J. 1975. Snowmelt - Runoff model for stream flow forecast. *Hydrology Research1* 6: 145-154.
McMaster, R., Sheppard, E. 2004. *Scale and geographic inquiry: nature, society and method*. Blackwell Publishing Ltd, Oxford.
Minder, J.R., Mote, P.W., Lundquist, J.D. 2010. Surface temperature lapse rates over complex terrain: Lessons from the Cascade Mountains. *Journal of Geophysical Research* 115: 1-13.
MINEM. 2019. *Anuario Estadístico de Electricidad*. MINEM (Ministerio de Energía y Minas), Lima.
Ministerio de Agricultura Pesca y Alimentación. 2019. *Informe Anual de Indicadores: Agricultura, Pesca y Alimentación*. Madrid.
Miró, J.R., Peña, J.C., Pepin, N., Sairouni, A., Aran, M. 2017. Key features of cold-air pool episodes in the northeast of the Iberian Peninsula (Cerdanya, eastern Pyrenees). *International Journal of Climatology* 38: 1105-1115.
Molotch, N.P., Colee, M.T., Bales, R.C., Dozier, J. 2005. Estimating the spatial distribution of snow water equivalent in an alpine basin using binary regression tree models: the impact of digital elevation data and independent variable selection. *Hydrological Processes* 19: 1459-1479.
Morán-Tejeda, E., Lorenzo-Lacruz, J., López-Moreno, J.I., Rahman, K., Beniston, M. 2014. Streamflow timing of mountain rivers in Spain: Recent changes and future projections. *Journal of Hydrology* 517: 1114-1127.
Murtagh, F., Legendre, P. 2014. Ward's Hierarchical Agglomerative Clustering Method: Which Algorithms Implement Ward's Criterion? *Journal of Classification* 31: 274-295.
Nadal-Romero, E., Cammeraat, E., Pérez-Cardiel, E., Lasanta, T. 2016. Effects of secondary succession and afforestation practices on soil properties after cropland abandonment in humid Mediterranean mountain areas. *Agriculture, Ecosystems and Environment* 228: 91-100.
Nitu, R., Roulet, Y.A., Wolff, M., Earle, M., Reverdin, A., C. Smith, J., Kochendorfer, S. et al. 2018. *Instruments and Observing Methods (Report No. 131). WMO Solid Precipitation Experiment (SPICE) (2012-2015)*. Geneva.
NOAA, NASA. 1976. *U.S. Standard Atmosphere*. 4.ª ed. U.S. Government Printing Office, Washington D.C.
Ollero Ojeda, A. 2000. Crecidas fluviales en la cuenca del Ebro desde 1980: estado de la cuestión, principales eventos y sistemas de prevención. *Serie Geográfica* 9: 151-162.
Pagès, M., Miró, J.R. 2010. Determining temperature lapse rates over mountain slopes using vertically weighted regression: a case study from the Pyrenees. *Meteorological Applications* 17: 53-63.
Pagès, M., Pepin, N., Miró, J. 2017. Measurement and modelling of temperature cold pools in the Cerdanya valley (Pyrenees), Spain. *Meteorological Applications* 24: 290-302.
Paredes, M., De la Puente, L. 2014. Protestas y negociaciones socioambientales. El caso de las industrias extractivas. En Damonte, G., Vila, G. (eds.), *Agenda de investigación en temas socioambientales en el Perú: Una aproximación desde las ciencias sociales*, pp. 75-105. Grupo de Estudios Ambiente y Sociedad, Lima.
Peña-Angulo, D., Trigo, R.M., Cortesi, N., González-Hidalgo, J.C. 2016. The influence of weather types on the monthly average maximum and minimum temperatures in the Iberian Peninsula. *Atmospheric Research* 178-179: 217-230.
Pepin, N., Bradley, R.S., Diaz, H.F., Baraer, M., Caceres, E.B., Forsythe, N., Fowler, H. et al. 2015. Elevation-dependent warming in mountain regions of the world. *Nature Climate Change* 5: 424-430.
Pepin, N., Kidd, D. 2006. Spatial temperature variation in the Eastern Pyrenees. *Weather* 61: 300-310.
Pepin, N., Losleben, M. 2002. Climate change in the Colorado Rocky Mountains: free air versus surface temperature trends. *International Journal of Climatology* 22: 311-329.
Pepin, N., Losleben, M., Hartman, M., Chowanski, K. 2005. A Comparison of SNOTEL and GHCN/CRU Surface Temperatures with Free-Air Temperatures at High Elevations in the Western United States: Data Compatibility

and Trends. *Journal of Climate* 18: 1967-1985.
Pepin, N., Maeda, E.E., Williams, R. 2016. Use of remotely sensed land surface temperature as a proxy for air temperatures at high elevations: Findings from a 5000m elevational transect across Kilimanjaro. *Journal of Geophysical Research: Atmospheres* 121: 9998-10,015.
Pepin, N., Seidel, D.J. 2005. A global comparison of surface and free-air temperatures at high elevations. *Journal of Geophysical Research* 110: 1-15.
Pino Peralta, S.L., Aguilar Azuero, H.R., Apolo Loayza, G.E., Sisalema Morejón, L.A. 2018. Aporte del sector agropecuario a la economía del Ecuador. Análisis crítico de su evolución en el período de dolarización. Años 2000 - 2016. *Revista Espacios* 39: 7-18.
Pomeroy, J.W., Fang, X., Marks, D.G. 2016. The cold rain-on-snow event of June 2013 in the Canadian Rockies - characteristics and diagnosis. *Hydrological Processes* 30: 2899-2914.
Pons, M., Johnson, P., Rosas-Casals, M., Sureda, B., Jover, È. 2012. Modeling climate change effects on winter ski tourism in Andorra. *Climate Research* 54: 197-207.
Pons, M., López-Moreno, J.I., Rosas-Casals, M., Jover. 2015. The vulnerability of Pyrenean ski resorts to climate-induced changes in the snowpack. *Climatic Change* 131: 591-605.
Pueyo, Y., Beguería, S. 2007. Modelling the rate of secondary succession after farmland abandonment in a Mediterranean mountain area. *Landscape and Urban Planning* 83: 245-254.
R-Core-Team. 2013. R: A Language and Environment for Statistical Computing.
Rasilla Álvarez, D.F., García-Codrón, J.C., Garmendia Pedraja, C. 2002. Los temporales de viento: propuesta metodológica para el análisis de un fenómeno infravalorado. En *Reunión Nacional de Climatología*, pp. 129-136.
Rasmusson, E.M., Carpenter, T.H. 1982. Variations in Tropical Sea Surface Temperature and Surface Wind Fields Associated with the Southern Oscillation/El Niño. *Monthly Weather Review* 110: 354-384.
Razik, S. 2014. *How magnetics and granulometry of continental margin sediments reflect terrestrial and marine environments of South America and West Africa*. Bremen University.
Real Academia Española. 2014. *Diccionario de la Lengua Española*. 23.ª ed. S.L.U. ESPASA LIBROS, Madrid.
Regniere, J., Bolstad, P. 1994. Statistical Simulation of Daily Air Temperature Patterns Eastern North America to Forecast Seasonal Events in Insect Pest Management. *Environmental Entomology* 23: 1368-1380.
Revuelto, J., Azorin-Molina, C., Alonso-González, E., Sanmiguel-Vallelado, A., Navarro-Serrano, F., Rico, I., López-Moreno, J.I. 2017. Meteorological and snow distribution data in the Izas Experimental Catchment (Spanish Pyrenees) from 2011 to 2017. *Earth System Science Data* 9: 993-1005.
Rolland, C. 2003. Spatial and Seasonal Variations of Air Temperature Lapse Rates in Alpine Regions. *Journal of Climate* 16: 1032-1046.
Rollenbeck, R., Bendix, J. 2011. Rainfall distribution in the Andes of southern Ecuador derived from blending weather radar data and meteorological field observations. *Atmospheric Research* 99: 277-289.
Ruiz Rivera, N., Galicia, L. 2016. La escala geográfica como concepto integrador en la comprensión de problemas socio-ambientales. *Investigaciones Geograficas* 89: 137-153.
de Saint-Exupéry, A. 1943. *Le Petit Prince*. 1.ª ed. Reynal, E., Hitchcock, C. (eds.),. Reynal & Hitchcock, New York.
Sanmiguel-Vallelado, A., López-Moreno, J.I., Morán-Tejeda, E., Alonso-González, E., Navarro-Serrano, F., Rico, I., Camarero, J.J. 2020. Variable effects of forest canopies on snow processes in a valley of the central Spanish Pyrenees. *Hydrological Processes* 34: 2247-2262.
Sarricolea, P., Meseguer-Ruiz, O., Martín-Vide, J., Outeiro, L. 2018. Trends in the frequency of synoptic types in central-southern Chile in the period 1961–2012 using the Jenkinson and Collison synoptic classification. *Theoretical and Applied Climatology* 134: 193-204.
SENAMHI. 2020. Mapa Climático Nacional. Disponible en: https://www.senamhi.gob.pe/?&p=mapa-climatico-del-peru [Accedido 1 de abril de 2020].
Sinergise Ltd. 2020. EO Broser - Home page. Disponible en: https://apps.sentinel-hub.com/eo-browser/.
Spellman, G. 2000. The application of an objective weather-typing system to the Iberian peninsula. *Weather* 55: 375-385.
Strahler, A.H., Strahler, A.N. 1997. *Geografía Física*. 3.ª ed. Omega (ed.),. Omega, Barcelona.
Takahashi, K., Mosquera, K., Reupo, J. 2014. El Índice Costero El Niño (ICEN): Historia y actualización. *Boletín Técnico del Instituto Geofísico del Perú* 1: 8-9.
Tomás-Burguera, M., Jiménez Castañeda, A., Luna Rico, M.Y., Morata, A., Vicente Serrano, S.M., González-Hidalgo, J.C., Beguería, S. 2016. Control de calidad de siete variables del banco nacional de datos de AEMET. En Asociación Española de Climatología Congreso (10. 2016. Alicante) (ed.), *X Congreso Internacional AEC: Clima, sociedad, riesgos y ordenación del territorio*, pp. 407-415. Alicante, Spain.
Trigo, R.M., DaCamara, C.C. 2000. Circulation Weather Types and their influence on the Precipitation regime in Portugal. *International Journal of Climatology* 20: 1559-1581.
USDMA. 2000. Vector Map Level 0 (VMAP0). Disponible en: https://www.lib.msu.edu/branches/map/findingaids/VMAP0/ [Accedido 13 de julio de 2017].
USGS. 2020. Earth Explorer - Home page. Disponible en: earthexplorer.usgs.gov [Accedido 7 de abril de 2020].

Vancutsem, C., Ceccato, P., Dinku, T., Connor, S.J. 2010. Evaluation of MODIS land surface temperature data to estimate air temperature in different ecosystems over Africa. *Remote Sensing of Environment* 114: 449-465.

Vicente-Serrano, S.M., Aguilar, E., Martínez, R., Martín-Hernández, N., Azorin-Molina, C., Sanchez-Lorenzo, A., El Kenawy, A. et al. 2017. The complex influence of ENSO on droughts in Ecuador. *Climate Dynamics* 48: 405-427.

Villanueva, M.J. 2018. Las lluvias y el deshielo disparan los caudales de los ríos y aumentan las reservas de los embalses. *Heraldo de Aragón*.

Villmow, J.R. 1962. Regional patterns of Climates in Europe according to the Thornthwaite Classification. *The Ohio Journal of Science* 62: 39-53.

Went, F.W. 1953. The effect of temperature on plant growth. *Annual Review of Plant Physiology* 4: 347-362.

Whiteman, C.D. 1982. Breakup of temperature inversions in deep mountain valleys: Part I. Observations. *Journal of Applied Meteorology and Climatology* 21: 270-289.

Whiteman, C.D., McKee, T.B. 1982. Breakup of temperature inversions in deep mountain valleys: Part II. Thermodynamic model. *Journal of Applied Meteorology and Climatology* 21: 290-302.

Whiteman, C.D., Pospichal, B., Eisenbach, S., Weihs, P., Clements, C.B., Steinacker, R., Mursch-Radlgruber, E., Dorninger, M. 2004. Inversion Breakup in Small Rocky Mountain and Alpine Basins. *Journal of Applied Meteorology and Climatology* 43: 1069-1082.

Wilcoxon, F. 1945. Individual Comparisons by Ranking Methods. *Biometrics Bulletin* 1: 80.

WMO. 2014. *Guide to Meteorological Instruments and Methods of Observation*. Geneva, Switzerland.

WMO. 2020. Permanent and Representative Members. *About us*. Disponible en: https://public.wmo.int/en/about-us/members/permanent-representatives [Accedido 8 de abril de 2020].

Zou, H., Zhu, J., Zhou, L., Li, P., Ma, S. 2014. Validation and application of reanalysis temperature data over the Tibetan Plateau. *Journal of Meteorological Research* 28: 139-149.

Apéndice I

BIBLIOMETRÍA Y CONTRIBUCIÓN EN LAS PUBLICACIONES

A continuación, se determinan las referencias completas de las publicaciones que forman parte del Compendio de publicaciones de la Tesis Doctoral, así como el factor de impacto (IF) del *Journal Citation Reports* (JCR) de cada revista, sus áreas de conocimiento y la contribución del doctorando al ser publicaciones en coautoría.

Publicación y justificación de la contribución del doctorando (Capítulo 3)

***Navarro-Serrano, F.**, López-Moreno, J., Azorin-Molina, C., Alonso-González, E., Tomás-Burguera, M., Sanmiguel-Vallelado, A., Revuelto, J., Vicente-Serrano, S.M. 2018. Estimation of near-surface air temperature lapse rates over continental Spain and its mountain areas. International Journal of Climatology 38: 3233-3249. DOI: https://doi.org/10.1002/joc.5497.*

Contribución: Francisco M. Navarro Serrano ha sido el principal responsable de todas las etapas de la investigación y de la redacción de todos los contenidos, discusión y conclusiones del manuscrito. El Dr. J.I. López Moreno ha tenido la idea original de la investigación y ha sido responsable de buena parte del desarrollo metodológico. El Dr. C. Azorín Molina ha supervisado cada una de las fases, y ha contribuido especialmente en la revisión del manuscrito. El Dr. M. Tomás-Burguera ha colaborado en la fase de control de calidad de los datos originales. Asimismo, todos los coautores han colaborado en la revisión de contenidos.

ISSN	IF 2019	IF 5 años	Área de Conocimiento	Ranking de la revista	Cuartil
0899-8418	3.928	4.611	Meteorology & Atmospheric Sciences	23 de 93	Q1

Publicación y justificación de la contribución del doctorando (Capítulo 4)

***Navarro-Serrano, F.**, López-Moreno, J.I., Domínguez-Castro, F., Alonso-González, E., Azorin-Molina, C., El-Kenawy, A., Vicente-Serrano, S.M. 2020. Maximum and Minimum air temperature lapse rates in the Andean region of Ecuador and Peru. International Journal of Climatology. En Prensa. DOI: https://doi.org/10.1002/joc.6574.*

Contribución: Francisco M. Navarro Serrano ha sido el principal responsable de todas las etapas de la investigación y de la redacción de todos los contenidos, discusión y conclusiones del manuscrito. El Dr. F. Domínguez ha contribuido de manera relevante en el proceso metodológico y en la supervisión de resultados y discusión. El Dr. J.I. López Moreno ha tenido la idea original de la investigación y ha supervisado cada una de las fases. El Dr. A. El-Kenawy ha colaborado intensamente en la fase de control de calidad y homogeneización de los datos originales. El Dr. C. Azorín Molina ha supervisado cada una de las fases, y ha contribuido especialmente en la revisión del manuscrito. Todos los coautores han colaborado en la revisión de contenidos. El artículo se encuentra actualmente aceptado y pendiente de publicación definitiva (En Prensa).

ISSN	IF 2019	IF 5 años	Área de Conocimiento	Ranking de la revista	Cuartil
0899-8418	3.928	4.611	Meteorology & Atmospheric Sciences	23 de 93	Q1

Publicación y justificación de la contribución del doctorando (Capítulo 5)

***Navarro-Serrano, F.**, López-Moreno, J.I., Azorin-Molina, C., Buisán, S., Domínguez-Castro, F., Sanmiguel-Vallelado, A., Alonso-González, E., Khorchani, M. 2019. Air temperature measurements using autonomous self-recording dataloggers in mountainous and snow covered areas. Atmospheric Research 224: 168-179. DOI: https://doi.org/10.1016/j.atmosres.2019.03.034.*

Contribución: Francisco M. Navarro Serrano ha sido el principal responsable de todas las etapas de la investigación, desde el diseño experimental, así como de la redacción de todos los contenidos, discusión y conclusiones del manuscrito. Los Drs. J.I. López Moreno y C. Azorín Molina han colaborado activamente en la revisión de resultados y discusión. El Dr. F. Domínguez ha contribuido de manera relevante en determinadas fases del diseño experimental. El Dr. S. Buisán ha contribuido activamente en la cesión de datos y en el acceso a las instalaciones de AEMET y el proyecto SPICE. Todos los coautores han participado de las tareas de trabajo de campo y han colaborado en la revisión de contenidos.

ISSN	IF 2019	IF 5 años	Área de Conocimiento	Ranking de la revista	Cuartil
0169-8095	4.676	4.639	Meteorology & Atmospheric Sciences	13 de 93	Q1

Publicación y justificación de la contribución del doctorando (Capítulo 6)

***Navarro-Serrano, F.**, López-Moreno, J.I., Azorin-Molina, C., Alonso-González, E., Aznárez-Balta, M., Buisán, S., Revuelto-Benedí, J. 2020. Elevation effects on air temperature in a topographically complex mountain valley in the Spanish Pyrenees. Atmosphere 11(6): 656. DOI: https://doi.org/10.3390/atmos11060656.*

Contribución: Francisco M. Navarro Serrano ha sido el principal responsable de todas las etapas de la investigación y de la redacción de todos los contenidos, discusión y conclusiones del manuscrito. El Dr. J.I. López Moreno ha tenido la idea original de la investigación y ha sido responsable de parte del desarrollo metodológico. El Dr. C. Azorín Molina ha supervisado cada una de las fases, y ha contribuido especialmente en la revisión del manuscrito. El Dr. S. Buisán ha contribuido activamente en la cesión de datos y en el acceso a las instalaciones de AEMET. Todos los coautores han participado de las tareas de trabajo de campo y han colaborado en la revisión de contenidos.

ISSN	IF 2019	IF 5 años	Área de Conocimiento	Ranking de la revista	Cuartil
2073-4433	2.397	2.437	Meteorology & Atmospheric Sciences	48 de 93	Q3

Publicación y justificación de la contribución del doctorando (Capítulo 7)					
*López-Moreno, J.I., **Navarro-Serrano, F.**, Azorin-Molina, C., Sánchez-Navarrete, P., González-Alonso, E., Rico, I., Morán-Tejeda, E., Buisán, S., Revuelto-Benedí, J., Pons, M., Vicente-Serrano, S.M. 2019. Air and wet bulb temperature lapse rates and their impact on snowmaking in a Pyrenean ski area. Theoretical and Applied Climatology 135(3-4): 1361-1373. DOI: https://doi.org/10.1007/s00704-018-2448-y.*					
Contribución: Francisco M. Navarro Serrando ha contribuido activamente en el diseño experimental, así como en la contextualización de la investigación y discusión de los resultados, trabajando activamente en la redacción del manuscrito y en las distintas fases metodológicas. El Dr. J.I. López-Moreno tuvo la idea original, y fue el máximo responsable de la generación de resultados y análisis, procediendo a la redacción de manera conjunta con Francisco M. Navarro Serrano. El Dr. C. Azorín Molina ha colaborado activamente en la revisión de resultados y del manuscrito final. Todos los coautores han participado de las tareas de trabajo de campo y han colaborado en la revisión de contenidos.					
ISSN	**IF 2019**	**IF 5 años**	**Área de Conocimiento**	**Ranking de la revista**	**Cuartil**
0177-798X	2.882	3.143	Meteorology & Atmospheric Sciences	40 de 93	Q2

Apéndice II

OTRAS CONTRIBUCIONES (Publicaciones en coautoría y Aportaciones a congresos)

Además de los cinco artículos de investigación publicados e incorporados en forma de capítulos en la presente Tesis Doctoral, el doctorando ha llevado a cabo otros trabajos colaborativos con miembros del Grupo de Investigación de Hidrología Ambiental (IPE – CSIC), lo que ha fructificado en la publicación de diversos trabajos académicos, así como en aportaciones a congresos nacionales e internacionales.

Listado de Publicaciones

1. El-Kenawy, A., Al Buloshi, A., Al-Awadhi, T., Alnasiri, N., **Navarro-Serrano, F.**, Al-Hatrushi, S., Robaa, S.M., Domínguez-Castro, F., McCabe, M., Schuwerack, P., López-Moreno, J.I., Vicente-Serrano, S.M. Evidence for intensification of meteorological droughts in Oman over the past four decades. *Atmospheric Research* (*en prensa*).
2. Alonso-González, E., López-Moreno, J.I., **Navarro-Serrano, F.**, Sanmiguel-Vallelado, A., Aznárez-Balta, M., Revuelto, J., Ceballos, A. 2020. Snowpack sensitivity to temperature, precipitation, and solar radiation variability over an elevational gradient in the Iberian mountains. *Atmospheric Research* 243: 104973. DOI: https://doi.org/10.1016/j.atmosres.2020.104973.
3. Alonso-González, E., López-Moreno, J.I., **Navarro-Serrano, F.**, Sanmiguel-Vallelado, A., Revuelto, J., Domínguez-Castro, F., Ceballos, A. 2020. Snow climatology for the mountains in the Iberian Peninsula using satellite imagery and simulations with dynamically downscaled reanalysis data. *International Journal of Climatology* 40: 477-491. DOI: https://doi.org/10.1002/joc.6223.
4. Sanmiguel-Vallelado, A., López-Moreno, J.I., Morán-Tejeda, E., Alonso-González, E., **Navarro-Serrano, F.**, Rico, I., Camarero, J.J. 2020. Variable effects of forest canopies on snow processes in a valley of the central Spanish Pyrenees. *Hydrological Processes* 34(10): 2247-2262. DOI: https://doi.org/10.1002/hyp.13721.
5. López Moreno, J.I., **Navarro-Serrano, F.**, Izaguirre, E., Alonso, E., Rico, I., Zabalza, J., Revuelto, J. 2019. Glacier and climate evolution in the Pariacacá Mountains, Peru. *Cuadernos de Investigación Geográfica* 46. En Prensa. DOI: https://doi.org/10.18172/cig.4331.
6. Alonso-González, E., López-Moreno, J.I., **Navarro-Serrano, F.**, Revuelto, J. 2019. Impact of North Atlantic Oscillation on the Snowpack in Iberian Peninsula Mountains. *Water* 12: 105. DOI: https://doi.org/10.3390/w12010105.
7. Alonso-González, E., López-Moreno, J.I., Gascoin, S., García-Valdecasas Ojeda, M., Sanmiguel-Vallelado, A., **Navarro-Serrano, F.**, Revuelto, J., Ceballos, A., Esteban-Parra, M.J., Essery, R. 2018. Daily gridded datasets of snow depth and snow water equivalent for the Iberian Peninsula from 1980 to 2014. *Earth System Science Data* 10: 303-315. DOI: https://doi.org/10.5194/essd-10-303-2018.
8. Domínguez-Castro, F., Vicente-Serrano, S.M., López-Moreno, J.I., Correa, K., Avalos, G., Azorin-Molina, C., El Kenawy, A., Tomás-Burguera, M., **Navarro-Serrano, F.**, Peña-Gallardo, M., Gimeno, L., Nieto, R. 2018. Mapping seasonal and annual extreme precipitation over the Peruvian Andes.

International Journal of Climatology 38(15): 5459-5475. DOI: https://doi.org/10.1002/joc.5739.

9. **Navarro-Serrano, F.**, López-Moreno, J.I. 2017. Spatio-temporal analysis of snowfall events in the Spanish Pyrenees and ther relationship to atmospheric circulation. *Cuadernos de Investigaciones Geográficas* 43: 233-254. DOI: https://doi.org/10.18172/cig.3042.
10. Revuelto, J., Azorin-Molina, C., Alonso-González, E., Sanmiguel-Vallelado, A., **Navarro-Serrano, F.**, Rico, I., Ignacio López-Moreno, J. 2017. Meteorological and snow distribution data in the Izas Experimental Catchment (Spanish Pyrenees) from 2011 to 2017. *Earth System Science Data* 9: 993-1005. DOI: https://doi.org/10.5194/essd-9-993-2017.
11. López-Moreno, J.I., Morán-Tejeda, E., Vicente-Serrano, S.M., Bazo, J., Azorin-Molina, C., Revuelto, J., Sánchez-Lorenzo, A. **Navarro-Serrano, F.**, Aguilar, A., Chura, O. 2016. Recent temperature variability and change in the Altiplano of Bolivia and Peru. *International Journal of Climatology* 36: 1773-1796. DOI: https://doi.org/10.1002/joc.4459.

Listado de Aportaciones a congresos

1. **Navarro-Serrano, F.**, López-Moreno, J.I., Buisán, S., Alonso-González, E., Sanmiguel-Vallelado, A. Mediciones de temperatura del aire mediante dataloggers en áreas nevadas y de montaña. *VII Congreso Ibérico de la International Permafrost Association*. Jaca, 25 a 27 de junio de 2019.
2. Alonso-González, E., **Navarro-Serrano, F.**, Revuelto, J., Ceballos, A. López-Moreno, J.I. Different snowpack responses to climatic variability over Iberian Peninsula. *VII Congreso Ibérico de la International Permafrost Association*. Jaca, 25 a 27 de junio de 2019.
3. López-Moreno, J.I., **Navarro-Serrano, F.**, Izaguirre, E., Alonso-González, E., Rico, I., Zabalza, J., Revuelto, J. Glacier and Climate evolution in the Pariacacá Mountains, Peru. *VII Congreso Ibérico de la International Permafrost Association*. Jaca, 25 a 27 de junio de 2019.
4. Alonso-González, E., **Navarro-Serrano, F.**, Revuelto, J., Ceballos, A., López-Moreno, J.I. The North Atlantic Oscillation influence on seasonal snowpack over different mountain ranges of Iberia. *VII Congreso Ibérico de la International Permafrost Association*. Jaca, 25 a 27 de junio de 2019.
5. López-Moreno, J.I., Pomeroy, J.W., Alonso-González, E., **Navarro-Serrano, F.**, Morán-Tejeda, E., Revuelto, J. Decoupling of Mountain snowpacks from Hydrology due to climate warming. *VII Congreso Ibérico de la International Permafrost Association*. Jaca, 25 a 27 de junio de 2019.
6. Sanmiguel-Vallelado, A., López-Moreno, J.I., Morán-Tejeda, E., Alonso-González, E., **Navarro-Serrano, F.**, Rico, I., Camarero, J.J. Influencia de las

masas forestales sobre la distribución espacial del manto de nieve y su variabilidad temporal en los Pirineos. *VII Congreso Ibérico de la International Permafrost Association*. Jaca, 25 a 27 de junio de 2019.

7. López-Moreno, J.I., Sanmiguel-Vallelado, A., Alonso-González, E., Rico, I., **Navarro-Serrano, F.**, Revuelto, J. Spatial and temporal differences in the effect of forest canopy on snow distribution: a case study in the Spanish Pyrenees. *2017 AGU FALL MEETING*. American Geophysical Union (AGU). New Orleans (USA), 11 a 15 de diciembre de 2017.
8. Vicente-Serrano, S.M., López-Moreno, J.I., Correa, K., Ávalos, G., Azorin-Molina, C., El-Kenawy, A., Tomás-Burguera, M., **Navarro-Serrano, F.**, Peña-Gallardo, M., Gimeno, L., Nieto, R.. Seasonal and annual daily precipitation risk maps for the Andean region of Peru. *First International Electronic Conference on the Hydrological Cycle*. 12 a 16 de noviembre de 2017.
9. Llorente-Pinto, J.M., **Navarro-Serrano, F.**, Alonso-González, E., Ceballos, A. Evolución reciente del manto de nieve en la España peninsular. *XXV Congreso de la Asociación de Geógrafos Españoles (AGE). Naturaleza, territorio y ciudad en un mundo global*. Madrid, 25 a 27 de octubre de 2017.
10. **Navarro-Serrano, F.**, López-Moreno, J.I., Alonso-González, E., Sanmiguel-Vallelado, A., Azorin-Molina, C. Gradientes de Temperatura Superficial en el Pirineo a escala regional. *V Snow and Avalanches Workshop (Pyrenean Symposium on Snow and Avalanches)*. Ordino (Andorra), 9 a 11 de octubre de 2017.
11. Alonso-González, E., López-Moreno, J.I., **Navarro-Serrano, F.**, Sanmiguel-Vallelado, A.. Evolución reciente del manto de nieve en el Pirineo. *V Snow and Avalanches Workshop (Pyrenean Symposium on Snow and Avalanches)*. Ordino (Andorra), 9 a 11 de octubre de 2017.
12. **Navarro-Serrano, F.**, López-Moreno, J.I., Alonso-González, E., Sanmiguel-Vallelado, A., Azorin-Molina, C., Vicente-Serrano, S.M. Gradientes de Temperatura en la Montaña Española. *II Encuentro Emeritense de Climatología*. Mérida, Extremadura, España. 25 a 26 de septiembre 2017.
13. **Navarro-Serrano, F.**, Alonso-González, E., Serrano-Notivoli, R., López-Moreno, J.I., Azorin-Molina, C., Sanmiguel-Vallelado, A. Análisis comparativo de superficie cubierta por nieve mediante imágenes NOAA-AVHRR, MODIS-MOD10A1 y FSM-WRF. *VI Congreso Ibérico de la International Permafrost Association*. Mieres, 21 a 23 de junio de 2017.
14. Alonso-González, E., López-Moreno, J.I., **Navarro-Serrano, F.**, Sanmiguel-Vallelado, A., Ceballos, A. Simulando el manto de nieve en la Península Ibérica para el periodo 1980 - 2014. *VI Congreso Ibérico de la International Permafrost Association*. Mieres, 21 a 23 de junio de 2017.
15. **Navarro-Serrano, F.**, López-Moreno, J.I., Alonso-González, E., Vicente-Serrano, S.M., Sanmiguel-Vallelado, A., Reig-Gracia, F., Azorin-Molina.

Gradientes de temperaturas en la Montaña Español. *10º Simposio de Meteorologia e Geofisica da APMG. 18º Encontro Luso Espanhol de Meteorologia*. Lisboa (Portugal), 20 a 22 de marzo de 2017.

Listado de Colaboraciones en Revistas Académicas

1. Remote Sensing of Environment (Elsevier). ISSN: 0034-4257. IF (JCR2019): 9.085. Q1. Revisión de 1 artículo.
2. International Journal of Climatology (Royal Meteorological Society). ISSN: 0899-8418. IF (JCR2019): 3.928. Q1. Revisión de 2 artículos.
3. Journal of Geophysical Research-Atmospheres (AGU Journal). ISSN: 2169-897X. IF (JCR2019): 3.821. Q2. Revisión de 1 artículo.
4. Regional Environmental Change (Springer). ISSN: 1436-3798. IF (JCR2019): 3.481. Q2. Revisión de 1 artículo.
5. Journal of Mountain Science (Springer). ISSN: 1672-6316. IF (JCR2019): 1.550. Q4. Revisión de 1 artículo.
6. Pirineos (Revistas CSIC). ISSN: 0373-2568. Revisión de 1 artículo.
7. Agua y Territorio (Revistas Científicas Universidad de Jaén). ISSN: 2340-8472. Revisión de 1 artículo.

Listado de Colaboraciones en ámbitos de Divulgación

1. Navarro-Serrano, F. Cálculo de gradientes de temperatura superficial en la Península Ibérica. Gaceta Instituto Pirenaico de Ecología 2017.
2. Equipo organizativo: "En Busca del Polen Perdido". Taller en conmemoración del Día Internacional de la Fascinación por las Plantas. Delegación CSIC Aragón. Zaragoza, 31 de mayo de 2017.
3. Conferencia: "Gradientes térmicos en el Pirineo y otras cordilleras españolas. Primeros pasos". IV Jornadas IPErinas 2016. Instituto Pirenaico de Ecología (IPE – CSIC). Zaragoza, 15 de diciembre de 2016.

Apéndice III

TRABAJO DE CAMPO

El trabajo de campo es un método experimental que permite la alimentación de modelos, y también la obtención de datos específicos para responder a cuestiones determinadas, todo ello realizándose sobre el terreno, aplicando procesos y técnicas diferentes al trabajo realizado en laboratorio o en gabinete. En la presente Tesis Doctoral, el trabajo de campo propio ha permitido la recolección de datos para dar respuesta a tres de los objetivos específicos, permitiendo llevar a cabo tres análisis diferentes, que ya se encuentran publicados. Además, parte del trabajo de campo se ha dado de forma colaborativa dentro del Grupo de Investigación de Hidrología Ambiental (IPE – CSIC), con lo que se ha colaborado con otros compañeros, y viceversa, con el objetivo de hacer campañas de trabajo de campo más prácticas y eficientes. Es por ello que en el siguiente listado aparecen emplazamientos finalmente no introducidos en la Tesis Doctoral.

Listado de campañas de campo y salidas en las que se expusieron resultados

1. 2016-11-16: Moncayo. Terrestral Laser Escaner. J.I. López Moreno; E. Alonso González.
2. 2016-11-24: Valle de Panticosa (laderas Garmo Negro y Tablato). Instalación de dos estaciones meteorológicas completas, así como sensores Tinytag-Plus-2 e iButton. J.I. López Moreno; E. Alonso González; A. Sanmiguel Vallelado; P. Sánchez Navarrete.
3. 2016-11-28 a 2016-11-29: Alto Campoo (Cantabria). Instalación de una estación meteorológica completa. E. Alonso González; J. Herrero; MeteoCampoo.
4. 2016-12-14: Delegación de AEMET en Aragón. Elaboración de diseño experimental. S. Buisán.
5. 2016-12-16: Canfranc – Estación. Instalación de sensores Tinytag-Plus-2. Santiago (observador meteorológico de Canfranc – Estación).
6. 2016-12-22: Daroca. Instalación de sensores Tinytag-Plus-2 e iButton. Yolanda (observadora meteorológica de Daroca).
7. 2017-01-11 – 2017-01-13: Hoyos del Espino (Ávila). Recogida de muestras y reunión de grupo de trabajo.
8. 2017-01-20: Canfranc – Estación. Instalación de sensores iButton.
9. 2017-01-27: Valle de Panticosa. Descarga de datos y relanzamiento de sensores iButton. Mediciones de espesor y densidad de nieve. A. Sanmiguel Vallelado; P. Sánchez Navarrete.
10. 2017-02-14: Daroca. Descarga de datos. Yolanda (observadora meteorológica de Daroca).
11. 2017-03-02: Valle de Panticosa. Descarga de datos.
12. 2017-03-02: Canfranc – Estación. Descarga de datos. Santiago (observador meteorológico de Canfranc – Estación).
13. 2017-03-08: Valle de Panticosa (ladera Garmo Negro). Mediciones de espesor y densidad de nieve. J.I. López Moreno; E. Alonso González; I. Rico; A. Sanmiguel Vallelado.
14. 2017-03-19 a 2017-03-23: Lisboa (Portugal). Congreso de la Asociación Portuguesa de Meteorológica y la Asociación Española de Meteorología. Presentación Oral (2017-03-20).
15. 2017-04-05: Valle de Panticosa (ladera Garmo Negro). Instalación de sensores Tinytag-Plus-2. J.I. López Moreno.

16. 2017-04-28: Glaciar Monte Perdido. Descarga de datos y relanzamiento de sensores Tinytag-Plus-2. J.I. López Moreno; E. Alonso González.
17. 2017-05-27: Valle del río Aragón (ladera Estiviellas). Descarga de datos y relanzamiento de sensores Tinytag-Plus-2. J.I. López Moreno.
18. 2017-05-30: Zaragoza. Curso práctico de manejo de drones de ala fija. J.I. López Moreno; I. Rico; E. Alonso González; P. Errea.
19. 2017-06-20 a 2017-06-23: Mieres (Asturias). Congreso de la International Permafrost Association y la Universidad de Oviedo. Presentación Oral (2017-06-21). J.I. López Moreno; E. Alonso González.
20. 2017-06-30: Sierra de Gredos (Ávila). Descarga de datos y relanzamiento de sensores Tinytag-Plus-2. J.I. López Moreno.
21. 2017-07-05: Valle del río Aragón (ladera Moleta). Descarga de datos e instalación de sensores Tinytag-Plus-2. J.I. López Moreno.
22. 2017-07-15: Valle de Panticosa (ladera Tablato). Descarga de datos e instalación de sensores Tinytag-Plus-2. J.I. López Moreno.
23. 2017-07-20: Valle de Panticosa (ladera Garmo Negro). Descarga de datos e instalación de sensores Tinytag-Plus-2. J.I. López Moreno.
24. 2017-08-01: Glaciar de Vignemale. Instalación de sensores Tinytag-Plus-2. J.I. López Moreno.
25. 2017-08-04: Aneto. Instalación de sensor Tinytag-Plus-2. J.I.. López Moreno.
26. 2017-08-06: Valle de Panticosa (ladera Garmo Negro). Descarga de datos. J.I. López Moreno.
27. 2017-08-10: Moncayo. Descarga de datos. J.I. López Moreno.
28. 2017-09-05: Valle de Panticosa (laderas Garmo Negro y Tablato). Instalación de sensores Tinytag-Plus-2. A. Sanmiguel Vallelado.
29. 2017-09-25 a 2017-09-26: Mérida. Congreso de Climatología. Presentación Oral (2017-09-25). S.M. Vicente-Serrano; M. Tomás-Burguera; F. Domínguez.
30. 2017-09-29. Valle de Panticosa. Instalación de sensores Tinytag-Plus-2. A. Sanmiguel Vallelado.
31. 2017-10-04: Glaciar de Monte Perdido. Descarga de datos e instalación de sensores Tinytag-Plus-2. J.I. López Moreno; E. Alonso González.
32. 2017-10-08 a 2017-10-11: Ordino (Andorra). Pyrenean Symposium on Snow and Avalanches. Presentación Oral (2017-10-09). E. Alonso González.
33. 2017-10-17: Aramón – Formigal. Curso de precipitación en el proyecto SPICE. S. Buisán.

34. 2017-11-15: Aramón – Formigal. Instalación de sensores Tinytag-Plus-2. M. Khorchani; P. Sánchez Navarrete.
35. 2017-11-30: Posets. Instalación de sensor Tinytag-Plus-2. J.I. López Moreno.
36. 2018-01-12: Canfranc – Estación. Instalación de sensores Tinytag-Plus-2 y alternativas de protección de radiación. Santiago (observador meteorológico de Canfranc – Estación).
37. 2018-01-23 a 2018-01-24: Valle de Panticosa (ladera Tablato). Mediciones de espesor y densidad de nieve. Descarga de sensores Tinytag-Plus-2. I. Rico; M. Khorchani.
38. 2018-03-21: Valle de Panticosa. Descarga y recogida de sensores Tinytag-Plus-2. A. Sanmiguel Vallelado.
39. 2018-05-31: Canfranc – Estación. Descarga de sensores Tinytag-Plus-2 y recogida de alternativas de protección de radiación.
40. 2018-05-31: Aramón – Formigal. Descarga de sensores Tinytag-Plus-2.
41. 2018-06-06: Aramón – Formigal. Descarga de sensores Tinytag-Plus-2 (restantes). M. Khorchani.
42. 2018-07-07: Valle del río Aragón (ladera Moleta). Descarga datos e instalación de sensores Tinytag-Plus-2. J.I. López Moreno.
43. 2018-07-14: Valle del río Aragón (ladera Estiviellas). Descarga de datos e instalación de sensores Tinytag-Plus-2. J.I. López Moreno.
44. 2018-07-18: Valle de Panticosa (ladera Tablato). Descarga de datos e instalación de sensores Tinytag-Plus-2. J.I. López Moreno.
45. 2018-08-07: Valle de Panticosa (ladera Garmo Negro). Descarga de datos y relanzamiento de sensores Tinytag-Plus-2. J.I. López Moreno.
46. 2018-09-19: Valle de Panticosa (ladera Garmo Negro). Mantenimiento de estaciones meteorológicas completas. A. Sanmiguel Vallelado; P. Sánchez Navarrete.
47. 2018-09-21: Valle de Panticosa (ladera Tablato). Mantenimiento de estaciones meteorológicas completas y descarga de sensores Tinytag-Plus-2. A. Sanmiguel Vallelado; P. Sánchez Navarrete.
48. 2018-09-28: Glaciar de Monte Perdido. Descarga de datos e instalación de sensores Tinytag-Plus-2. J.I. López Moreno; E. Alonso González.
49. 2019-02-15: Glaciar de Vignemale. Descarga y recogida de sensores Tinytag-Plus-2. J.I. López Moreno; E. Alonso González.
50. 2019-03-19: Sierra de Gredos (Ávila). Descarga de datos y relanzamiento de sensores Tinytag-Plus-2. J.I. López Moreno.

51. 2019-06-04 a 2019-06-08: Ginebra (Suiza). Meteorological Technology Word Expo 2019.
52. 2019-06-23: Valle del río Aragón (ladera Estiviellas). Descarga y recogida de sensores Tinytag-Plus-2. J.I. López Moreno.
53. 2019-06-24 a 2019-06-25: Jaca. Congreso de la International Permafrost Association y el Instituto Pirenaico de Ecología (IPE-CSIC). Póster. J.I. López Moreno; J. Zabalza; E. Alonso González.
54. 2019-06-28: Valle del río Aragón (ladera Moleta). Descarga y recogida de sensores Tinytag-Plus-2. J.I. López Moreno.
55. 2019-07-03: Valle de Panticosa (ladera Garmo Negro). Descarga y recogida de sensores Tinytag-Plus-2. J.I. López Moreno; Álvaro (estudiante en prácticas).
56. 2019-07-20: Valle de Panticosa (ladera Garmo Negro). Descarga y recogida de sensores Tinytag-Plus-2. J.I. López Moreno.
57. 2019-08-01: Valle de Panticosa (ladera Tablato). Descarga y recogida de sensores Tinytag-Plus-2. J.I. López Moreno.
58. 2019-09-13: Glaciar de Monte Perdido. Descarga de datos e instalación de sensores Tinytag-Plus-2. J.I. López Moreno; E. Alonso González.
59. 2019-11-18 a 2019-11-19: Refugio de la Renclusa. Toma de muestras y reunión de trabajo. J.I. López Moreno; E. Alonso González; A. Sanmiguel Vallelado; J. Revuelto Benedí; C. Azorin Molina; M. Aznárez.
60. 2019-11-22: Cuenca Experimental de Izas. Instalación de sensores Tinytag-Plus-2. E. Alonso González; J. Revuelto; J.I. López Moreno.
61. 2019-11-27: Valle de Panticosa (ladera Garmo Negro). Instalación de sensores Tinytag-Plus-2. J.I. López Moreno; J. Revuelto; E. Alonso González.
62. 2019-11-29: Valle de Panticosa (ladera Tablato). Instalación de sensores Tinytag-Plus-2. J.I. López Moreno; J. Revuelto; E. Alonso González.
63. 2019-12-18: Valle de Panticosa (ladera Garmo Negro). Comprobación de configuración de sensores Tinytag-Plus-2.

Apéndice IV

CARTA DE ACEPTACIÓN DE PUBLICACIÓN "EN PRENSA"

Navarro-Serrano, F., López-Moreno, J.I., Domínguez-Castro, F., Alonso-González, E., Azorin-Molina, C., El-Kenawy, A., Vicente-Serrano, S.M. 2020. Maximum and Minimum air temperature lapse rates in the Andean region of Ecuador and Peru. *International Journal of Climatology*. En Prensa. DOI: https://doi.org/10.1002/joc.6574.

Fecha: 22/04/20 [02:44:45 CEST]
De: cs-author@wiley.com
Para: fnavarro@ipe.csic.es
Asunto: Published: Your article is now published in Early View!

Dear Francisco Navarro-Serrano,

Your article Maximum and Minimum Air Temperature Lapse Rates in the Andean region of Ecuador and Peru in International Journal of Climatology has the following publication status: Published as Early View

To access your article, please click the following link to register or log in:

https://authorservices.wiley.com/index.html#register

You can also access your published article via this link: http://dx.doi.org/10.1002/joc.6574

If you need any assistance, please click here to view our Help section.

Sincerely,

Wiley Author Services

Manuscripts with Decisions

ACTION	STATUS	ID	TITLE	SUBMITTED	DECISIONED
	ED: Huth, Radan AE: Aguilar, Enric EOS: Menzies, Deborah • Accept (26-Mar-2020) view decision letter	JOC-19-0528.R2	Maximum and Minimum Air Temperature Lapse Rates in the Andean region of Ecuador and Peru View Submission	21-Jan-2020	26-Mar-2020

International Journal of Climatology

Decision Letter (JOC-19-0528.R2)

From: enric.aguilar@urv.cat
To: fnavarro@ipe.csic.es, nlopez@ipe.csic.es, f.dominguez.castro@gmail.com, e.alonso@ipe.csic.es, cesar.azorin-molina@gu.se, kenawy@mans.edu.eg, svicen@ipe.csic.es
CC:
Subject: JOC-19-0528.R2 - Decision on Manuscript
Body: 26-Mar-2020

Dear Mr Navarro-Serrano

I have reviewed your revised manuscript "Maximum and Minimum Air Temperature Lapse Rates in the Andean region of Ecuador and Peru" and I believe that you have satisfactorily addressed the issues raised by the reviewers. Therefore, I am happy to accept your paper for publication in the International Journal of Climatology. Congratulations!

Your article cannot be published until you have signed the appropriate license agreement. Within the next few days you will receive an email from Wiley's Author Services system which will ask you to log in and will present you with the appropriate licence for completion. Any authors who work for an official government department should select as primary the appropriate license (for example Crown Copyright in the UK) for their work.

If you are a member of the Royal Meteorological Society, and the corresponding author, please be aware that you are eligible for a 20% discount on your fee for Open Access publication (if you select this option). If you are unaware of your member discount code, please contact alison.brown@rmets.org.

Please note that you can request changes of the typeset proofs only during the typesetting process and strictly BEFORE the official online publication (Early View). We are unable to accept requests to modify manuscripts which have already completed the typesetting process and have been published online.

Please note, citations to your paper are counted as soon as your paper is published online in EarlyView. A citation requires only the author names, paper title, journal title and year the paper was first published online (e.g. in EarlyView) and DOI to be valid. To make sure any paper is cited correctly always use the DOI.

Thank you for your fine contribution and while I look forward to receiving more papers from you, I may also wish to call upon your expertise as a reviewer in the future. Therefore, please ensure that your account details are accurate with respect to your areas of expertise.

Sincerely,

Dr Enric Aguilar
Associate Editor, International Journal of Climatology
enric.aguilar@urv.cat

Escuela de Doctorado

Universidad Zaragoza

Tesis Doctoral
Zaragoza, 2020